An investigation into the reliability performance of bridges designed according to TMH-7

by
Suzanne Esther Basson

Thesis presented in fulfilment of the requirements for the degree of Master of Engineering in Civil Engineering in the Faculty of Engineering at Stellenbosch University

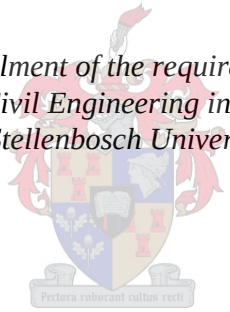

Supervisor: Prof Roman Lenner

March 2020

Declaration

By submitting this thesis electronically, I declare that the entirety of the work contained therein is my own, original work, that I am the sole author thereof (save to the extent explicitly otherwise stated), that reproduction and publication thereof by Stellenbosch University will not infringe any third party rights and that I have not previously in its entirety or in part submitted it for obtaining any qualification.

Date: ……

Abstract

South Africa's bridge design code, called Technical Methods for Highways 7 (TMH-7), was last revised in 1988 and is partially based on an outdated code. Since then, the road freight industry has expanded significantly, further encouraged by changes to the traffic regulations. The expected reliability performance of TMH-7 in catering for the increased traffic demand is not clear.

The purpose of this study is to investigate the structural performance of a new highway bridge designed according to TMH-7 and loaded with actual traffic loads. The study focus on the performance of TMH-7 for normal traffic conditions i.e. NA loading. A reliability analysis can provide a reliability index that measures the safety level of the structure.

For the investigation, reliability analyses were performed for two case studies, based on actual traffic load effects derived from site-specific Weigh-in-Motion (WIM) data. The load effect is represented by the bending moment at midspan of a simply supported bridge. For both case studies the extreme traffic load effects were extracted and described in a probabilistic manner. By means of statistical projection the maximum load effect distribution for a 50-year reference period was obtained. The limit state function was then formulated to define the failure mode at the ultimate limit state (ULS). The First Order Reliability Method (FORM) was used to obtain an overall reliability index and the results were interpreted by comparing the reliability index to target values from existing standards.

For the reliability analysis in the first case study, failure occurs when the actual traffic load effects exceed the design load effect for NA loading. Spans ranging from 5 to 50 metres were investigated. It was found that NA loading generally performs well for a typical highway bridge, especially for longer spans ranging from 30 to 50 metres. However, a poor reliability performance is seen for short narrow span bridges (especially for 5 m and 10 m spans), which agrees with previous studies.

In the second case study, a critical element reliability analysis was conducted on a spine beam of a 20 m reinforced concrete twin spine deck. Failure occurs when the load effects exceed the resistance of the critical spine beam. High reliability indices were obtained, which indicate that NA loading is performing well for the bending moment capacity of a 20 m span bridge. Furthermore, a sensitivity analysis revealed that the traffic load and model uncertainty for resistance, have the most significant effect on the obtained reliability indices.

With regard to bending moments at midspan, deficiencies in the traffic load model for NA loading were identified. Spans were also identified where design could be optimised to be more cost-effective. The study contributes to an improved understanding of the performance of TMH-7 for normal traffic conditions and can help direct future revisions of the traffic load model. It is recommended to extend the study to include other load effect types and to provide separate probabilistic descriptions for different loading event types.

Opsomming

Suid-Afrika se brugontwerpkode, Tegniese Metodes vir Snelweë 7 (TMH-7), was laas opgedateer in 1988 en is gedeeltelik gebaseer op ‘n uitgedateerde kode. Sedertdien het die padvrag-industrie aansienklik uitgebrei, aangemoedig deur veranderinge in die verkeersregulasies. Dit is onduidelik watter betroubaarheidsprestasie van TMH-7 verwag kan word, gegewe die toenemende verkeersbehoefte.

Die doel van die studie is om die strukturele werkverrigting van ‘n nuwe brug op ‘n snelweg, wat ontwerp is volgens TMH-7, met werklike verkeersbelasting te ondersoek. Die studie fokus op die doeltreffendheid van TMH-7 vir normale verkeerstoestande, m.a.w. NA-belasting. ‘n Betroubaarheidsanalise kan gebruik word om ‘n betroubaarheidsindeks te verkry wat die struktuur se veiligheidsvlak meet.

Die ondersoek behels die uitvoering van ‘n betroubaarheidsanalise vir twee gevallestudies wat gebaseer is op die las-effek van werklike verkeersbelasting, wat afgelei is van terrein-spesifieke Weeg-in-Beweging data. Die buigmoment by midspan van ‘n enkel-span brug verteenwoordig die las-effek. Die maksimum las-effekte van die verkeersbelasting was bepaal en beskryf op ‘n waarksynlikheidswyse. Statistiese projeksie was gebruik om die maksimum las-effekte vir ‘n 50-jaar verwysingsperiode te bepaal. Daarna was die grenstoestand van swigting geformuleer by faling. Die Eerste Orde Betroubaarheidsmetode was gebruik om ‘n algehele betroubaarheidsindeks te vind, en die resultate was geïnterpreteer deur die betroubaarheidsindeks te vergelyk met teikenwaardes van bestaande standaarde.

Faling in die eerste gevallestudie vind plaas wanneer die werklike las-effekte van die verkeer die ontwerp las-effek van NA-belasting oorskrei. Spanlengtes van 5 tot 50 meter was ondersoek. Daar is bevind dat NA-belasting goed presteer vir ‘n tipiese snelwegbrug, veral vir langer spanne tussen 30 en 50 meter. ‘n Swak betroubaarheidsvlak word egter gesien vir kort en smal spanlengtes (veral tussen 5 en 10 meter), wat ooreenstem met vorige studies.

‘n Kritiese-element betroubaarheidsanalise was uitgevoer op ‘n flensbalk van ‘n 20 m gewapende beton brugdek met twee geflensde balke. Faling vind plaas wanneer die las-effekte die weerstand van die balk oorskry. Hoë betroubaarheidsindekse was verkry, wat aandui dat NA-belasting goed presteer vir die buigmomentkapasitiet van ‘n 20 m span brug. Verder het ‘n sensitiwiteitsanalise die verkeersbelasting en model-onsekerheid vir weerstand geïdentifiseer as die veranderlikes wat die grootste invloed het op die betroubaarheidsindekse.

Sover dit buigmomente by midspan betref, was tekortkominge in die verkeersbelastingsmodel vir NA-belasting geïdentifiseer, sowel as spanlengtes waar ontwerp geoptimiseer kan word om meer koste-effektief te wees. Die studie dra by tot 'n beter begrip van die doeltreffendheid van TMH-7 vir normale verkeerstoestande en kan dien as riglyn vir toekomstige hersienings van die verkeersbelastingsmodel. Dit word aanbeveel om die studie uit te brei om ook ander las-effek tipes in te sluit en om aparte waarskynlikheidsbeskrywings te gee vir verskillende tipes las-gebeurtenisse.

Acknowledgements

First and foremost, I would like to thank my Heavenly Father for His provision and guidance throughout the research process. This thesis is for Him.

I would like to thank the following people:

- Dr Roman Lenner, for his guidance, mentorship and patience throughout the research process.
- Pierre van der Spuy, Prof De Wet and Dr Sýkora for their advice and insights.
- N3 Toll Concession and Bakwena Concession for providing the Weigh-in-Motion data.
- The Wilhelm Frank Trust for funding.
- My family and friends, especially Robert, Biancé and Nicola, for their encouragement, love and understanding.
- My parents for their constant love and support. Thank you for always being my number one supporters.

Table of Contents

List of Figures

List of Tables

List of Abbreviations

CDF	Cumulative distribution function
COV	Coefficient of variation
EN	Eurocode
FORM	First Order Reliability Method
GEV	Generalised extreme value
ISO	International Standards Organisation
iid	Independent and identically distributed
JCSS	Joint Committee on Structural Safety
LLDF	Lateral load distribution factor
LN	Two-parameter lognormal
LN3	Three-parameter lognormal
MLE	Maximum likelihood estimation
MLF	Multiple lane reduction factor
N	Normal
N1	National Route 1
N3	National Route 3
SANS	South African National Standard
TMH-7	Technical Methods for Highways 7
UDL	Uniformly distributed load
ULS	Ultimate limit state
WIM	Weigh-in-Motion

List of Symbols

A_s	Area of steel reinforcement
b	Effective flange width
$\boldsymbol{D}$	Vector of partial derivatives
d	Effective depth to tension reinforcement
E	Load effect
E	Modulus of elasticity
E_{model}	Traffic load effects before model uncertainty is included
e_d	Design value of the load effect
F	Probability distribution function
F_{cc}	Compression force in concrete
F_E	Probability distribution function of the load effect
F_k	Characteristic load
$F_{LN,U}$	Probability distribution function of a standardised lognormal variable
$F_{LN,X}$	Probability distribution function of a lognormal variable
F_{LN3}	Probability distribution function of the three-parameter lognormal distribution
F_R	Probability distribution function of the resistance
F_{st}	Tension force in reinforcement
F_U	Probability distribution function of a standardised random variable
F_X	Probability distribution function of a random variable
F_Z	Probability distribution function of the limit state
$F_{50\ years}$	Probability distribution function for 50-year maximum load effects
f	Probability density function
f_{cu}	Concrete cube strength
f_E	Probability density function of the load effect
$f_{LN,U}$	Probability density function of a standardised lognormal variable

f_{LN3}	Probability density function of the three-parameter lognormal distribution
f_R	Probability density function of the resistance
f_X	Probability density function of a random variable
f_y	Steel yield strength
f_Z	Probability density function of the limit state
$f_{50\ years}$	Probability density function for 50-year maximum load effects
$f(\boldsymbol{X})$	Joint probability density function
G	Dead load
G_w	Superimposed dead load
i	Location of item in list
k	Correction factor to account for partial loading of an influence line
L	Effective loaded length
L_i	Loaded length of any previously calculated base length portion i
L_p	Loaded length of the p-th part
L_s	Equivalent or effective span length
LLDF_1	Lateral load distribution factor corresponding to Q_1
LLDF_2	Lateral load distribution factor corresponding to Q_2
LLDF_3	Lateral load distribution factor corresponding to Q_3
l	Log-likelihood
$M_{d,G}$	Design moment for permanent loads
$M_{d,Q}$	Design moment for variable loads
$M_{d,R}$	Design moment for resistance
M_G	Dead load moment
M_{GW}	Moment due to superimposed dead loads
M_Q	Variable load moment
M_R	Resistance moment
M_u	Ultimate moment of resistance

m	Sample mean
NA	Normal traffic loading
NB	Abnormal traffic loading
Nb1	Slow lane in northbound direction
Nb2	Fast lane in northbound direction
NC	Super loading
n	Number of items in list
P	Probability
p_f	Probability of failure
Q	Traffic load (50 years)
Q_a	Average nominal NA loading per metre of notional lane
Q_{ap}	Nominal distributed NA loading on p-th loaded part
$Q_{combined}$	Combined load effect carried by critical spine beam
Q_i	Loading intensity of any previously calculated base length portion i
Q_{max}	Maximum load effect per month
Q_n	Traffic load effect in n-th traffic lane (furthest away from critical spine beam)
Q_1	Traffic load effect in first traffic lane (closest to critical spine beam)
Q_2	Traffic load effect in second traffic lane
Q_3	Traffic load effect in third traffic lane
$\{Q_{combined}\}$	Vector of combined load effects per month
R	Resistance
r_d	Design value of the resistance
S^*	Notation for design load effect in TMH-7
Sb1	Slow lane in southbound direction
Sb2	Fast lane in southbound direction
s	Sample standard deviation
s	Simplified compression block depth

U	Standardised random variable
U_E	Standardised variable of the load effect
U_R	Standardised variable of the resistance
u	Realisation of standardised random variable
u_0	Standardised value corresponding to $z = 0$
u'	Modified standardised variable
u^*	Design point of standardised random variable
$\boldsymbol{U}$	Vector of standardised random variables
$\boldsymbol{u}^*$	Vector of the standardised design point
w	Distributed load
w	Sample skewness
X	Random variable
x	Realisation of a random variable
x_0	Upper or lower bound of the three-parameter lognormal distribution
x^*	Design point of a random variable
$\boldsymbol{X}$	Vector of random variables
$\boldsymbol{x}$	Vector of random variable realisations
$\boldsymbol{x}^*$	Vector of design values
Z	Limit state
z	Internal lever arm
z	Realisation of the limit state
$Z'(\boldsymbol{U})$	Limit state expressed in terms of vector of standardised random variables
$Z(\boldsymbol{X})$	Limit state expressed in terms of vector of random variables
α	Sensitivity factor
α	Skewness
α_E	Sensitivity factor of the load effect
α_R	Sensitivity factor of the resistance

α^2	Relative importance of variable
$\boldsymbol{\alpha}$	Vector of sensitivity factors
β	Reliability index
β_E	Load effect index
β_R	Resistance index
β_t	Target reliability index
γ	Global safety factor
γ_E	Partial factor for the load effect
γ_{fL}	Partial load factor
γ_{f3}	Partial effect factor
γ_R	Partial factor for the resistance
δ	Scale parameter
θ	Model uncertainty
θ_E	Load effect model uncertainty
θ_G	Permanent load model uncertainty
θ_Q	Traffic load model uncertainty
θ_R	Resistance model uncertainty
κ	Shape parameter
λ	Location parameter
μ	Mean
μ_E	Mean value of the load effect
μ_R	Mean value of the resistance
μ_X	Mean value of a random variable
μ_Z	Mean value of the limit state
μ_X^e	Mean of the equivalent normal distribution
ρ_{RE}	Correlation coefficient between resistance and load effect
σ	Standard deviation

σ_E	Standard deviation of the load effect
σ_R	Standard deviation of the resistance
σ_X	Standard deviation of a random variable
σ_Z	Standard deviation of the limit state
σ_X^e	Standard deviation of the equivalent normal distribution
φ_2	Swiss impact factor

1 Introduction

1.1 Background

Bridges form part of the road transport network of a country. In South Africa, transport is identified as one of the most important national assets as it plays a key role in socio-economic development (Maina and De Beer, 2008). It is thus important to ensure that the design, construction and maintenance of this network are looked after and able to cater for the traffic demand. Traffic loading is the most significant variable action considered in road and bridge design and thus requires careful attention to ensure a sound road network.

The current code of practice for the design of highway bridges in South Africa is called Technical Methods for Highways 7 (TMH-7). It consists of three parts, whereas the traffic load models are formulated in Part 2. The code was first published in 1981 and is largely based on the CEB FIP Model Code for Concrete Structures of 1978, the British Code BS5400 and the National Building Code of Canada (CSRA, 1981). It is important to understand the context in which South Africa's bridge design code was written, relative to the development of the road freight industry in South Africa. The context subsequently explained, surfaces the reasons why this research study is important.

For most of the 20th century, the development of road freight transport in South Africa was restricted by regulations in order to protect the railway industry. In 1977 the gradual deregulation of road transportation commenced in order to allow for freer competition between the road and railway industry (Janse van Rensburg, 1996). By 1988 the complete economic deregulation of road transportation was implemented (Stander and Pienaar, 2005), with the prerequisite that the Road Transport Quality System be adhered to, as presented in Act 93 of the National Road Traffic Act of 1996 (DOT, 2013). To date this system has not been implemented and evidently poor control and management of road transport operations were seen after the deregulation in 1988 (Havenga, Simpson and De Bod, 2014).

In light of the above, TMH-7 was published before the deregulation of road transport in 1988. The traffic load model was derived based on research done by Dr A.C. Liebenberg prior to March 1974, formulated according to South Africa's road traffic regulations of 1974 (Oosthuizen *et al.*, 1991). In light of knowledge at the time, provisions were made to the load model to account for possible future developments and overloading of heavy vehicles. In 1988, the Committee of State Road Authorities (CSRA) found shortcomings in the traffic load model

for normal traffic conditions, called NA loading (Oosthuizen *et al.*, 1991). Subsequently, revisions were made to the NA loading in 1988, in which 6 kN/m was added to the distributed load and the axle load was increased by 20 %. Notwithstanding the revisions made to TMH-7, Oosthuizen *et.al*. (1991) found that NA loading was still inadequate in providing for short and narrow span bridges up to 10 m in length. It was proposed to amend the axle load with a 25 % increase and to conduct a general revision of TMH-7 (Oosthuizen *et al.*, 1991), however, these proposals were not put into effect. Concern is further raised by the fact that TMH-7 is largely based on the loading provisions of the British Code BS5400, which has since been updated and superseded by the Eurocodes. Anderson (2006) conveys the importance of also designing for NB loading, representing abnormal loading, in order to cover the shortcomings seen for short span bridges.

Since the last revision of TMH-7 in 1988, an exponential growth in heavy freight vehicles have been seen over the past few decades, which led to road freight becoming the dominant mode of freight transport in South Africa. In 2004 it was estimated that approximately 70 % of all freight in South Africa was carried by heavy vehicles and by 2013 it increased to 76 % (Bosman, 2004; DOT, 2013). Furthermore, amendments to the traffic regulations have exacerbated the situation and have led to changes in the traffic characteristics and the volume of heavy vehicles on the road. Significant changes include an increase in the permissible vehicle mass from to 56 t in 1989 (Parliamentary Monitoring Group, 2000), an increase in legal axle mass from 8200 kg to 9000 kg in 1993 (DOT, 2013), and also the increase in allowable heavy vehicle dimensions. The influence of these changes on the performance of the code is still undetermined. According to the Department of Transport (2013), a growing concern has been raised regarding the levels of overloading recorded in South Africa. The National Transport Masterplan 2050 (2013) sheds light on the ineffectiveness of overloading control systems in many areas of the national route system.

1.2 Problem Statement

The background of TMH-7 and heavy traffic characteristics in South Africa raise concerns regarding the present performance of TMH-7 in catering for the increased traffic demand. TMH-7 is partially based on an outdated code and was written in a time prior to exponential growth in the road freight industry, accompanied by significant changes to the traffic regulations in the country. Deficiencies in the traffic load model for normal traffic conditions

have been identified and the matter of revising the code has been recommended by previous studies.

A globally acceptable approach in verifying the performance of a design code is to measure the safety level or reliability index it achieves. Other design codes have used the probabilistic analysis of traffic data to derive rational traffic load models. The model is then calibrated based on a target reliability index in order to limit the probability of failure related to a certain reference period. Presently, such a measure is not available for TMH-7, as the traffic load model was not calibrated based on a target reliability index. Due to a lack of statistical data on traffic at the time, the load model was derived based on a credibility approach (CSRA, 1981). The approach made use of engineering judgement and experience in conjunction with deterministic methods to model idealised vehicle combinations to represent the traffic loading (Anderson, 2006).

Recent advances in the development and quality of Weigh-in-Motion (WIM) technology have allowed for better characterisation of the current traffic loading on bridges in South Africa. The purpose of this study is to perform a reliability analysis on a bridge designed according to TMH-7 for normal traffic conditions, and loaded with actual traffic loading derived from WIM data. From this a reliability index can be obtained, related to a certain reference period, that measures the safety level of the bridge. By comparing the obtained reliability index to existing target reliability indices, the results can provide valuable insights into the reliability performance of TMH-7 in catering for the current traffic demand.

1.3 Objectives

The primary objective of this study is to investigate the reliability performance of TMH-7, and more specifically the traffic load model for normal traffic conditions, i.e. NA loading. This is achieved by conducting reliability analyses for two case studies based on actual traffic load effects derived from site-specific WIM data.

The following sub-objectives are relevant to both case studies:

- Decide on a statistical approach to assess the extreme traffic load effects.
- Determine the statistical characteristics describing the extreme traffic load effects.
- Select applicable probabilistic models to represent the extreme traffic load effects.
- Assess the selected probabilistic models by means of goodness-of-fit tests.

- Find the maximum load effect distribution for a certain reference period.
- Formulate the relevant limit state function describing the failure mode.
- Conduct a reliability analysis according to the limit state function, in order to obtain the reliability index.
- Compare the obtained reliability indices to target reliability indices used in national and international standards.

1.4 Motivation

Concerns have been raised that the traffic load model in TMH-7 for normal traffic conditions shows deficiencies, and that the model should be revised based on a probabilistic analysis of actual traffic data in South Africa (Oosthuizen *et al.*, 1991; Anderson, 2006). Moreover, it is unclear what reliability performance can be expected from TMH-7 in catering for the current traffic demand. The reliability index obtained from a reliability analysis provides a way of quantifying the safety level provided by the code. As such, it can be determined whether TMH-7 is performing adequately to design a bridge for normal traffic conditions.

The reliability analysis provides for the identification of shortcomings and deficiencies in the code for different span lengths, which can then be used to rectify them. If the code is underperforming at the ultimate limit state (ULS), the structure is viewed unsafe and structural failure may occur. However, when the code is performing too conservatively, it may lead to overdesign which neglects the cost optimisation principles. Thus, the study is valuable as it estimates the reliability level of TMH-7 for normal traffic conditions, and it identifies deficiencies in the load model. In addition to this, the results provide a measure of assurance of the validity of TMH-7 as the code of practice.

1.5 Scope and Limitations

The study is limited to the investigation of two case studies, where a reliability analysis is performed on a bridge designed according to TMH-7 and loaded with the actual traffic loading derived from WIM data. Only the traffic load model for normal traffic conditions, i.e. NA loading, is considered, and the investigation is based on the design of a new highway bridge. The traffic load effect considered, is the bending moment at midspan of a simply supported bridge, i.e. sagging moments. Subsequently, the focus is on the performance of a bridge at

ULS. Furthermore, the study investigates free flow traffic, which is assumed to govern extreme traffic load effects for short to medium span bridges ranging from 5 to 50 metres (Bruls *et al.*, 1996; Caprani and O'Brien, 2009). These span lengths also represent the majority of highway bridges in South Africa (Van der Spuy and Lenner, 2019). As WIM data only provides static loading, the dynamic load effects of moving traffic on a bridge are excluded from the study. Consequently, only static load effects are considered.

The two case studies are based on WIM data from two different national routes. The first case study is based on WIM data from Roosboom station on the National Route 3 (N3) between Durban and Johannesburg. The second case study is based on WIM data from the National Route 1 (N1) near Kilner Park, north of Pretoria. The two WIM sites were chosen firstly because they are located on major freight corridors in South Africa (DOT, 2013). Secondly, because Roosboom station has been investigated in a number of previous studies (Lenner, De Wet and Viljoen, 2017; Van der Spuy and Lenner, 2018; Sifre and Lenner, 2019) and may serve as reference station. Kilner Park on the other hand is the only station measuring four traffic lanes, which makes it suitable to investigate a multiple lane bridge. Both WIM sites have three or more years of recorded measurements, and the data is deemed to be of good quality (De Wet, 2010a).

The scope of each case study is dictated by the number of traffic lanes measured at the WIM site. In the first case study, only the slow (outer) lane data is available. A one-lane bridge carrying slow lane traffic is not representative of a typical highway bridge. Therefore, the decision has been made to only consider the traffic loading part in the reliability analysis. That is, the traffic load effects on the bridge are included, but the bridge resistance and dead loads are ignored. The investigation considers span lengths of 5 to 50 metres, in increments of 5 metres.

In the second case study, data for a slow and fast lane in both directions are available. As more than one lane of data is available, it can be used to design a bridge which is more representative of a typical highway bridge. The case study utilises a two-lane, single span bridge for the analysis. A critical element reliability analysis is performed, where the resistance, dead load and traffic load effects of the critical member are included. This is followed by a sensitivity analysis to determine the relative significance of the resistance, dead loads and traffic load effects on the obtained reliability results.

The WIM data for both case studies were processed in a previous study done by Van der Spuy and Lenner (2019), who used a moving load analysis to derive the traffic load effects from the complete set of cleaned and calibrated WIM data. As access is limited to the unprocessed WIM data, it is difficult to look at subsets of the data and to identify specific loading events. For instance, whether the critical loading event is produced by a single heavy truck or side-by-side trucks. Furthermore, it is difficult to make a distinction between illegally overloaded standard trucks and permit trucks. Overloading is a growing concern in South Africa (DOT, 2013; Lenner, De Wet and Viljoen, 2017), and as NA loading in TMH-7 makes provision for overloading of legal vehicles (Anderson, 2006), it is deemed acceptable to consider the whole data set of traffic load effects in this study.

It is difficult to predict future trends in traffic, as the variation of traffic volumes and configurations are highly dependent on the economy, new regulations and technological developments (Caprani and O'Brien, 2009). Traffic growth is thus considered outside the scope of this study. If there is concern about the actual change in traffic conditions over time, the reliability performance of a bridge will need to be reassessed on a periodic basis.

1.6 Thesis Outline

Chapter 1: Introduction

The first chapter provides background on the traffic load model in TMH-7 and the development of the road freight industry in South Africa. Thereafter, the problem statement, motivation and objectives are stated, followed by the scope and limitations of the study.

Chapter 2: Literature Review

Background is provided on TMH-7's load model for normal traffic conditions. It also includes background on different approaches to assess extreme traffic load effects. The concepts of probabilistic modelling and reliability theory are discussed, followed by a summary of the First Order Reliability Method (FORM).

Chapter 3: Roosboom Case Study

This chapter presents the case study on WIM data from Roosboom station on the N3. The methodology for the case study is thoroughly explained, which include the procedure on how the reliability analysis was performed. Thereafter, the results and conclusions of the findings are discussed.

Chapter 4: Kilner Park Case Study

This chapter presents the case study on WIM data from a site near Kilner Park on the N1. The methodology for the case study is detailed, which includes the execution of the critical element reliability analysis and sensitivity analysis. This is followed by results and concluding remarks.

Chapter 5: Conclusion and Recommendations

A summary of the findings for both case studies are given, and recommendations are made for future research in this field of study.

2 Literature Review

2.1 Introduction

The chapter provides relevant information and explanations of important concepts to better understand the remaining chapters. The key discussion points include a brief summary of TMH-7's traffic load model for normal traffic conditions and a description of Weigh-in-Motion (WIM) data and statistical methods for investigating traffic load effects. Concepts of probability theory and structural reliability are also discussed, which include a description of the relevant probabilistic models and an outline of the First Order Reliability Method (FORM).

2.2 Overview of NA Loading in TMH-7

2.2.1 *Background to Limit State Design in Context of TMH-7*

TMH-7 is based on the concept of Limit State Design as defined by the International Standards Organisation in ISO 2394 (2015). It allows for a semi-probabilistic design, where the limit state defines a distinct condition that needs to be met in order for the structure to perform satisfactory (Holický, 2009). For the ultimate limit state (ULS), this is typically defined by the condition that the load effects should not exceed the resistance of the structure for the duration of its specified design life.

Design standards generally specify characteristic values for the load effects and resistance of the structure based on a prescribed probability of exceedance corresponding to a specific reference period (Holický *et al.*, 2015). The characteristic value describing the basic variable is a function of its distribution type and variability, but independent of a reliability level or specified design life (Holický *et al.*, 2015). The characteristic values for the load effects and resistance are then multiplied or divided by applicable partial factors to obtain the design values for the basic variables. The design value for the load effects is more than its characteristic value, whereas the design value for the resistance is less than its characteristic value. The partial factors are derived from statistical information on the basic variable and a target reliability index (Holický *et al.*, 2015). A reliability index is a measure of the safety level of the structure (Holický, 2009).

Although TMH-7 defines characteristic values and partial factors to obtain design values for the traffic load effects, the values were not derived based on probability theory. The characteristic load effects are represented by nominal traffic load effects that were obtained

deterministically by the credibility approach. This approach used engineering judgement and past experience to select idealised heavy vehicle combinations to provide the worst loading events (CSRA, 1981; Anderson, 2006). The characteristic values, represented by the nominal traffic load effects, were thus not based on the statistical interpretation of actual traffic data. According to CSRA (1981), the partial factors also do not consider probabilistic concepts and were conservatively derived based on engineering judgement.

2.2.2 *TMH-7 Traffic Load Model*

Traffic load effects can be measured in terms of bending moments and shear forces induced in the bridge due to vehicles moving over the bridge. The traffic load model is found in Part 2 of TMH-7 and it is used to model the traffic loading on different span lengths. The model was developed to account for all combinations of traffic load conditions and are used to obtain design values that produce the most unfavourable traffic load effects. The design traffic load and dead load are then used to find the required resistance of the bridge.

The traffic load model considers three types of live loading: normal loading (NA), abnormal loading (NB) and super loading (NC). Each type is applied separately to the bridge, and NA and at least 24 units of NB loading need to be considered for all highway bridges. According to TMH-7 (CSRA, 1981), NA loading represents normal traffic conditions on a highway, consisting of the most severe arrangements of legal vehicles. NB loading describes an abnormally heavy vehicle, whereas NC loading represents multi-wheeled trailer combinations with controlled hydraulic suspension and steering (CSRA, 1981). The scope of this study entails the investigation of NA loading.

2.2.3 *NA Loading*

The load model for NA loading makes use of a floating lane notional lane width, where the notional lanes do not represent the actual traffic lanes, but are used for the purpose of applying the loading. The notional lanes are equal in width, but the width varies depending on the number of notional lanes required for the specific carriageway width. The carriageway width is defined as the width of the bridge deck between kerbs, which include the shoulders and traffic lanes. The required number of notional lanes are outlined in TMH-7 Section 2.6.2. (CSRA, 1981) and summarised in Table 2.1 for transparency.

Table 2.1: Number of notional lanes required for a specific carriageway width (CSRA, 1981).

Carriageway width (m)	**Number of notional lanes**
4.8 up to and including 7.4	2
Above 7.4 up to and including 11.1	3
Above 11.1 up to and including 14.8	4
Above 14.8 up to and including 18.5	5
Above 18.5 up to and including 22.2	6

The load model for NA loading is characterised by a nominal uniformly distributed line load (UDL) that is applied in the longitudinal direction of any continuous part of a notional lane. Simultaneously, a single nominal axle load (or knife edge load) is applied to each notional lane.

The UDL is depended on the effective loaded length (L) that TMH-7 (CSRA, 1981) defines as the 'aggregate length of the separate parts loaded in any single notional lane or combination of notional lanes in one or more carriageways'. Here *parts* refer to sections of the notional lanes that are loaded to obtain the most adverse load effects at a specific location on the bridge. The loading curve describing the application of the UDL is illustrated in Figure 2.1, where the UDL is denoted by Q_a and measured in kN/m. For a continuous loaded length of up to 36 m, a UDL of 36 kN/m is applied in the longitudinal direction. For loaded lengths exceeding 36 m, the UDL value is obtained from Equation 2.1.

$$Q_a = \frac{180}{\sqrt{L}} + 6 \tag{2.1}$$

The axle load applied per notional lane, can be calculated from Equation 2.2 and is measured in kN. The symbol n refers to the loading sequence number corresponding to the relevant notional lane (CSRA, 1981).

$$Axle\ load\ = \frac{144}{\sqrt{n}} \tag{2.2}$$

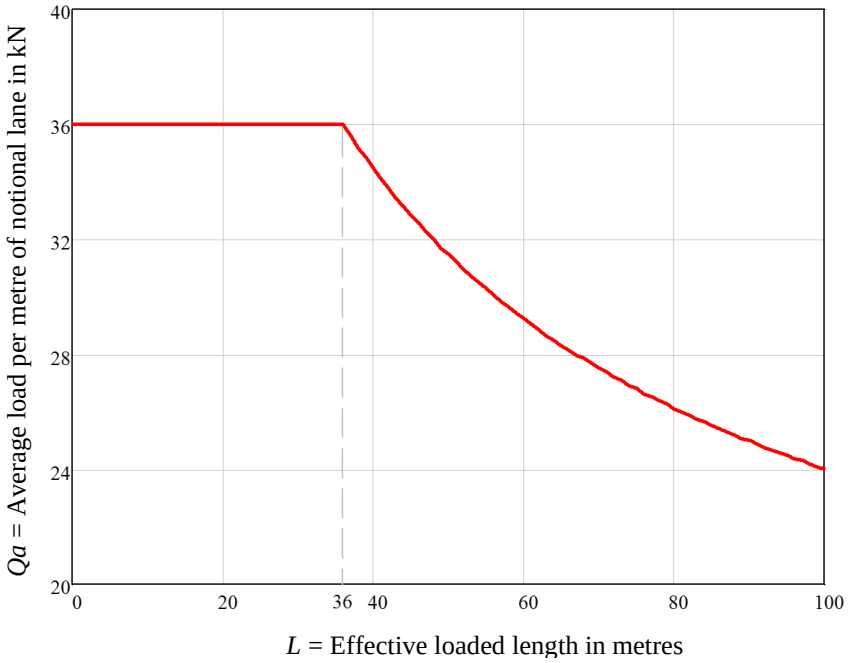

Figure 2.1: Loading curve for type NA loading (CSRA, 1981)

NA loading considers the dynamic effects of moving traffic on the bridge with the Swiss impact factor, denoted by φ_2. The factor is expressed in Equation 2.3, where L_s represents the equivalent (or effective) span length in metres. For a simply supported bridge, L_s is generally the distance between the centres of support. The Swiss impact factor is already accounted for in the NA loading. For this study the WIM data are producing static load effects and thus the impact factor needs to be removed from NA loading to make it static.

$$\varphi_2 = 0.05\left(\frac{100 + L_s}{10 + L_s}\right) \tag{2.3}$$

2.2.4 *NA Loading Application*

Depending on the purpose of the investigation, the UDL for NA loading can be determined by means of a global analysis or by parts. When the traffic load effects are determined by a global analysis, an average UDL is obtained for the aggregate loaded length and applied to the loaded parts of each notional lane. To illustrate, consider a 20 m single span bridge with thee notional lanes, where the maximum bending moment at midspan is of interest. The average UDL applied to each notional lane can be calculated with Equation 2.1, where Q_a denotes the average UDL and L is the aggregate loaded length, i.e. 60 m. The global bending moment at midspan

due to the UDL can be calculated with $wL^2/8$, where w is equal to three times Q_a and L denotes an effective span length of 20 m. Figure 2.2 illustrates the application of an average UDL, denoted by Q_a, over three notional lanes.

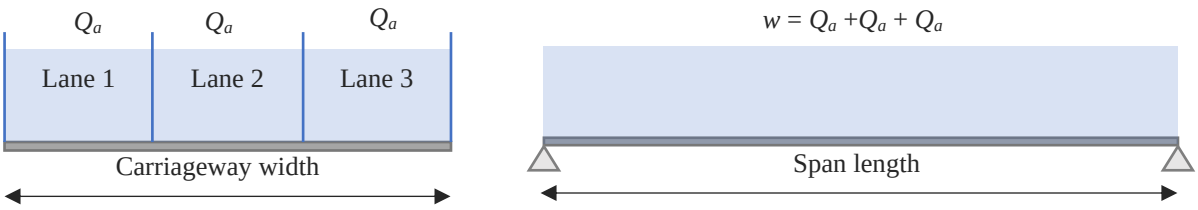

Figure 2.2: Cross-section (left) and longitudinal section (right) of average UDL (Q_a) applied to three notional lanes.

When a critical element is of interest, parts of the notional lanes should be loaded in a sequence that produces the maximum load effects for the critical element. In this case, the analysis makes use of Equation 2.4, which determines the UDL (in kN/m) that should be applied to the p-th loaded part, denoted by Q_{ap}. TMH-7 (CSRA, 1981) provides the following definitions for the notations in Equation 2.4. $\sum_{i=1}^{p} L_i$ is the sum of all loaded lengths (in metres) up to and including the p-th part. The loaded length of the p-th part is denoted by L_p. Q_a is the intensity of loading (in kN/m) obtained from the loading curve in Figure 2.1 for $\sum_{i=1}^{p} L_i$. L_i is the length (in metres) of any previously calculated base length portion i. Q_i is the intensity of loading (in kN/m) applied to any previously calculated base length portion i.

$$Q_{ap} = \left(Q_a \sum_{i=1}^{p} L_i - \sum_{i=1}^{p-1} Q_i L_i \right) / L_p \tag{2.4}$$

To illustrate, again consider a 20 m single span bridge, where the maximum bending moment at midspan is of interest. Three notional lanes with three loaded parts are considered, i.e. i = 1,2,3. The three loaded parts are loaded with Q_{a1}, Q_{a2} and Q_{a3}, as obtained from Equation 2.4. The global bending moment at midspan due to the UDL's can again be obtained with $wL^2/8$, but here w represents the sum of the UDL's (Q_{a1} + Q_{a2} + Q_{a3}). Figure 2.3 illustrates the application of NA loading by parts, where Q_{a1}, Q_{a2} and Q_{a3} represent the UDL applied to each loaded part over the three notional lanes.

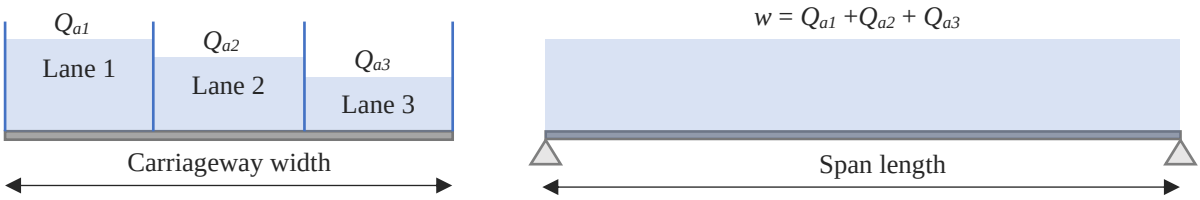

Figure 2.3: Cross-section (left) and longitudinal section (right) of UDL (Q_{ap}) applied by parts over three notional lanes.

Both methods mentioned above obtain the same global load effects. A requirement applicable to both methods is that the UDL for any loaded part should not exceed 36 kN/m. Furthermore, the UDL should be adjusted with a correction factor, i.e. a *k*-factor. The *k*-factor is chosen based on the shape of the influence line describing the longitudinal distribution of the load effect under consideration. It is a measure to account for the possibility that partial loading of an influence line may result in a larger load effect, than using a uniformly distributed load with lower intensity over the relevant base portion of the influence line (CSRA, 1981). A *k*-factor of 1.1 is applicable for the bending moment at midspan of a simply supported bridge.

In addition to the UDL calculated by either of the above methods, the axle load per notional lane is calculated from Equation 2.2 and positioned in each notional lane to produce the most adverse effects on the section of interest. The maximum characteristic load effect is then calculated when the UDL and axle loads are applied simultaneously over the notional lanes. A detailed explanation of the longitudinal and transverse distribution of the UDL and axle loads can be found in Section 2.6.3.2. of TMH-7 (CSRA, 1981).

2.2.5 *Design Load Effects*

For ULS, the obtained characteristic traffic load effects obtained from NA loading are multiplied by partial factors to obtain the design load effects. TMH-7 Part 1 (1981) provides a description of the partial load factors. Equation 2.5 can be used to calculate the design load effects. F_k denotes the characteristic load, whereas S^* denotes the design load effect. The partial load factor and partial effect factor are denoted by γ_{fL} and γ_{f3}, respectively.

$$S^* = \gamma_{f_3}(\text{effects of } \gamma_{fL} F_k) \tag{2.5}$$

The factor γ_{fL} is a function of γ_{f1} and γ_{f2}, and depends on the combination of loads as outlined in TMH-7, Section 5 of Part 2 (1981). γ_{f1} accounts for unfavourable deviations from the nominal load. γ_{f2} is a combination factor introducing the reduced probability that the nominal values will be reached simultaneously for all load types present. γ_{f3} account for uncertainties in modelling the load effects, unforeseen conditions, the random nature of variables and the importance of the limit state under consideration (CSRA, 1981).

For NA loading at ULS, the design traffic load effects are typically obtained with γ_{fL} equal to 1.5 and γ_{f3} equal to 1.1, which results in an overall partial factor of 1.65. For dead load, γ_{fL} is equal to 1.2 and γ_{f3} is also equal to 1.1, which results in an overall partial factor of 1.32.

2.3 Probabilistic Modelling

This section provides an overview of basic concepts in probability theory as well as a description of probabilistic models relevant to the study.

2.3.1 *Concepts of Probability Theory*

Probabilistic modelling can be used as a statistical tool to characterise a phenomenon or event based on historical data. It accounts for the randomness or unpredictable behaviour of an event, which prevent the exact prediction of a future outcome of the event (Mitrani and Mitrani, 1998). A quantity whose outcome is uncertain is called a random variable, denoted by X (Coles, 2001). A random variable can take on any value in a set of possible outcomes, called the sample space, consisting of real numbers (Coles, 2001). A realisation or outcome of the random variable X is called an event, denoted by x, and it describes a subset of the sample space (Chang, 2013).

A random variable can either be discrete or continuous. A discrete random variable's sample space is countable with distinct values, while a continuous random variable's sample space is uncountable and usually based on measurements (Montgomery and Runger, 2014). For most applications in engineering, including traffic load effect measurements, the random variable is continuous (Chang, 2013). Therefore, the focus of this section is on the probabilistic modelling of continuous random variables.

A random variable can be described by a probability distribution function and a corresponding probability density function. The probability distribution function (also called cumulative distribution function) is denoted by $F(x)$, where x can take on any value in the sample space.

$F(x)$ assigns probabilities to the various values in the sample space, and the function output ranges between 0 and 1. Some values may have larger probabilities of occurring than other values. The function is presented in Equation 2.6, where P denotes the probability of not exceeding any real value x (Coles, 2001).

$$F(x) = P(X \leq x) \tag{2.6}$$

The probability of X assuming a value within the interval $[x_1 ; x_2]$ is shown in Equation 2.7 (Holický, 2013).

$$P(x_1 \leq X \leq x_2) \; = \; F(x_2) - F(x_1) \tag{2.7}$$

If the probability distribution function is differentiable, it can be used to find the probability density function, denoted by $f(x)$. The probability density function is equal to the first derivative of the probability distribution function, as expressed in Equation 2.8 (Coles, 2001). The function is always positive and the integral of $f(x)$ for $-\infty < x < \infty$ is equal to 1 (Montgomery and Runger, 2014). The probability distribution function can be written as an integral of the probability density function, as shown in Equation 2.9. The area under the probability density function equals the probability that a realisation x of the random variable X will fall in the considered interval. A histogram describing the relative frequency of intervals in the sample space, can be used to approximate the probability density function if needed (Montgomery and Runger, 2014).

$$f(x) = \frac{dF(x)}{dx} \tag{2.8}$$

$$F(x) = \int_{-\infty}^{x} f(x)\, dx \tag{2.9}$$

The concepts of a population and sample are important to understand. The population is defined as the complete set of possible realisations x of the random variable X, which can be finite or infinite (Holický, 2009). The population is then described by the probability distribution function and probability density function. Population parameters, also called model parameters, are incorporated in the functions and describe the selected probabilistic model.

More frequently the probabilistic model is described by moment parameters, which include the population mean, variance and skewness. The moment parameters are dependent on the selected probabilistic model and its model parameters. The population mean describes the average measurement and it indicates the location of the centre of the probability density function. The population variance indicates the relative dispersion of the population about the mean. The relative dispersion is often represented by the standard deviation, which equals the square root of the variance. Lastly, the population skewness describes the shape of the density distribution function and subsequently the degree of asymmetry of the population (Holický, 2009).

The population mean (μ) is calculated from the first moment about the origin as shown in Equation 2.10. The formulation of the standard deviation (σ) is based on the second central moment, as shown in Equation 2.11. Whereas the population skewness (α) is based on the third central moment and determined with Equation 2.12. The notation in the equations are adopted from the *Reliability analysis for structural design* (Holický, 2009). Another parameter that describes the dispersion of the population about the mean is called the coefficient of variation (COV). It is the ratio of the standard deviation to the mean, expressed as σ / μ.

$$\mu = \int x\, f(x)\, dx \tag{2.10}$$

$$\sigma = \sqrt{\int (x - \mu)^2\, f(x)\, dx} \tag{2.11}$$

$$\propto = \frac{1}{\sigma^3} \int (x - \mu)^3\, f(x)\, dx \tag{2.12}$$

In most cases, only a number of measurements are available to describe the random variable X. The measured data contain a subset of realisations x_i from the population and the subset is called a sample (Holický, 2009). For x_i, $i = 1, 2, 3, \ldots, n$ and n is equal to the sample size. Holický (2009) defines a very small sample as $n \leq 10$ and a large sample as $n \geq 30$. The sample becomes more representative of the population as the sample size increases, enabling the use of the sample to draw inferences regarding the population.

The properties of the sample can be described by sample characteristics, also called moment characteristics. These properties are unbiased point estimates of the moment parameters describing the population. The moment characteristics primarily include the sample mean, variance and skewness. The sample mean (m) is calculated from the first moment about the origin as seen in Equation 2.13. The sample standard deviation (s) and skewness (w) are calculated from Equation 2.14 and 2.15, respectively, which are based on the second and third central moments (Holický, 2009). Additionally, the sample coefficient of variation (COV) is described by the ratio s/m.

$$m = \frac{1}{n}\sum_i x_i \tag{2.13}$$

$$s = \sqrt{\frac{\sum_i (x_i - m)^2}{n-1}} \tag{2.14}$$

$$w = \frac{n}{(n-1)(n-2)s^3}\sum_i (x_i - m)^3 \tag{2.15}$$

This section conveys the concept of probabilistic modelling, which entails describing a random variable with a probabilistic model. There are numerous probabilistic models (or distribution types) available, and the applicable model is dependent on the properties of the random variable. The relevant probabilistic models for the study are discussed in the following sections.

2.3.2 *Description of Probabilistic Models*

2.3.2.1 *Normal Distribution*

This section makes reference to Montgomery and Runger's book on *Applied Statistics and Probability for Engineers* (2014), which provides a comprehensive understanding of the normal (N) distribution. The normal distribution, also called Gaussian distribution, is the most widely used continuous distribution. It plays an important role in the central limit theorem, where the averages from the repetitions of a random experiment represent a random variable, which tends to a normal distribution as the repetitions increase.

The sample space of a normal random variable X has an infinite range $-\infty < x < \infty$. The model parameters include the mean (μ) and standard deviation (σ), where $-\infty < \mu < \infty$ and $\sigma > 0$.

The probability density function can be described by a symmetric bell-shaped curve. As no asymmetry is present for the normal distribution, the skewness is zero and the probability that a measurement is located more than 3σ away from the mean is very small. The probability of an interval tends asymptotically to zero the further away the interval is from the mean. Owing to symmetry, the probability of X being less than or equal to the mean is 0.5 (or 50 %). The probability density function is expressed in Equation 2.16, followed by the probability distribution function in Equation 2.17.

$$f(x) = \frac{1}{\sqrt{2\pi}\sigma} e^{-\frac{1}{2\sigma^2}(x-\mu)^2} \tag{2.16}$$

$$F(x) = \frac{1}{\sqrt{2\pi}\sigma} \int_{-\infty}^{x} e^{-\frac{1}{2\sigma^2}(x-\mu)^2} dx \tag{2.17}$$

The normal random variable X with μ and σ, can be transformed with Equation 2.18 to the standardised random variable U. The standardised variable U has a mean of 0 and a standard deviation of 1. When X represents a normal variable, U is also normally distributed. The probability distribution function of the standardised variable U is given in Equation 2.19, and the solutions are available in standard statistical tables. The tables are useful in finding solutions for the probability distribution function and density function of the normal distribution. Moreover, both Equation 2.18 and 2.19 are applicable for any distribution. Here, the distance between x and μ is equal to $u\sigma$.

$$U = \frac{X - \mu}{\sigma} \tag{2.18}$$

$$F_U(u) = P(U \leq u) \tag{2.19}$$

Figure 2.4 illustrates the probability density function and probability distribution function for a normal distribution, where the model parameters vary. Different mean and standard deviations are considered in order to show the influence of the model parameters on the functions. The notation N(μ,σ) is used to describe the normal distribution. The probability density distribution for N(10,1) in Figure 2.4 is used to convey the definition of the mean (μ) and standard deviation (σ). When the standard deviation decreases, the probability density distribution becomes narrower and the slope of the probability distribution function becomes

steeper, as less variation is seen in the distribution. When the mean increases the functions shift to the right.

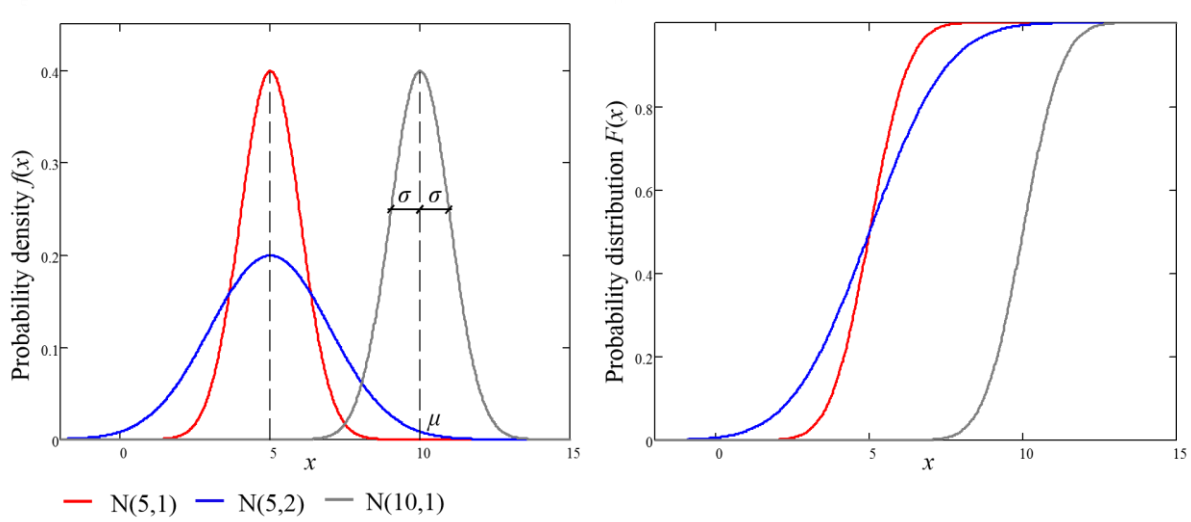

Figure 2.4: Probability density function (left) and probability distribution function (right) for normal distribution, denoted by N(μ,σ).

2.3.2.2 *Lognormal Distribution*

The content of this section is based on Holický (2013), unless stated otherwise. The lognormal distribution is described by the general three-parameter lognormal (LN3) distribution. It is an asymmetric distribution with a lower or upper bound, denoted by x_0. The sample space is limited to the interval $x_0 < x < \infty$, when it has a lower bound and $\infty < x < x_0$, when it has an upper bound. The model parameters for the distribution consist of the mean (μ), standard deviation (σ) and skewness (α). The bound (x_0) can also be used instead of the skewness.

The skewness is a measure of asymmetry, and therefore also describes the tail behaviour of the probabilistic distribution. That is, it provides information on the distribution of the sample data to the left or right of the mean. If the skewness is positive (right skewness), it means that more of the sample data is located on the right side of the mean, also referred to as the right tail. If the skewness is negative (left skewness), it means that more of the sample data is located on the left side of the mean, named the left tail. The larger the skewness, the more sample data is located on the one side. The LN3 distribution can have a left or right tail, where the tail decays faster than a power-type tail, meaning that it asymptotically tends faster to zero (Papalexiou and Koutsoyiannis, 2013).

The lognormal distribution relates to the normal distribution in the following way: If the random variable *X* is lognormally distributed, the transformed variable *Y* (see Equation 2.20) is normally distributed. In Equation 2.20, *ln* is the natural logarithm.

$$Y = ln|X - x_0| \tag{2.20}$$

The bound x_0 can be calculated with Equation 2.21, where *c* is a coefficient relating the bound to the skewness. If the skewness is positive, the distribution has a lower bound and if the skewness is negative, the distribution has an upper bound. When the skewness is equal to zero, the lognormal distribution represents a normal distribution.

$$x_0 = \mu - \frac{\sigma}{c} \tag{2.21}$$

The expression for *c* is provided in Equation 2.22 and the expression for the skewness is provided in Equation 2.23.

$$c = \left[\left(\sqrt{\alpha^2 + 4} + \alpha\right)^{\frac{1}{3}} - \left(\sqrt{\alpha^2 + 4} - \alpha\right)^{\frac{1}{3}}\right] 2^{-\frac{1}{3}} \tag{2.22}$$

$$\alpha = c^3 + 3c \tag{2.23}$$

The LN3 distribution can be derived from the normal distribution by modifying the standardised random variable $u = (x - \mu)/\sigma$. Where *x* is a data point of the sample, and μ and σ are the mean and standard deviation of the LN3 distribution. The modified standardised variable is denoted by *u'* and formulated in Equation 2.24. The sign(α) is equal to +1 when the skewness of the LN3 distribution is positive. When the skewness is negative, the sign(α) is equal to -1.

$$u' = \frac{ln\left(\left|u + \frac{1}{c}\right|\right) + ln\left(|c|\sqrt{1 + c^2}\right)}{\sqrt{ln(1 + c^2)}} sign(\alpha) \tag{2.24}$$

Equation 2.24 can be used to obtain the probability density function $f_{LN,U}(u)$ and probability distribution function $F_{LN,U}(u) = F_{LN,X}(x)$ of the LN3 distribution. The two distributions are shown in Equation 2.25 and 2.26, respectively, where $f_U(u')$ and $F_U(u')$ represent the

probability density function and probability distribution function of the standardised normal variable.

$$f_{LN,U}(u) = \frac{f_U(u')}{\left(\left|u + \frac{1}{c}\right|\right)\sqrt{ln(1+c^2)}} \tag{2.25}$$

$$F_{LN,X}(x) = F_{LN,U}(u) = F_U(u') \tag{2.26}$$

The LN3 distribution can be reduced to a two-parameter distribution, commonly known as the lognormal (LN) distribution. The model parameters only consist of the mean (μ) and standard deviation (σ). Here the bound (x_0) is equal to zero and it always represents a lower bound. Therefore, the LN distribution always has a positive skewness. The coefficient c is equal to the COV, described by the ratio σ/μ. Equation 2.23 can be re-written to express the skewness (α) of the LN distribution in terms of the COV (see Equation 2.27).

$$\alpha = \left(\frac{\sigma}{\mu}\right)^3 + 3\left(\frac{\sigma}{\mu}\right) \tag{2.27}$$

Figure 2.5 illustrates how a change in skewness affects the probability density function of a lognormal distribution. In the figure a two-parameter lognormal distribution is used, described by LN(μ,σ). The lower bound (x_0) is equal to zero and the skewness (α) is positive. When the skewness increases, the area under the probability density function at the right tail becomes larger. That is because a larger portion of the sample data is now situated on the right side of the mean. As the COV increases, the relative dispersion of the sample data about the mean also increases and the curve widens. This leads to the observation that the peak of the probability density function lowers.

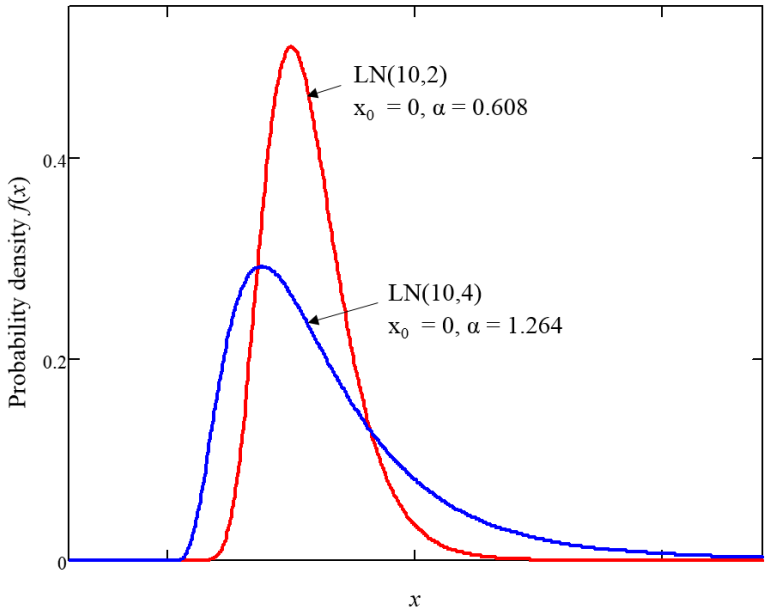

Figure 2.5: Probability density function of lognormal distribution, denoted by LN(μ,σ).

2.3.2.3 *Generalised Extreme Value Distribution*

This section refers to Coles' (2001) description of the generalised extreme value (GEV) distribution, unless stated otherwise. The GEV distribution is an asymmetric distribution representing extreme data. The minimum values or maximum values can be extracted from a sample to form a new data set. The focus of this section is on the GEV distribution for maximum values, as it is applicable to the study. The model parameters include the location (λ), scale (δ) and shape (κ) parameters (Castillo *et al.*, 2005). The location parameter is a measure of the centre values of the sample data, while the scale parameter is a measure of the dispersion of the sample data. The shape parameter is important as it describes the tail behaviour of the distribution, which determines the interval of the sample space. The probability distribution function of the GEV distribution is shown in Equation 2.28.

$$F(x) = e^{-\left[1+\kappa\left(\frac{x-\lambda}{\delta}\right)\right]^{-\frac{1}{\kappa}}} \tag{2.28}$$

The random variable X can take on any value x, as long as the condition in Equation 2.29 is satisfied. The following are true for the parameters: $-\infty < \lambda < \infty$, $\delta > 0$ and $-\infty < \kappa < \infty$.

$$1 + \kappa\frac{(x-\lambda)}{\delta} > 0 \tag{2.29}$$

The GEV distribution combines the extreme limit distributions Gumbel, Fréchet and Weibull into a single distribution. When the shape parameter tends to zero ($\kappa \to 0$), the GEV distribution represents the Gumbel distribution, also called the extreme Type I distribution. The distribution is defined on an infinite interval $-\infty < x < \infty$, where the right tail decays exponentially. That is, the tail tends faster to zero than a power-type tail. Another attribute of the Gumbel distribution is that it has a fixed skewness (α) of 1.14 (Holický, 2009).

When the shape parameter exceeds zero ($\kappa > 0$), the GEV distribution represents the Fréchet distribution, also called the extreme Type II distribution. The Fréchet distribution has a lower bound and is defined on the interval $\lambda - \delta/\kappa \leq x < \infty$. The right tail decays in a polynomial manner, i.e. at a slower rate than the tail of the Gumbel distribution. Furthermore, the skewness (α) is larger than 1.14 (Holický, 2009).

Lastly, when the shape parameter is less than zero ($\kappa < 0$), the GEV distribution represents the Weibull distribution for maxima, also called an extreme Type III distribution. The distribution has a finite upper bound, thus x falls within the interval $-\infty < x \leq \lambda - \delta/\kappa$. The skewness ($\alpha$) is less than 1.14 (Holický, 2009).

Figure 2.6 illustrates the probability density function for the GEV distribution when $\kappa < 0$, $\kappa = 0$ and $\kappa > 0$. The GEV distribution is denoted by GEV(λ, δ, κ).

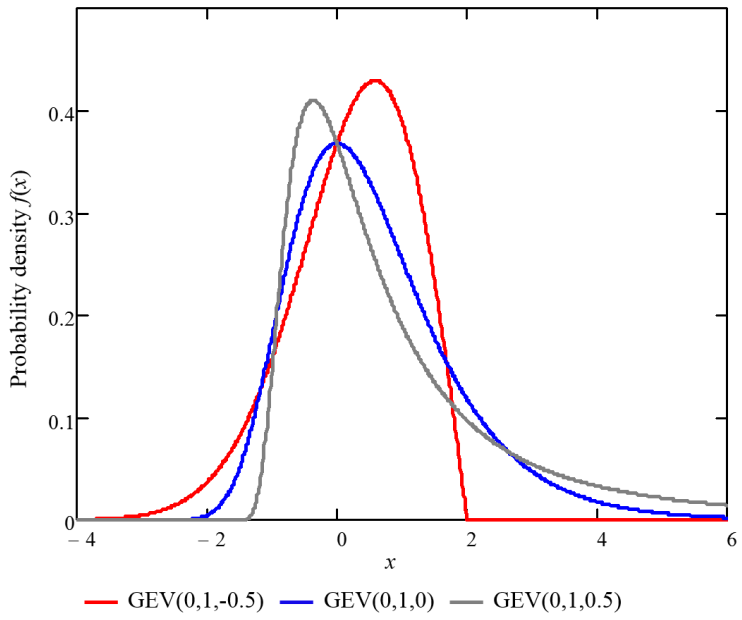

Figure 2.6: Probability density function for the generalised extreme value distribution, denoted by GEV(λ, δ, κ).

The extreme value theorem is similar to the central limit theorem, except extreme data is considered and the extreme limit distributions (Gumbel, Fréchet and Weibull) are of importance. For the theorem to be valid, the extreme data needs to be independent and identically distributed (iid). Variables are considered independent when the one variable do not affect the other variables. The variables are identically distributed when all the variables have the same probability distribution function. Extreme values representing maximum values can be extracted from a random experiment. The data set of extreme values increases as the number of repetitions of the random experiment increases. As the sample size of extreme values tends to infinity, the distribution will tend to one of the extreme limit distributions, which represents the distribution's maximum domain of attraction. For instance, the normal and lognormal distributions tend to a Gumbel distribution (Castillo *et al.*, 2005). Another characteristic of the GEV distribution is that it is max-stable, which means that a GEV distribution will remain a GEV distribution as the sample size tends to infinity.

2.4 Assessment of Extreme Traffic Load Effects

2.4.1 *Weigh-In-Motion Data and Traffic Load Effects*

Extreme traffic load effects are obtained from critical loading events on the bridge. It is important to adequately characterise extreme traffic load effects as they are used in evaluating the reliability performance of a bridge design code and also in deriving new traffic load models.

Free flowing traffic governs the critical loading events for short to medium span bridges, i.e. spans less than or equal to 50 metres (Bruls *et al.*, 1996; Caprani and O'Brien, 2009). Generally, critical loading events for short to medium span bridges can be caused by a single heavy truck or by the simultaneous occurrence of two or three trucks (Enright and O'Brien, 2013). These events can include trucks following each other, side-by-side or staggered in two traffic lanes (Ghosn, Sivakumar and Moses, 2011). For shorter spans, e.g. 5 to 10 metres, the critical loading event can be governed by a single axle or a group of axles (Anderson, 2006; Žnidarič *et al.*, 2015).

The advancement of WIM technologies has allowed for the extensive collection of good quality traffic data. There are various applications of WIM data, which include pavement management and planning, monitoring and prosecution of overloading, developing new bridge load models, site-specific bridge assessment and evaluating existing load models (Enright, Caprani and O'Brien, 2011; Lenner, De Wet and Viljoen, 2017). The focus of this study is on the latter,

where the reliability performance of TMH-7 for normal traffic conditions is considered. Thus, the focus of the literature review is on the derivation of traffic load effects from the WIM data to characterise the heavy traffic characteristics on a bridge.

WIM systems are widely used in South Africa with the primary focus of measuring static axle loads of moving vehicles. The WIM data goes through a review process where the data is scrubbed of measurements not satisfying the quality control checks and WIM errors are filtered out (Ghosn, Sivakumar and Moses, 2011). A locally developed post-calibration method called the Truck Tractor (TT) method provides a series of data quality checks applied to the data after it has been collected (De Wet, 2010b, 2010a). The method has been approved by the South African National Road Authority (SANRAL) and is incorporated in the new Technical Methods for Highways 8 (TMH-8), a document on traffic and axle load monitoring methodologies and procedures (COTO, 2014). Furthermore, specifications for the provision of traffic and WIM monitoring services are provided in TMH-3 (COTO, 2013).

Literature confirms that the quality of WIM data in South Africa is of an internationally acceptable standard after it is cleaned and calibrated (De Wet, 2010a; Lenner, De Wet and Viljoen, 2017). The majority of WIM sensors in the country consist of a bending plate embedded in the road surface, often only in the left wheel path of the traffic lane (De Wet, 2010a; Lenner, De Wet and Viljoen, 2017). The WIM measurements typically include the date, time of arrival, number of axles, axle weights and axle spacings.

In the past, traffic load effects were often derived from simplified methods based on single vehicle events (Nowak, 1994; Nowak and Rakoczy, 2013). However, literature shows that maximum load effects can be governed by multiple truck events and thus a moving load analysis that accounts for such events is deemed more appropriate (Žnidarič *et al.*, 2015). The analysis entails arranging the measured vehicles in each traffic lane into a convoy with appropriate gaps, and moving the convoy over the bridge (Žnidarič *et al.*, 2015). As the convoy moves over the bridge it runs through the applicable influence line. The traffic load effect is then obtained by the superposition of the response of each vehicle in the convoy. As a result, traffic load effects are obtained that account for both single and multiple truck events.

2.4.2 *Statistical Approaches in Assessing Extreme Traffic Load Effects*

From literature it is evident that the main purpose for determining the traffic load effects, is one of two options. It is either to find the characteristic load effect corresponding to a certain

probability of exceedance and reference period, or to obtain the maximum load effect distribution for a certain reference period and determine the corresponding fractile for the characteristic load effect. Two methods are alternately used in literature to estimate maximum load effects for a specified reference period, i.e. either statistical extrapolation or a Monte Carlo simulation.

2.4.2.1 *Statistical Extrapolation Approach*

For the statistical extrapolation approach, a probabilistic distribution is fitted either to the whole set of measured traffic load effects, or only to the upper part or a set of periodic maxima. This mostly comprises using a probability plot where a distribution is fitted to the data and extrapolated graphically to obtain the characteristic load effect corresponding to a certain reference period. Or, a distribution is fitted to the load effects and raised to an appropriate power to obtain the maximum load effect distribution for the reference period of interest. A great variety of methods have been used in literature to conduct a statistical extrapolation. Literature reveals that the method applied varies according to the location of the WIM station, the number of heavy vehicles recorded in the data set and the method of traffic data collection (Doan, Sparling and Feldman, 2016).

Right Tail Fitting

Right tail fitting entails the fitting of a distribution to the upper part of the measured traffic load effects. This approach eliminates less critical load effects and reduces the number of different types of loading events considered (O'Brien *et al.*, 2015). In this way, an improved representation of the extreme load effects is provided. Furthermore, it is said that the tail region of the traffic load effects can be well-represented by a single distribution, which may not necessarily be true for the whole data set (O'Brien *et al.*, 2015).

Different assumptions have been made in defining the right tail of the traffic load effects, and it is greatly dependent on engineering judgement. Castillo (1988) recommends using the upper $2\sqrt{n}$ of the traffic load effects, where n is the number of load effects in the whole data set. Enright (2010) specifies the right tail region as the upper 30 % of the data set, while Sivakumar *et al.* (2011) fit a normal distribution to the upper 5 % of the traffic load effects. The right tail region can also be chosen visually at the point where there is a change in slope on the

probability plot paper (Nowak and Rakoczy, 2013; Žnidarič *et al.*, 2015). A few prominent right tail fitting techniques are listed below.

a) Normal Probability Plot

A popular approach in literature has been to plot the traffic load effects on a normal probability plot that is based on an inverse cumulative distribution function of a standard normal variable (Doan, Sparling and Feldman, 2016). A normal distribution is then fitted to the whole plot (Nowak, 1999) or only to the right tail (or upper part) of the plot, which is then statistically extrapolated. Some authors have fitted a straight line (Nowak, 1989; Nowak and Hong, 1991) or a curved line (Nowak, 1993, 1994) to the right tail of the plot.

Doan *et al.* (2016) conducted a study to test the method of fitting a distribution to the right tail of the traffic load effects plotted on a normal probability plot. The study found that the distribution best describing the right tail varied from site to site which prevented the selection of a single distribution that best fits the critical load effects for all WIM sites. For example, the study found that the lognormal distribution best described the critical load effects at one site, while the normal distribution best described the critical load effects at another site (Doan, Sparling and Feldman, 2016).

b) Block Maxima Approach

The block maxima method is a well-known right tail fitting technique, where the maximum load effects are extracted from equal-size, non-overlapping time periods called block periods. For instance, the daily maximum load effects can be obtained by extracting the maximum load effect per day. Here the block period would then be represented by a day. A distribution is then fitted to the block maximum load effects and extrapolated to obtain maximum load effects for another reference period. Žnidarič *et al.* (2015) explains the use of probability plot paper for the visual interpretation of the block maxima. A distribution can then be fitted to the whole data set of block maxima or only to the right tail of the block maxima on the probability plot. The decision is based on whether the block size is able to adequately represent the extreme load effects or not.

The block maxima method allows for time-referencing the load effects and provides a more representative data set of the critical load effects, i.e. extreme load effects (O'Brien *et al.*,

2015). The selection of the block period is usually restricted by the duration of the recorded period (Žnidarič *et al.*, 2015). Furthermore, if the block period is chosen too small, the data set will include less critical load effects that can influence the extrapolated results (Hajializadeh *et al.*, 2012). If the block period is too large, the data set may be too small, and it may neglect valuable data points also describing the critical load effects (O'Brien *et al.*, 2015).

Previous studies have considered a variety of applications for the block maxima method. Ghosn and Moses (1985) fit a normal distribution to the maximum load effects for a block period of 2.4 hours, which is then raised to an appropriate power to obtain the maximum load effect distribution for a 50-year reference period. Cooper (1995, 1997) raises the distribution of the measured load effects to an appropriate power to obtain the 4.5-day block maxima. Hwang *et al.* (2014) fit a lognormal distribution to the maximum load effects. The GEV distribution is more common at present, as it is theoretically more appropriate in describing extreme load effects (Žnidarič *et al.*, 2015).

The GEV family of distributions consist of the Gumbel (type I), Fréchet (type II) and Weibull (type III) distribution, depending on the right tail behaviour (Coles, 2001). In using the GEV distribution, the choice between the three limit distributions are avoided. Getachew and O'Brien (2007) fit a GEV distribution to the daily maxima, similarly Hajializadeh *et al.* (2012) fit the GEV distribution to the daily and annual maxima, and compare it to other distributions such as the lognormal, log-gamma and log-logistic distribution.

The GEV distribution is usually constrained to the Weibull and Gumbel distributions (O'Brien, Connor and Arrigan, 2012) in representing maximum traffic load effects. The Fréchet distribution has a very long, power-type right tail (Papalexiou and Koutsoyiannis, 2013), which does not agree with the physical bounds of traffic loading (O'Brien *et al.*, 2015). In addition, it leads to unrealistically large extrapolated values. Sivakumar *et al.* (2011) fit a Gumbel distribution to the right tail of weekly maxima, and raises the distribution with a power to obtain the maximum load effect distribution. Buckland *et al.* (1980) fit a Gumbel distribution to a block period of three months. The Weibull distribution has also been used in numerous studies (Enright, 2010; O'Brien, Connor and Arrigan, 2012). It has an upper bound which limits the extrapolated maximum load effects obtainable.

c) Peak Over Threshold Approach

The Peak over Threshold (POT) approach can be used as an alternative to the block maxima approach. This method considers the load effects above a certain threshold value and fits a Generalised Pareto distribution to the data set. One disadvantage to the method, is that the threshold value is selected based on engineering judgement and could lead to a misrepresentation of the right tail (O'Brien *et al.*, 2015).

d) Rice Formula

Another approach favoured in some studies, is the Rice formula. The Rice formula is applied to the upper part or right tail of an outcrossing rate histogram (Cremona, 2001). Therefore, a proper threshold value should be chosen to define the right tail region. Furthermore, a normally distributed process is used to describe the time variations of traffic load effects on bridges (Cremona, 2001). The Rice formula has for instance been used in the background studies of the Eurocodes.

Concluding Remarks on Statistical Extrapolation

O'Brien *et al.* (2015) conducted a study to investigate the accuracy of seven statistical inference methods used in literature for the extrapolation of traffic load effects. The extrapolated maximum load effects for each method were compared to long-run simulations to assess the accuracy of the method. It was found that the GEV and POT approaches generally obtained accurate extrapolated maximum load effects. Even though the normal distribution and Rice formula lack statistical foundation for dealing with extreme data, it was found that they also performed well. The study concludes that the extrapolated results are more sensitive to the sample size and assumptions regarding the right tail, than to the statistical inference method chosen (O'Brien *et al.*, 2015).

From literature it is evident that the extrapolation process can involve considerable uncertainty, as it is influenced by the distribution type, the sample size available and the power with which the distribution is raised (Hajializadeh *et al.*, 2012; Doan, Sparling and Feldman, 2016). It is thus important to choose the distribution type that best fits the site-specific data, and that the measuring period is large enough to provide a reliable characterisation of the right tail of the traffic load effects.

If the measuring period is too small, it may exclude critical loading events caused by extremely heavy vehicle combinations. This is a concern for many countries, where the measuring periods are quite short and only stretch over a few months and maximum a year (Doan, Sparling and Feldman, 2016). In some countries, the recorded data is even limited to a few days or weeks due to the cost of data collection (Hajializadeh *et al.*, 2012). Sivakumar *et al.* (2011) suggest that a period of a year is sufficient to develop a traffic load model.

2.4.2.2 *Monte Carlo Simulation*

Monte Carlo simulation uses random sampling from a set of measured data to generate a large number of random values, consistent with the main trend in the measured data (Ghosn, Sivakumar and Moses, 2011). The parameters describing the traffic are fitted with statistical distributions in order to simulate new traffic data. These parameters are obtained from the WIM data and include characteristics such as the gross-vehicle weight (GVW), axle load and spacing, truck speed and daily truck volumes for each lane (Hajializadeh *et al.*, 2012).

Literature varies in the application of the Monte Carlo simulation. Traffic load effects can be simulated for a short period of time (typically a few years) and then fitted with a distribution to extrapolate and obtain maximum load effects for a certain reference period. For instance, Caprani *et al.* (2008) provide up to 5 years of traffic load effects and extrapolate with a fitted GEV distribution. Zhou *et al.* (2013) provide 2000 days of simulated traffic load effects, which are then fitted with a GEV distribution and extrapolated to obtain the maximum load effect distribution. Caprani and O'Brien (2009) simulate a set of a 1000 daily maxima.

A more recent application of the Monte Carlo simulation approach is to conduct a long-run simulation. For a long-run simulation, traffic is generated for thousands of years, which allows for the direct determinisation of the maximum load effects for the lifetime or other reference period (Enright, Caprani and O'Brien, 2011; Enright and O'Brien, 2013). For instance, Hajializadeh *et al.* (2012) make use of a simulation period of 5000 years.

The main advantage to the Monte Carlo approach, is that the simulation can address axial configurations and multiple truck events that were not necessarily present in the measuring period (Žnidarič *et al.*, 2015). In addition to this, the simulation approach improves the representation of the extreme load effects, especially when the data set is very small. However, there are some concerns that need to be acknowledged. If the measuring period is too small to adequately represent the traffic load effects, it will influence the quality of the simulated traffic.

As the simulation is based on the collected data, the simulated traffic load effects for larger periods may become unreliable (Ghosn, Sivakumar and Moses, 2011). If the generation period is large, the simulation may become too computationally intensive, and a simpler approach may be more favourable to use. In such a case, a short simulation period followed by statistical extrapolation may be more viable.

2.5 Structural Reliability

This section describes basic concepts of structural reliability theory, which include the definition of reliability and different safety measures. Thereafter, the fundamental and general reliability problems are discussed, which include the formulation of the limit state function and the determination of the reliability index and probability of failure. The First Order Reliability Method (FORM) is outlined, followed by a brief description of the semi-probabilistic design method. Lastly, different target reliability indices from existing design codes are summarised.

2.5.1 *Reliability Concepts*

The response of a structure is dependent on its resistance and the magnitude of the applied load. The structural response is then considered adequate if the performance requirements (or reliability conditions) for the structure are met. ISO 2394 (2015) provides a formal definition of reliability: it is the ability of a structure to satisfy given requirements under specified conditions during its intended design life. These requirements are called limit states. For instance, the requirements can be associated with the structural safety, where collapse or a form of structural failure is prevented. This is called the ultimate limit state (ULS). It can also refer to conditions of normal use, such as limiting deflections and cracks. This is called the serviceability limit state (SLS).

Structural reliability or safety is concerned with the violation of the performance requirements. If the considered limit state is violated, the structure is in an undesirable state (Holický, 2009). A safe or desirable state is assumed when the limit state is satisfied. There are different measures of structural reliability. According to the Joint Committee on Structural Safety (JCSS), these measures can be described by safety levels according to whether the method is deterministic, semi-probabilistic or probabilistic.

The safety levels are described as follows:

- *Level 0* is a deterministic method, where a global safety factor (γ) is specified in the code. For the structure to be deemed safe, the ratio between the resistance (R) and load (E) should be equal to or more than the prescribed safety factor. The shortcoming of this method is that it does not properly account for uncertainties related to the resistance and load of the structure (Skrzypczak, Słowik and Buda-Ożóg, 2017).
- *Level 1* is a semi-probabilistic method based on the limit state principle. Predefined characteristic values are used to describe the resistance (R) and load effect (E). Thus, no distribution functions are used. A partial safety factor is then assigned to each parameter, denoted by γ_R and γ_E, which typically exceeds a value of 1. The structure is deemed safe when the inequality, $R/\gamma_R \geq \gamma_E E$, is satisfied. Although this is still a simplified method, it is an improvement to Level 0 in accounting for uncertainties.
- *Level 2* makes use of probabilistic approximation methods, e.g. FORM or Second Order Reliability method (SORM). Probability distributions are assigned to the resistance (R) and load (E) parameters, where the parameters are described in terms of their mean and standard deviation. E and R are now referred to as basic variables. Generally, the variables are correlated and non-normal, which are then transformed by the method into uncorrelated and standardised normal variables. The transformed variables are used to determine a reliability index (β) which serves as measure of the reliability or safety level of the structure. The structure is deemed safe when the obtained reliability index is equal to or more than the required target reliability index (β_t). In practice, design codes commonly apply Level 1, where the partial factors have been calibrated with Level 2 methods to satisfy a target reliability index.
- *Level 3* employs the full probabilistic method and calculates the probability of failure (p_f), i.e. the probability of not satisfying the limit state. Typical methods include numerical integration and Monte Carlo simulation. The calculated probability of failure should be less than or equal to the permissible probability of failure. Level 2 and Level 3 explicitly make provision for the uncertainties of the relevant parameters.
- *Level 4* uses the total expected cost of the structure to formulate an optimisation criterion (Van Gelder, Proske and Vrijling, 2009). It considers the benefits and costs related to construction, maintenance and repairs, consequences of failure and interests of capital (Madsen, Krenk and Lind, 2006). The design is acceptable when it maximises the difference between the benefits and costs linked to the structure.

2.5.2 *The Fundamental Reliability Problem*

In its simplest form, the reliability of a structure can be defined by the inequality $R > E$, where R is the resistance and E is the load effect (Thoft-Christensen and Nowak, 1997). The inequality can be re-written as $R \leq E$ to define the failure mode. The limit state function, also called the reliability margin, is denoted by Z and formulated in Equation 2.30.

$$Z = R - E \tag{2.30}$$

The limit state $Z = 0$ represents the boundary between the safe and unsafe domain. The probability of failure (p_f) can be expressed as the probability that R is exceeded by E. Thus, when $Z > 0$ the structure is safe and when $Z \leq 0$, structural failure occurs (Holický, 2009). Equation 2.31 provides an expression for p_f.

$$p_f = P(R - E \leq 0) \tag{2.31}$$

When R and E are random variables, they can be described by probability distributions, where $F_R(x)$ and $F_E(x)$ denote the probability distribution functions and $f_R(x)$ and $f_E(x)$ denote the probability density functions. The variable X, with realisations x, is used to express both R and E.

Structural reliability can be explained by the special case where the two random variables, R and E, are assumed to be normally distributed. The variable Z will then also have a normal distribution with a mean (μ_Z) and standard deviation (σ_Z) described by Equation 2.32 and 2.33 (Holický, 2009). Here ρ_{RE} denotes the correlation coefficient between R and E, which is equal to zero if R and E are mutually independent variables (Holický, 2009).

$$\mu_Z = \mu_R - \mu_E \tag{2.32}$$

$$\sigma_z = \sqrt{\sigma_R^2 + \sigma_E^2 + 2\rho_{RE}\sigma_R^2\sigma_E^2} \tag{2.33}$$

According to Equation 2.31, p_f is defined as $P(Z \leq 0)$. The expression can now be re-written in terms of the probability distribution function of Z, denoted by $F_Z(z)$ (see Equation 2.34).

$$p_f = P(Z \leq 0) = F_Z(0) \tag{2.34}$$

Usually $F_Z(z)$ can be obtained by transforming the random variable Z into the standardised random variable U (see Section 2.3.2.1). Equation 2.35 calculates the standardised value u_0, which corresponds to $z = 0$.

$$u_0 = \frac{(0 - \mu_Z)}{\sigma_Z} = -\frac{\mu_Z}{\sigma_Z} \tag{2.35}$$

In Equation 2.36 the probability of failure p_f is now expressed in terms of the standardised random variable U.

$$p_f = P(Z \leq 0) = F_Z(0) = F_U(u_0) \tag{2.36}$$

Figure 2.7 illustrates the probability density function of the reliability margin Z, denoted by $f_Z(z)$ (Holický, 2009). The shaded area under the curve is equivalent to the probability of failure p_f. Equation 2.35 can be re-written as $\mu_Z = -u_0 \sigma_Z$.

With Z being normally distributed, the reliability index, denoted by β, is equal to $-u_0$ and can be expressed by the relationship in Equation 2.37, derived from Equation 2.32, 2.33 and 2.35 (Holický, 2009). The variables R and E are typically assumed independent with $\rho_{RE} = 0$. Thus, β is the distance between μ_Z and the origin ($z = 0$), measured in units of σ_Z. This means that the value of the reliability index indicates the number of standard deviations needed to reach the mean from the origin. The higher the β-value, the higher the reliability level for the given limit state function.

$$\beta = \frac{\mu_Z}{\sigma_Z} = \frac{\mu_R - \mu_E}{\sqrt{\sigma_R^2 + \sigma_E^2 + 2\rho_{RE}\sigma_R^2\sigma_E^2}} \tag{2.37}$$

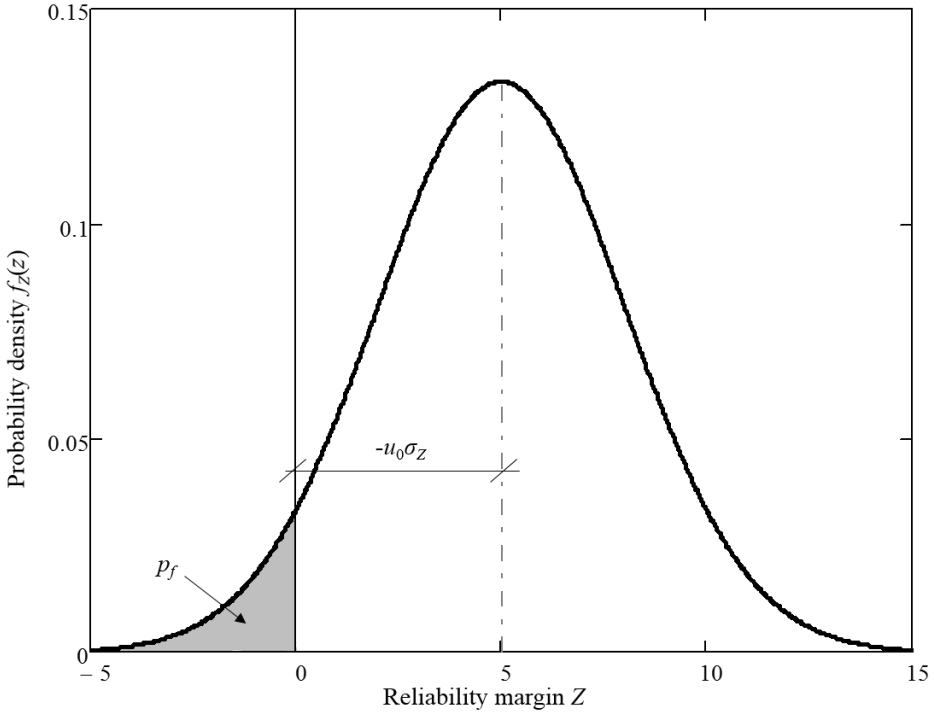

Figure 2.7: Probability density function of reliability margin Z (Holický, 2009).

The reliability index β relates to the probability of failure p_f of the structure. When p_f decreases, β increases. The relation is shown in Equation 2.38, where F_U denotes the probability distribution function of a standardised normal distribution. The relation is valid for all distribution types, and thus not only for the normal distribution.

$$p_f = F_U(-\beta) \tag{2.38}$$

As the numerical value of β is more comprehensive, it is often used instead of p_f to measure the reliability level of the structure (Holický, 2009). It is important to know that the parameters β and p_f are notional values used primarily in the development of consistent design rules. These parameters are not necessarily representative of the actual failure rate of the structure, which is highly dependent on human error (Holický, 2009).

When considering a more general case where the two variables R and E are not normally distributed, the reliability margin Z is also non-normal. The probability of failure is then expressed as the simultaneous occurrence of event A and event B. Where event A is equal to $P(x < E < x + dx)$ and event B is equal to $P(R < x)$. Figure 2.8 illustrates the probability density functions for R and E and defines the terms x and dx.

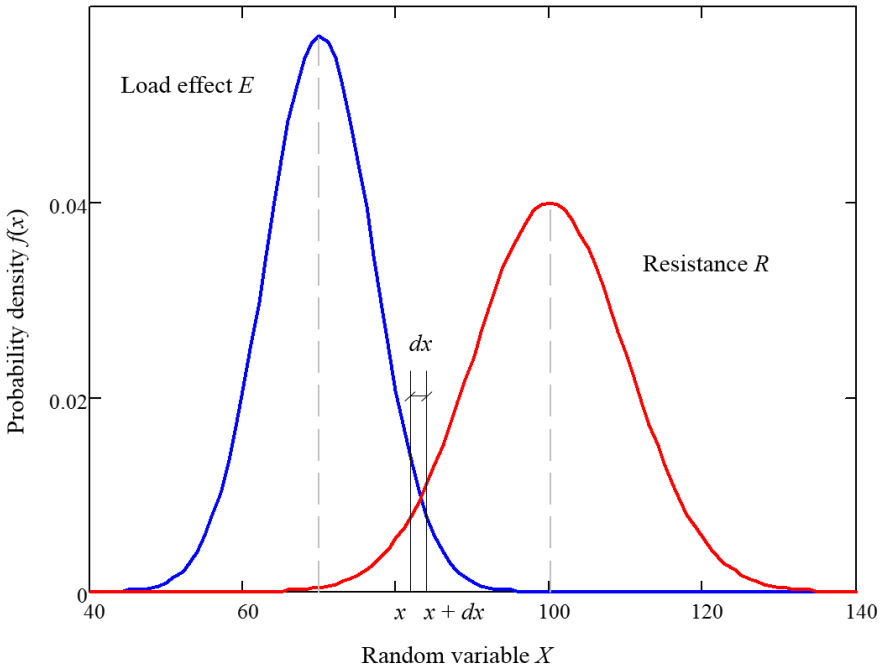

Figure 2.8: Probability distribution functions for load effect *E* and resistance *R* (Holický, 2009).

The variables *R* and *E* are assumed mutually independent, which produce the expression in Equation 2.39 for p_f (Thoft-Christensen and Nowak, 1997). An important remark is that the results are greatly influenced by the chosen distribution types for *R* and *E*.

$$p_f = \int_{-\infty}^{\infty} F_R(x) f_E(x)\, dx \tag{2.39}$$

2.5.3 *The General Reliability Problem*

Often the limit state function *Z* is non-linear and consists of more than two random variables. This means that the resistance *R* and load effect *E* are functions of random variables. The resistance can include random variables describing material and geometric properties, whereas the load effect can include applied loads and in some cases also material and geometric properties (Lee, 2011). The limit state function *Z* is then a function of the vector of random variables $\boldsymbol{X} = \{X_1, X_2, \ldots, X_n\}$, where *n* is the number of random variables. Their realisations are given by the vector $\boldsymbol{x} = \{x_1, x_2, \ldots, x_n\}$. Equation 2.40 formulates the limit state function *Z* for the multivariate case.

$$Z(X_1, X_2, \dots, X_n) = Z(\boldsymbol{X}) \tag{2.40}$$

The limit state $Z(\boldsymbol{X}) = 0$ represents the boundary between the safe and unsafe domain. The probability of failure p_f is then given by Equation 2.41, where $f(\boldsymbol{X})$ is the joint probability density function of all the random variables considered in the vector $\boldsymbol{X}$ (Holický, 2009). In addition, the reliability index β can also be found using Equation 2.38.

$$p_f = P(Z(\boldsymbol{X}) \leq 0) = \int_{Z(\boldsymbol{X}) \leq 0} f(\boldsymbol{X})\, d\boldsymbol{X} \tag{2.41}$$

Reliability is the probability that the random variables $\boldsymbol{X}$ are in the safe region, defined by $Z(\boldsymbol{X}) > 0$. Equation 2.41 can be used to describe the reliability in terms of p_f. Subsequently, the reliability is expressed in Equation 2.42 as $(1 - p_f)$.

$$1 - p_f = P(Z(\boldsymbol{X}) > 0) = \int_{Z(\boldsymbol{X}) > 0} f(\boldsymbol{X})\, d\boldsymbol{X} \tag{2.42}$$

The integral in Equation 2.41 may be difficult to solve and usually requires numerical simulation methods, e.g. Monte Carlo simulation. A major disadvantage of this method is the high computational cost (Manoj, 2016). As a result, approximation methods such as FORM are the most popular procedures to compute the probability of failure. In comparison to simulation methods, FORM is computationally more efficient as it only needs a small number of iterations for convergence (Manoj, 2016). This is especially the case for low probabilities of failure. The following section outlines the FORM-analysis.

2.5.4 *First Order Reliability Method*

FORM is a simple and efficient approximation method to perform a reliability analysis and to obtain a reliability index for the structure. Most of the commercially available software products include the FORM-analysis, and thus it can easily be implemented. FORM is able to consider non-linear limit state functions with correlated non-normal variables, and reduce it to a simple normally distributed variable problem (Du, 2005).

Consider the multivariate case where the random variables are represented by the vector $\boldsymbol{X} = \{X_1, X_2, \dots, X_n\}$, and the limit state function is expressed as $Z(\boldsymbol{X})$. As a first step, FORM

transforms the basic variables into mutually independent, standardised normal variables that are represented by the vector ***U*** (Du, 2005).

Figure 2.9 provides a two-dimensional graph of the joint probability density function for the resistance variable (*R*) and load effect variable (*E*). The density contours correspond to different levels of the probability density. The transformation of the original variables (*R* and *E*) from the *X*-space to the *U*-space, i.e. the standardised space, is shown in Figure 2.9. The transformed variables are denoted by U_R and U_E, respectively.

Two conditions needs to be satisfied to transform the original basic variables into their equivalent normal variables at a given point ***x**** (Holický, 2009). The first condition states that the probability distribution functions for the basic variables should stay the same before and after the transformation. This is called the Rosenblatt transformation and it is shown in Equation 2.43. The variables μ_X^e and σ_X^e denote the mean and standard deviation of the transformed normal variables.

$$F_X(x^*) = F_U\left(\frac{x^* - \mu_X^e}{\sigma_X^e}\right) \tag{2.43}$$

The second condition requires that the probability density functions of the original basic variables must be equivalent to the transformed normal variables' probability density functions (see Equation 2.44) (Holický, 2009).

$$f_X(x^*) = \frac{1}{\sigma_X^e} f_U\left(\frac{x^* - \mu_X^e}{\sigma_X^e}\right) \tag{2.44}$$

The mean and standard deviation of the equivalent normal distribution can be calculated with Equation 2.45 and 2.46, in accordance with the two conditions.

$$\mu_X^e = x^* - \sigma_X^e\left[F_U^{-1}\left(F_X(x^*)\right)\right] \tag{2.45}$$

$$\sigma_X^e = \frac{1}{f_X(x^*)} f_U\left[\frac{x^* - \mu_X^e}{\sigma_X^e}\right] = \frac{1}{f_X(x^*)} f_U\left[F_U^{-1}\left(F_X(x^*)\right)\right] \tag{2.46}$$

According to Holický (2009), the main steps of the FORM-analysis can be summarised as follows. The basic variables are transformed into standardised normal variables. Subsequently, also the limit state function $Z(\boldsymbol{X}) = 0$ is transformed into $Z'(\boldsymbol{U}) = 0$ in the *U*-space. The limit

state function is generally non-linear, and FORM approximates the limit state function using the first order Taylor expansion. This means that a tangent is fitted to the limit state function at the design point. The design point is the point on the limit state function $Z'(\boldsymbol{U}) = 0$ closest to the origin, and it is found by an iteration process. The reliability index β is then determined as the shortest distance from the design point to the origin in the *U*-space. Finally, the probability of failure is obtained from $p_f = F_U(-\beta)$, where F_U denotes the probability distribution function of a standardised normal distribution. Figure 2.9 includes the non-linear limit state function, the tangent at the design point, and the reliability index in the *U*-space (Holický, 2009).

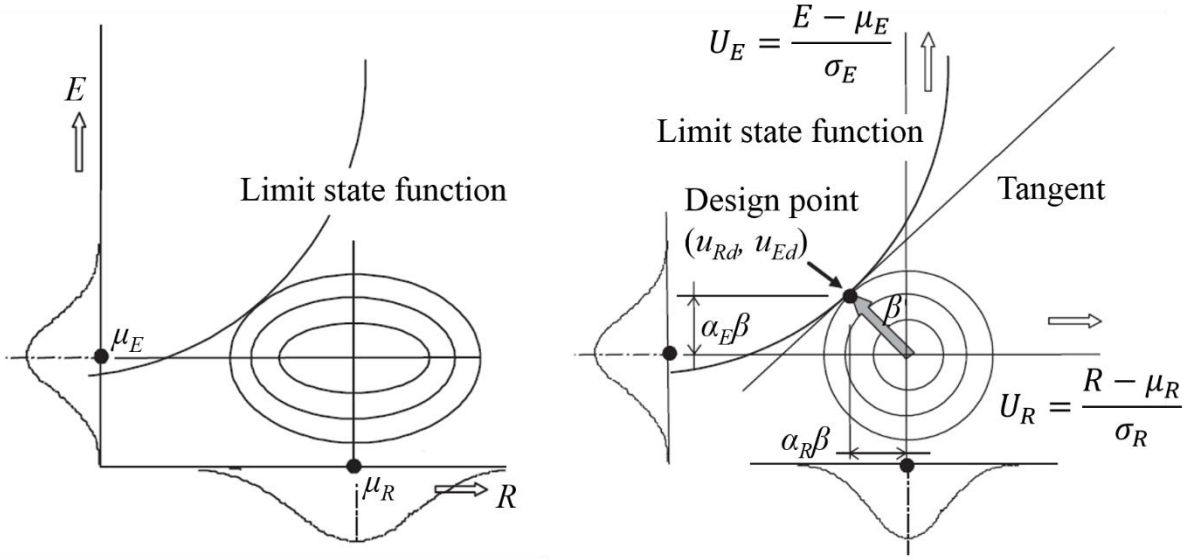

Figure 2.9: First Order Reliability Method. a) Original basic variables *R* and *E*. b) Transformed variables U_R and U_E (Holický, 2009).

The FORM-analysis uses an iteration process to find the design point and to solve the reliability problem. According to Holický (2009), the iteration process can be summarised by the following ten steps:

1. The performance requirement is specified and the corresponding limit state function $Z(\boldsymbol{X}) = 0$ is formulated. Probabilistic models are selected to describe the relevant basic variable in the vector $\boldsymbol{X} = \{X_1, X_2, \ldots, X_n\}$.
2. Initial values are assumed for the design point $\boldsymbol{x^*} = \{x_1^*, x_2^*, \ldots, x_n^*\}$. For example, the mean can be used for the basic variables (n-1) and the last basic variable can be determined from the limit state function $Z(x^*) = 0$.
3. The equivalent normal distributions of the original basic variables can be obtained at the point $\boldsymbol{x^*} = \{x_1^*, x_2^*, \ldots, x_n^*\}$, using Equation 2.45 and 2.46.

4. The original design point $\boldsymbol{x^*} = \{x_1^*, x_2^*, \ldots, x_n^*\}$ is transformed with Equation 2.47, to find the standardised design point $\boldsymbol{u^*} = \{u_1^*, u_2^*, \ldots, u_n^*\}$ for the standardised random variables $\boldsymbol{U} = \{U_1, U_2, \ldots, U_n\}$. Here $i = 1, 2, ..., n$, where n is the number of basic variables.

$$u_i^* = \frac{x_i^* - \mu_{Xi}^e}{\sigma_{X_i}^e} \tag{2.47}$$

5. Partial derivatives of the limit state function with respect to the standardised random variables $\boldsymbol{U} = \{U_1, U_2, \ldots, U_n\}$ are assessed at the design point. The partial derivatives can be represented by the vector $\boldsymbol{D} = \{D_1, D_2, ..., D_n\}$, where D_i is expressed in Equation 2.48.

$$D_i = \frac{\partial Z}{\partial U_i} = \frac{\partial Z}{\partial X_i}\frac{\partial X_i}{U_i} = \frac{\partial Z}{\partial X_i}\sigma_{X_i}^e \tag{2.48}$$

6. The vector $\boldsymbol{D} = \{D_1, D_2, ..., D_n\}$ together with the standardised design point $\boldsymbol{u^*} = \{u_1^*, u_2^*, \ldots, u_n^*\}$, are used to estimate the reliability index β (see Equation 2.49). The reliability index can be compared to a target reliability index, to measure the performance of the structure.

$$\beta = -\frac{\{D\}^T\{u^*\}}{\sqrt{\{D\}^T\{D\}}} \tag{2.49}$$

7. The directional vector $\boldsymbol{\alpha} = \{\alpha_1, \alpha_2, ..., \alpha_n\}$ from the origin to the design point, is formulated in Equation 2.50. The vector consists of sensitivity factors that describe the influence of each basic variable on the reliability index. The sensitivity factor is denoted by α to be consistent with literature. However, the same notation is used for the skewness of a probability distribution. One should not confuse the two terms with each other, as they do not have the same meaning.

$$\{a\} = \frac{\{D\}}{\sqrt{\{D\}^T\{D\}}} \tag{2.50}$$

8. A new design point is calculated with Equation 2.51 and 2.52 for n-1 standardised and original basic variables.

$$u_i^* = \alpha_i \beta \tag{2.51}$$

$$x_i^* = \mu_{X_i}^e - u_i^* \sigma_{X_i}^e \tag{2.52}$$

9. The design point of the *n*-th basic variable is determined from the limit state function $Z(\boldsymbol{x}^*) = 0$.
10. For the iteration process, steps 3 to 9 are repeated until the reliability index β and the design point $\boldsymbol{x}^*$ reach the desired degree of accuracy.

2.5.5 *Semi-Probabilistic Design Concept*

Various simplifications are made in order to practically apply reliability concepts in operational design codes. The semi-probabilistic method, also called the design value method, serves as an important step between probabilistic design methods and the partial factor method (Holický *et al.*, 2015).

The design value method is based on the fundamental principle that the codified design load effect (e_d) should not exceed the codified design resistance (r_d). The design values are deterministic, and the structure is deemed reliable when the condition in Equation 2.53 is satisfied. Generally, the design load effect should account for the design values of loads, geometric properties and model uncertainties. The design resistance should consider the design values of material properties, geometric properties and model uncertainties. Model uncertainty is a significant variable, as it accounts for the uncertainty associated with idealising or approximating the physical behaviour of a structure with a mathematical model (Faber, 2009).

$$e_d < r_d \tag{2.53}$$

In design, the overall reliability level, described by the reliability index β, can be split into the resistance part and load effect part (CEN, 2002). The resistance part is described by the resistance index $\beta_R = \alpha_R \beta$, where α_R is the sensitivity factor from FORM. Similarly, the load effect index is given as $\beta_E = \alpha_E \beta$, where α_E is the FORM sensitivity factor for the load effect variable. The expressions for β_R and β_E are derived from Equation 2.51 in the FORM-analysis.

The design values, r_d and e_d, can be obtained from Equation 2.54 and 2.55, where $F_U(u)$ denotes the probability distribution function of a standardised normal distribution. Here, β describes a target reliability index, specified by the design code, for which the structure is deemed reliable. The sensitivity factors, α_R and α_E, should satisfy the condition $|\alpha| \leq 1$. Moreover, α_R is always positive, while α_E is negative for unfavourable load effects. The Eurocode, EN 1990, recommends α_R = 0.8 and α_E = -0.7 for dominant variables, i.e. variables that are considered the most significant for the structure.

$$P(R \leq r_d) = F_U(-\alpha_R \beta) = F_U(\beta_R) \tag{2.54}$$

$$P(E > e_d) = F_U(+\alpha_E \beta) = F_U(\beta_E) \tag{2.55}$$

Depending on the probabilistic models describing R and E, Equation 2.56 and 2.57 can be used to calculate the design values r_d and e_d. Here, the design values are fractiles corresponding to the probabilities obtained in Equation 2.54 and 2.55. $F_R(x)$ and $F_E(x)$ denote the probabilistic distribution functions for R and E.

$$P(R \leq r_d) = F_R(r_d) \tag{2.56}$$

$$P(E > e_d) = 1 - \ P(E \leq e_d) = 1 - F_E(e_d) \tag{2.57}$$

According to the partial factor method, the design values for the basic variables (x_d) are described in terms of a characteristic value (x_k) and a partial factor (γ). The characteristic value is specified based on a prescribed probability of exceedance corresponding to a specific reference period. The characteristic value is then multiplied or divided by a partial factor to obtain the design value needed to secure the desired reliability level for the structure. A partial factor accounts for model uncertainty and variability of the basic variable. Equation 2.58 and 2.59 show the resistance (γ_R) and load effect (γ_E) partial factors.

$$\gamma_R = \frac{r_k}{r_d} \tag{2.58}$$

$$\gamma_E = \frac{e_k}{e_d} \tag{2.59}$$

Equation 2.54 to 2.57 show how the codified design values for the resistance and load effect can be found when a target reliability index is specified. These equations can also be used to verify the reliability performance provided by the design code. Probabilistic descriptions, $F_R(x)$ and $F_E(x)$, for the variables R and E can be derived from actual data. With the codified design values (r_d and e_d) known, the probability expressions $P(R \leq r_d)$ and $P(E > e_d)$ can be found. Assuming α_R = 0.8 and α_E = -0.7, the actual reliability index β can be estimated with Equation 2.54 or 2.55. As a result, the actual reliability index can then be compared to the target reliability index to measure the reliability performance of the structure.

2.5.6 *Target Reliability Levels*

According to ISO 2394 (2015), the target reliability index is primarily concerned with the consequences of failure and the relative cost of safety measures. The properties of the basic variables are related to a reference period, and so the reliability index also corresponds to a reference period. Holický (2009) states that the reference period may or may not coincide with the design working life, and defines the design working life as follows: The design working life is the assumed period for which the structure needs to fulfil its purpose, allowing scheduled maintenance without substantial repairs. For example, the reliability of a structure with an intended design working life of a 100 years may be verified with data related to a 50-year reference period.

The reliability performance of a structure is usually assessed by comparing the determined reliability index (β) with the target reliability index (β_t). For optimum design, it is required that the structure is designed in such a way that the determined reliability index approximates the target reliability index.

EN 1990 (CEN, 2002) specify three reliability classes to categorise the target reliability indices for the different limit states. The reliability classes include RC3, RC2 and RC1. From RC3 to RC1, the consequences for loss of human life or economic, social or environmental

consequences range from high to low. The target reliability indices (β_t) for ULS are summarised in Table 2.2. EN 1990 is based on a default target reliability index of 3.8 for a 50-year reference period (CEN, 2002). This target value corresponds to the reliability class RC2 with medium consequences of failure. For EN 1990, the target reliability index can be interpreted as the reliability level to be reached on average.

Table 2.2: Reliability classes and recommended target reliability indices (β_t) for ULS (CEN, 2002).

Reliability class	**Target reliability index (βt)**	
	1-year reference period	50-year reference period
RC3	5.2	4.3
RC2	4.7	3.8
RC1	4.2	3.3

ISO 2394 (2015) provides target reliability indices based on the relative cost of safety measures and consequences of failure. Table 2.3 summarises the target reliability indices valid for the ultimate, fatigue and serviceability limit states. Similar to Table 2.2, target reliability indices β_t = 3.1, β_t = 3.8 or β_t = 4.3 may be considered for ULS.

Table 2.3: Target reliability indices (β_t) for life time (ISO 2394, 2015).

Relative cost of safety measures	**Consequences of failure**			
	Small	Some	Moderate	Great
High	0	1.5	2.3	3.1
Moderate	1.3	2.3	3.1	3.8
Low	2.3	3.1	3.8	4.3

SANS 10160 (2019) is the South African National Standard for buildings and industrial structures. It specifies β_t = 3.0 for a 50-year reference period. This target value corresponds to the same class of structures considered in EN 1990 and ISO 2394 when β_t = 3.8. Here, the target value of 3.0 is interpreted as a constraint, which represents the minimum β that may be obtained (Retief, Dunaiski and eds., 2009).

3 Roosboom Case Study

3.1 Introduction

This chapter investigates the traffic loading on the National Route 3 (N3) Toll Road between Durban and Johannesburg. It entails a reliability analysis based on the observed traffic load effects on the N3 and the design traffic load model provided in Technical Methods for Highways 7 (TMH-7) (CSRA, 1981). The investigation aims to determine the reliability performance of a bridge designed according to TMH-7 and loaded with actual traffic loads. More specifically, the focus is on the performance of TMH-7's traffic load model for normal traffic conditions, i.e. NA loading.

The case study makes use of traffic load effects derived from Weigh-in-Motion (WIM) data collected at Roosboom station situated on the N3. The road is made up of four traffic lanes, from which WIM data is measured for the slow lane (outer traffic lane) in both directions. The N3 is known to be a heavy freight route connecting Durban's port to Gauteng, which makes it appropriate for this study. Another favourable consideration of Roosboom station, is that it has been operational since November 2000 and delivers good quality WIM measurements for the slow lanes (De Wet, 2010a). Thus, an extensive database is available for providing a good representation of the traffic conditions on the N3.

Seven consecutive years of WIM data from 2010 to 2016 were used in this case study to represent the slow lane traffic in the northbound direction. The traffic load effects were obtained from a previous study (Van der Spuy and Lenner, 2018). Furthermore, the reliability analysis was based only on the traffic load effects on the bridge and thus ignored the bridge resistance and dead loads. The investigation considered span lengths ranging from 5 to 50 metres to find preliminary results for the reliability performance of NA loading in TMH-7.

The phase of the research reported in this chapter was presented at the 7th International Conference on Structural Engineering, Mechanics and Computation (SEMC) and published in its proceedings (Basson and Lenner, 2019).

3.2 Methodology

The main objective of this case study was to carry out a reliability analysis based only on the traffic load effects. The case study commenced by selecting a statistical approach to assess the

extreme traffic load effects. Statistical characteristics were then obtained to describe the extreme load effects and to identify applicable models to represent the data set. The maximum likelihood estimation (MLE) method enabled the estimation of the model parameters for the selected models, while goodness-of-fit tests verified the credibility of the selection. These tests entailed diagnostic plots and hypothesis testing. Furthermore, the representative extreme load effect distribution was statistically projected to obtain the maximum load effect distribution related to a 50-year reference period. This was done in order to compare the results from the reliability analysis to target reliability indices that correspond to a 50-year period. Based on the statistical projection, a single model was chosen from the applicable models to represent the extreme load effects for the reliability analysis.

The limit state function was formulated to describe the failure mode, i.e. when the extreme traffic load effects exceed the design load effect. Different design scenarios were defined and the First Order Reliability Method (FORM) was used to conduct the reliability analysis. The results provided reliability indices that correspond to a 50-year reference period and measured the reliability level for each span length. A comparison between the obtained reliability indices and target values from existing standards, allows for an interpretation of the reliability performance of NA loading in TMH-7.

3.3 Calculation and Assessment of Traffic Load Effects

3.3.1 *Overview of Traffic Load Effect Calculation*

In the derivation of the traffic load effects, Van der Spuy and Lenner (2018) first cleaned the WIM data using Golem. Golem is a technique developed by a South African transportation engineer, M. Slavik, to address errors in WIM data. The data was then post-calibrated using the Truck Tractor method (De Wet, 2010a, 2010b). Both methods are locally developed and applicable to South African WIM data.

With the help of WIM data characteristics such as vehicle and axle weight, axle spacing, speed, date and timestamp, the traffic load effects on a bridge can be derived. The use of influence lines together with the moving load analysis is the most applicable approach in finding the traffic load effects on variable span lengths (Van der Spuy and Lenner, 2019). The approach allows for maximum traffic load effects to be produced by a single heavy vehicle or multiple heavy vehicles travelling close to each other in the same lane. In this way, a better

representation of the extreme load effects on the bridge are provided, especially for longer span lengths.

In the derivation of the traffic load effects, it was difficult to make a distinction between standard trucks, illegally overloaded trucks and permit trucks. Therefore, the data set of traffic load effects account for a mixture of loading events, which means that not all the load effects are identically distributed. This is recognised in Section 1.5 as a limitation for the study.

The procedure for the moving load analysis is explained as follows. The speed and timestamp are used to find the distance between vehicles crossing the bridge. The vehicles, presented as axle weights and axle spacings, are then positioned in a long convoy in the appropriate order. Throughout the analysis, the speed of the vehicles is assumed to remain constant. The convoy is then moved over a bridge and the resultant load effects are measured. Van der Spuy and Lenner (2018) moved the convoy over a range of span lengths in increments of 0.444 m, which corresponds to 0.02 s at a speed of 80 km/h. At each time step, the bending moment at midspan was measured and the maximum load effect per day was recorded.

3.3.2 *Statistical Approach in Assessing Extreme Traffic Load Effects*

The literature review in Section 2.4.2 reveals that the statistical approaches in assessing extreme traffic load effects are quite diverse, and that the approach may be chosen subjectively according to the author's discretion. For this case study the block maxima method was chosen, as it is a well-established method for assessing traffic load effects (refer to Section 2.4.2). By taking a large enough block period, dependencies between loading events are deemed to disappear. After assessing the traffic load effects for a block size of a day, a week and a month, it was decided to consider the maximum traffic load effect per month, i.e. monthly maxima. The observation period of seven years was long enough to extract a large enough sample of monthly maxima from the measured traffic load effects. By choosing monthly maxima, the decision to choose what percentage of the traffic load effects are applicable to the right tail, is avoided.

The monthly maxima approach is similar to fitting a distribution to the right tail of daily maxima, as it limits the data set to critical extreme load effects. By choosing monthly maxima, instead of daily and weekly maxima, temporal variations in load effects (e.g. caused by weekends and holidays) are deemed to disappear. Thus, the less critical loading events are ignored, and the range of loading event types considered, are reduced. A single distribution is

deemed adequate to represent the extreme traffic load effects (O'Brien *et al.*, 2015). Thus, for this study a single distribution was fitted to the monthly maxima in representing the extreme load effects. The monthly maxima were assumed independent and identically distributed (iid), which is typically found to be an underlying assumption in literature (O'Brien *et al.*, 2015). The assumption of iid is often made with the purpose of simplifying arguments used in statistical inference. The assumption also serves as a prerequisite for important theorems, such as the Central Limit Theorem and the Extreme Value Theorem (Coles, 2001).

The traffic load effect distribution can be raised to an appropriate power to obtain the maximum load effect distribution for a specific reference period (refer to Section 3.4.5). The power is equal to the number of block periods that occur in the reference period. As the block period of a month is larger than a block period of a day or week, the monthly maxima distribution will be raised to a smaller power than when daily or weekly maxima were to be used. A smaller power is desirable, as even small discrepancies in the data will lead to large discrepancies when raised to a high power. Thus, the simplifying assumption of iid has less of an effect on the estimated maximum load effect distribution when monthly maxima are used.

3.4 Probabilistic Modelling of Traffic Load Effects

3.4.1 *Statistical Characteristics of Monthly Maxima*

The statistical characteristics of the monthly maxima were found in order to determine applicable probabilistic models to represent the data. The sample characteristics of the monthly maxima data set can be described by the moment characteristics, which are unbiased point estimates of the population parameters (Holický, 2009). The moment characteristics primarily include the sample mean, variance and skewness, where the square root of the variance provides the standard deviation. Equation 2.13, 2.14 and 2.15 in Section 2.3.1 were used to determine the moment characteristics. In addition, the coefficient of variation (COV), describing the ratio between the standard deviation and mean, was also determined.

The change in sample characteristics from daily maxima and weekly maxima to monthly maxima was assessed. The change in sample mean, COV and skewness are illustrated in Figure 3.1. The graphs show that as the block period increases, the mean value increases, while the COV and skewness decrease. The mean value increases as the data set is limited to critical extreme load effects. Furthermore, the COV and skewness decrease as the range of loading event types are reduced.

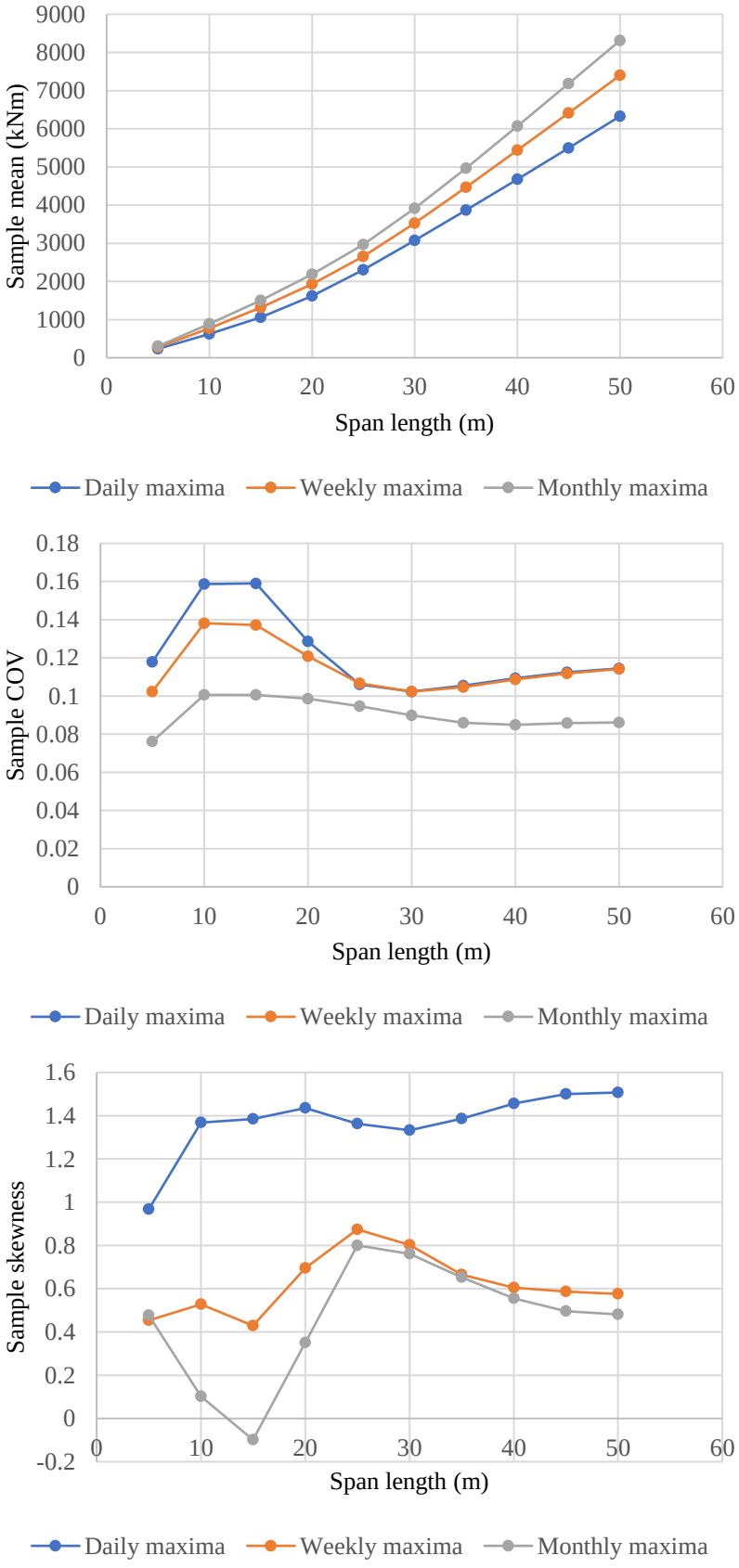

Figure 3.1: Sample mean (top), sample COV (middle) and sample skewness (bottom) for daily, weekly and monthly maxima.

The sample characteristics of the monthly maxima of each span length are summarised in Table 3.1. A maximum value of 0.101 is obtained for the COV. The COV is an indication that the monthly maxima have a narrow distribution shape and that most of the values are located close to the mean. The skewness for all span lengths are less than 1, with a maximum value of 0.8. The skewness is positive for all span lengths except for a 15 m span. A positive value indicates a right skewness (i.e. a right tail), where a number of larger load effects occur further away from the central part of the distribution. The opposite is true for a negative skewness, where the left tail of the distribution is longer, meaning that a number of smaller load effects occur further away from the central part of the distribution. The skewness for the 10 m and 15 m spans is close to zero, which indicates a distribution that approaches a normal distribution.

Table 3.1: Sample characteristics of monthly maxima.

Span length (m)	Mean (kNm)	Standard deviation (kNm)	COV	Skewness
5	302.0	23.0	0.076	0.476
10	884.8	89.0	0.101	0.103
15	1504.8	151.4	0.101	-0.099
20	2186.0	215.5	0.099	0.351
25	2968.0	281.1	0.095	0.800
30	3914.4	352.0	0.090	0.762
35	4969.6	427.0	0.086	0.653
40	6069.9	515.7	0.085	0.555
45	7182.6	617.0	0.086	0.496
50	8310.9	716.2	0.086	0.481

3.4.2 *Selection of Applicable Models*

There are discrepancies as to which distribution type should be used to represent the extreme traffic load effects. The different approaches vary from fitting a normal or lognormal distribution to fitting extreme value distributions, such as the generalised extreme value (GEV) family (refer to Section 2.4.2). The extreme value distributions can be statistically justified for dealing with extreme data (Coles, 2001). Nevertheless, it is recommended to explore a wider range of distributions when considering actual data, as other distributions may be more suitable in representing the site-specific data. With this in mind, the following procedure was used to select applicable models for the monthly maxima.

An approach developed by Holický (2013) together with the sample characteristics of the monthly maxima, were considered in finding applicable models to represent the monthly maxima. It utilises the COV and skewness of a sample to find an appropriate model to represent the data (Holický, 2013). The originally considered distributions include the normal, two-parameter lognormal, three-parameter lognormal, beta, gamma and Gumbel distribution. The approach was amended to also include the GEV family of distributions for maxima, namely the Gumbel, Fréchet and Weibull distribution.

The modified approach adopted from Holický (2013) is illustrated in Figure 3.2, where the COV is denoted by V. For each span length, the skewness and COV from the sample characteristics were used to plot points on the diagram in Figure 3.2. Most of the points are located above the two-parameter lognormal line, which suggests that the three-parameter lognormal (LN3) distribution or Weibull distribution (for maxima) is appropriate to model the monthly maxima. The generalised extreme value (GEV) distribution can be used to represent the Weibull distribution, as it corresponds to the Weibull distribution when the skewness is less than 1.14. Also, that is when the shape parameter of the GEV distribution is less than zero. See Chapter 2 Section 2.3.2 for a detailed discussion of the LN3 distribution and GEV distribution.

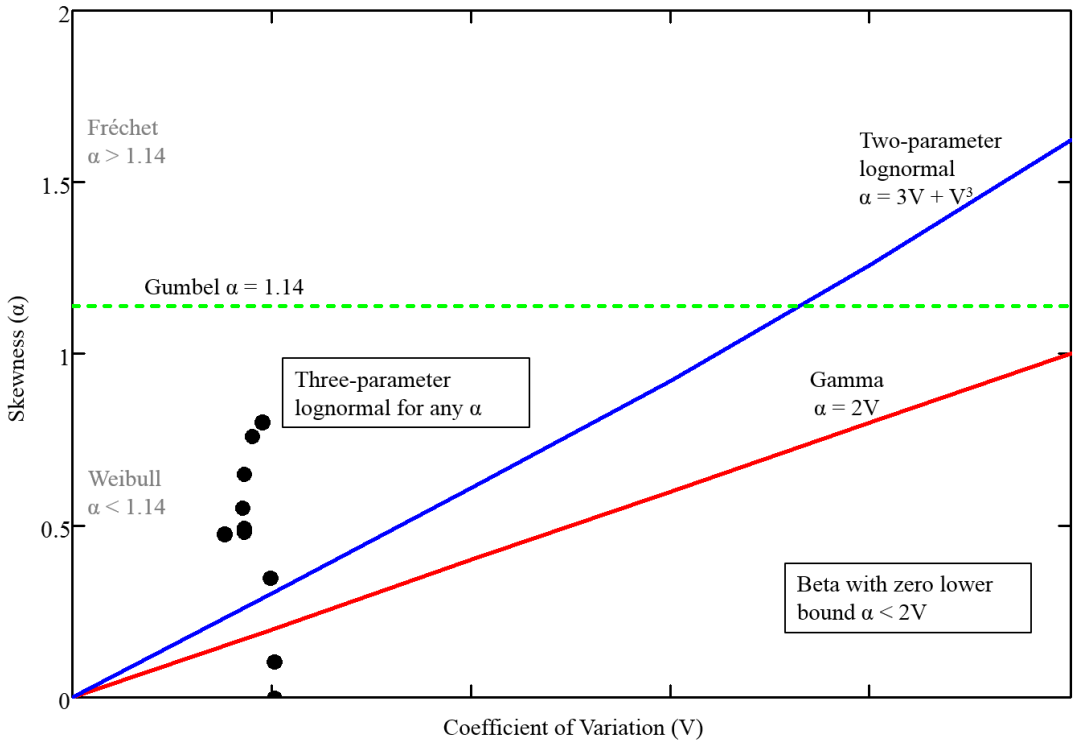

Figure 3.2: A diagram where the relation between skewness and coefficient of variation is used to find applicable models to represent the monthly maxima for each span length (Holický, 2013).

Both the LN3 distribution and GEV distribution are asymmetrical and have three model parameters. Both models are flexible in allowing for positive or negative skewness's and can thus cater for different sample characteristics obtained from the different span lengths. As a result, the LN3 distribution and GEV distribution were further investigated to decide on an appropriate model.

3.4.3 *Estimation of Model Parameters*

When working with block maxima, it is widely accepted and deemed reliable to use MLE in estimating unknown model parameters for a distribution fitted to the data set (Ferreira and De Haan, 2013). Thus, MLE was used in this study to estimate the values of the model parameters that best describe the monthly maxima. It does so by maximising the likelihood function, or the equivalent log-likelihood function with respect to the model parameters (Castillo *et al.*, 2005). Consequently, the likelihood function obtains parameter estimates which maximise the probability of obtaining the observed maxima (Coles, 2001). In doing so, the agreement between the chosen model and the observed monthly maxima is optimised. Estimates of the model parameters are called maximum likelihood estimators (Coles, 2001).

In Equation 3.1 and 3.2, $L(\theta)$ denotes the likelihood function, whereas $l(\theta)$ denotes the log-likelihood function. $f(x_i; \theta)$ represents the probability density function of the selected model, θ denotes the model parameter, n is the number of observations in the sample, and x_i denotes independent realisations of the random variable X, where i ranges from 1 to n.

$$L(\theta) = \prod_{i=1}^{n} f(x_i; \theta) \tag{3.1}$$

$$l(\theta) = log\, L(\theta) = \sum_{i=1}^{n} log\, f(x_i; \theta) \tag{3.2}$$

The GEV distribution has three model parameters, namely, the location, scale and shape parameters. The LN3 distribution has a different set of model parameters, namely, the mean, standard deviation and skewness. The maximum likelihood estimators for the GEV distribution were obtained in *R*, a statistical software. For the LN3 distribution, a mathematical software called *Mathcad* (PTC, 2006) was used to numerically obtain the estimators (refer to Appendix

A for the *Mathcad* sheet). The maximum likelihood estimators for both distribution types are summarised in Table 3.2.

Table 3.2: Maximum likelihood estimates of the model parameters.

Span length (m)	**GEV distribution**			**LN3 distribution**		
	Location (kNm)	Scale (kNm)	Shape	Mean (kNm)	Standard deviation (kNm)	Skewness
5	292.5	20.4	-0.128	302.0	23.0	0.622
10	852.9	86.3	-0.268	884.8	88.6	0.221
15	1458.1	154.9	-0.372	1504.8	150.8	-0.224
20	2097.6	194.5	-0.149	2186.2	217.7	0.645
25	2845.3	235.1	-0.066	2968.0	279.1	0.792
30	3762.9	296.9	-0.075	3914.4	349.6	0.771
35	4784.3	360.1	-0.073	4969.9	429.8	0.860
40	5838.5	437.7	-0.077	6070.7	525.8	0.921
45	6917.8	531.4	-0.096	7183.7	631.3	0.910
50	8006.3	621.7	-0.106	8311.8	728.4	0.838

To compare the moment parameters of the two distribution types, the mean, standard deviation and skewness for the GEV distribution were derived from the location, scale and shape parameters. Similar to using the moment characteristics to obtain the sample properties, the moment parameters were determined to describe the population properties of the GEV distribution. The difference is that the sample properties are obtained directly from the sample values, while the moment parameters are obtained from the probability distribution and its model parameters.

The moment parameters include the population mean, variance and skewness, where the standard deviation is equal to the square root of the variance. Equation 2.10, 2.11 and 2.12 in Section 2.3.1 were used to determine these parameters for the GEV distribution. The monthly maxima represent the random variable X, while the probability density function is denoted by $f(x)$.

A summary of the statistical parameters describing the GEV and LN3 distributions is given in Table 3.3. It includes the mean, standard deviation, COV and skewness of the monthly maxima

described by each distribution. The comparison of the distributions reveals that relatively similar values are obtained for the statistical parameters.

Table 3.3: Comparison of statistical parameters for monthly maxima.

Span length (m)	**GEV distribution**				**LN3 distribution**			
	Mean (kNm)	Standard deviation (kNm)	COV	Skewness	Mean (kNm)	Standard deviation (kNm)	COV	Skewness
5	301.9	22.7	0.075	0.522	302.0	23.0	0.076	0.622
10	884.2	86.8	0.098	0.029	884.8	88.6	0.100	0.221
15	1504.2	148.4	0.099	-0.281	1504.8	150.8	0.100	-0.224
20	2184.6	212.9	0.097	0.440	2186.2	217.7	0.100	0.645
25	2966.5	278.7	0.094	0.790	2968.0	279.1	0.094	0.792
30	3913.7	348.7	0.089	0.750	3914.4	349.6	0.089	0.771
35	4967.7	423.6	0.085	0.758	4969.9	429.8	0.086	0.860
40	6060.1	512.9	0.085	0.741	6070.7	525.8	0.087	0.921
45	7178.2	610.7	0.085	0.655	7183.7	631.3	0.088	0.910
50	8305.6	707.3	0.085	0.612	8311.8	728.4	0.088	0.838

3.4.4 *Assessment of Selected Models*

Goodness-of-fit tests were used to assess the quality of both the LN3 and GEV distribution in representing the monthly maxima. The tests consist of diagnostic plots and hypothesis testing, whereas the former is the primary focus. *R* software (R Core Team, 2018) was used to perform the goodness-of-fit tests for both distribution types and the *R* code is provided in Appendix B.

The assessment of the diagnostic plots also allows for the investigation of different block periods to describe the extreme load effects. Thus, diagnostic plots for daily, weekly and monthly maxima are presented in Section 3.4.4.3, to verify the use of monthly maxima in representing the extreme traffic load effects.

3.4.4.1 *Diagnostic Plots*

Diagnostic plots are used to assess the goodness-of-fit of models graphically. The most significant are the Q-Q plot (Quantile plot) and P-P plot (Probability plot), called probability plots. The Q-Q plot compares the empirical quantiles from the data set to the corresponding

theoretical quantiles obtained from the selected distribution (Coles, 2001; Castillo *et al.*, 2005). It is also more sensitive to deviations in the tails, which is of importance in this study (Fisher, 1983). The P-P plot compares the cumulative probabilities of the empirical and theoretical quantiles and are more sensitive to the centre values (Fisher, 1983).

The LN3 distribution is analogous to the two-parameter lognormal (LN) distribution. Both have the same skewness and standard deviation, but different mean values (Sangal and Biswas, 1970). This is because the LN distribution has a lower bound at zero, while the LN3 distribution can have a lower or upper bound of any value. Hence, the LN3 distribution can easily be assessed by subtracting the bound value from each data point and by fitting a LN distribution to the shifted data (*NIST/SEMATECH e-Handbook of Statistical Methods*). This simplified assessment approach was followed and the diagnostic plots were obtained using the *fitdistrplus* package (Delignette-Muller and Dutang, 2015) in *R*. It includes the probability plots, a density plot and cumulative distribution function (CDF) plot. The density plot is a plot where the density distribution function is fitted to the frequency histogram of the monthly maxima. The CDF plot compares the theoretical and empirical cumulative distribution functions. Moreover, it obtains the probability of non-exceedance ranging from 0 to 1.

The GEV distribution diagnostic plots were obtained using the *ismev* package in *R* (Heffernan and Stephenson, 2018). It includes the probability plots, density plot and the return level plot. The return level plot indicates which distribution type is represented by the GEV distribution. When the plot is concave, the right tail has no finite bound and the shape parameter exceeds zero (Coles, 2001). This is when the GEV distribution represents a Fréchet distribution. When the plot is a straight line, the shape parameter is zero and the Gumbel distribution is represented. Lastly, when the plot is convex, the distribution has an upper bound and represents a Weibull distribution for maxima (Coles, 2001).

For illustrative purposes, the four diagnostic plots for the LN3 and GEV distribution are shown in Figure 3.3 and Figure 3.4 for a 5 m span. The data is measured in kNm. The diagnostic plots for all span lengths can be found in Appendix C for the LN3 and GEV distribution.

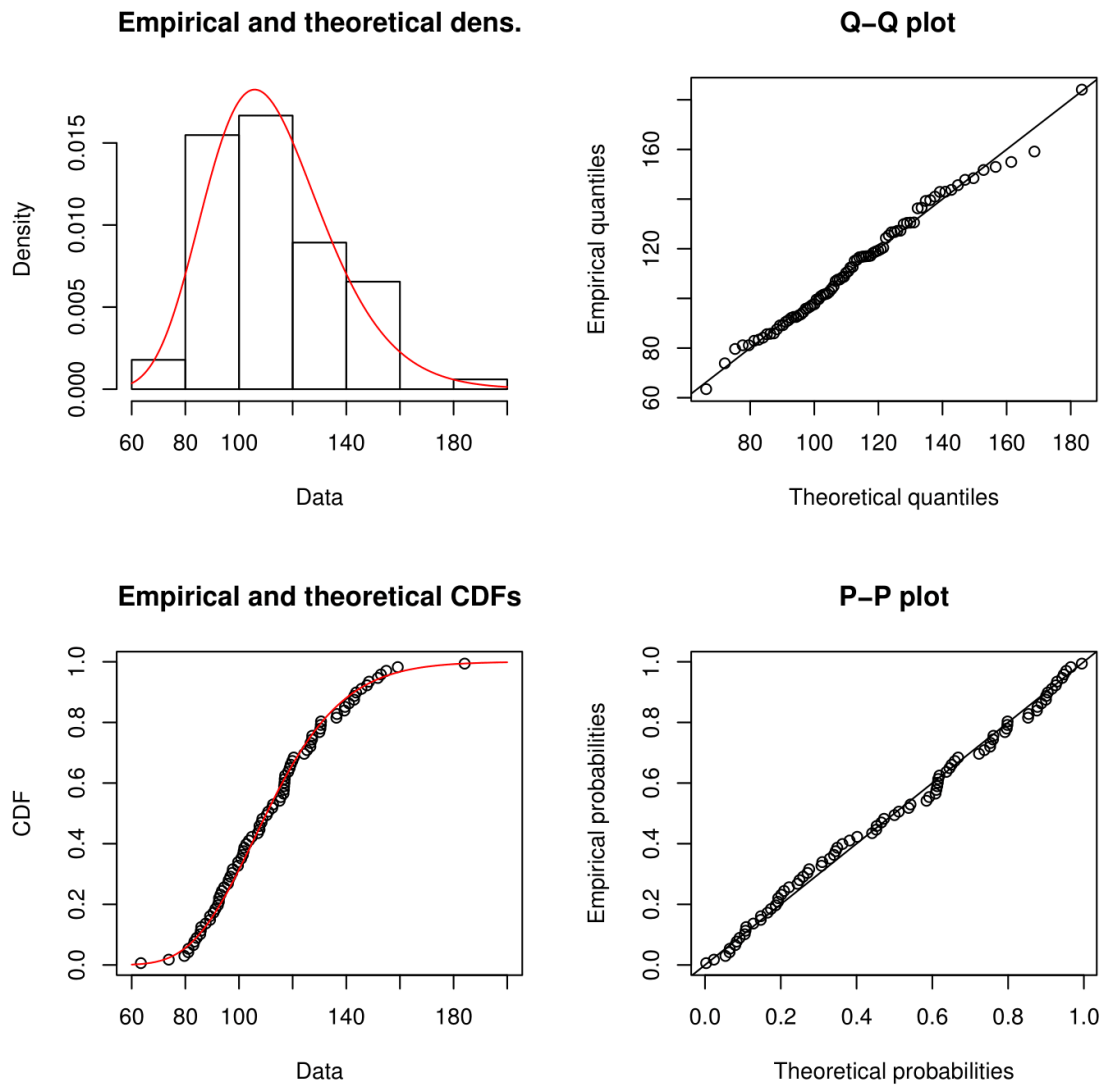

Figure 3.3: Diagnostic plots for the monthly maxima of a 5 m span represented by the LN3 distribution.

Visual inspection of the diagnostic plots indicates that both distributions fit the data well. For the probability plots, the data forms an approximate linear pattern for all span lengths. The validity of the fitted models are further supported by the corresponding probability density functions that fit the histograms of the data quite well. The CDF plots for the LN3 distribution give similar results to the density plots. The return level plots for the GEV distribution show that the shape parameter is negative but varies in value.

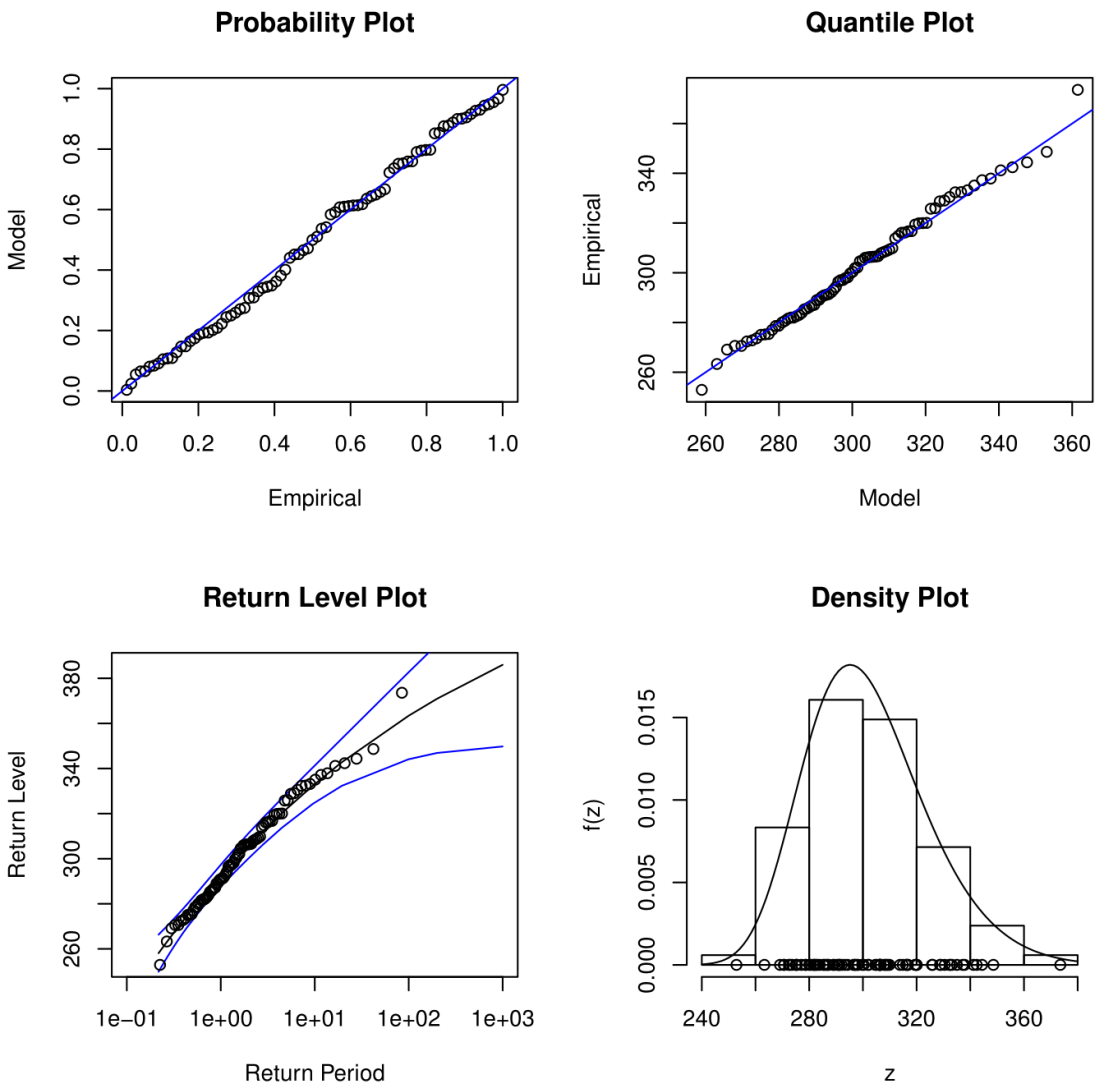

Figure 3.4: Diagnostic plots for the monthly maxima of a 5 m span represented by the GEV distribution.

The normal distribution can also be used to confirm that the monthly maxima can be lognormally distributed. It is well known that a random variable *X* has a lognormal distribution if the transformed variable *Y*, as seen in Equation 3.3, is normally distributed (Holický, 2013). The LN3 distribution bound is denoted by x_0. Equation 3.3 was used to transform the monthly maxima and to fit a normal distribution to the transformed data using the *fitdistrplus* package in *R* (Delignette-Muller and Dutang, 2015).

$$Y = ln(X - xo) \tag{3.3}$$

The diagnostic plots for the normal distribution based on the transformed data, are provided in Appendix C. For illustrative purposes, the diagnostic plots for a 5 m span are shown in Figure 3.5.

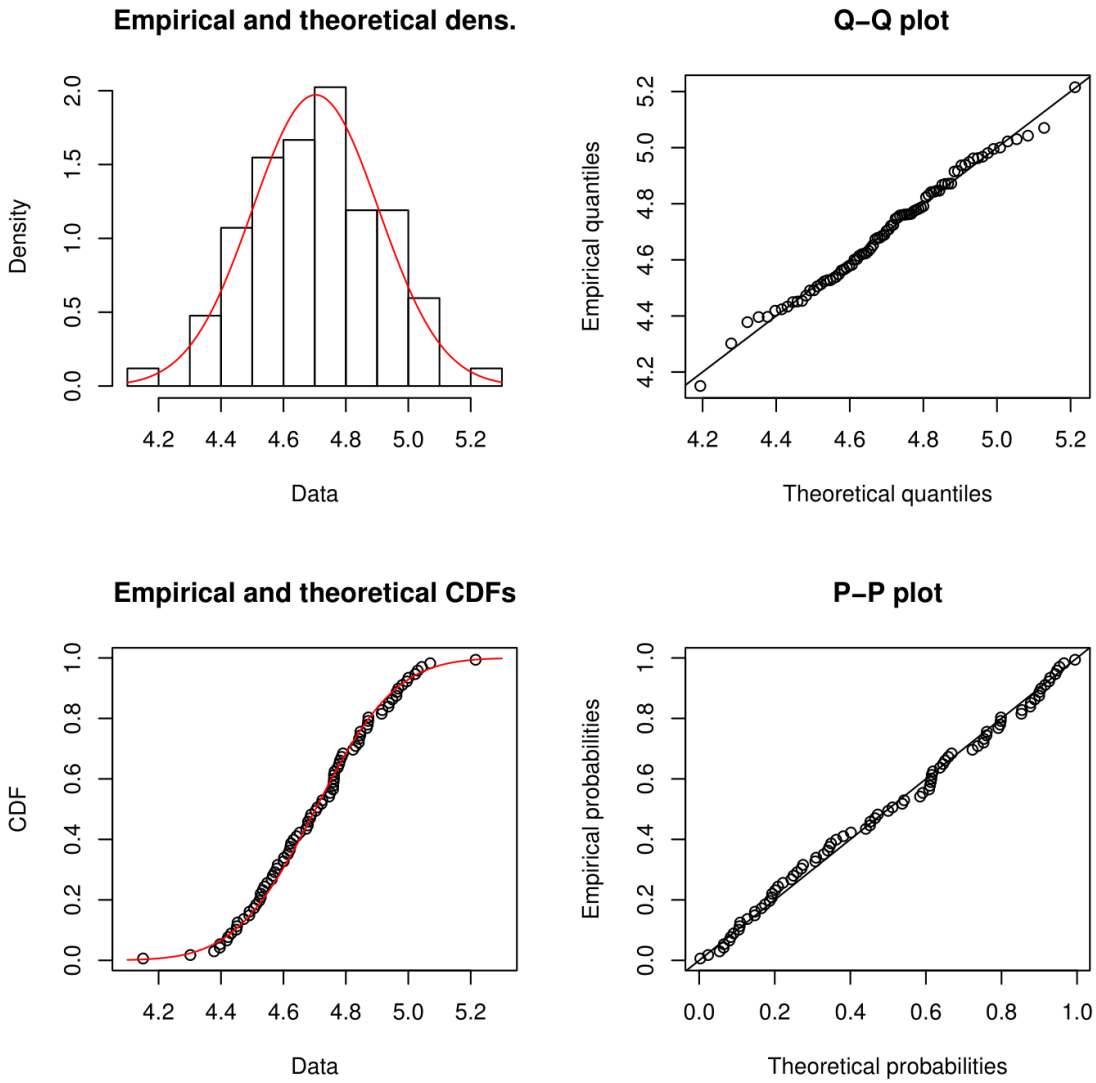

Figure 3.5: Diagnostic plots of the normal distribution fitted to the monthly maxima transformed in accordance with Equation 3.3.

The probability plots in Figure 3.5 show that the transformed monthly maxima form a linear pattern. The density plot and CDF plot also show that the normal distribution is a good fit. This confirms that the monthly maxima are lognormally distributed and can be well-represented by the LN3 distribution.

3.4.4.2 *Goodness-of-fit Statistics*

Goodness-of-fit statistics were used as a numerical measure to substantiate the results obtained from the graphical methods. It was decided to use the modified Anderson-Darling test. The advantage of this test is that it gives more weight to the tails of the distribution, in comparison to other EDF (empirical distribution function) tests (Stephens, 1979).

The modified Anderson-Darling test produces two results, namely the *A*-statistic and *p*-value. The *p*-value determines whether the data follows the selected distribution or not. It is compared to a chosen significance level. When the *p*-value exceeds the significance level, the null hypothesis is accepted, and it is concluded that the data can come from the fitted distribution (Stephens, 1979). The opposite is true for a *p*-value less than or equal to the significance level. A value of 0.05 is commonly accepted for the significance level (Fisher, 2006), which simply means that there is a 5% risk that the null hypothesis is rejected, while it should be accepted (Minitab Express™ Support, 2019).

The modified Anderson-Darling test for the transformed data fitted with a normal distribution, was performed in *R* using the *fitdistrplus* package (Delignette-Muller and Dutang, 2015). The resultant *p*-values are summarised in Table 3.4. The results show that the *p*-value for each span length exceeds the significance level of 0.05. The smallest *p*-value of 0.063 is seen for a 20 m span, while a maximum value of 0.951 is seen for a 30 m span. The results confirm that the transformed data can be represented by a normal distribution and that the monthly maxima can be lognormally distributed.

The modified Anderson-Darling test for the GEV distribution was performed using the *gnFit* package in *R* (Saeb, 2018). The *p*-values for the GEV distribution are provided in Table 3.5. The resultant *p*-values are relatively similar to those in Table 3.4. The *p*-values for all span lengths exceed the value of 0.05. This concludes that the monthly maxima data can also be well-represented by the GEV distribution.

Table 3.4: Anderson-Darling *p*-values for the normal distribution fitted to the monthly maxima transformed in accordance with Equation 3.3.

Span length (m)	5	10	15	20	25	30	35	40	45	50
***p*-value**	0.724	0.273	0.150	0.063	0.581	0.951	0.929	0.421	0.349	0.585

Table 3.5: Anderson-Darling *p*-values for the GEV distribution fitted to the monthly maxima.

Span length (m)	5	10	15	20	25	30	35	40	45	50
***p*-value**	0.751	0.450	0.331	0.091	0.583	0.956	0.916	0.418	0.385	0.603

3.4.4.3 *Comparison of Block Periods*

A Q-Q plot is a valuable tool in assessing the goodness-of-fit of a distribution to the lower and upper tails of the data set. In this study it was used to show that by fitting a distribution to a smaller block period, such as a day or a week, less critical load effects will draw attention away from the right tail.

The procedure used to obtain the Q-Q plots for the daily and weekly maxima agrees with what was done for the monthly maxima. The procedure entails estimating the model parameters for the LN3 and GEV distributions using MLE. For the LN3 distribution the data is transformed, and a LN distribution is fitted to the shifted data in *R*. Concurrently, the data is also fitted with a GEV distribution in *R*. The Q-Q plots for both distributions revealed that the quality of the fit to the right tail improved as the block period became larger. For illustrative purposes, the Q-Q plots for a 10 m span fitted with a LN3 distribution are shown in Figure 3.6.

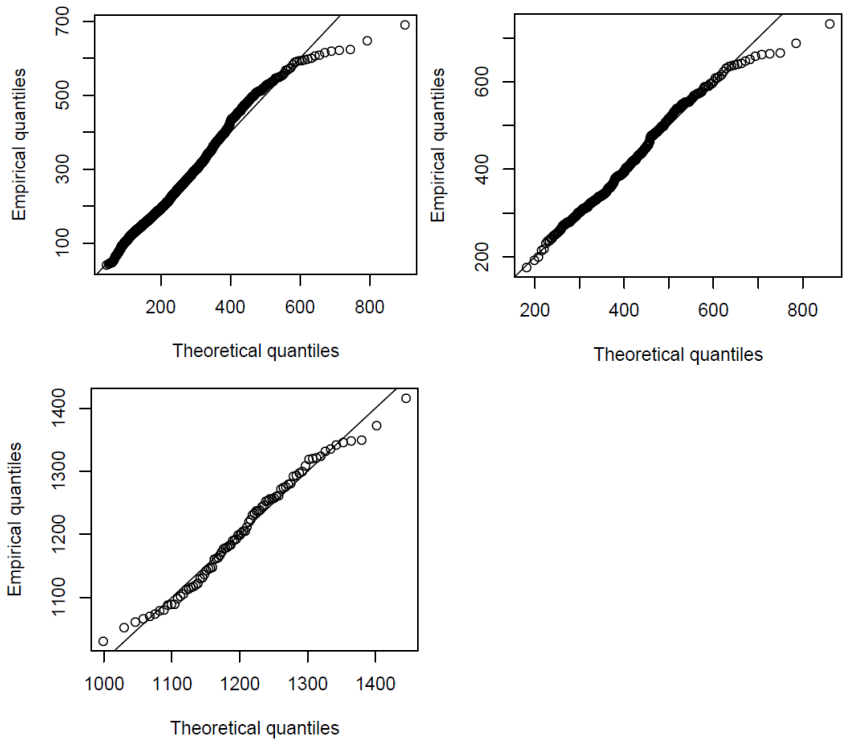

Figure 3.6: Q-Q plots for a 10 m span fitted with a LN3 distribution. Daily maxima (top left), weekly maxima (top right) and monthly maxima (bottom).

From Figure 3.6 it is evident that a poor distribution fit is seen for daily maxima and a more accurate fit is seen for monthly maxima. The results verify that a block period of a month is more appropriate to use in representing extreme load effects.

3.4.5 *50-year Maximum Load Effect Distribution*

The maximum load effect distribution can be found for a 50 year reference period by statistically projecting the monthly maxima distribution using the theorem adopted from (Coles, 2001). A 50-year reference period was selected, in order to compare the obtained reliability indices to target reliability indices from existing standards, which typically correspond to a 50-year period.

The theorem is formulated in Equation 3.4 and 3.5. It assumes that the random variables X_1 to X_n are iid, where n is the number of random variables in the observation period (Coles, 2001). $F(x)$ is the probability distribution function describing X, where x is any realisation of X. The random variable Y represents the maximum value of X per observation period. For this case study, n is the number of monthly maxima obtained in a 50-year period and Y represents the maximum load effects for a block period of 50 years, i.e. the 50-year maxima. The distribution function $F_n(x)$ of the random variable Y can be obtained by raising the original distribution function $F(x)$ to the n-th power. Thus, for this case study n equals 600 (12 times 50).

$$Y = max\{X_1, X_2, \ldots, X_n\} \tag{3.4}$$

$$\begin{aligned} F_n(x) = P(Y \leq x) &= P(X_1 \leq x, X_2 \leq x, \ldots, X_n \leq x) \\ &= P(X_1 \leq x) \times P(X_2 \leq x) \times \ldots \times P(X_n \leq x) \\ &= [F(x)]^n \end{aligned} \tag{3.5}$$

Equation 3.5 was used in *Mathcad* to obtain the 50-year maximum load effect distribution ($F_{600}(x)$) for both the LN3 distribution and the GEV distribution. Hereafter, the 50-year maximum load effect distribution is denoted by $F_{50\ years}(x)$. The probability density function for the 50-year maximum load effects, denoted by $f_{50\ years}(x)$, was obtained from the first derivative of $F_{50\ years}(x)$. The derivation is formulated in Equation 3.6, as described in (Castillo *et al.*, 2005).

$$f_n(x) = \frac{d}{dx} F_n(x) = n\, f(x)\, [F(x)]^{n-1} \tag{3.6}$$

The mean, standard deviation, COV and skewness for the 50-year maximum load effect distribution were obtained from the moment parameters described in Equation 2.10, 2.11 and 2.12 in Section 2.3.1. When the monthly maxima are represented by the GEV distribution, the obtained 50-year maximum load effect distribution is also a GEV distribution. This is in accordance with Theorem 3.2 in *An Introduction to Statistical Modelling of Extreme Values* (Coles, 2001), as the GEV distribution is max-stable. The moment parameters and COV for the 50-year maximum load effect distribution are summarised in Table 3.6. A comparison between the monthly maxima distribution and the 50-year maximum load effect distribution, shows that the skewness stays the same, while the mean increases and the standard deviation and COV decreases.

On the contrary, when the monthly maxima are represented by a LN3 distribution, the obtained 50-year maximum load effect distribution may not necessarily also resemble a LN3 distribution. This is because the LN3 distribution is not max-stable. According to Castillo *et al.* (2005), a lognormal distribution fitted to maximum values converges to a Gumbel distribution as the power *n*, with which it is raised, tends to infinity. By comparing the obtained 50-year maximum load effect distribution to a LN3 distribution with the same moment parameters, it was concluded that the 50-year maximum load effect distribution can still be approximated by a LN3 distribution. In other words, the obtained functions, $F_{50\ years}(x)$ and $f_{50\ years}(x)$, can be approximated by the cumulative distribution function, $F_{LN3}(x)$, and probability density function, $f_{LN3}(x)$, of the LN3 distribution when it has the same moment parameters as the 50-year maximum load effect distribution. For illustrative purposes, the comparison of the cumulative distribution functions and probability density functions for a 5 m span are shown in Figure 3.7 and Figure 3.8, respectively.

The moment parameters for the 50-year maximum load effect distribution, obtained from the LN3 distribution, are summarised in Table 3.6. A comparison of the monthly maxima distribution and the 50-year maximum load effect distribution reveals that the mean and right skewness increases, while the standard deviation and COV decreases.

Table 3.6: Statistical parameters of the 50-year maximum load effect distribution for the GEV distribution and LN3 distribution.

Span length (m)	**GEV distribution**				**LN3 distribution**			
	Mean (kNm)	Standard deviation (kNm)	COV	Skewness	Mean (kNm)	Standard deviation (kNm)	COV	Skewness
5	385.7	10.0	0.026	0.522	396.2	15.7	0.040	1.056
10	1122.2	15.6	0.014	0.029	1188.5	40.9	0.034	0.865
15	1839.8	13.7	0.007	-0.281	1924.6	43.1	0.022	0.667
20	2933.7	82.2	0.028	0.440	3085.8	152.2	0.049	1.067
25	4151.1	182.6	0.044	0.790	4192.9	222.4	0.053	1.139
30	5366.0	216.2	0.040	0.750	5435.8	273.5	0.050	1.128
35	6739.4	265.5	0.039	0.758	6907.5	363.0	0.053	1.172
40	8187.0	314.1	0.038	0.741	8497.9	467.4	0.055	1.205
45	9599.8	330.7	0.034	0.655	10085.6	556.1	0.055	1.196
50	11045.0	358.7	0.032	0.612	11567.6	604.0	0.052	1.161

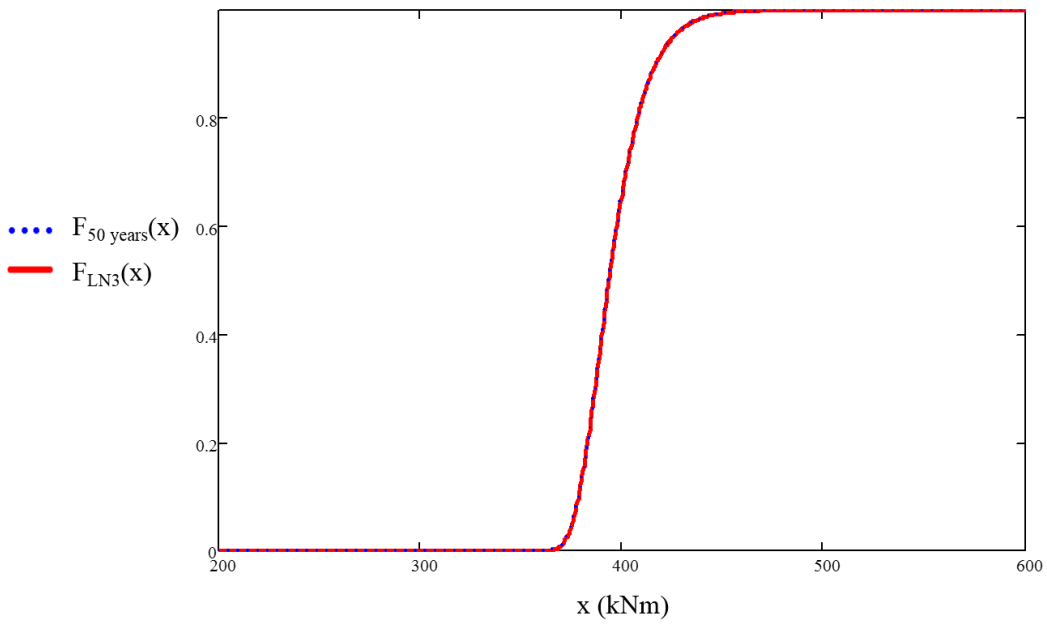

Figure 3.7: Comparison of 50-year maximum load effect distribution with a LN3 distribution with the same moment parameters: cumulative distribution plot for a 5 m span.

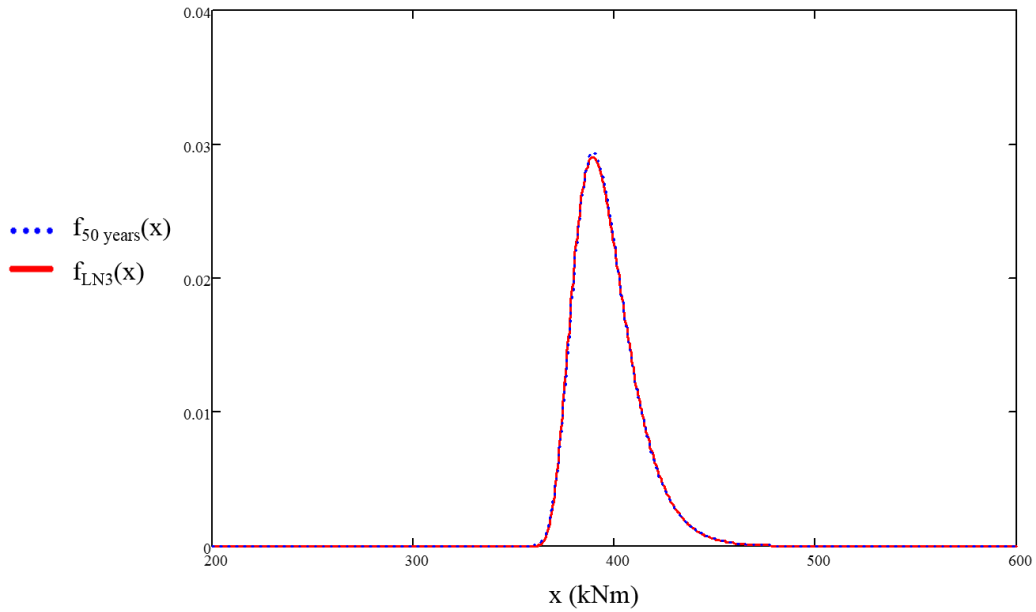

Figure 3.8: Comparison of 50-year maximum load effect distribution with a LN3 distribution with the same moment parameters: probability density plot for a 5 m span.

3.4.6 *Concepts on the Reliability Analysis of Traffic Load Effects*

The overall reliability level, described by the reliability index β, can be split into the resistance (R) part and load effect (E) part (CEN, 2002). For this case study, the load effect part is of interest, where the reliability level is expressed with the load effect index (β_E) equal to $\alpha_E\beta$. The variable α_E is a sensitivity factor obtained from FORM, which describes the relative importance of the load effects in obtaining β (CEN, 2002).

For the case study, α_E denotes the sensitivity factor for the traffic load effects. It is dependent on many factors, such as the load ratio between the traffic load and dead load and the probabilistic description of the resistance variables of the bridge, which was not included in this case study. Therefore as a simplification, it was decided to use a value of -0.7 recommended by the Eurocode, EN 1990, to represent α_E (CEN, 2002). This value is prescribed when traffic load is the leading action. In general, traffic load dominates for short to medium span bridges, but as the span length increases the dead load increases in significance. Therefore, this value is appropriate for short spans, while it is more conservative for longer spans.

When only traffic load effects are considered, the reliability analysis of one random variable can be considered. The failure mode is then defined as the instance the actual traffic load effects exceed the design load effect. The actual traffic load effects are seen as a random variable, described by the 50-year maximum load effect distribution. Whereas the design load effect is

described by a deterministic value determined from the traffic load model in TMH-7 for NA loading.

According to the design value method, the design load effect can be described as a fractile value of the 50-year maximum load effect distribution ($F_{50\ years}(x)$). The probability of failure (p_f) is then represented by the probability that the design load effect (e_d) is exceeded by the traffic load effects (E). The p_f can be calculated with Equation 3.7. The probability distribution function of a standardised normal distribution ($F_U(x)$) relates β_E to p_f, as seen in Equation 3.8.

$$p_f = P(E > e_d) = 1 - F_{50\ years}(e_d) \tag{3.7}$$

$$p_f = F_U(+\alpha_E \beta) = F_U(-0.7\beta) \tag{3.8}$$

3.4.7 *Decision on Representative Model for Reliability Analysis*

Concerns were raised regarding the application of the GEV distribution in the reliability analysis, which led to the decision to use the LN3 distribution. In the case of the GEV distribution, the negative shape parameters imply that the Weibull distribution is fitted to the monthly maxima. The Weibull distribution for maxima has an upper bound, i.e. a finite end-point in the right tail, and its maximum domain of attraction remains a Weibull distribution (Castillo *et al.*, 2005). This means that the 50-year maximum load effect distribution obtained by the GEV distribution is also described by the Weibull distribution.

The concern with using the Weibull distribution is that the upper bound remains unchanged irrespective of the reference period projected to (Basson and Lenner, 2019). This means that the 50-year maximum load effect distribution has the same upper bound as the monthly maxima distribution. For illustrative purposes, Figure 3.9 shows how the probability density functions for a 15 m and 20 m span are pressed up and shifted towards the vertical upper bound, as it is projected to a 50-year reference period.

When considering the GEV distribution, it was determined that for span lengths of 15, 20 and 35 to 50 metres, the design load effect exceeds the upper bound and cannot be used as a fractile of the distribution function to obtain the probability of failure (see Equation 3.7). Therefore, for these span lengths the probability of failure is zero. Moreover, the probability of failure

remains zero even if the design value is very close to the upper bound. This is substantiated by the condition in Equation 3.9 (Coles, 2001), which is not satisfied by the 50-year maximum load effect distribution for the mentioned span lengths, when x is equal to the design load effect. In Equation 3.9, x denotes the traffic load effects and λ, δ and κ represent the location, scale and shape parameters of the GEV distribution. See Table 3.8 in Section 3.5.2 for a summary of the calculated design load effects obtained from TMH-7.

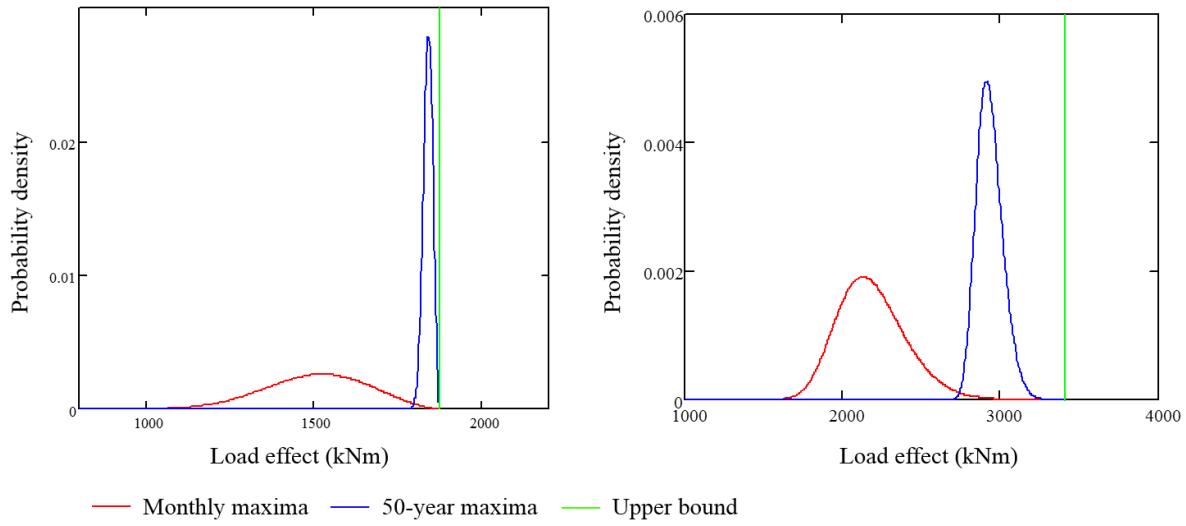

Figure 3.9: Monthly maxima distribution and 50-year maximum load effect distribution for a 15 m span (left) and 20 m span (right) fitted with a GEV distribution.

$$\{x : 1 + \kappa \frac{(x - \lambda)}{\delta} > 0\} \tag{3.9}$$

When considering the design load effects from TMH-7 based on one notional lane (see Table 3.8 in Section 3.5.2), the probability of failure is significantly large for 5 m and 10 m spans, whereas it is equal to zero for 15 m and 20 m spans due to the upper bound being less than the design values. The large difference in results for the short spans seems unrealistic, and thus reinforces the question whether the fixed upper bound is reasonable.

As a result, it was decided to use the LN3 distribution for the reliability analysis instead of the GEV distribution. Mainly because it is questioned whether the monthly maxima upper bound for the GEV distribution is still valid for the 50-year reference period. In addition, the LN3 distribution shows a similar fit to the monthly maxima as the GEV distribution, and the unbounded right tail allows for the investigation of the design load effects (Basson and Lenner, 2019).

3.5 Reliability Analysis for Traffic Load Effects

3.5.1 *Formulation of Limit State Function*

For the reliability analysis, only the traffic load effects were considered. As discussed in Section 3.4.6, failure is then defined as the instance the traffic load effects (E) exceed the design load effect (e_d).

For the final reliability analysis, model uncertainty (θ_E) related to the traffic load effects must be included. It takes account of the uncertainties associated with the selected theoretical model, owing to the simplification of actual conditions (Holický, 2009). E_{model} represents the traffic load effects before θ_E is included. A multiplicative relationship between θ_E and E_{model} can be used to find the traffic load effects (E) after θ_E is included. This relationship is shown in Equation 3.10, followed by the resultant limit state function (Z) in Equation 3.11. Failure occurs when Z is negative.

$$E = \theta_E \, E_{model} \tag{3.10}$$

$$Z = e_d - \theta_E \, E_{model} \tag{3.11}$$

The reliability index in this investigation was obtained by means of FORM, implemented in the *Comrel* software package (RCP, 2007). The FORM-analysis utilised the limit state function in Equation 3.11 to find the probability of failure (p_f) and load effect index (β_E) associated with the traffic load effects on each span length. The design load effect (e_d) is a deterministic value provided by TMH-7 for NA loading, while θ_E and E_{model} are random variables. In agreement with literature (JCSS, 2001; fib COM3 TG3.1, 2016), θ_E is represented by a LN distribution with a mean of 1.0 and a COV of 0.1. For this case study, E_{model} is described by a LN3 distribution with moment parameters as provided in Table 3.6. Finally, the overall reliability index β was obtained for each span length by dividing β_E with the sensitivity factor α_E equal to 0.7 (refer to Section 3.4.6).

3.5.2 *Reliability Results and Discussion for Different Design Scenarios*

Different design scenarios were considered to gain the most insight into the reliability performance of TMH-7 for normal traffic conditions, when only the slow lane WIM data is available. The four different design scenarios allow for a thorough exploration of the slow lane data and extends the investigation to consider narrow span bridges and more typical highway bridges. Furthermore, it considers the influence of the number of notional lanes on the design and performance of the bridge. Table 3.7 provides an overview of the four design scenarios, which include the number of actual traffic lanes on the bridge and the number of notional lanes used to design the bridge.

Table 3.7: Overview of design scenarios.

Design scenario	**Description**
1	1 traffic lane; 1 notional lane
2	1 traffic lane; 3 notional lanes
3	2 traffic lanes; 3 notional lanes
4	2 traffic lanes; 2 notional lanes

For each design scenario, the design load effects were obtained from the traffic load model in TMH-7 Part 2 for NA loading (CSRA, 1981). The traffic load model makes use of a floating lane notional lane width, where the number of notional lanes is governed by the carriageway width (CSRA, 1981). The design load effects were calculated using the global analysis, as described in Chapter 2 Section 2.2.4, thus it describes the total load effects on the bridge. The design values account for partial load factors, γ_{fL} = 1.5 and γ_{f3} = 1.1, as defined in Section 2.2.5 of Chapter 2. Furthermore, the dynamic impact factor obtained by the Swiss formula in Equation 2.3 of Chapter 2, was removed from the NA loading to obtain the static design load effects. The resultant design traffic load effects for the ultimate limit state (ULS) are summarised in Table 3.8 for each span length. The design values represent the maximum obtained bending moments at midspan when designing for one, two and three notional lanes.

Table 3.8: Design traffic load effects (in kNm) for ULS determined from NA loading in TMH-7.

Span length (m)	One notional lane	Two notional lanes	Three notional lanes
5	357.5	650.6	915.1
10	1048.2	1960.0	2811.3
15	2082.6	3953.1	5742.7
20	3465.0	6902.2	8895.0
25	5197.5	9720.0	12546.0
30	7281.3	12887.8	16661.4
35	9717.1	16384.9	21215.7
40	13057.2	20195.2	26189.4
45	15689.0	24306.0	31566.9
50	18499.0	28706.8	37335.1

For each span length, the overall reliability index (β) was determined, corresponding to a 50-year reference period. The results were then compared to target reliability indices (β_t) from existing standards that correspond to this period. EN 1990 (2002) recommends a β_t of 3.8 for ULS, while the South African National Standard, SANS 10160 (2019), use a β_t of 3.0. The following sections describe each design scenario and discuss the corresponding results.

3.5.2.1 *Design Scenario 1*

The first design scenario considered the extreme case of using one notional lane to design and cater for the traffic load effects of one traffic lane. This case does not typically present itself for highway bridges, as most highway bridges consist of two or more traffic lanes. Even when only one traffic lane is present on the bridge, the shoulder widths contribute to carriageway widths exceeding 4.8 metres, which requires two or more notional lanes for design (CSRA, 1981; Burrell, Mitchell and Wolhuter, 2002). Nevertheless, theoretically a narrow bridge requiring only one notional lane for design can exist and thus requires investigation (CSRA, 1981). Moreover, this case provides insightful findings on the performance of TMH-7, and more specifically the traffic load model for different span lengths. Table 3.8 provides the design load effects for one notional lane and Table 3.9 provides the obtained reliability indices (β) for each span length.

The results presented in Table 3.9 show that for short spans ranging from 5 to 25 metres, the overall β is less than 3.8, with a probability of failure approaching a hundred percent for 5 m

and 10 m spans. This design scenario reveals that a poor reliability performance is seen for short, narrow span bridges. It agrees with literature findings that NA loading shows deficiencies for short narrow span bridges ranging from 5 to 10 metres (Oosthuizen *et al.*, 1991; Anderson, 2006).

Table 3.9 shows that for spans 30 to 50 metres, β is equal to or more than 3.8. Thus, TMH-7 maintains an adequate reliability level for these span lengths when only traffic load effects are considered. The extreme case of using one notional lane also reveals the inherent conservatism of NA loading for longer spans, evidently seen in the relatively high β values for 30 to 50 m spans. Anderson (2006) found similar results and explains that it is owing to the way NA loading was derived for longer spans. The following factors may play a role: the combination of idealised vehicles applied to the span and assumptions made regarding overloading and the application of a partial load factor.

To complete the investigation of the design scenario, β was also compared to a target value of 3.0. Table 3.9 shows that for spans ranging from 5 to 25 metres β is less than 3.0, while for spans 30 to 50 metres β exceeds a value of 3.0.

Table 3.9: Overall reliability indices (β) for the first design scenario.

Span length (m)	5	10	15	20	25	30	35	40	45	50
Reliability index (β)	-1.23	-1.58	1.21	1.65	2.84	3.79	4.29	5.12	5.24	5.62

3.5.2.2 *Design Scenario 2*

The second design scenario considered a typical ramp design for a one-lane bridge. A basic lane width of 3.7 m was chosen, with a shoulder width of 2.5 m on both sides (Burrell, Mitchell & Wolhuter, 2002). The width allows vehicles to pass by a broken-down truck and provides an accessible road width while maintenance and repairs are in process. The total carriageway width equalled 8.7 m, which resulted in the extreme case of using three notional lanes to cater for the traffic load effects of one traffic lane.

The 50-year maximum load effect distribution was used for the reliability analysis (see Section 3.4.5), together with the design load effects obtained for three notional lanes (see Table 3.8). The obtained β for each span length is given in Table 3.10. As expected, β attains a very high

value in comparison to the target values of 3.8 and 3.0, and for most span lengths β exceeds a value of 10. Thus, the probability of failure is negligibly small. The results indicate that TMH-7 is very conservative in this design scenario. Recall that the results are based on global load effects on the bridge. The reliability results may differ when considering the load effects imposed on a critical member of the bridge.

Table 3.10: Overall reliability indices (β) for the second design scenario.

Span length (m)	5	10	15	20	25	30	35	40	45	50
Reliability index (β)	9.68	10.82	15.01	10.55	10.28	10.64	10.35	10.11	10.22	10.70

3.5.2.3 *Design Scenario 3*

In consideration of the extreme case presented in the second design scenario, a more realistic design would be to allow for future expansion of the one-lane bridge to a two-lane bridge. Thus, for the third design scenario, two traffic lanes were fitted on the one-lane bridge described in Section 3.5.2.2. The same design load effects were used as for the second design scenario (see Table 3.8).

The WIM data in this case study is limited to a single measured lane, i.e. the slow lane. In order to investigate a two-lane bridge, the slow lane data needs to be utilised in such a way as to find representative load effects for the adjacent lane. A conservative assumption was made that the second lane of loading could be obtained by multiplying the slow lane load effects with a multiple lane reduction factor (MLF). The factor reduces the loading in the second lane to account for the low probability of adjacent lanes being simultaneously loaded with multiple heavy vehicles (Bakht and Mufti, 2015).

A new method for obtaining MLFs was locally developed by Van der Spuy *et al.* (2019), which proposes a MLF of 0.752 to be used to obtain the traffic load effects in the second traffic lane. The derivation of this value is based on WIM data on the National Route 1 (N1) near Kilnerpark, and it is deemed applicable to other WIM sites with comparable traffic conditions (Van der Spuy *et al.*, 2019). Roosboom and Kilner Park WIM sites are both situated on heavy freight routes. Therefore, it is a reasonable assumption to use an MLF of 0.752 in the Roosboom

case study. This assumption should be superseded by actual traffic load effects, if the WIM data at Roosboom station is extended in the future to include the second traffic lane.

The sum of the traffic load effects in the two lanes describe the global traffic load effects for the two-lane bridge. By using the MLF, the global traffic load effects can be found by multiplying the traffic load effects in the slow lane with a factor of 1.752. The monthly maxima distribution for the two traffic lanes has the same skewness and COV as the monthly maxima distribution obtained in Section 3.4 for one traffic lane. The only difference is that it has a larger mean and standard deviation. The same procedure was used as described in Section 3.4.3 to 3.4.5, where a LN3 distribution was fitted to the monthly maxima for two traffic lanes, and projected to obtain the 50-year maximum load effect distribution, which is also represented by a LN3 distribution.

The design load effects for three notional lanes were used in the reliability analysis. The overall β values are presented in Table 3.11, which shows that β exceeds the target values of 3.8 and 3.0 for all span lengths, except for a 5 m span where β is just below 3.8. The results conclude that TMH-7 provides a good reliability performance for all spans in this design scenario. The reliability indices also seem more reasonable than the extremely high values obtained for the second design scenario.

Table 3.11: Overall reliability indices (β) for the third design scenario.

Span length (m)	5	10	15	20	25	30	35	40	45	50
Reliability index (β)	3.77	4.16	7.51	6.06	6.22	6.56	6.44	6.34	6.47	6.90

3.5.2.4 *Design Scenario 4*

The fourth design scenario aims at investigating a narrow two-lane bridge, which is designed with two notional lanes (see Table 3.8). The actual traffic load effects correspond to two lanes of WIM data as in the third design scenario.

The reliability results are presented in Table 3.12. For short spans ranging from 5 to 25 metres, the overall β is less than 3.8. Whereas for spans 30 to 50 metres, β is equal to or more than 3.8. When comparing β to a target value of 3.0, only spans 5 to 15 metres obtain values smaller than 3.0. The trend in the results is similar as for the first design scenario, where a narrow one-

lane bridge was investigated. The findings indicate that NA loading again does not provide an adequate reliability level for short narrow span bridges, but performs satisfactory for longer spans.

Table 3.12: Overall reliability indices (β) for the fourth design scenario.

Span length (m)	5	10	15	20	25	30	35	40	45	50
Reliability index (β)	-0.72	-0.69	2.33	3.24	3.6	3.91	3.87	3.84	3.99	4.37

Table 3.13 provides an overview of the reliability results for the four design scenarios. It consists of the reliability indices obtained for each span length.

Table 3.13: Overall reliability indices (β) provided for each design scenario and corresponding to a 50-year period.

Span length (m)	**Design scenario 1**	**Design scenario 2**	**Design scenario 3**	**Design scenario 4**
5	-1.23	9.68	3.77	-0.72
10	-1.58	10.82	4.16	-0.69
15	1.21	15.01	7.51	2.33
20	1.65	10.55	6.06	3.24
25	2.84	10.28	6.22	3.60
30	3.79	10.64	6.56	3.91
35	4.29	10.35	6.44	3.87
40	5.12	10.11	6.34	3.84
45	5.24	10.22	6.47	3.99
50	5.62	10.70	6.90	4.37

3.5.2.5 *General Findings*

The results for the reliability analyses were considered before and after model uncertainty was included. The findings reveal that β decreases when model uncertainty is included. This is because the new distribution function for the load effects has a larger standard deviation than the distribution function before model uncertainty is included. The findings also show that the larger the COV of model uncertainty relative to that of the load effects, the larger the influence

of model uncertainty on β. In general, the influence of the model uncertainty is seen to decrease from short spans to longer spans.

Before model uncertainty was included, it was found that an irregular jump in β values occurred at a 15 m span. The determined β values were much larger than the β values obtained for the 10 m and 20 m adjacent span lengths. The β values smoothed out to more regular values when model uncertainty was included, as it had a large influence on β for 15 m spans. It is known that individual axles and axle sets govern the extreme load effects for 5 to 15 m spans (Anderson, 2006). The sample characteristics show that 10 m and 15 m spans have the lowest skewness and tend towards a normal distribution (see Section 3.4). This could be explained by the possibility that a certain axle set, e.g. a tridem axle, with a limited range of axle weights and spacing, governs the extreme loading events. The 15 m span is the only span with a negative skewness for monthly maxima, thus it takes longer to converge to its maxima domain. As a result, the 15 m span has the lowest 50-year skewness and COV. These characteristics make the 15 m span distribution much more sensitive to the location of the design load effects, in comparison to other span lengths. However, as these results are only based on a single WIM station, different results may be obtained for other stations.

3.6 Chapter Summary

This chapter discussed the case study based on WIM data from Roosboom station located on the N3. The main purpose was to investigate the reliability performance of TMH-7 in catering for normal traffic conditions on a highway bridge. This was done by performing a reliability analysis for simply supported spans ranging from 5 to 50 metres, based only on the traffic load effects. The load effect is represented by the bending moment at midspan.

The block maxima approach was applied to extract the maximum load effect per month from the WIM-based traffic load effects. With the sample skewness and COV known, applicable models were identified to represent the monthly maxima. It included the GEV distribution (representing the Weibull distribution for maxima) and the LN3 distribution. MLE provided estimates for the model parameters, while goodness-of-fit tests assessed the quality of fit of the models. The 50-year maximum load effect distribution was then obtained by means of statistical projection of the monthly maxima distribution. Furthermore, it was decided to use the LN3 distribution for the reliability analysis.

The reliability analysis was performed for four design scenarios, using FORM in *Comrel*. The limit state function included the design load effects for NA loading in TMH-7, the load effect model uncertainty and the actual traffic load effects described by the 50-year maximum load effect distribution. Lastly, the obtained reliability indices were compared to target values to estimate the reliability performance of each span length.

3.7 Conclusion

The different design scenarios provide insight into the reliability performance of NA loading for different span lengths. The results show that NA loading is not performing satisfactory for short, narrow span bridges, especially for 5 and 10 m spans. That is, when the number of notional lanes equal the number of traffic lanes on the bridge. The findings agree with previous studies that identified deficiencies in the traffic load model for short, narrow span bridges (Oosthuizen *et al.*, 1991; Anderson, 2006). However, this design scenario is not typical for highway bridges, owing to the geometry of a highway bridge deck (Burrell, Mitchell and Wolhuter, 2002) and the way notional lanes are defined in TMH-7 with floating lane widths (CSRA, 1981). For a highway bridge, the number of notional lanes typically exceeds the number of traffic lanes. As a result, the findings show that TMH-7 performs satisfactory for short and medium span bridges, ranging from 5 to 50 metres.

In addition, the results for the design scenarios reveal that TMH-7 is inherently conservative in its design for longer spans. This is evidently seen for spans ranging from 30 to 50 metres, where the obtained reliability indices exceed the target reliability indices. This finding may be the result of decisions that were made during the derivation of NA loading for longer spans. That is, decisions regarding the idealised vehicle combinations, overloading and the application of partial load factors (Anderson, 2006).

It is recommended for future studies to update the assumed sensitivity factor of -0.7 for the traffic load effects. The value is a reasonable assumption for short spans, where the traffic load is deemed to be the leading action. However, as the span length increases, the dead load of the bridge will become more dominant, leading to a reduced sensitivity of the reliability performance to the traffic load on the bridge. For this case study, a smaller sensitivity factor for longer spans would mean that the overall reliability indices would increase even more, supporting the finding that NA loading overestimates sagging moments for longer spans.

Furthermore, future research should also investigate the reliability performance of NA loading for shear forces. Anderson (2006) refers to Liebenberg's work on deriving the traffic load model for NA loading, where it is stated that the form of the loading curve was dictated by shear forces. Oosthuizen *et al.* (1991) found that NA loading also showed deficiencies for shear forces in short, narrow span bridges up to 10 m in length. There is thus a need to extend the investigation to include shear forces, as it may represent the critical load effect for some spans.

4 Kilner Park Case Study

4.1 Introduction

In this chapter, a reliability analysis of a bridge is conducted based on traffic load effects obtained from Weigh-in-Motion (WIM) data on the National Route 1 (N1). The site is located near Kilner Park in the Gauteng Province of South Africa. The WIM data includes measurements for four traffic lanes, i.e. two traffic lanes in both the northbound and southbound direction. They consist of the outer lane, identified as the slow lane, and the second outer lane, identified as a fast lane. The N1 is known to be a heavy freight route and three years of WIM data from 2015 to 2017 are available to provide a good representation of the traffic conditions at this site.

Access to four lanes of WIM data allows for the investigation of a typical highway bridge with more than one traffic lane. It was decided to conduct a critical element reliability analysis, which includes the resistance, permanent load and traffic load imposed on the critical member in proportion to transverse stiffness. The analysis provides a way to measure the reliability performance of the critical member. For optimum design, failure of a bridge is assumed to occur when the critical member fails. The failure mode under consideration is defined as follows: Failure occurs when the ultimate bending moment capacity of the critical member is exceeded by the load effects imposed on it.

The scope of this case study is limited to the investigation of a single span bridge designed for two traffic lanes with paved shoulders. The load effect under consideration is the bending moment at midspan for the ultimate limit state (ULS). It was decided to investigate a 20 m reinforced concrete bridge with a twin spine deck, where the critical member is represented by a single flanged spine beam. A 20 m span is typically found in highway bridges. Furthermore, a twin spine deck is an economical choice for the design of a 20 m span bridge (Benaim, 2008).

4.2 Methodology

The main objective of this case study was to carry out a critical element reliability analysis on the selected critical member. The first step was to design the twin spine deck according to Technical Methods for Highways 7 (TMH-7). The sizing of members was primarily based on the guidelines set out in Robert Benaim's book on *The Design of Prestressed Concrete Bridges: Concepts and Principles* (2008). After finding the geometric and material properties of the

bridge deck, the properties were used to model the bridge deck in *Midas Civil*. A simple grillage analysis served to obtain the design load effects of the critical spine beam in accordance with the loading requirements of TMH-7 Part 2 (CSRA, 1981). The loading accounts for the permanent load and traffic load on the bridge deck, where the traffic load is representative of NA loading in TMH-7. Provisions of TMH-7 Part 3 (CSRA, 1989) subsequently allowed for the calculation of the required reinforcement quantities.

The second step focused on finding the load effects generated in the critical spine beam due to the actual traffic on the bridge. A simple transverse influence line from the grillage model, along with the traffic load effects corresponding to the WIM data, led to the calculation of the total combined traffic load effects in the spine beam.

The third step considered the probabilistic modelling of the combined traffic load effects in the spine beam. The block maxima approach enabled the assessment of the extreme traffic load effects, where a block period of a month was considered. Thereafter, the parameters of the selected model were estimated with the maximum likelihood estimation (MLE) method. In order to determine the applicability of the selected model to the data set, diagnostic plots and hypothesis testing were utilised. This was followed by the statistical projection of the monthly maxima distribution to obtain the maximum load effect distribution for a 50-year reference period.

Finally, the fourth step proceeded with the formulation of the limit state function to describe the failure mode in terms of the resistance, dead load and traffic load effects for the critical spine beam. The probabilistic description of the traffic load effects is based on the WIM data, while the rest of the basic variables are described by probabilistic models adopted from literature. The First Order Reliability Method (FORM), along with the limit state function, was then employed to perform the critical element reliability analysis. As a result, the analysis obtained reliability indices corresponding to a 50-year period that were compared to target reliability indices. Lastly, a sensitivity analysis was conducted to determine the relative contribution of each variable on the obtained reliability indices.

4.3 Bridge Deck Design and Analysis

4.3.1 *Bridge Deck Properties*

This section describes the properties of the 20 m twin spine deck. Some advantages of the twin spine deck over a solid slab deck, is that it increases the reinforced concrete lever arm and reduces the self-weight of the deck (Benaim, 2008). The dimensions of a twin spine deck of an existing reinforced concrete bridge in South Africa (Van der Spuy and Niehaus, 2019), were considered to find preliminary dimensions for the bridge deck. The dimensions were then amended for a 20 m span length and to concur with the guidelines set out in Benaim's book on *The Design of Prestressed Concrete Bridges: Concepts and Principles* (2008). The cross-sectional layout of the bridge deck, together with the traffic lane arrangement, is provided in Figure 4.1.

The following decisions were made regarding the geometric properties of the bridge deck:

- According to Benaim (2008), the ratio between the span of the side cantilever and the span of the centre slab should range between 2.3 and 2.8. This ratio prevents the spine beams from rotating under dead loads. For the bridge deck, it was decided to use a side cantilever of 2.75 m and a centre slab of 6.45 m, which obtains a ratio of 2.345.
- The span/depth ratio of a simply supported span generally ranges between 1/20 and 1/15 (Benaim, 2008). Benaim (2008) recommends a minimum ratio of 1/20 and a more typical ratio of 1/18 for twin spine decks. A 1/20 ratio was decided on, which resulted in a 1 m deck height. Furthermore, a trapezoidal web with a bottom width of 1.8 m was selected for the spine beams.
- Benaim (2008) recommends a minimum slab thickness of 200 mm for cantilevers that span between 1.4 to 1.7 metres, depending on the loading code used. When the cantilever has a longer span, a haunch should be added to the cantilever with a root thickness equal to or more than 1/7 or 1/9 of the cantilever length (Benaim, 2008). The cantilever length refers to the distance from the edge of the cantilever to the root of the haunch. For the bridge deck, this length was calculated as 1.75 m. Thus, it was decided to use a 200 mm slab thickness for the edge of the cantilever, which increases to 300 mm at the root of the haunch.
- The slab between spine beams should provide sufficient transverse stiffness for the deck, in order to effectively distribute loads transversely to the spine beams. A slab thickness of (clear span)/25 to (clear span)/20 is recommended, where the clear span

stretches between the two spine beams (Benaim, 2008). For the bridge deck, a slab thickness of 250 mm was chosen for a clear span of 4.45 m.

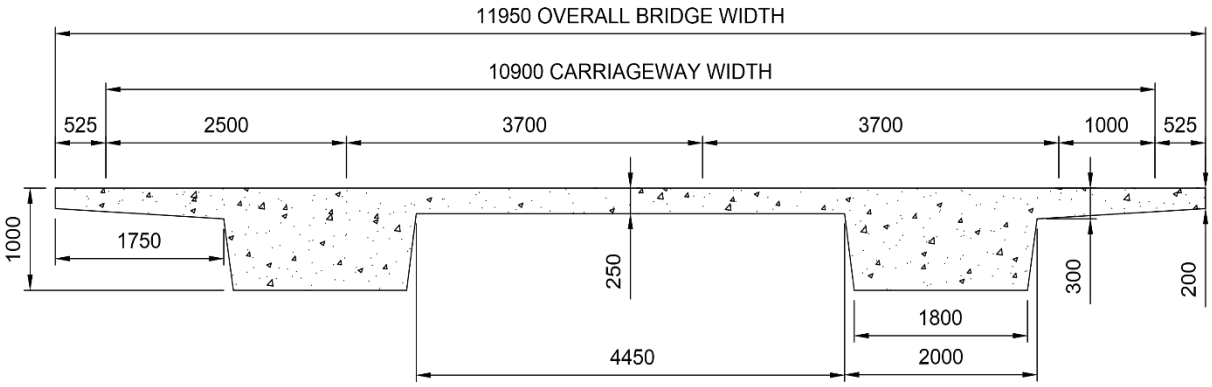

Figure 4.1: Cross-section of bridge deck with the lane arrangement (units in mm).

For the material properties of the bridge deck, a concrete cube strength (f_{cu}) of 50 MPa was selected, which corresponds to a modulus of elasticity (E) of 34 GPa. Moreover, it was decided to use a density of 25 kN/m^3 for the reinforced concrete.

For the bridge analysis, dead loads and superimposed dead loads, along with the traffic load were considered. The dead load consists of the self-weight of the bridge deck (see Figure 4.1), while the superimposed dead loads include the asphalt road surfacing and parapets on the deck. A thickness of 40 mm (SANRAL, 2010) and a density of 21 kN/m^3 (CSRA, 1989) were assumed for the asphalt surfacing. Typically, a F-shape Type A parapet is used for a highway bridge (SANRAL, 2012). Therefore, the weight of the parapets was represented by a line load of 10 kN/m placed on both edges of the bridge deck in the longitudinal direction.

4.3.2 *Bridge Deck Analysis in Midas Civil*

The bridge deck was modelled in *Midas Civil* (MIDAS, 2016), an engineering software used for the design of bridges and other civil structures, using a simple grillage analysis. A grillage analysis involves modelling a structure using a two-dimensional grid pattern and assuming linear-elastic behaviour. The grid pattern allows for the bridge deck to be seen as a series of longitudinal and transverse elements rigidly connected at the nodes. The grid layout for this case study is illustrated in Figure 4.2, where the longitudinal and transverse members are

identified. Moreover, the cross-sectional properties of the spine beams, representing the longitudinal members, are shown in Figure 4.3.

The deck slab was modelled using 2 m wide beams, representing the transverse members. The beams provided for the actual stiffness of the slab by describing the member thickness in accordance with the slab thickness in Figure 4.1. No density was assigned to the transverse members as not to introduce additional loading.

A dummy beam was created as a longitudinal member on the edge of the bridge deck, in order to apply the parapet line load to the deck. No density was assigned to the dummy beam, and it was given a very small cross-section to make its stiffness negligible.

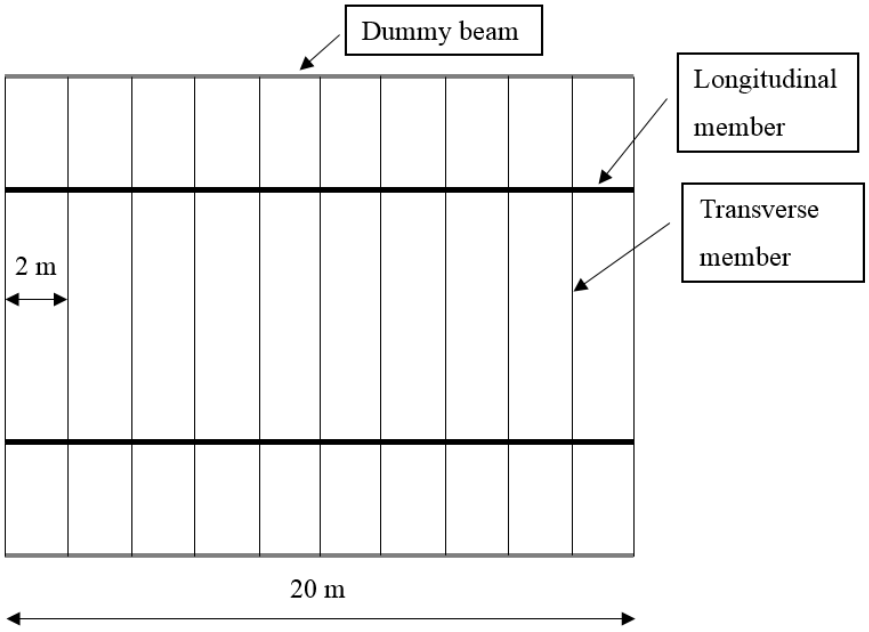

Figure 4.2: Plan view of grid layout of bridge deck.

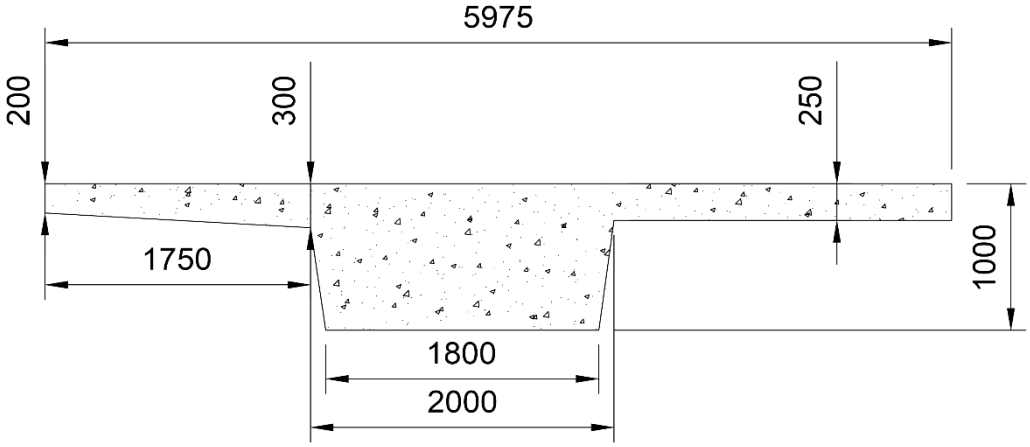

Figure 4.3: Cross-section of spine beam modelled in *Midas Civil* as a longitudinal member.

The bridge was assumed simply supported; thus, provision was made for pinned connections. The node numbering of the grillage model is shown in Figure 4.4. Node 12 and 23 were prevented from translation in the x, y and z-direction, while node 22 and 33 were prevented from translation in the y and z-direction.

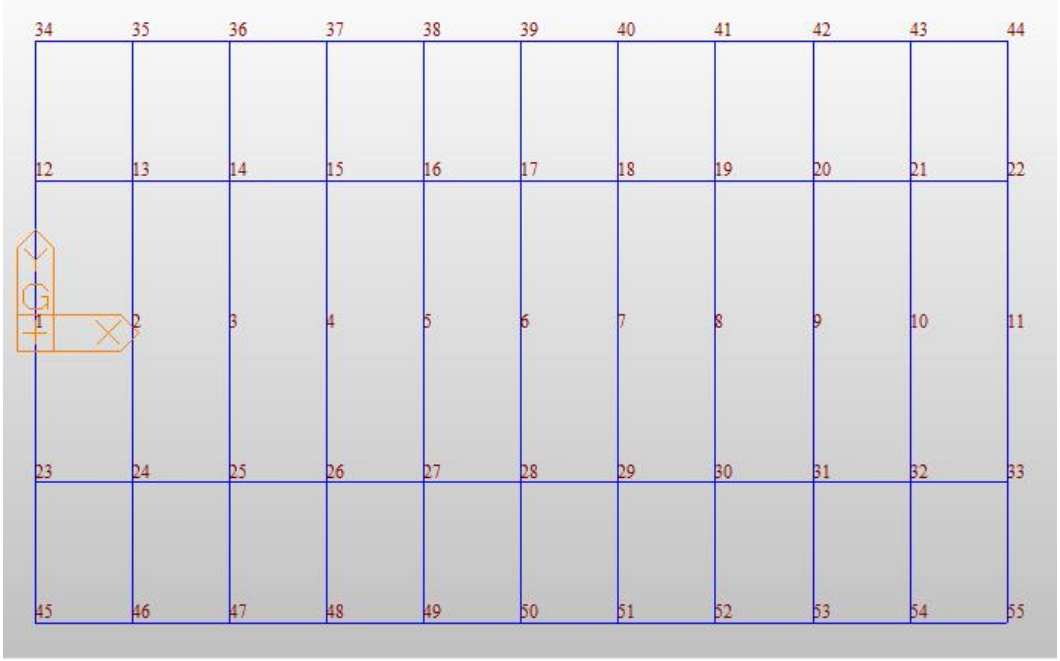

Figure 4.4: Plan view of node numbering for grillage model in *Midas Civil*.

The loading, as set out in Section 4.3.1, was applied to the grillage model. *Midas Civil* has TMH-7's traffic load model built in, which allows NA loading to be applied on the bridge deck. Regular optimisation is recommended for NA loading, where the loading is shifted between the extreme left, middle or extreme right of the traffic lane, to obtain the worst loading position. *Midas Civil* also allows for the partial loading of an influence line in order to obtain the maximum loading at the specific location. Thus, it alleviates the need to compensate for partial loading with the *k*-factor, as discussed in Section 2.2.4.

A carriageway width of 10.9 m requires three notional lanes, with a width of 3.633 m each, to be considered for NA loading (CSRA, 1981). For the analysis, a vehicle width of 1.9 m was assumed (CSRA, 1981). *Midas Civil* applies the NA loading as a moving load. When the point of interest is specified, the NA loading is positioned in such a way as to provide the worst loading at that point. The loading is then accordingly converted to represent a static load. For the bridge deck, the point of interest was specified at node 17 (see Figure 4.4), which is the

mid-section of the selected critical spine beam. The corresponding loading arrangement is shown in Figure 4.5. As the deck is symmetrical, either one of the spine beams could have been selected as the critical spine beam.

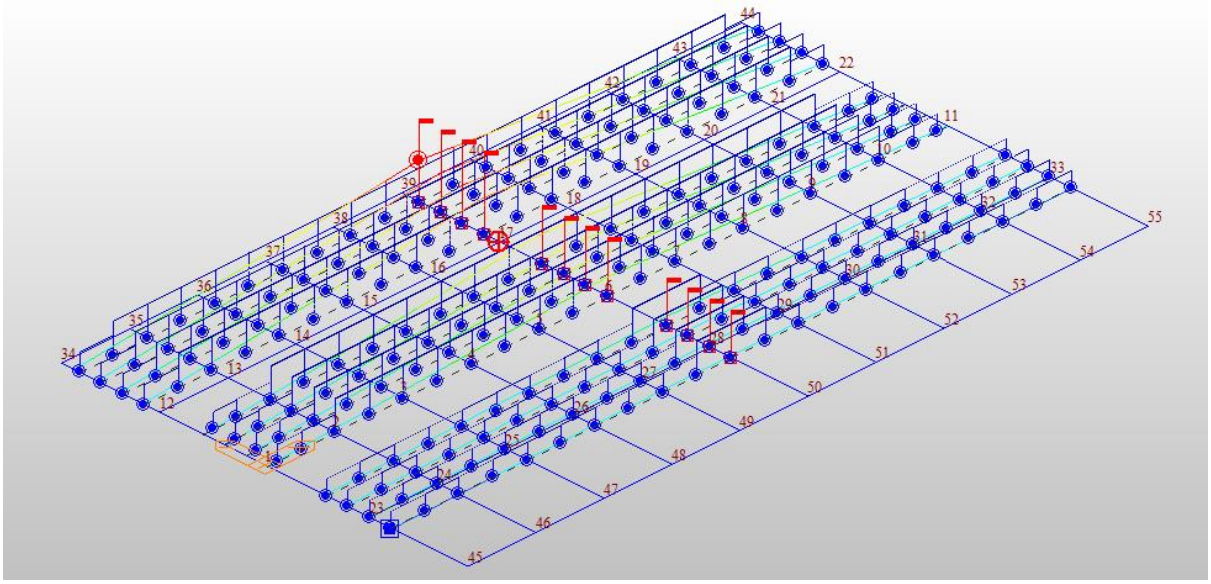

Figure 4.5: Position of NA loading for design of spine beam at midspan.

Partial factors were applied to the loading in order to find the ultimate design bending moment for the spine beam at midspan. The ULS partial factors are based on Combination 1 of Table 17 in TMH-7 Part 2 (CSRA, 1981), and consist of the partial load factor (γ_{fL}) and the partial effect factor (γ_{f3}). For the dead load and superimposed dead loads, γ_{fL} = 1.2 and γ_{f3} = 1.1 were applied (CSRA, 1981), which equates to a partial factor of 1.32. For NA loading, γ_{fL} = 1.5 and γ_{f3} = 1.1 were used (CSRA, 1981), which equates to a partial factor of 1.65. NA loading accounts for dynamic load effects with the Swiss impact factor (φ_2), which for a 20 m simply supported bridge is equal to 0.2 (see Equation 2.3 in Section 2.2.3). In order to obtain static load effects from NA loading in the analysis, the Swiss impact factor was removed by dividing NA loading with a factor of 1.2.

The unfactored global reaction forces and bending moments at midspan were obtained from the grillage analysis. Unfactored load effects refer to characteristic load effects, i.e. before partial factors are applied. To confirm the soundness of the grillage model, these values were compared to unfactored global reaction forces and bending moments calculated by hand. The comparison is presented in Table 4.1.

The results show that the grillage model adequately represents the bridge deck. The small difference shown for the parapet bending moment is due to the small longitudinal stiffness of the dummy beam. The difference between the NA loading results is caused by the difference in the way partial loading of an influence line is addressed. The grillage model allows for a partial loading of an influence line, and thus eliminates the use of a *k*-factor, whereas the analytical model uses a *k*-factor to account for partial loading. As can be seen from the results, the analytical model produces more conservative load effects due to the approximate *k*-factor.

Table 4.1: Check global reactions and bending moments for the grillage model.

Load component	**Reaction force at support (kN)**		**Bending moment at midspan (kNm)**	
	Grillage model	Analytical model	Grillage model	Analytical model
Dead load	1460.6	1460.6	7303.1	7303.1
Parapets	200	200	1006.7	1000
Asphalt surfacing	91.6	91.6	457.8	457.8
NA loading	863.7	941.2	5279.5	5390.8

From the grillage model, the design bending moment for ULS was found for the selected critical spine beam at midspan. The design value for each load component is shown in Table 4.2. Table 4.2 also includes the characteristic (unfactored) moment for each load component, which is later used in the reliability analysis (see Section 4.6).

Table 4.2: Maximum bending moment of critical spine beam at midspan.

Load component	**Maximum bending moment at ULS (kNm)**	
	Unfactored	Factored
Dead load	3651.6	4820.1
Parapets	503.3	664.4
Asphalt surfacing	228.9	302.2
NA loading	3528.3	5821.6
Total = Σ(load components)	7912.1	11608.3

4.3.3 *Spine Beam Design*

The bending moment resistance of the spine beam at midspan is dependent on the area of longitudinal steel reinforcement provided at the section. With the ultimate design bending

moment known, the required area of steel reinforcement was determined. For design, the spine beam cross-section was idealised as a T-beam. The idealised cross-section of the spine beam is shown in Figure 4.6. The geometric properties were calculated to give an adequate representation of the spine beam properties. Attention was given especially to the cross-sectional area, the moment of inertia, and the centroid of the section.

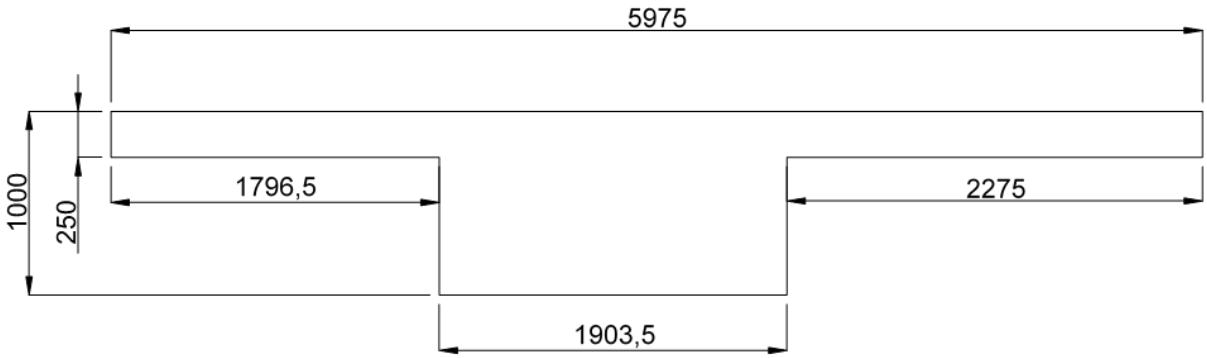

Figure 4.6: Idealised cross-section of spine beam.

Table 4.3 provides the input parameters assumed for the calculation of the steel reinforcement in the spine beam. The parameters are primarily based on TMH-7 Part 3 (CSRA, 1989), though the South African National Standard, SANS 10100-1 (2000), was also consulted. Two layers of steel reinforcement was assumed, which resulted in an average effective depth (d) of 895 mm from the top of the beam to the tension reinforcement.

Table 4.3: Input parameters to determine the steel reinforcement.

Input parameter	**Measurement**
Effective flange width	5.7 m
Coarse aggregate size	19 mm
Spacer bar between layers	20 mm
Nominal cover	40 mm
Shear link diameter	16 mm
Steel bar diameter	40 mm
Steel yield strength	450 MPa

The ultimate moment of resistance is equal to the sum of the design bending moments for the permanent and variable loads. The calculation is done with Equation 4.1, where $M_{d,R}$ is the

ultimate moment of resistance, $M_{d,G}$ is the design moment for permanent loads and $M_{d,Q}$ is the design moment for variable loads. The permanent loads include the dead load and superimposed dead loads of the bridge deck, while the variable load represents the traffic load. According to the grillage model (see Table 4.2), $M_{d,R}$ is equal to 11608.3 kNm for the spine beam.

$$M_{d,R} = M_{d,G} + M_{d,Q} \tag{4.1}$$

Equation 4.2 and 4.3, obtained from TMH-7 Part 3 (CSRA, 1989), were simultaneously solved to obtain the area of tension reinforcement (A_s) for the spine beam. For the equations, f_y denotes the steel yield strength, z denotes the internal lever arm, b denotes the effective flange width and d denotes the effective depth to the tension reinforcement. The ultimate moment of resistance is denoted by M_u and it is equal to the value obtained for $M_{R,d}$.

$$M_u = 0{,}87 f_y A_s z \tag{4.2}$$

$$z = \left[1 - \frac{1{,}1 f_y A_s}{f_{cu} b d}\right] d \tag{4.3}$$

The solution for the tension reinforcement is summarised in Table 4.4. The section is ductile with $z = 0.93d$ and the compression block situated in the flange. Moreover, no compression reinforcement is required. For the reinforcement layout, 15 bars were placed in the first bottom layer and 14 bars in the second bottom layer, with a clear spacing of 75 mm between bars.

Table 4.4: Area of tension reinforcement for the spine beam.

Properties	**Measurement**
Area of Y-40 bar	1256.6 mm^2
A_s required	35587 mm^2
No. of bars required	28.3
No. of bars provided	29
A_s provided	36442 mm^2

4.4 Traffic Load Effects on Critical Spine Beam

This section considers the actual traffic load effects obtained from WIM data. The objective was to find the influence of the traffic load effects in each traffic lane, on the critical spine beam. First, the influence line describing the lateral load distribution over the carriageway width was obtained. Depending on the position of the traffic lane on the bridge deck, the concurrent traffic load effects in each lane were multiplied by lateral load distribution factors to obtain the load contribution of each lane on the critical spine beam.

4.4.1 *Lateral Load Distribution*

The lateral distribution of loading on the bridge deck was considered in order to accurately characterise the traffic load effects imposed on the critical spine beam. Benaim (2008) explains the structural response of a spine beam when a load is applied to its centreline at midspan. The rotation of the spine beam is prevented by the stiffness of the slab surrounding the load. This allows load effects to be generated in the slab, which transfers a proportion of the loading to the other spine beam. A transverse influence line can be used to describe the proportion of longitudinal bending moment carried by the spine beam at the section of interest. This is done by positioning a unit point load or longitudinal distributed load at the section, and varying its position across the carriageway width (Benaim, 2008).

For the study, a uniformly distributed line load applied over the span of the bridge was chosen as unit load to represent the traffic loading on the bridge. As the full length of a truck can be carried by a 20 m span bridge, a uniformly distributed load is deemed more representative than a unit point load.

The grillage model in *Midas Civil* (Section 4.3.2) was used to obtain the influence line for the lateral load distribution on the critical spine beam at midspan. A longitudinal unit load of 10 kN/m was placed on the edge of the carriageway and moved across the carriageway width. At each position, the bending moment in the critical spine beam was measured at midspan and the lateral load distribution factor (LLDF) was determined. The LLDF is simply the ratio between the bending moment generated in the spine beam and the global bending moment on the bridge deck.

Table 4.5 summarises the proportion of the global bending moment carried by each spine beam, corresponding to the position of the unit load on the carriageway width. For illustrative

purposes, the critical spine beam is called Beam 1 and the other spine beam is called Beam 2. The table also includes the LLDFs for the critical spine beam, i.e. Beam 1. In Table 4.5, Location 1 and 11 are positioned at the edges of the carriageway width. Location 3 and 9 are at the centreline of Beam 1 and 2, respectively. And Location 6 is at the centreline of the carriageway width, where the global bending moment is distributed evenly between the two spine beams.

Table 4.5: Lateral load distribution at midspan.

Location	**Position from edge of carriageway width closest to Beam 1 (m)**	**Bending moment in Beam 1 (kNm)**	**Bending moment in Beam 2 (kNm)**	**LLDF for Beam 1**
1	0	588	-88	1.18
2	1.177	515	-15	1.03
3	2.354	442	58	0.88
4	3.386	378	122	0.76
5	4.418	314	186	0.63
6	5.450	250	250	0.50
7	6.482	186	314	0.37
8	7.514	122	378	0.24
9	8.546	58	442	0.12
10	9.723	-15	515	-0.03
11	10.900	-88	588	-0.18

The LLDFs are illustrated in Figure 4.7, where the line describes the proportion of the global bending moment in Beam 1.

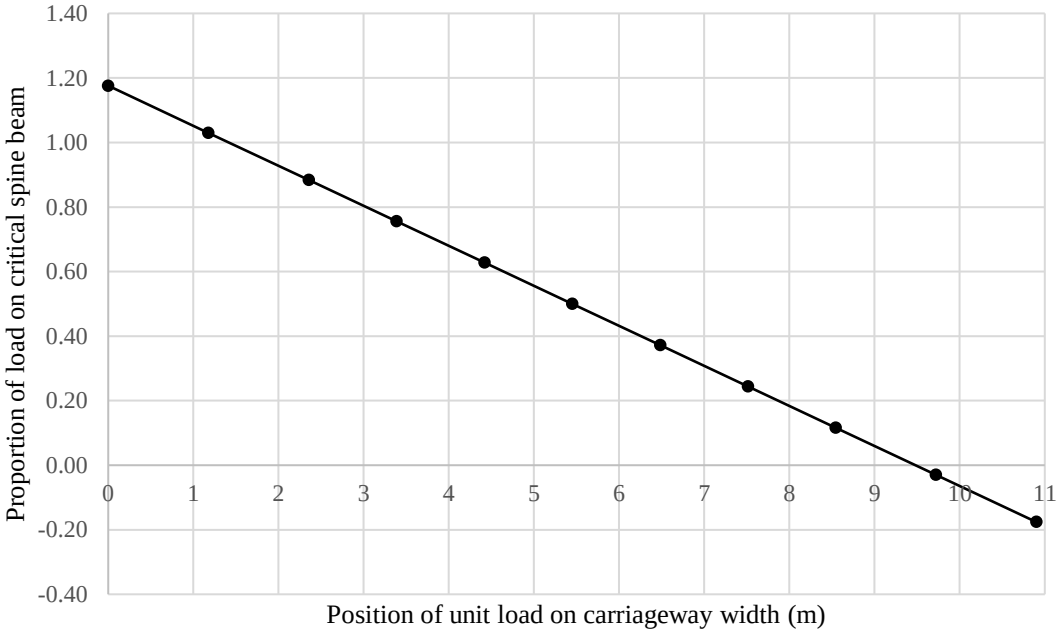

Figure 4.7: Lateral influence line of critical spine beam at midspan.

4.4.2 *Calculation of Load Effects on Critical Spine Beam*

The traffic load effects used in this case study are described by the bending moment at midspan and based on WIM data from a site near Kilner Park on the N1. The traffic load effects were obtained from a previous study (Van der Spuy *et al.*, 2019) that used a moving load analysis to derive the traffic load effects in each traffic lane. An overview of the calculation of the traffic load effects is given in Chapter 3 Section 3.3.1. In addition, the time history of the traffic load effects was used to find the concurrent load effects in each traffic lane (Van der Spuy *et al.*, 2019), i.e. the load effects that occur simultaneously.

The concurrent load effects at any given time can be combined, along with their corresponding LLDFs, to obtain the combined load effects carried by the critical spine beam. This is illustrated in Equation 4.4, where Q_1, Q_2,…, Q_n represent concurrent traffic load effects in each traffic lane. Here, n is the number of traffic lanes on the bridge, Q_1 is the load effect in the first traffic lane (closest to the critical spine beam), Q_2 is the load effect in the second traffic lane and Q_n is the load effect in the n-th traffic lane (furthest away from the critical spine beam). Here, Q_1, Q_2,..., Q_n represent load effects that occur at the same time. The combined load effects, relating to the concurrent load effects and their respective LLDFs, are denoted by $Q_{combined}$.

$$Q_{combined} = LLDF_1(Q_1) + LLDF_2(Q_2) + \ldots + LLDF_n(Q_n) \quad (4.4)$$

A discussion follows, where firstly it is explained how the relevant LLDFs for each traffic lane were determined. Secondly, it describes how the actual traffic lanes were used in different combinations to find the combined load effects on the critical spine beam. The different combinations are called load cases. Lastly, it describes how the maximum load effects on the critical spine beam were extracted from the data set of combined load effects.

With the help of the influence line in Figure 4.7, the LLDF for each traffic lane on the bridge was determined. The 20 m span bridge is designed for two traffic lanes with a width of 3.7 m each. In order to represent the worst loading on the critical spine beam, the actual traffic lanes were shifted to the edge of the carriageway width closest to the critical spine beam. The vehicle centreline was assumed to follow the traffic lane centreline. The position of each traffic lane's centreline on the carriageway width was obtained and then used to find the LLDF at that position. Subsequently, the centrelines of the first and second traffic lane were positioned at 1.85 m and 5.55 m from the edge of the carriageway width. As a result, the corresponding LLDFs for the first and second traffic lanes are 0.95 and 0.49, as shown in Figure 4.8.

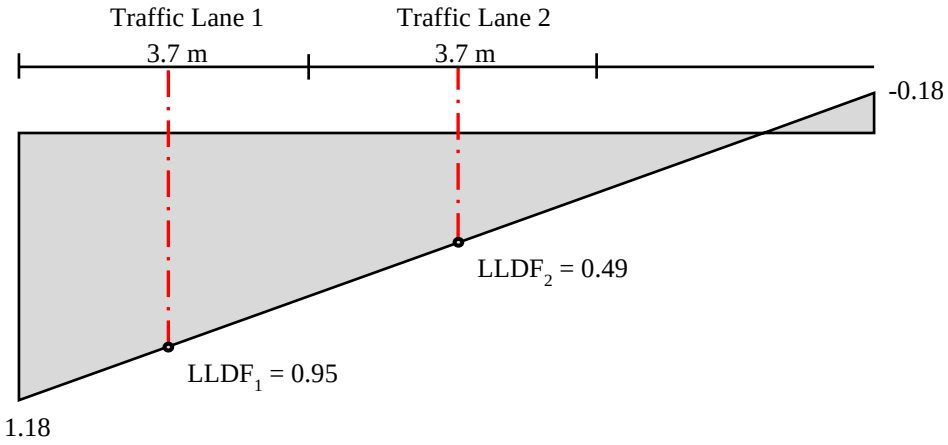

Figure 4.8: Lateral load distribution factors corresponding to the position of traffic load effects in two lanes.

Following the investigation of two traffic lanes, three traffic lanes were fitted on the bridge deck to determine the influence an additional traffic lane would have on the combined load effects. A traffic lane width of 3.5 m was assumed, and the lanes were shifted to the edge of the carriageway width. Subsequently, the centrelines of the first, second and third traffic lanes

were found at 1.75 m, 5.25 m and 8.75 m from the edge of the carriageway width. The corresponding LLDFs are 0.96, 0.52 and 0.09, as seen in Figure 4.9. The LLDF of 0.09 for the third traffic lane is very small. Hence, the loading in this lane has a very small contribution to the combined load effects imposed on the critical spine beam.

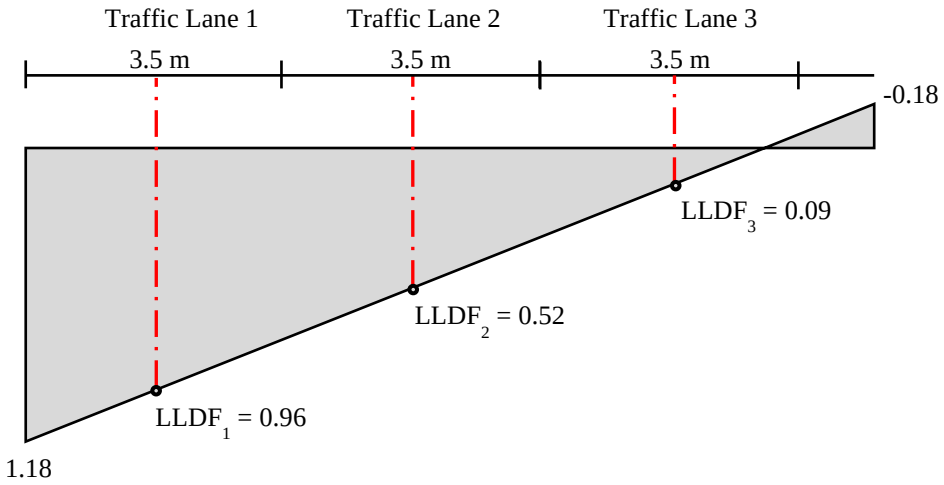

Figure 4.9: Lateral load distribution factors corresponding to the position of traffic load effects in three lanes.

The WIM station provides data for the two outer traffic lanes in the northbound (*Nb*) and southbound (*Sb*) direction. Figure 4.10 shows the notation adopted from (Van der Spuy *et al.*, 2019) to describe the traffic lanes. The notations *Nb1* and *Sb1* refer to the slow lanes, while *Nb2* and *Sb2* refer to the fast lanes in the northbound and southbound direction.

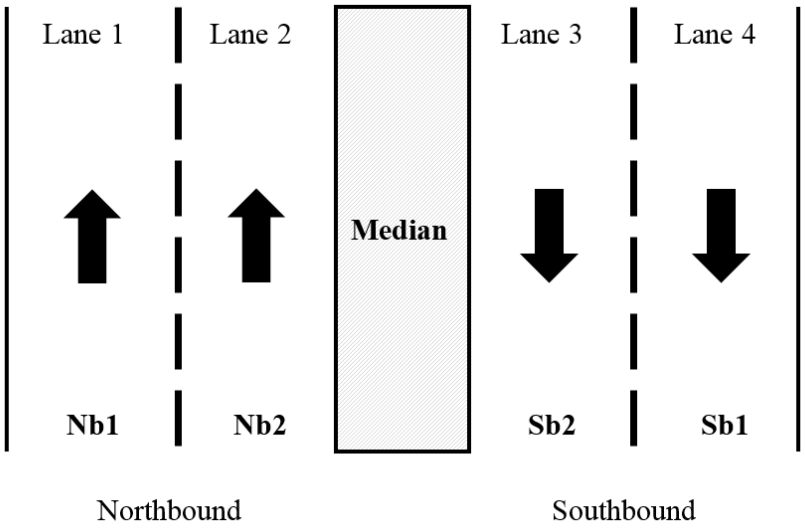

Figure 4.10: Traffic lane notation.

For the case study, different load cases were considered in calculating the combined load effects on the critical spine beam. The load cases are described by different combinations of the actual traffic lanes on the bridge deck. Moreover, the load cases provide for the possibility that the critical spine beam may be located under the slow lane (outer lane) or the fast lane (inner lane). That is, considering a single direction of traffic and the fact that the bridge is symmetrical with only two spine beams.

The load cases, describing two traffic lanes on the bridge, are presented in Table 4.6. The table shows which traffic lane is located above the critical spine beam. This traffic lane relates to $LLDF_1$ equal to 0.95, and thus the load effects in this lane correspond to Q_1 (see Equation 4.4). The other traffic lane then relates to $LLDF_2$ equal to 0.49, and the load effects in this lane correspond to Q_2 in Equation 4.4.

Table 4.6: Load cases used to find combined load effects on critical spine beam, when considering two traffic lanes.

Load Case	**Traffic lane corresponding to Q_1**	**Traffic lane corresponding to Q_2**
1	*Nb1*	*Nb2*
2	*Sb1*	*Sb2*
3	*Nb2*	*Nb1*
4	*Sb2*	*Sb1*
5	*Nb1*	*Sb1*
6	*Sb1*	*Nb1*

The load cases, for three traffic lanes fitted on the bridge deck, are presented in Table 4.7. The three lanes consist of a slow lane (outer lane) and two fast lanes, which represents the typical lane arrangement of three lanes in one direction. Here, the critical spine beam is assumed below the slow lane. Thus, the slow lane relates to $LLDF_1$ equal to 0.96, and the traffic load effects in this lane correspond to Q_1 in Equation 4.4. The second traffic lane relates to $LLDF_2$ equal to 0.52 and the traffic load effects correspond to Q_2. Lastly, the third traffic lane relates to $LLDF_3$ equal to 0.09 and the traffic load effects correspond to Q_3.

Table 4.7: Load cases used to find combined load effects on critical spine beam, when considering three traffic lanes.

Load Case	**Traffic lane corresponding to Q_1**	**Traffic lane corresponding to Q_2**	**Traffic lane corresponding to Q_3**
7	*Nb1*	*Nb2*	*Sb2*
8	*Sb1*	*Sb2*	*Nb2*

Similar to Roosboom Case Study in Chapter 3, the block maxima approach was utilised to assess the extreme traffic load effects on the critical spine beam. With three years of data available, the sample size was deemed sufficient to use a block period of a month. This block period eliminates temporal variations and less critical loading events that would surface in a smaller block period. By using a large enough block period, the dependencies between loading events are also eliminated.

For each load case, the combined load effects were captured at time steps of 0.02 s, thus, providing a continuous output of bending moments at midspan. Equation 4.4 is restated in Equation 4.5, to show how the maximum load effect per month, denoted by Q_{max}, is extracted from the combined load effects per month, denoted by the vector $\{Q_{combined}\}$.

$$\{Q_{combined}\} = LLDF_1\{Q_1\} + LLDF_2\{Q_2\} + \ldots + LLDF_n\{Q_n\}$$
$$Q_{max} = max\{Q_{combined}\} \tag{4.5}$$

Equation 4.5 was used to extract Q_{max} for each month in the recorded period of three years. The new data set consists of the monthly maximum load effects carried by the critical spine beam, hereafter referred to as combined monthly maxima. A data set of combined monthly maxima were obtained for each load case.

To give an example, consider Load Case 1, where *Nb1* is situated above the critical spine beam and *Nb2* is the adjacent traffic lane. Then, *Nb1* corresponds to $LLDF_1$ and *Nb2* corresponds to $LLDF_2$. Considering Equation 4.5, the concurrent load effects in *Nb1* and *Nb2* are then denoted by Q_1 and Q_2, respectively. The combined load effects ($Q_{combined}$), obtained from the concurrent load effects and corresponding LLDFs, are then captured every 0.02 seconds for the duration of the recorded period. Finally, the maximum load effect per month is extracted from the combined load effects to obtain a data set of combined monthly maxima.

4.5 Probabilistic Modelling of Traffic Load Effects

The extreme traffic load effects are represented by the combined monthly maxima. This section provides a discussion on the assessment and probabilistic modelling of the extreme traffic load effects, in finding the maximum load effect distribution for a 50-year reference period. This period agrees with target reliability indices found in existing standards such as the Eurocode, EN 1990.

4.5.1 *Statistical Characteristics and Model Selection*

For each load case, the statistical characteristics describing the combined monthly maxima were obtained. The sample mean, standard deviation, skewness and coefficient of variation (COV) were calculated according to Equation 2.13, 2.14 and 2.15 in Section 2.3.1. These characteristics are summarised in Table 4.8 for each load case.

Table 4.8 shows that two traffic lanes in the southbound direction (Load Case 2 and 4) provide a larger mean for the combined monthly maxima, compared to two traffic lanes in the northbound direction (Load Case 1 and 3). As the traffic load effects corresponding to Q_1 have the largest LLDF, the combined monthly maximum is typically obtained at the time increment when the maximum load effect from Q_1 occurs. Table 4.8 further shows that the COV of the load cases varies between 0.061 and 0.081. The skewness varies between a minimum of 0.301 for Load Case 4 and 1.839 for Load Case 3. This shows that the right tail of the distribution is quite sensitive to which traffic lanes are considered together and which traffic lane is situated closest to the critical spine beam.

Load Case 5 and 6 represent two slow lanes on the bridge. One would assume that more heavy side-by-side trucks would be present for these cases, and that at least the mean value would be larger than for load cases with a slow lane and a fast lane (see Load Case 1 to 4). However, Table 4.8 shows that Load Case 5 and 6 have similar characteristics to Load Case 1 to 4. This suggests that the combined monthly maximum generally occurs when the maximum load effect for Q_1 occurs and there is a small or no load effect in the other lane. Furthermore, the characteristics of Load Case 7 and 8 (with three traffic lanes) are similar to that of the load cases with two traffic lanes. This may be because the contribution of the third traffic lane on the critical spine beam is negligibly small.

Table 4.8: Sample characteristics for combined monthly maxima on critical spine beam.

Load Case	Mean (kNm)	Standard deviation (kNm)	COV	Skewness
1	1948.7	158.2	0.081	0.408
2	2053.4	137.6	0.067	0.777
3	1849.0	112.4	0.061	1.839
4	1985.0	153.1	0.077	0.301
5	1955.3	135.6	0.069	0.413
6	2005.1	126.7	0.063	0.450
7	1987.3	155.4	0.078	0.380
8	2101.5	136.2	0.065	1.010

A similar approach to Roosboom Case Study was followed to select an applicable model to represent the combined monthly maxima. The sample skewness and COV for each load case can be used to find an applicable model to represent the sample. This approach was developed by Holický (2013) and adjusted to include the Fréchet and Weibull distribution. The relation between the COV and skewness was used to plot the characteristics of each load case on the diagram in Figure 4.11, where the COV is denoted by V. From the figure it can be seen that the sample skewness varies considerably, which makes the three-parameter lognormal (LN3) distribution an appropriate model.

The generalised extreme value (GEV) distribution can represent the Gumbel, Fréchet or Weibull distribution for maximum values. The GEV distribution was also assessed, but only for comparative purposes. It was decided not to use the Weibull distribution in order to avoid characterising the combined monthly maxima with a fixed upper bound, which remains constant irrespective of the reference period projected to. See Chapter 3 Section 3.4.7 for more on this topic. It was also decided not to use the Gumbel distribution, as the fixed skewness could overestimate or underestimate the combined monthly maxima. In using the LN3 distribution to assess the extreme traffic load effects, the case study stays consistent with Roosboom Case Study.

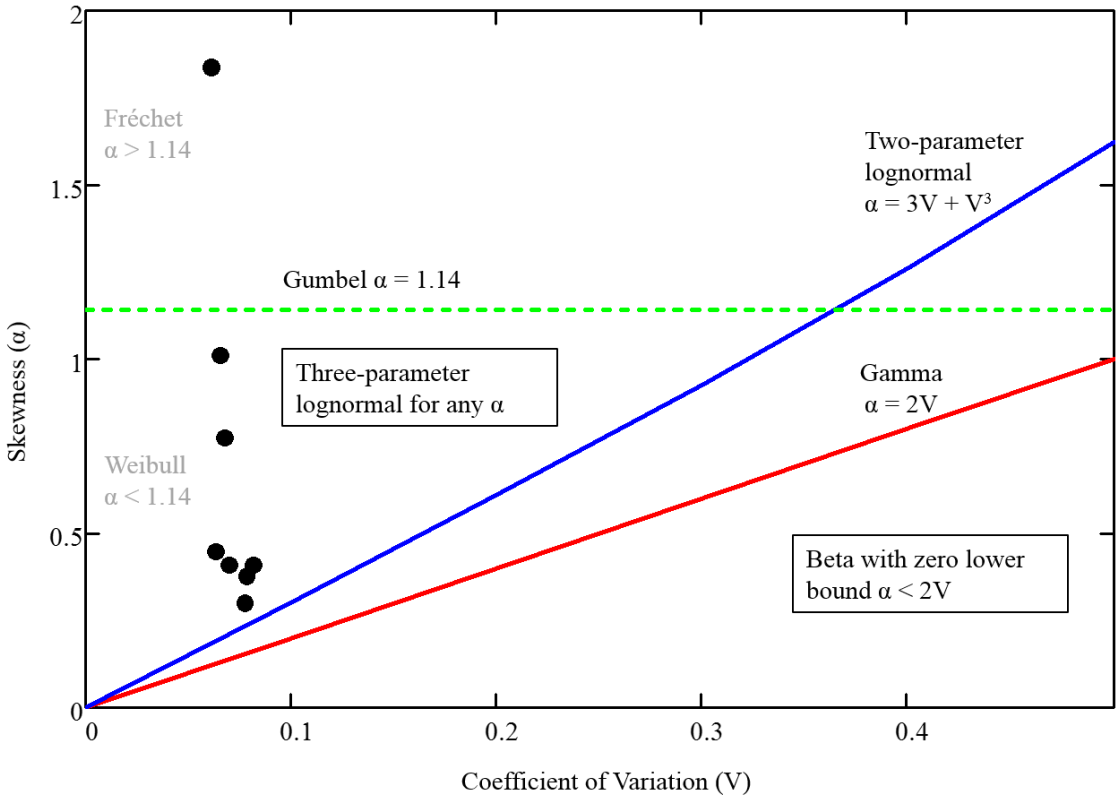

Figure 4.11: A diagram where the relation between skewness and coefficient of variation is used to find applicable models to represent the combined monthly maxima for each load case (Holický, 2013).

4.5.2 *Estimation of Model Parameters and Assessment of Selected Model*

Goodness-of-fit tests were used to assess the quality of fit of the LN3 distribution in representing the combined monthly maxima. The tests consist of diagnostic plots and hypothesis testing, whereas the former is the primary focus. The *R* code in Appendix B provides the procedure to apply the goodness-of-fit tests.

MLE was used in *Mathcad* to estimate the model parameters describing the combined monthly maxima for each load case. The log-likelihood function in Section 3.4.3 Equation 3.2 was used to obtain the MLE parameters, which include the mean, standard deviation and skewness. The MLE parameters are summarised in Table 4.9, together with the COV and lower bound of the LN3 distribution.

Table 4.9: MLE parameters for combined monthly maxima fitted with a LN3 distribution.

Load Case	Mean (kNm)	Standard deviation (kNm)	Skewness	COV	Bound (kNm)
1	1949.1	162.7	1.025	0.083	1455.4
2	2053.9	142.6	1.370	0.069	1722.5
3	1849.3	112.5	1.880	0.061	1650.6
4	1985.1	153.9	0.665	0.078	1279.7
5	1955.3	134.2	0.519	0.069	1171.2
6	2005.1	125.6	0.553	0.063	1316.1
7	1987.6	158.2	0.897	0.080	1443.3
8	2102.1	141.1	1.614	0.067	1818.2

The MLE parameters were then used to find diagnostic plots in *R* to graphically confirm the appropriateness of using the LN3 distribution. The diagnostic plots primarily include the Q-Q plot and P-P plot, followed by plots for the theoretical and empirical probability density function and cumulative distribution function (CDF). Definitions of the diagnostic plots are given in Chapter 3 Section 3.4.4.1, and in summary they show the accuracy of the theoretical model in representing the empirical model.

The LN3 distribution can easily be assessed by subtracting the bound value from each data point and by fitting a two-parameter lognormal (LN) distribution to the shifted data (*NIST/SEMATECH e-Handbook of Statistical Methods*). This simplified assessment approach was followed and the diagnostic plots were obtained using the *fitdistrplus* package in *R* (Delignette-Muller and Dutang, 2015). For illustrative purposes, Figure 4.12 shows the diagnostic plots for Load Case 2, where the data is measured in kNm. Appendix D contains the diagnostic plots for all the load cases.

Visual inspection of the diagnostic plots shows that the LN3 distribution fits the combined monthly maxima reasonably well. The points on the Q-Q plot and P-P plot show a fairly linear pattern, indicating that the data can be represented by the LN3 distribution. This is confirmed by the density plot and CDF plot. The least linear fit is seen for Load Case 1, 5 and 7. This observation is discussed at the end of this section. The diagnostic plots for the LN3 distribution were compared to the GEV distribution diagnostic plots. The comparison showed that the diagnostic plots for the two models gave similar fits. The diagnostic plots for the GEV distribution can be found in Appendix D, however, the study proceeded with using the LN3 distribution to represent the combined monthly maxima.

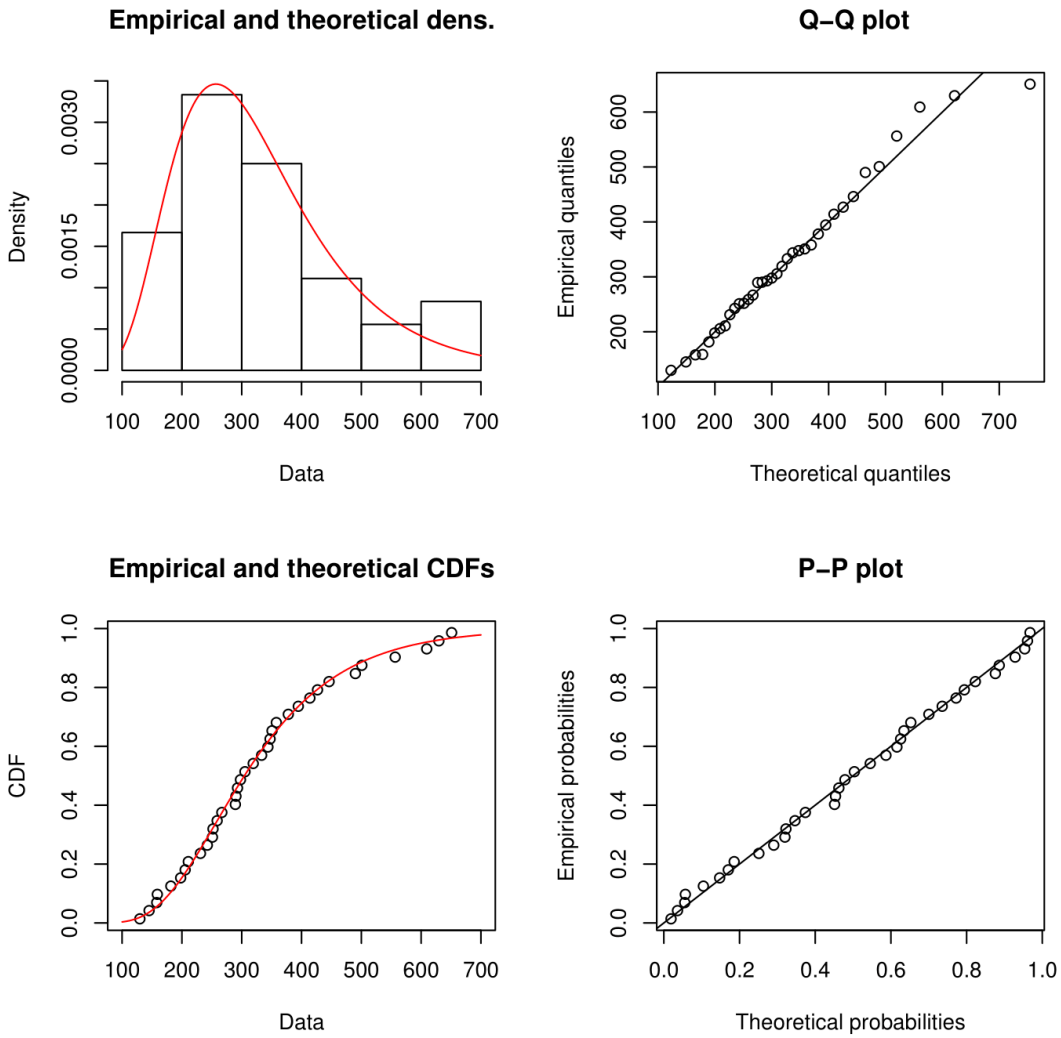

Figure 4.12: Diagnostic plots provided in *R* for Load Case 2 fitted with the LN3 distribution.

The modified Anderson-Darling test was used as a numerical measure to substantiate the results obtained from the diagnostic plots. The test provides a *p*-value that should be higher than a general significance level of 0.05, in order for the selected model to be accepted. A higher *p*-value provides a higher confidence in the selected model to represent the data set.

The relationship between the LN3 distribution and normal distribution was utilised to perform the modified Anderson-Darling test for each load case. A random variable X, in this case the combined monthly maxima, can be transformed to $Y = \log(X - x_0)$, where x_0 is the bound of the LN3 distribution fitted to X. If Y is normally distributed, then X is lognormally distributed. Thus, for the modified Anderson-Darling test the combined monthly maxima were transformed, and a normal distribution was fitted to the transformed data. The *p*-value obtained for each load case is listed in Table 4.10. It shows that the *p*-values exceed a significance level

of 0.05, which confirms that the LN3 distribution can be used to represent the combined monthly maxima.

Table 4.10: Anderson-Darling *p*-values for the normal distribution fitted to the transformed, combined monthly maxima

Load Case	***p*-value**
1	0.112
2	0.981
3	0.882
4	0.630
5	0.145
6	0.891
7	0.110
8	0.710

The results show relatively high *p*-values for all the load cases, except for Load Case 1, 5 and 7 that have much lower *p*-values. This observation concurs with what was seen in the diagnostic plots. What these three load cases have in common is that the traffic load effects from *Nb1* represents Q_1. That is, the concurrent traffic load effects in the northbound slow lane has the greatest contribution to the combined monthly maxima.

The traffic characteristics of *Nb1* were investigated to acquire a better understanding of the results for Load Case 1, 5 and 7. First only the maximum load effects produced in *Nb1* per month were considered. Secondly, the global traffic load effects on the bridge were considered for *Nb1* together with *Nb2*. The data set included the unfactored, combined monthly maxima obtained from the concurrent load effects, i.e. no LLDFs were included. Visual inspection of the probability plots for both cases did not show a prominent deviation from a linear pattern. However, the deviations in the probability plots and the lower *p*-values for Load Case 1, 5 and 7, suggest that the combined monthly maxima imposed on the critical spine beam may originate from a mixture of loading events. For example, the combined monthly maxima may include side-by-side truck events together with single or following truck events.

The study is limited to processed data that makes no distinction between different loading events. It is therefore recommended that future research should investigate ways for separating different loading events and fitting distributions to the individual loading event types. For each

loading event type, the load effects are then deemed identically distributed. Caprani *et al.* (2008) for instance have explored fitting separate GEV distributions to different loading event types and combining the results using a composite distribution statistics model. They found that this approach is less conservative than fitting a distribution to a mixture of loading events, and provides more accurate results when statically projecting to another reference period. Although the above-mentioned limitation is acknowledged in this study, a good fit is seen for the rest of the load cases, i.e. Load Case 2, 3, 4, 6 and 8, when fitting a LN3 distribution to the combined monthly maxima. It is thus deemed acceptable to still use a single distribution to represent the combined monthly maxima.

4.5.3 *50-year Maximum Load Effect Distribution*

The combined monthly maxima were used to obtain the maximum load effect distribution for a 50-year reference period ($F_n(x)$). This was done by raising the probability distribution function for the combined monthly maxima ($F(x)$) to an appropriate power n. A 50-year reference period was selected to compare the obtained reliability indices to target reliability indices corresponding to this period. The statistical projection is formulated in Equation 4.6, and the theory is discussed in Chapter 3 Section 3.4.5. Traffic load effects are represented by the random variable X, with realisations x. And the number of combined monthly maxima in a 50-year period is denoted by n and equals 600 (12 x 50). The calculation was done in *Mathcad*.

$$F_n(x) = [F(x)]^n \tag{4.6}$$

It was established that the 50-year maximum load effect distribution can be adequately represented by a LN3 distribution. The moment parameters for the 50-year maximum load effect distribution were determined in *Mathcad* using Equation 2.10, 2.11 and 2.12 in Section 2.3.1. The parameters include the mean, standard deviation and skewness.

Table 4.11 presents the moment parameters together with the COV and lower bound of the 50-year maximum load effect distribution. The COV ranges from 0.032 to 0.074 and a significant right skewness is seen, which varies between 1.006 and 1.656 depending on the load case.

Table 4.11: Statistical parameters of the 50-year maximum load effect distribution, represented by a LN3 distribution.

Load Case	Mean (kNm)	Standard deviation (kNm)	Skewness	COV	Bound (kNm)
1	2730.0	157.2	1.252	0.058	2333.6
2	2823.6	177.2	1.419	0.063	2424.3
3	2550.8	189.7	1.656	0.074	2177.4
4	2626.6	109.6	1.077	0.042	2309.1
5	2480.9	83.3	1.006	0.034	2223.6
6	2504.2	80.6	1.022	0.032	2259.3
7	2711.2	137.8	1.190	0.051	2347.1
8	2922.0	204.9	1.534	0.070	2490.9

4.6 Critical Element Reliability Analysis

This section presents the procedure and results for the reliability analysis performed on the critical spine beam. This is followed by a discussion on the sensitivity analysis, where the relative importance of the basic variables on the obtained reliability level is identified.

4.6.1 *Formulation of Limit State Function*

A limit state function was formulated to determine the reliability performance of the bending moment capacity of the critical spine beam at ULS. The formulation of the limit state function (Z) is based on the basic requirement that the resistance (R) should be larger than the load effect (E) (Holický, 2009). Structural failure occurs when Z is negative, i.e. $E \geq R$. The structure is deemed safe when $Z \geq 0$.

The basic limit state function is shown in Equation 4.7. The basic variables in the limit state function are random in nature and assumed independent of each other. Each basic variable is described by a probabilistic model in terms of its mean and standard deviation. The mean of each basic variable is obtained in terms of its characteristic or nominal value.

$$Z = R - E \tag{4.7}$$

The limit state function can be refined to represent the bending limit state function for the structure, as seen in Equation 4.8. The resistance moment (M_R) should be larger than the sum of the permanent load moments (M_G and M_{GW}) and variable load moment (M_Q). For the critical element reliability analysis, M_R represents the resistance moment of the critical spine beam. M_G represents the dead load moment due to the self-weight of the critical spine beam. M_{GW} represents the moments imposed on the critical spine beam by the superimposed dead loads, i.e. parapets and asphalt surfacing. A distinction is made between M_G and M_{GW} to allow for different statistical characteristics. M_Q describes the moments imposed on the critical spine beam by the traffic load on the bridge.

The limit state function accounts for the uncertainties introduced by the probabilistic models representing the basic variables. Model uncertainty is a significant variable, as it accounts for the uncertainties associated with idealising or approximating the physical behaviour of a structure with a mathematical model (Faber, 2009). The variable for model uncertainty is denoted by θ and introduced into the limit state function by a multiplicative relationship, as shown in Equation 4.8. The model uncertainty corresponding to the resistance, permanent loads and variable loads are denoted by θ_R, θ_G and θ_Q, respectively. Model uncertainty does not necessarily have to be divided between permanent and variable loads, but the distinction allows for different statistical characteristics. For this study, it was assumed that the sample size of traffic load effects is large enough to ignore statistical uncertainty. Exploration of statistical uncertainty is recommended for future research.

$$Z = \theta_R M_R - [\theta_G(M_G + M_{GW}) + \theta_Q M_Q] \tag{4.8}$$

The bending limit state function can further be detailed to describe M_R in terms of the area of reinforcement, denoted by A_s. The variable A_s describes the area of tension reinforcement in the bottom of the critical spine beam at midspan. To express M_R in terms of A_s, Equation 4.9 and 4.10 were considered, where z is the internal lever arm, d is the effective depth to the tension reinforcement, s is the simplified compression block depth and f_y is the steel yield strength.

$$M_R = f_y A_s z \tag{4.9}$$

$$z = d - \frac{s}{2} \tag{4.10}$$

To find s in terms of A_s, Equation 4.11 was used, where F_{st} represents the tension force in the reinforcement and F_{cc} represents the resultant force of the concrete compression stresses. Moreover, f_{cu} denotes the concrete cube strength and b denotes the effective flange width. According to TMH-7 Part 3 (CSRA, 1989), a value of 0.67 relates the concrete cube strength to the bending strength in a flexural member.

$$\begin{aligned} F_{st} &= F_{cc} \\ f_y As &= 0{,}67 f_{cu} bs \\ s &= \left[\frac{f_y A_s}{0{,}67 f_{cu} b}\right] \end{aligned} \tag{4.11}$$

A new expression for the resistance moment, M_R, was found by substituting Equation 4.10 and 4.11 into Equation 4.9. The final bending limit state function for the critical spine beam is shown in Equation 4.12. Here, G, G_w and Q represent the bending moment variables associated with the dead load, superimposed dead loads and traffic load on the critical spine beam.

$$Z = \theta_R f_y A_s \left[1 - \frac{f_y A_s}{1.34 f_{cu} bd}\right] d - \theta_G (G + G_w) - \theta_Q Q \tag{4.12}$$

4.6.2 *Statistical Description of Basic Variables*

The basic variables in the bending limit state function are represented by probabilistic models to account for the variability in measurements. They were selected based on literature, except for the traffic load effects, which were based on actual data. Unless stated otherwise, the basic variables presented in this section were adopted from Holický's book *Reliability analysis for structural design*, Table 1 of Annex 4 (2009). Holický (2009) provides conventional theoretical models for basic variables that are primarily based on working documents of the Joint Committee on Structural Safety (JCSS, 2001). Whenever convincing data is available, the uncertainties presented in the statistical description of the basic variables should be further reduced.

The basic variables and their probabilistic models are given in Table 4.12, where the following abbreviations are applicable: N for normal, LN for two-parameter lognormal, LN3 for three-

parameter lognormal and Det for a deterministic value. The subscript *k* denotes the characteristic value of the variable. The following sections provide a discussion on the basic variables summarised in Table 4.12.

Table 4.12: Conventional probabilistic models for the basic variables.

Name of basic variable		**Symbol of basic variable (*X*)**	**Unit**	**Distribution type**	**Mean (μ_X)**	**Standard deviation (σ_X)**
Dead load		G	kNm	N	G_k	$0.05\mu_X$
Superimposed dead load		G_w	kNm	N	G_{wk}	$0.1\mu_X$
Traffic load (50 years)		Q	kNm	LN3	(see Table 4.11)	(see Table 4.11)
Concrete strength		f_{cu}	kPa	LN	$f_{cuk} + 1.645\sigma_X$	$0.18\mu_X$
Yield strength		f_y	kPa	LN	$f_{yk} + 1.645\sigma_X$	30E+03
Effective flange width		b	m	Det	b_k	0
Effective depth to reinforcement		d	m	N	d_k	$0.02\mu_X$
Area of reinforcement		A_s	m^2	N	$1.02*A_s$(nom)	$0.02\mu_X$
Permanent load model uncertainty		θ_G	-	N	1	$0.07\mu_X$
Traffic load model uncertainty		θ_Q	-	LN	1	$0.1\mu_X$
Resistance model uncertainty	**Probabilistic model 1**	θ_R	-	LN	1	$0.06\mu_X$
	Probabilistic model 2	θ_R	-	LN	1.1	$0.1\mu_X$
	Probabilistic model 3	θ_R	-	LN	1.2	$0.15\mu_X$

4.6.2.1 *Geometric Properties*

The statistical description of basic variables, such as the geometric properties of a concrete cross-section and steel reinforcement, have been extensively investigated in literature and are well-established (fib COM3 TG3.1, 2016). The geometric properties include variables such as the effective flange width (b), the effective depth to reinforcement (d) and the area of steel reinforcement (A_s). The values in Table 4.12 are based on normal quality control measures. It is typically found that b and d have a bias of 1, meaning that the mean value is equal to the

characteristic value (Holický, 2009). Whereas the area of steel bars (A_s) has a slight bias of 1.02 (Holický, 2009). The variable d was taken to be normally distributed with a standard deviation of $0.02\mu_X$ (Lenner and Sýkora, 2017). The reliability analysis showed that b had a negligible contribution to the obtained reliability index, and was therefore applied as a deterministic quantity.

4.6.2.2 *Material Properties*

Holický (2009) recommends a mean of ($f_k + 2\sigma$) for the steel yield strength (f_y) and concrete strength (f_{cu}), instead of ($f_k + 1.645\sigma$). Meaning that in reality, the specified 5 % characteristic value (f_k) actually represents a 2 % characteristic value. This is based on sample inspection that suggests that better quality production standards are maintained in European countries (Holický, Retief and Wium, 2010). The 5 % characteristic value is equivalent to a 95 % probability of exceedance, whereas a 2 % characteristic value represents a 98 % probability of exceedance. Nevertheless, for this case study the 5 % characteristic strength specified in TMH-7 (CSRA, 1989) was used, i.e. ($f_k + 1.645\sigma$), as the same level of quality is not necessarily realised by South African production standards (Mensah, 2015). A fixed standard deviation of 30 MPa was used for f_y and a conservative standard deviation of $0.18\mu_X$ (fib COM3 TG3.1, 2016) was assumed for f_{cu}, to account for uncertainties in the quality control level.

4.6.2.3 *Permanent Loads*

The statistical description of the dead load (G) and superimposed dead loads (G_w) of the bridge are dependent on the volume and density of the members. The variability of the two properties are greatly influenced by the tolerances on the dimensions of the cross-section and the production quality of the materials (CIB, 1989). Both G and G_w are normally distributed with a mean equal to the characteristic value, however, G generally has a lower variability than G_w. A standard deviation of $0.05\mu_X$ was assumed for G, as the cross-section of the twin spine deck is symmetrical and fairly simple with a constant cross-section along the span. A standard deviation of $0.10\mu_X$ was assumed for G_w. For instance, to account for variability in the thickness of the asphalt surfacing that can differ significantly. These values agree with literature sources (Von Sholten *et al.*, 2004; Holický, 2009).

4.6.2.4 *Load Effect Model Uncertainty*

The following model uncertainties were introduced into the limit state function. It is recommended to use a traffic load model uncertainty (θ_Q) that is lognormally distributed with a mean of 1.0 and a COV of 0.1 (JCSS, 2001; Holický and Sýkora, 2012; fib COM3 TG3.1, 2016). The permanent load model uncertainty (θ_G) is considered normally distributed with a mean of 1.0 and a COV ranging between 0.05 and 0.1 (Holický, 2009). Moreover, θ_G should generally be set equal to or less than θ_Q. For the investigation, a COV of 0.07 was assumed for θ_G based on literature (Steenbergen and Vrouwenvelder, 2010; Lenner and Sýkora, 2017), and owing to the simplicity of the spine beam cross-section.

4.6.2.5 *Resistance Model Uncertainty*

More variability is seen in literature for the statistical description of the resistance model uncertainty (θ_R). Therefore, three probabilistic models were considered to investigate the influence of different parameters for the mean and COV. A two-parameter lognormal (LN) distribution is typically used to describe θ_R. The three probabilistic models are summarised in Table 4.13 with the appropriate references.

Table 4.13: Different probabilistic models describing the resistance model uncertainty θ_R.

Probabilistic model	**Distribution type**	**Mean (μ)**	**COV (σ/μ)**	**Reference**
1	LN	1.0	0.06	fib COM3 TG3.1 (2016)
2	LN	1.1	0.1	Sýkora *et al.* (2015)
3	LN	1.2	0.15	JCSS (2001)

It has been mentioned in literature that the JCSS Model Code provides fairly general and limited information on the selection of a mean value and COV for θ_R (Holický, Retief and Wium, 2010; Lenner and Sýkora, 2017). According to *fib* Bulletin 80 (2016), the mean of 1.2 and COV of 0.15 provided by JCSS account for members experiencing bending in the presence of axial and shear forces, and that smaller uncertainties can be expected for pure bending. For sound reinforced concrete cross-sections, the COV can even reduce to values in the order of 2 to 5 % (fib COM3 TG3.1, 2016). Thus, the first two probabilistic models are more appropriate in representing the resistance model uncertainty. Consequently, the focus is on the reliability

results obtained for the first and second probabilistic models. The third probabilistic model, based on JCSS, is only included for comparative purposes.

4.6.3 *Input Parameters for Limit State Function*

Finally, the input parameters of the basic variables are presented in Table 4.14. The resistance and permanent load properties of the critical spine beam were obtained from the bridge design in Section 4.3. The permanent load properties were obtained from the unfactored bending moments, provided in Table 4.2, which represent the characteristic values. A_s is based on the nominal (design) value, provided in Table 4.4, which was obtained for the spine beam under NA loading and permanent loads. The traffic load properties were derived from actual WIM data and it is described by the 50-year maximum load effect distribution presented in Table 4.11 for Load Case 1 to 8. By designing the bridge according to TMH-7 and loading it with the actual traffic load effects, the reliability performance of TMH-7 can be estimated.

Table 4.14: Statistical input parameters for basic variables in bending limit state function.

Name of basic variable		**Symbol of basic variable (X)**	**Unit**	**Distribution type**	**Mean (μ_X)**	**Standard deviation (σ_X)**
Dead load		G	kNm	N	3651.6	182.6
Superimposed dead load		G_w	kNm	N	732.2	73.2
Traffic load (50 years)		Q	kNm	LN3	(see Table 4.11)	(see Table 4.11)
Concrete strength		f_{cu}	kPa	LN	71E+03	12.8E+03
Yield strength		f_y	kPa	LN	499.4E+03	30E+03
Effective flange width		b	m	Det	5.7	0
Effective depth to reinforcement		d	m	N	0.895	0.018
Area of reinforcement		A_s	m^2	N	37.2E-3	0.74E-3
Permanent load model uncertainty		θ_G	-	N	1	0.07
Traffic load model uncertainty		θ_Q	-	LN	1	0.1
Resistance model uncertainty	**Probabilistic model 1**	θ_R	-	LN	1	0.06

Name of basic variable		Symbol of basic variable (X)	Unit	Distribution type	Mean (μ_X)	Standard deviation (σ_X)
Resistance model uncertainty	**Probabilistic model 2**	θ_R	-	LN	1.1	0.11
	Probabilistic model 3	θ_R	-	LN	1.2	0.18

4.6.4 *Reliability Analysis Results and Discussion*

The critical element reliability analysis was conducted on the bending limit state function. It involved a time-invariant analysis performed in the reliability software called *Comrel* (RCP, 2007), using FORM. The FORM-analysis determined the overall reliability index (β) and corresponding probability of failure (p_f) for a 50-year reference period. The results for the reliability analysis are provided in Table 4.15. It contains the results for Load Case 1 to 8 in accordance with the three probabilistic models selected to describe the resistance model uncertainty (θ_R).

Table 4.15: Reliability indices (β) and probability of failure (p_f) corresponding to a 50-year reference period.

Load Case	Probabilistic model 1		Probabilistic model 2		Probabilistic model 3	
	β	p_f	β	p_f	β	p_f
1	7.08	7.38E-13	6.61	1.98E-11	5.60	1.08E-08
2	6.63	1.73E-11	6.45	5.70E-11	5.52	1.74E-08
3	6.34	1.18E-10	6.36	9.91E-11	5.72	5.34E-09
4	7.56	2.07E-14	6.78	5.96E-12	5.70	6.00E-09
5	7.81	2.99E-15	6.96	1.75E-12	5.83	2.85E-09
6	7.78	3.71E-15	6.93	2.06E-12	5.81	3.19E-09
7	7.32	1.27E-13	6.66	1.37E-11	5.62	9.41E-09
8	6.20	2.88E-10	6.17	3.45E-10	5.42	2.97E-08

The results in Table 4.15 show that a high reliability level is achieved for the ultimate bending capacity of the critical spine beam. For the different probabilistic models, β ranges between 5.42 and 7.81. When compared to typical target reliability indices (β_t) of 3.8 (CEN, 2002) and 3.0 (SABS, 2019) corresponding to a 50-year period, the obtained β is seen to be much higher. This observation shows that TMH-7 is providing a good reliability performance for the bending

capacity of a 20 m span bridge, when designed according to NA loading. According to Tabsh and Nowak (1991) and Matos *et al.* (2019), uneconomically high β-values (larger than 5-6) could be expected for structures in a good condition.

Table 4.15 shows that the first probabilistic model for θ_R obtains the highest β-values, where β varies with a maximum difference of 1.61 between load cases. Whereas, the third probabilistic model obtains the lowest β-values. The results show that the statistical description of θ_R has a large influence on the reliability results, which agrees with literature (Allaix, 2007; Holický, Retief and Wium, 2010). Consider Load Case 5, where the p_f ranges between 2.99E-15 and 2.85E-09 depending on the description of θ_R. When the mean and COV of θ_R increases, the corresponding β-value decreases and the p_f increases. In short, the larger the uncertainty or variability in the resistance model, the less confidence there is in the safety of the structure. The smallest β-values are obtained in Load Case 8, which is characterised by three traffic lanes positioned on the bridge, where the slow lane in the southbound direction (*Sb1*) has the largest loading contribution on the critical spine beam.

It is important to note that the obtained reliability results for the 20 m twin spine deck may not necessarily be true for other types of 20 m span bridges. The deck type and material type of a bridge may have a significant influence on the reliability performance of a critical member (Tabsh and Nowak, 1991), as it influences the self-weight, required reinforcement and transverse stiffness of the deck. Although a twin spine deck is recommended for a 20 m span bridge (Benaim, 2008), other bridge deck types can also be considered, e.g. multiple T-girders or a box-girder. Additionally, bridges can have different material types, i.e. reinforced concrete or prestressed concrete. With this in mind, TMH-7 needs to cater for a wide range of practical design situations for a 20 m span bridge. Therefore, it is recommended for future research to explore other design situations to determine whether the reliability results concur with what is found for the twin spine deck.

4.6.5 *Sensitivity Analysis Results and Discussion*

A sensitivity analysis was performed on the basic variables in the limit state function, using FORM. The FORM-analysis produces sensitivity factors, denoted by α, which describe the significance of each variable in the reliability analysis. The larger the α-factor, the larger the influence of the basic variable on the obtained β-value. The relative importance of each variable on the obtained β-value can be assessed with α^2, where the sum of α^2 for all the variables are

equal to 1. The relative importance (α^2) of each basic variable is presented in Table 4.16 as percentage values, where α^2 for all the basic variable in the limit state function sums to 100 %. Except for the traffic load effects, the basic variables are based on theoretical models.

For every load case in Table 4.16, the basic variables with the three largest α^2-values are colour-coded for each probabilistic model. As discussed in Section 4.6.2.5, the focus is primarily on the first and second probabilistic models. The results show that depending on the load case, the resistance model uncertainty (θ_R) or the traffic load effects (Q) have the most significant effect on the obtained β.

Table 4.16: Relative importance (α^2) of the basic variables provided as a percentage (%).

Load Case	Basic variable	θ_R	f_y	A_s	f_{cu}	d	G	Q	G_W	θ_G	θ_Q
1	Prob. model 1	15.21	13.69	1.69	0.16	1.96	1.44	49.00	0.25	3.61	12.96
	Prob. model 2	51.84	17.64	1.96	0.25	2.25	2.89	7.84	0.49	6.76	9.00
	Prob. model 3	72.25	10.89	1.21	0.16	1.44	1.96	2.25	0.36	4.84	4.84
2	Prob. model 1	10.24	9.61	1.00	0.16	1.21	0.81	65.61	0.09	1.96	10.24
	Prob. model 2	43.56	14.44	1.69	0.16	1.96	1.96	20.25	0.36	4.84	9.61
	Prob. model 3	70.56	10.89	1.21	0.16	1.44	1.69	3.24	0.25	4.84	5.29
3	Prob. model 1	6.25	5.76	0.64	0.09	0.81	0.36	77.44	0.04	1.00	7.29
	Prob. model 2	19.36	6.25	0.81	0.09	0.81	0.49	64.00	0.09	1.44	6.76
	Prob. model 3	68.89	10.24	1.21	0.16	1.44	1.96	5.76	0.25	4.84	4.84
4	Prob. model 1	30.25	28.09	3.24	0.36	3.61	4.41	5.76	0.64	10.24	13.69
	Prob. model 2	54.76	18.49	2.25	0.25	2.56	3.24	2.25	0.49	7.84	7.84
	Prob. model 3	72.25	10.89	1.21	0.16	1.44	1.96	1.00	0.36	5.29	4.84
5	Prob. model 1	31.36	29.16	3.61	0.36	4.00	4.84	2.25	0.81	11.56	12.25
	Prob. model 2	54.76	18.49	2.25	0.25	2.56	3.61	1.00	0.49	8.41	7.29
	Prob. model 3	73.96	10.89	1.21	0.16	1.44	2.25	0.49	0.36	5.29	4.41
6	Prob. model 1	31.36	29.16	3.61	0.36	4.00	4.84	1.96	0.81	11.56	12.25
	Prob. model 2	56.25	18.49	2.25	0.25	2.56	3.61	1.00	0.49	8.41	7.29
	Prob. model 3	73.96	10.89	1.21	0.16	1.44	2.25	0.49	0.36	5.29	4.41
7	Prob. model 1	23.04	22.09	2.56	0.25	2.89	2.89	25.00	0.49	6.76	14.44
	Prob. model 2	53.29	17.64	1.96	0.25	2.25	2.89	4.41	0.49	7.29	9.00
	Prob. model 3	72.25	10.89	1.21	0.16	1.44	1.96	1.69	0.36	4.84	4.84
8	Prob. model 1	8.41	7.84	0.81	0.09	1.00	0.49	70.56	0.09	1.44	9.00
	Prob. model 2	27.04	9.00	1.00	0.09	1.21	0.81	49.00	0.16	2.25	9.00
	Prob. model 3	68.89	10.24	1.21	0.16	1.44	1.69	5.29	0.25	4.41	5.76

Table 4.16 shows that for the first probabilistic model, Q shows the largest contribution to β for Load Case 1, 2, 3 and 8, while θ_R shows the largest contribution for Load Case 4, 5 and 6. For Load Case 7, Q and θ_R show similar results. These results can be explained by considering the skewness and COV of Q for each load case (see Table 4.11). When Q governs, its skewness and COV are the largest relative to its parameters in the other load cases. When Q shows the smallest skewness and COV relative to other load cases, θ_R governs. This concludes that the significance of the traffic load effects (Q) is highly sensitive to its variability and tail behaviour. It also shows that the sensitivity of β to θ_R is dependent not only on the COV of θ_R, but also on the skewness and COV of Q.

The results show that θ_R is the most significant variable for all load cases in the second probabilistic model, except for Load Case 3 and 8 where Q governs. From Table 4.11 it can be seen that Q has the largest skewness and COV for Load Case 3 and 8, and thus shows significance. In the third probabilistic model, θ_R has the largest significance, as its COV is much larger than any of the other basic variables.

In addition to the above findings, the steel yield strength (f_y) consistently shows a significant contribution to β, with α^2-values reaching a maximum value of 29.16 %. This observation can be attributed to the standard deviation of 30 MPa recommended for f_y (Holický, 2009), which leads to a relatively high COV of 0.06. Its influence on β is further enhanced by its expression in the bending limit state function, where f_y is raised to the power of two. Actual measurements may lead to a smaller COV, which will reduce the relative importance of f_y and increase the obtained β-value. Furthermore, Table 4.16 shows that the traffic load model uncertainty (θ_Q) and dead load model uncertainty (θ_G) can reach a maximum value of 14.44 % and 11.56 %, respectively. Thus, θ_Q and θ_G also have a considerable contribution on the reliability results.

An important remark is that the relative importance of the basic variables may change for other span lengths. This can partially be explained by the change in ratio between the traffic load (Q) and permanent loads (G and G_w). In general, the permanent loads increase as the span length increases, leading to a larger relative importance. Concurrently, the significance of the traffic load decreases. The probabilistic description of the traffic load will also look differently for other span lengths, as different loading events will become more prominent. For instance, single axles or axle sets govern for shorter spans, whereas for longer spans, multiple truck event becomes more important. As a result, the description of the COV and skewness may vary and influence the relative importance of the traffic load. Lastly, the geometric properties of the

bridge deck will change for different span lengths, which will influence the relative importance of the resistance variables.

4.7 Chapter Summary

This chapter discussed the case study based on WIM data from a station near Kilner Park, located on the N1. The main purpose was to investigate the reliability performance of TMH-7 in catering for normal traffic conditions on a highway bridge. This was done by conducting a critical element reliability analysis.

For the analysis, a 20 m reinforced concrete twin spine deck was selected, where the spine beam represented the critical member. The bridge deck was designed in accordance with NA loading in TMH-7, and analysed in *Midas Civil* using a grillage analysis. Thereafter, the concurrent traffic load effects derived from the WIM data, along with their lateral load distribution factors, were used to obtain the total traffic load effects carried by the critical spine beam. This was done for different load cases, describing different traffic lane combinations. The block maxima approach was applied, where the maximum load effect per month was extracted. This was followed by the probabilistic modelling of the extreme traffic load effects using the LN3 distribution. MLE provided estimates for the model parameters, while goodness-of-fit tests assessed the quality of fit of the model. Through statistical projection, the 50-year maximum load effect distribution was then obtained and used to represent the traffic load variable in the bending limit state function. The probabilistic description of the other basic variables was acquired from literature.

Finally, to perform the critical element reliability analysis, FORM was utilised in *Comrel*, together with the bending limit state function. The analysis obtained reliability indices, which were then compared to target values to draw conclusions on the reliability performance of the bending moment capacity of the spine beam. In addition, a sensitivity analysis was performed to determine the relative importance of each basic variable on the reliability index.

4.8 Conclusion

Based on the work done in this chapter, conclusions can be drawn concerning the reliability performance of a 20 m span bridge, designed according to NA loading in TMH-7 and carrying traffic load effects derived from WIM data. The critical element reliability analysis obtained

reliability indices for a 50-year period that are much higher than the target values of 3.8 and 3.0 (see Table 4.15). The results indicate that the beam resistance is substantially higher than the load effects applied to it. Thus, the results suggest that a design according to TMH-7 provides a good reliability performance for the bending moment capacity of a 20 m span bridge. However, the bridge deck type and material type can have an influence on the reliability performance of the bridge. Therefore, it is recommended for future research to explore different design situations, in order to confirm that a 20 m span in general agrees with the high reliability results obtained in this case study.

The results from the sensitivity analysis show that the resistance model uncertainty and traffic load obtain the largest sensitivity factors, depending on the load case. A high sensitivity factor signifies that the variable has a large influence on the obtained reliability index. The findings suggest that TMH-7 is conservative in its representation of normal traffic conditions for a 20 m span. Notwithstanding, the reliability performance of NA loading may differ for other load effects, such as hogging moments and shear forces. Therefore, further study is recommended to determine the performance of NA loading for other load effects.

Actual data improves the uncertainty quantification of a variable, which in turn influences the relative importance of the variable and the obtained reliability index. Therefore, it is recommended that future research should verify and improve the theoretical probabilistic models of the basic variables. This is especially important for the resistance model uncertainty, which largely influences the reliability results. In addition, the yield strength and model uncertainties for load effects also show a noticeable significance.

When considering the monthly maximum traffic load effects carried by the critical spine beam, the diagnostic plots showed deviations from a linear fit for some load cases. This suggests that the data set of monthly maxima are not completely iid (independent and identically distributed) and may originate from a mixture of loading events. The study is limited to processed data that makes no distinction between these loading events. It is therefore recommended that future research should identify and separate single truck events, following truck events and side-by-side truck events and fit distributions to the individual loading events. This will improve the assumption of iid and also lead to more reliable results.

In describing the extreme traffic load effects derived from WIM data, different probabilistic descriptions were obtained for each load case. The COV and skewness of the model varied, depending on whether the traffic moved in the northbound or southbound direction and whether

a slow lane or a fast lane was located above the critical spine beam. Moreover, the sensitivity analysis reveals that the relative importance of the traffic load is highly sensitive to the COV. Therefore, it is recommended for future reliability analyses to investigate different load cases in order to find the governing load case for the critical member under consideration.

Furthermore, different loading events may govern for other span lengths. For instance, for shorter spans, single axles or axle sets may become more critical. Therefore, no direct correlation can be drawn between the reliability performance of a 20 m span bridge and the performance of other span lengths. Consequently, other span lengths will need to be investigated to obtain a more comprehensive understanding of the overall reliability performance of TMH-7 for normal traffic conditions. The procedure set out in this case study can serve as guideline for future studies.

5 Conclusion and Recommendations

5.1 Conclusion

The structural performance of a bridge is essential in ensuring a sound road transport network. South Africa's bridge design code, called Technical Methods for Highways 7 (TMH-7), is partially based on an outdated code and the traffic load model was last revised in 1988. Since then, the road freight industry has expanded significantly, further exacerbated by changes to the traffic regulations. As a result, the question was raised as to whether TMH-7 is still able to cater for the current traffic demand.

The purpose of this study was to carry out an investigation into the reliability performance of bridges designed according to TMH-7 and loaded with actual traffic loads. Past studies have identified deficiencies in TMH-7's traffic load model for normal traffic conditions, called NA loading (Oosthuizen *et al.*, 1991; Anderson, 2006). In response, the study focused on the investigation of the reliability performance of TMH-7 for normal traffic conditions. For the investigation, the performance of a bridge at the ultimate limit state (ULS) was of concern, where the load effect was represented by the bending moment at midspan of a simply supported bridge.

In achieving the study's purpose, reliability analyses were performed for two case studies, based on actual traffic load effects derived from site-specific Weigh-in-Motion (WIM) data. For each reliability analysis, a reliability index was obtained to measure the reliability level of the structure. The obtained reliability indices were compared to target reliability indices from existing standards to draw inferences with regard to the reliability performance of TMH-7 for normal traffic conditions.

For both case studies, the sub-objectives were achieved. The traffic load effects describing the extreme loading events, were extracted and described in a probabilistic manner using the three-parameter lognormal (LN3) distribution. The maximum load effect distribution was obtained, relating the extreme traffic load effects to a 50-year reference period. The limit state function was formulated to describe the failure mode. The First Order Reliability Method (FORM) was then used to conduct the reliability analysis and to obtain a reliability index. Lastly, the reliability indices were compared to target values of 3.8 (CEN, 2002) and 3.0 (SABS, 2019) corresponding to a 50-year period.

For the first case study (discussed in Chapter 3), only the traffic load effects were considered in the reliability analysis. The limit state function defined failure as the instance the actual traffic load effects exceed the design value for NA loading. The overall reliability indices for short to medium spans were obtained for different design scenarios. It was found that NA loading generally performs well for spans ranging from 5 to 50 metres. However, a poor reliability performance is seen for short narrow span bridges, especially for 5 m and 10 m spans. That is, when the number of traffic lanes is equal to the number of notional lanes for NA loading. The findings agree with Oosthuizen *et al.* (1991) and Anderson (2006), who also found deficiencies in NA loading for short and narrow span bridges. Notwithstanding, a highway bridge typically exhibits more traffic lanes than the number of notional lanes, owing to the geometry of the bridge deck (Burrell, Mitchell and Wolhuter, 2002) and the way notional lanes are defined in TMH-7 with floating lane widths (CSRA, 1981). The results also conclude that NA loading is inherently conservative in its design for longer spans. This is evident for 30 m to 50 m spans. This finding may be attributed to decisions made regarding idealised vehicle combinations, overloading and partial load factors in deriving the load model for NA loading.

The reliability analysis in the first case study is valuable, as it identifies deficiencies in TMH-7 for normal traffic conditions. It also identifies span lengths that achieve a high reliability performance, where design could be optimised to be more cost-effective.

The second case study is discussed in Chapter 4. A critical element reliability analysis was performed on the spine beam of a 20 m reinforced concrete bridge with a twin spine deck. The limit state function accounted for the resistance and permanent loads in accordance with TMH-7, whereas the traffic load was based on WIM data. Failure was defined as the instance the load effects exceed the resistance of the spine beam. The comparison of the overall reliability indices revealed that the obtained reliability indices far exceeded the target values. This concludes that TMH-7 NA loading is providing a high reliability performance for the bending moment capacity of the 20 m span bridge. The results agree with the findings in the first case study, where high reliability indices were obtained for a typical highway bridge with a 20 m span.

A sensitivity analysis in the second case study identified the traffic load effects and resistance model uncertainty as having the greatest influence on the reliability performance of the spine beam. The results suggest that NA loading is conservative in its representation of traffic load effects on a 20 m span bridge. Revision of the load model for a 20 m span could lead to potential

cost savings. However, other load effect types will need to be investigated to confirm this observation.

With regard to bending moments at midspan, the findings indicate that TMH-7 is able to cater for the current normal traffic conditions, although concern is raised for short narrow span bridges. The study consists of an investigation into the reliability performance of TMH-7 for normal traffic conditions. Therefore, the findings are insightful but not conclusive in representing the overall reliability performance of TMH-7 for normal traffic conditions. Future research is recommended to confirm and elaborate on the performance of TMH-7.

5.2 Recommendations

The study reveals the enormity of the task to verify the reliability performance of TMH-7 and that it consists of many different components. Recommendations can assist future research in making this task more attainable.

It is recommended for future research to make use of the extensive database of WIM data, available at different locations in South Africa, to verify and confirm the findings in this study. The focus should be on WIM stations on heavy freight routes. The investigation should be extended to include load effects described by the shear forces and hogging moments on single and continuous spans, as appropriate. These load effects may supersede sagging moments in representing the failure mode of the structure, and thus provide more insight into the performance of the load model. Moreover, future research should examine the dynamic load effects of moving traffic on a bridge, as it may have a significant effect on the reliability performance.

For the analysis of normal traffic conditions, it is recommended to find a way to identify and separate loading events caused by standard trucks, illegally overloaded trucks and permit trucks. Probabilistic models are sensitive to different types of loading events. Therefore, by fitting distributions to the individual loading event types, the accuracy of the probabilistic models will improve. This will also lend further support to the assumption of iid (independent and identically distributed) for the extreme traffic load effects. Another consideration is that for multiple lane bridges, a mixture of loading event types becomes more prominent. It may include single truck, following trucks and side-by-side truck events that require different probabilistic descriptions. The study is limited to processed data that makes no distinction

between these loading events. Similar as before, it is recommended that future research should identify and separate these loading event types and fit distributions to them individually. This will improve the assumption of iid and also lead to more accurate results.

It is further recommended to extend the critical element reliability analysis to other span lengths and bridge deck types, where the dead load, geometric properties and transverse stiffness of the bridge will differ. Moreover, different loading events will govern for different span lengths. Therefore, no direct correlation can be drawn between the reliability performance of one span length and another. The procedure used in Chapter 4 can serve as guideline to perform critical element reliability analyses for other span lengths. The broadened investigation will provide a better understanding of the overall reliability performance of NA loading.

Furthermore, except for the traffic load effect variable, the basic variables in the reliability analysis were obtained from literature. The literature sources provide rather general probabilistic descriptions of the basic variables and they are not specific to South Africa. Therefore, when possible, future research should use actual measurements to improve the probabilistic description of the model uncertainties and resistance variables related to quality control. It is especially important for the resistance model uncertainty, which was shown to have a large influence on the reliability results.

The work presented in this thesis contributes to an improved understanding of the reliability performance of a bridge designed according to TMH-7 for normal traffic conditions. With regard to bending moments at midspan, the study was able to identify deficiencies in the traffic load model for NA loading. It also identified spans where design could be optimised to be more cost-effective. These insights can help direct future revisions of the traffic load model for normal traffic conditions.

6 References

Allaix, D. L. (2007) Bridge Reliability Analysis with an Up-to-Date Traffic Load Model. Politecnico di Torino.

Anderson, J. R. B. (2006) Review of South African live load models for traffic loading on bridge and culvert structures using Weigh-in-Motion (WIM) data. University of Cape Town.

Bakht, B. and Mufti, A. (2015) Bridges: Analysis, Design, Structural Health Monitoring, and Rehabilitation. Springer.

Basson, S. E. and Lenner, R. (2019) 'Reliability verification of bridges designed according to TMH-7', in Zingoni, A. (ed.) Proceedings of the 7th International Conference on Structural Engineering, Mechanics and Computation. Cape Town: CRC Press.

Benaim, R. (2008) The Design of Prestressed Concrete Bridges: Concepts and Principles. New York: Taylor & Francis.

Bosman, J. (2004) 'Traffic Loading Characteristics of South African Heavy Vehicles', in Eight (8th) International Symposium on Heavy Vehicles, Weights and Dimensions. Loads, Roads and the Information Highway, pp. 14–18.

Bruls, A., Croce, P., Sanpaolesi, L. and G, S. (1996) 'ENV1991 – Part 3: traffic loads on bridges; calibration of load models for road bridges', in Proceedings of IABSE Colloquium on Basis of Design and Actions on Structures. Delft, The Netherlands: IABSE, pp. 439–454.

Buckland, P. G., Navin, P. D., Zidek, J. M. and McBride, J. P. (1980) 'Proposed vehicle loading for long span bridges', Journal of Structural Engineering, ASCE, 106(4), pp. 915–931.

Burrell, R. C., Mitchell, M. F. and Wolhuter, K. M. (2002) Geometric design guidelines. South African Roads Agency Limited.

Caprani, C. C. and O'Brien, E. J. (2009) 'Estimating Extreme Highway Bridge Traffic Load Effects', in Proceedings of the International Conference on Structural Safety and Reliability (ICOSSAR'09).

Caprani, C. C., O'Brien, E. J. and Mclachlan, G. J. (2008) 'Characteristic traffic load effects from a mixture of loading events on short to medium span bridges', Structural Safety, 30(5), pp. 394–404.

Castillo, E. (1988) Extreme Value Theory in Engineering. Boston: Academic Press.

Castillo, E., Hadi, A. S., Balakrishnan, N. and Sarabia, J. M. (2005) Extreme Value and Related Models with Applications in Engineering and Science. John Wiley & Sons, inc.

CEN (2002) EN 1990:2002, Basis of Structural Design. Brussels: European Commitee of Standardization.

Chang, K. H. (2013) Product Performance Evaluation using CAD/CAE: The Computer Aided Engineering Design Series. Academic Press.

CIB (1989) CIB Report Publication 115: Actions on Structures Self-weight Loads, International Council for Research and Innovation in Building and Construction.

Coles, S. (2001) An Introduction to Statistical Modeling of Extreme Values. London: Springer.

Cooper, D. I. (1995) 'The determination of highway bridge design loading in the United Kingdom from traffic measurements', in The First European Conference on Weigh-in-Motion of Road Vehicles. Zurich.

Cooper, D. I. (1997) 'Development of short span bridge-specific assessment live loading', Safety of bridges, pp. 64–89.

COTO (2013) TMH 3: Specifications for the Provision of Traffic and Weigh-in-Motion Monitoring Service, SANRAL. Pretoria.

COTO (2014) TMH 8. Traffic and Axle Load Monitoring Procedures, SANRAL. Pretoria.

Cremona, C. (2001) 'Optimal extrapolation of traffic load effects', Structural Safety, 23, pp. 31–46.

CSRA (1981) TMH 7 Code of Practice for the Design of Highway Bridges and Culverts in South Africa. Parts 1 and 2. Pretoria: Committee of State Road Authorities, Department of Transport.

CSRA (1989) TMH 7 Part 3: Code of Practice for the Design of Highway Bridges and Culverts in South Africa. Pretoria: Committee of State Road Authorities, Department of Transport.

Delignette-Muller, M. L. and Dutang, C. (2015) 'fitdistrplus : An R Package for Fitting Distributions', Journal of Statistical Software, 64(4).

Doan, K., Sparling, B. and Feldman, L. (2016) 'STR-846: Methods of Comparing Extreme Load Effects Based on Weigh-in-Motion Data', in Proceedings of the CSCE Annual Conference

(Resilient Infrastructure). London.

DOT (2013) National transport master plan (natmap) 2050 Chapter 7: Freight Transport, Department of Transport. South Africa.

Du, X. (2005) 'First order and second reliability methods', in Probabilistic engineering design, pp. 1–33.

Enright, B. (2010) Simulation of traffic loading on highway bridges. University College Dublin.

Enright, B., Caprani, C. and O'Brien, E. (2011) 'Modelling of highway bridge traffic loading: some recent advances', Applications of Statistics and Probability in Civil Engineering, 111.

Enright, B. and O'Brien, E. J. (2013) 'Monte Carlo simulation of extreme traffic loading on short and medium span bridges', Structure and Infrastructure Engineering, 9(12), pp. 1267–1282.

Faber, M. H. (2009) Basics of Structural Reliability, DRAFT, Swiss Federal Institute of Technology ETH. Zürich, Switzerland.

Ferreira, A. and De Haan, L. (2013) 'On the block maxima method in extreme value theory', arXiv preprint arXiv:1310.3222.

fib COM3 TG3.1 (2016) 'fib Bulletin 80: Partial factor methods for existing concrete structures'. Edited by R. Caspeele, R. Steenbergen, and M. Sykora. Germany: Fédération internationale du béton.

Fisher, N. I. (1983) 'Graphical Methods in Nonparametric Statistics : A Review and Annotated Bibliography', International Statistical Review, 51(1), pp. 25–58.

Fisher, R. A. (2006) Statistical methods for research workers. Edinburgh: Genesis Publishing Pvt Ltd.

Van Gelder, P. H. A. J. M., Proske, D. and Vrijling, J. K. (2009) Proceedings of the 7th International Probabilistic Workshop. Delft, The Netherlands: Dirk Proske Verlag.

Getachew, A. and O'Brien, E. J. (2007) 'Simplified site-specific traffic load models for bridge assessment', Structure and Infrastructure Engineering, 3(4), pp. 303–311.

Ghosn, M. and Moses, F. (1985) 'Markov renewal model for maximum bridge loading', Journal of Engineering Mechanics, ASCE, 111(9), pp. 1093–1104.

Ghosn, M., Sivakumar, B. and Moses, F. (2011) Protocols for Collecting and Using Traffic Data

in Bridge Design, Report of national cooperative highway research program. Washington, DC. USA: Transportation Research Board.

Hajializadeh, D., O'Brien, E. J., Enright, B., Caprani, C. C., Sheils, E. and Wilson, S. P. (2012) 'Probabilistic study of lifetime load effect distribution of bridges', in 6th International ASRANet Conference for Integrating Structural Analysis, Risk and Reliability. London.

Havenga, J. H., Simpson, Z. P. and De Bod, A. (2014) 'South Africa's freight rail reform: A demand-driven perspective', Journal of Transport and Supply Chain Management, 8(1), pp. 1–7.

Heffernan, J. E. and Stephenson, A. G. (2018) ismev: An Introduction to Statistical Modeling of Extreme Values, R package version 1.42.

Holický, M. (2009) Reliability Analysis for Structural Design. First. Stellenbosch: SUN MeDIA.

Holický, M. (2013) Introduction to probability and statistics for engineers. Springer.

Holický, M., Retief, J. V, Diamantidis, D. and Viljoen, C. (2015) 'On Standardization of the Reliability Basis of Structural Design', in 12th International Conference on Applications of Statistics and Probability in Civil Engineering. Vancouver: ICASP12.

Holický, M., Retief, J. and Wium, J. (2010) 'Partial factors for selected reinforced concrete members: Background to a revision of SANS 10100-1', Journal of the South African Institution of Civil Engineering, 52(1), pp. 37–44.

Holický, M. and Sýkora, M. (2012) 'Conventional probabilistic models for calibration of codes', Applications of Statistics and Probability in Civil Engineering, (1970), pp. 969–976.

Hwang, E. S., Nguyen, S. H. and Nguyen, Q. H. (2014) 'Development of serviceability limit state design criteria for stresses in prestressed concrete girders', KSCE Journal of Civil Engineering, 18(7), pp. 2143–2152.

ISO 2394 (2015) General principles on reliability for structures. 4th edn. Geneve: International Standards Organisation.

Janse van Rensburg, R. A. J. (1996) The History of the Rail Transport Regulatory Environment in South Africa.

JCSS (2001) Probabilistic Model Codes, Joint Committee on Structural Safety working materials. Available at: http://www.jcss.ethz.ch/.

Lee, L. S. (2011) 'Rehabilitation and service life estimation of bridge superstructures', in Service Life Estimation and Extension of Civil Engineering Structures. Woodhead Publishing, pp. 117–142.

Lenner, R. and Sýkora, M. (2017) 'Partial factors for imposed loads in areas for storage and industrial use', Structure and Infrastructure Engineering, 13(11), pp. 1425–1436.

Lenner, R., De Wet, D. P. G. and Viljoen, C. (2017) 'Traffic characteristics and bridge loading in South Africa', Journal of the South African Institution of Civil Engineering, 59(4), pp. 34–46.

Madsen, H. O., Krenk, S. and Lind, N. C. (2006) Methods of structural safety. Courier Corporation.

Maina, J. W. and De Beer, M. (2008) 'Improved performance evaluation of road pavements by using measured tyre loading', in Proceedings of the 2nd CSIR Biennial Conference (Science Real and Relevant). Pretoria, South Africa: CSIR, p. 13.

Manoj, N. R. (2016) First Order Reliability Method: Concepts and Application, Physical Review E. Delft University of Technology.

Matos, J. C., Moreira, V. N., Valente, I. B., Cruz, P. J. S., Neves, L. C. and Galvão, N. (2019) 'Probabilistic-based assessment of existing steel-concrete composite bridges – Application to Sousa River Bridge', Engineering Structures. Elsevier, 181, pp. 95–110.

Mensah, K. K. (2015) Reliability Assessment of Structural Concrete with Special Reference to Stirrup Design. Stellenbosch University.

MIDAS (2016) 'Midas Civil'. MIDAS Information Technology Co.

Minitab Express Support (2019) Interpret all statistics and graphs for Normality Test, Minitab, LCC. Available at: https://support.minitab.com/en-us/minitab-express/ (Accessed: 16 January 2019).

Mitrani, Isi and Mitrani, Israel (1998) Probabilistic Modelling. Cambridge University Press.

Montgomery, D. C. and Runger, G. C. (2014) Applied Statistics and Probability for Engineers. 6th edn. United States of America: John Wiley & Sons, Inc.

NIST/SEMATECH e-Handbook of Statistical Methods (2012). Available at: https://www.itl.nist.gov/div898/handbook/ (Accessed: 28 June 2019).

Nowak, A. S. (1989) 'Probabilistic basis for bridge design codes', in International Conference on Structural Safety and Reliability. San Francisco, pp. 2019–2026.

Nowak, A. S. (1993) 'Live load model for highway bridges', Structural Safety, 13, pp. 53–66.

Nowak, A. S. (1994) 'Load model for bridge design code', Canadian Journal of Civil Engineering, 21(1), pp. 36–49.

Nowak, A. S. (1999) Calibration of LRFD bridge design code (No. Project C12-33 FY'88-'92).

Nowak, A. S. and Hong, Y. K. (1991) 'Bridge live load models', Journal of Structural Engineering, ASCE, 117(9), pp. 2757–2767.

Nowak, A. S. and Rakoczy, P. (2013) 'WIM-based live load for bridges', KSCE Journal of Civil Engineering, 17(3), pp. 568–574.

O'Brien, E. J. et al. (2015) 'A review of probabilistic methods of assessment of load effects in bridges', Structural Safety. Elsevier, 53, pp. 44–56.

O'Brien, E. J., Connor, A. J. O. and Arrigan, J. E. (2012) 'Procedures for Calibrating Eurocode Traffic Load Model 1 for National Conditions', in Biondini & Frangopol (ed.) Bridge Maintenance, Safety, Management, Resilience and Sustainability. London: Taylor & Francis.

Oosthuizen, A. P. C., Meintjies, C. J., Trumpelmann, V., Peters, D., Ullmann, K. K. A. B. and Oppermann, G. H. P. (1991) TMH7 Part 2: Traffic Loading (1991) Proposed Substitution of Section 2.6., CSRA, Department of Transport. Cape Town.

Papalexiou, S. M. and Koutsoyiannis, D. (2013) 'Battle of extreme value distributions : A global survey on extreme daily rainfall', Water Resources Research, 49(1), pp. 187–201.

Parliamentary Monitoring Group (2000) Spoornet programme & structure: Briefing. Available at: https://pmg.org.za/committee-meeting/4365/ (Accessed: 21 February 2019).

PTC (2006) Mathcad 14. version 14.0.0.163, Parametric Technology Corporation.

R Core Team (2018) R: A language and environment for statistical computing, version 3.5.0, R Foundation for Statistical Computing. Vienna, Austria.

RCP (2007) 'Comrel: Componental Reliability. Version 8.1.0.0'. Munchen, Germany: RCP Consult GmbH. Available at: www.strurel.de.

Retief, J. V, Dunaiski, P. E. and Eds. (2009) Background to SANS 10160: Basis of structural design and actions for buildings and industrial structures. AFRICAN SUN MeDIA.

SABS (2000) SANS 10100-1. The structural use of concrete – Part 1: Design, South African

Bureau of Standards. Pretoria.

SABS (2019) SANS 10160-1:2019. Basis of structural design and actions for buildings and industrial structures, South African Bureau of Standards. Pretoria.

Saeb, A. (2018) gnFit: Goodness of Fit Test for Continuous Distribution Functions, R package version 0.2.0.

Sangal, B. P. and Biswas, A. K. (1970) 'The 3-Parameter Lognormal Distribution and Its Applications in Hydrology', Water Resources Research, 6(2), pp. 505–515.

SANRAL (2010) Table 6000/1 Project document: Project specifications, The South African National Roads Agency Limited.

SANRAL (2012) SANRAL Structural Drawings, The South African National Roads Agency Limited. Available at: https://www.nra.co.za/live/content.php?Category_ID=206 (Accessed: 22 May 2019).

Von Sholten, C., Enevoldsen, I., Arnbjerg-Nielsen, T., Randrup-Thomsen, S., Sloth, M., Engelund, S. and Faber, M. (2004) Reliability-Based Classification of the Load Carrying Capacity of Existing Bridges, Road Directorate.

Sifre, S. P. and Lenner, R. (2019) 'Bridge assessment reduction factors based on Monte Carlo routine with copulas', Engineering Structures. Elsevier, 198, p. 109530.

Skrzypczak, I., Słowik, M. and Buda-Ożóg, L. (2017) 'The application of reliability analysis in engineering practice–reinforced concrete foundation', Procedia Engineering, 193, pp. 144–151.

Van der Spuy, P. F. and Lenner, R. (2018) 'Developing a new bridge live load model for South Africa', in Proceedings of the ninth international conference on bridge maintenance, safety and management (IABMAS), pp. 1405–1410.

Van der Spuy, P. F. and Niehaus, H. J. (2019) 'Design of the new Olifants river arch bridge in the Western Cape province of South Africa', in Zingoni, A. (ed.) Proceedings of the 7th International Conference on Structural Engineering, Mechanics and Computation. Cape Town: CRC Press.

Van der Spuy, P. and Lenner, R. (2019) 'Towards a New Bridge Live Load Model for South Africa', Structural Engineering International. Taylor & Francis, 0(0), pp. 1–7.

Van der Spuy, P., Lenner, R., De Wet, T. and Caprani, C. (2019) 'Multiple lane reduction factors based on multiple lane weigh in motion data', Structures. Elsevier, 20, pp. 543–549.

Stander, H. J. and Pienaar, W. J. (2005) 'Land freight issues in South Africa', in Proceedings of the 24th Annual Southern African Transport Conference. Pretoria, South Africa: SATC, pp. 1027–1037.

Steenbergen, R. D. J. M. and Vrouwenvelder, A. C. W. M. (2010) 'Safety philosophy for existing structures and partial factors for traffic loads on bridges', Heron, 55(2), pp. 123–140.

Stephens, M. A. (1979) The Anderson-Darling Statistic, Department of Statistics, Stanford University. Stanford.

Sýkora, M., Holický, M., Prieto, M. and Tanner, P. (2015) 'Uncertainties in resistance models for sound and corrosion-damaged RC structures according to EN 1992-1-1', Materials and Structures/Materiaux et Constructions. Springer Netherlands, 48(10), pp. 3415–3430.

Tabsh, S. W. and Nowak, A. S. (1991) 'Reliability of Highway Girder Bridges', Journal of Structural Engineering, 117(8), pp. 2372–2388.

Thoft-Christensen, P. and Nowak, A. S. (1997) 'Principles of Bridge Reliability: application to design and assessment codes', in International Symposium on The Safety of Bridges. London.

De Wet, D. P. G. (2010a) Post-Calibration and Quality Management of Weigh-in-Motion Traffic Data. Stellenbosch University.

De Wet, D. P. G. (2010b) 'WIM calibration and data quality management', Journal of the South African Institution of Civil Engineering, 52(2), pp. 70–76.

Zhou, X. Y. et al. (2013) 'Applying Weigh-in-motion traffic data to reliability based assessment of bridge structures', in ICOSSAR2013, 11th International Conference on Structural Safety. France.

Žnidarič, A., Kreslin, M., Leahy, C., O'Brien, E. J., Schmidt, F. and Pederson, C. (2015) Guidelines on collecting WIM data and forecasting of traffic load effects on bridges, Re-GEN D3. 1 Report.

Appendices

Appendix A: Maximum Likelihood Estimation

This appendix provides an example to show the implementation of the maximum likelihood estimation (MLE) method in *Mathcad*. The method is used to determine the model parameters of the three-parameter lognormal (LN3) distribution. Moreover, the example makes use of the monthly maxima data set for a 50 m span, as discussed in Chapter 3 Section 3.4.3.

Figure A.1 shows the expression used in *Mathcad* for the probability density function of the LN3 distribution, where m denotes the mean, s denotes the standard deviation and w denotes the skewness. The expression originates from the equations in Section 2.3.2.2.

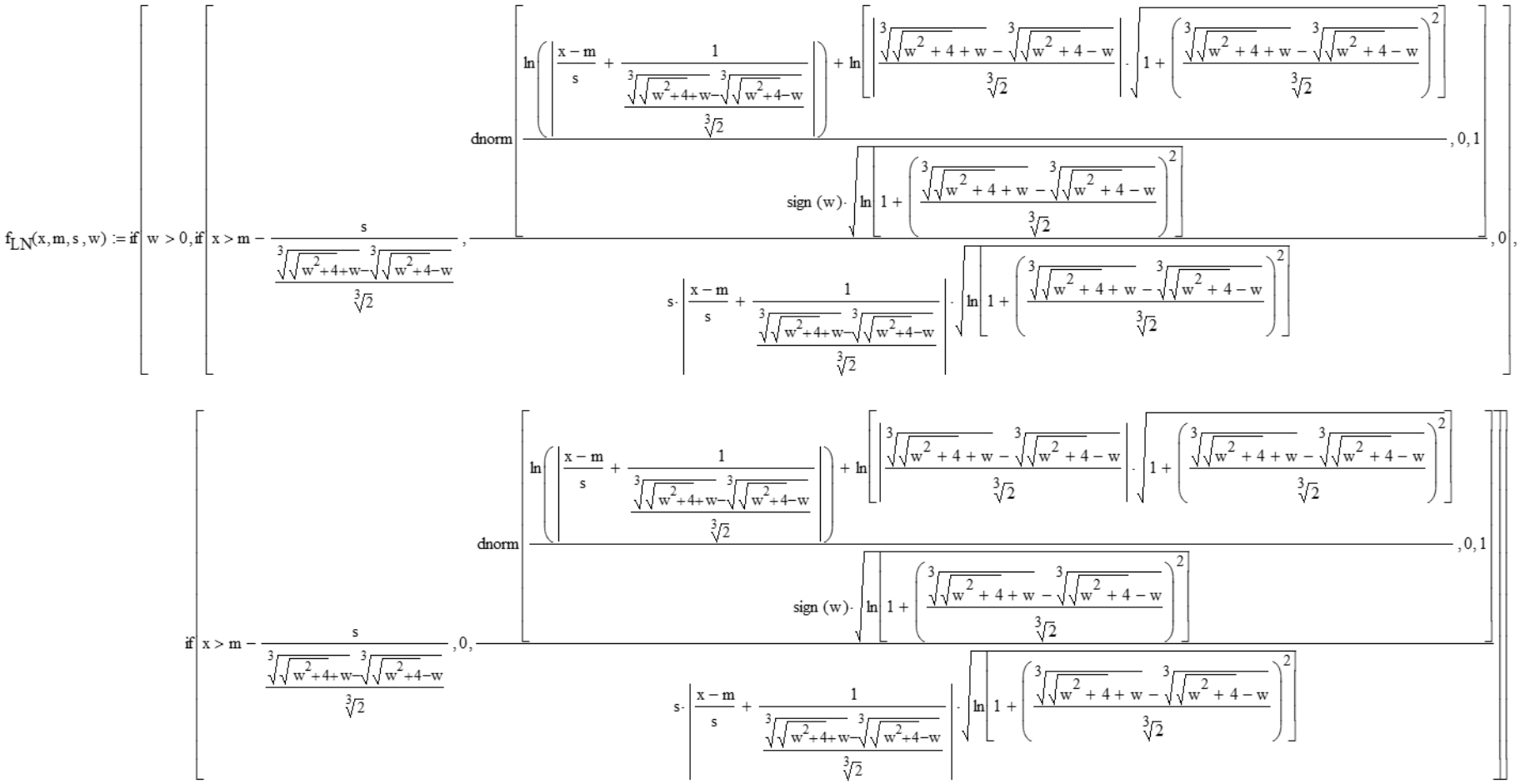

Figure A.1: Probability density function for LN3 distribution, written in terms of mean (m), standard deviation (s) and skewness (w).

Example in Mathcad to illustrate MLE:

ORIGIN := 1

Monthly maxima for 50 m span (measured in kNm):

data =

	1	2	3	4	5	6
1	$8.032 \cdot 10^3$	$8.481 \cdot 10^3$	$7.468 \cdot 10^3$	$8.618 \cdot 10^3$	$7.731 \cdot 10^3$	...

Sample size:

$n := cols(data)$ $n = 84$

Use sample characteristics to provide initial values for the model parameters:

μ - mean
σ - standard deviation
V - coefficient of variation
w - skewness

$\mu_M := mean(data^T)$ $\sigma_M := Stdev(data^T)$ $V_M := \frac{\sigma_M}{\mu_M}$ $w_M := skew(data^T)$

$\mu_M = 8310.95$ $\sigma_M = 716.20$ $V_M = 0.086$ $w_M = 0.481$

Maximum likelihood estimation (MLE) of model parameters for LN3 distribution:

$$MLM(\mu_{MLM}, \sigma_{MLM}, w_{MLM}) := \sum_{i=1}^{n} \ln\left[f_{LN}\left[(data^T)_i, \mu_{MLM}, \sigma_{MLM}, w_{MLM}\right]\right]$$

$\mu_{MLM} := \mu_M$ $\sigma_{MLM} := \sigma_M$ $w_{MLM} := w_M$

Given $0.5 \cdot \sigma_M \le \sigma_{MLM} \le 1.5 \cdot \sigma_M$

$0.8 \cdot \mu_M \le \mu_{MLM} \le 1.2 \cdot \mu_M$

$$\begin{pmatrix} \mu \\ \sigma \\ w \end{pmatrix} := \text{Maximize}\left(\text{MLM}, \mu_{\text{MLM}}, \sigma_{\text{MLM}}, w_{\text{MLM}}\right) \qquad \begin{pmatrix} \mu \\ \sigma \\ w \end{pmatrix} = \begin{pmatrix} 8311.847 \\ 728.42 \\ 0.838 \end{pmatrix}$$

$$V := \frac{\sigma}{\mu} \qquad V = 0.088$$

MLE parameters:

$\mu = 8311.85$ $\sigma = 728.42$ $V = 0.088$ $w = 0.838$

Appendix B: *R* Code

The *R* code on the following page represents the procedure to obtain the diagnostic plots for each distribution type, along with the application of the modified Anderson-Darling test. The procedure is applicable to both case studies presented in Chapter 3 and Chapter 4.

```
library(evd)

library(fitdistrplus)

library(ismev)

library(VGAM)

library(extRemes)

library(survival)

library(SPREDA)

library(stats4)

library(FAdist)

library(nortest)

library(gnFit)


getwd()

d<-read.table("Sagging moments monthly max (84).txt", header=FALSE, sep="
")
print(d)

 collection<-data.matrix(d)
 noCol<-ncol(collection)
 noRow<-nrow(collection)

 mean.vec <-matrix(nrow=noCol, ncol=1)
 sd.vec <-matrix(nrow=noCol, ncol=1)

 m<-read.table("MLE parameters for LN3.txt", header=FALSE, sep="")
 print(m)

 ln3MLE<-data.matrix(m)
 skewvec<-ln3MLE[,3]
 boundvec<-ln3MLE[,4]

 cat("Number of columns ",noCol)


 #Normal distribution fitted to transformed data

 for(j in 1:noCol){

   cat("Column = ",j)
   col<-collection[,j]
   boundi<-boundvec[j]
```

```
  for(k in 1:noRow){
    col[k]<-log(abs(col[k]-boundi))
  }

  normfit<-fitdist(col,"norm",method="mle")

  mean.vec[j,]<- normfit$estimate[1]
  sd.vec[j,]<- normfit$estimate[2]

  print(ad.test(col))
  plot(normfit)
  print(normfit)

}


# Lognormal distribution fitted to shifted data

for(j in 1:noCol){

  cat("Column = ",j)
  col<-collection[,j]
  bound<-boundvec[j]
  skew<-skewvec[j]

  if(skew>0){
    for(k in 1:noRow){
    col[k]<-col[k]-bound
    }
  }
   else{
      for(k in 1:noRow){
        col[k]<-((-1)*col[k])+bound
      }
    }

  lnormfit<-fitdist(col,"lnorm",method="mle")

  plot(lnormfit)
  print(gofstat(lnormfit))
  print(lnormfit)

}


#Generalised Extreme Value distribution fitted to data

for(j in 1:noCol){

  cat("Column = ",j)
  col<-collection[,j]

  fgevfit<-gev.fit(col, ydat=NULL, mul=NULL,sigl=NULL,shl=NULL,
```

```
                    mulink=identity,siglink=identity,shlink=identity,
                    muinit=NULL,siginit=NULL,shinit=NULL,
                    show=TRUE)

  gev.diag(fgevfit)
  gnfit(col,"gev",pr=fgevfit$mle)

}
```

Appendix C: Diagnostic Plots for Roosboom Case Study

The relevant diagnostic plots for Chapter 3 Section 3.4.4.1 are provided in this section. The data represents the monthly maxima (measured in kNm) for each span length. Figure C.1 to Figure C.10 show the diagnostic plots for the normal distribution fitted to the transformed data. The diagnostic plots for the three-parameter lognormal (LN3) distribution are shown in Figure C.11 to Figure C.20, where a two-parameter lognormal (LN) distribution is fitted to the shifted data. The diagnostic plots include the Q-Q plot, P-P plot, density plot and cumulative distribution (CDF) plot, as described in Section 3.4.4.1. This is followed by the diagnostic plots for the generalised extreme value (GEV) distribution fitted to the data. The diagnostic plots for the GEV distribution are presented in Figure C.21 to Figure C.30, which include the Q-Q plot, P-P plot, density plot and return level plot.

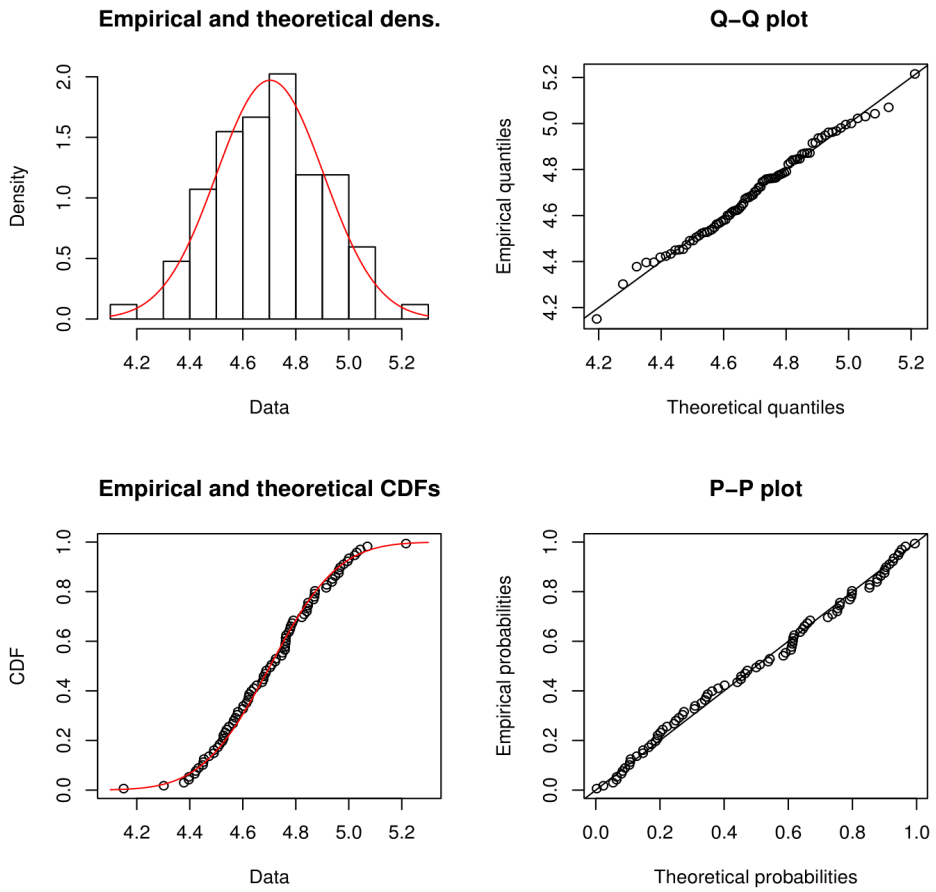

Figure C.1: Diagnostic plots for 5 m span: normal distribution fitted to transformed monthly maxima.

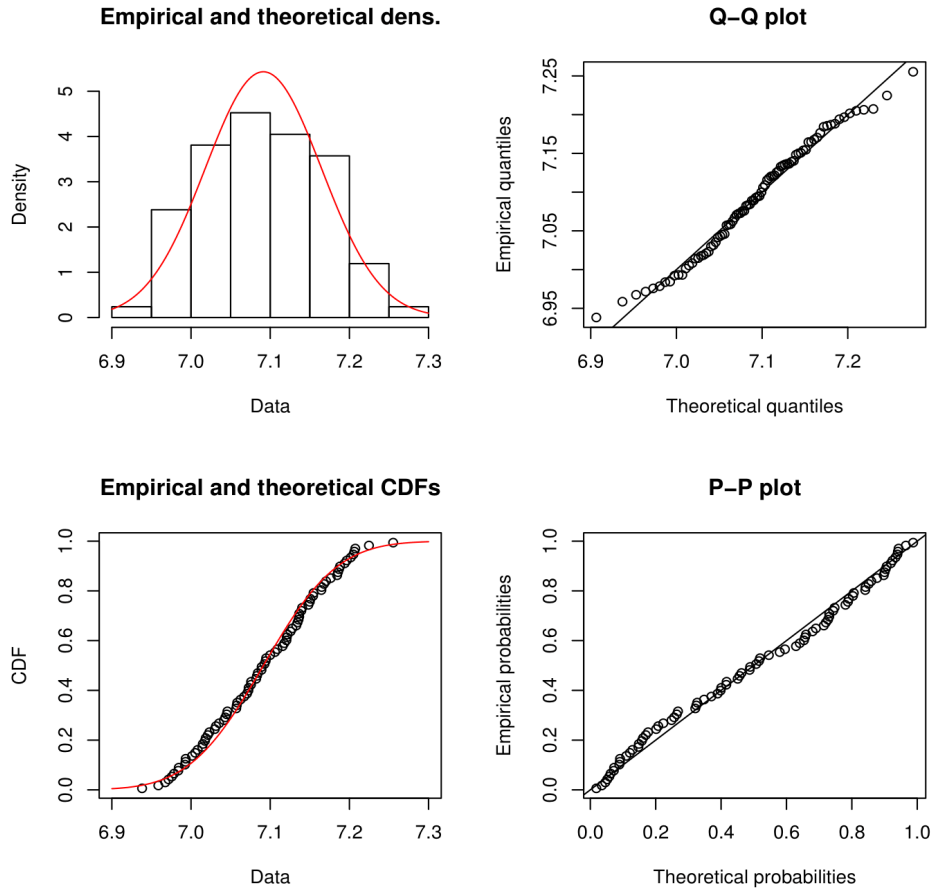

Figure C.2: Diagnostic plots for 10 m span: normal distribution fitted to transformed monthly maxima.

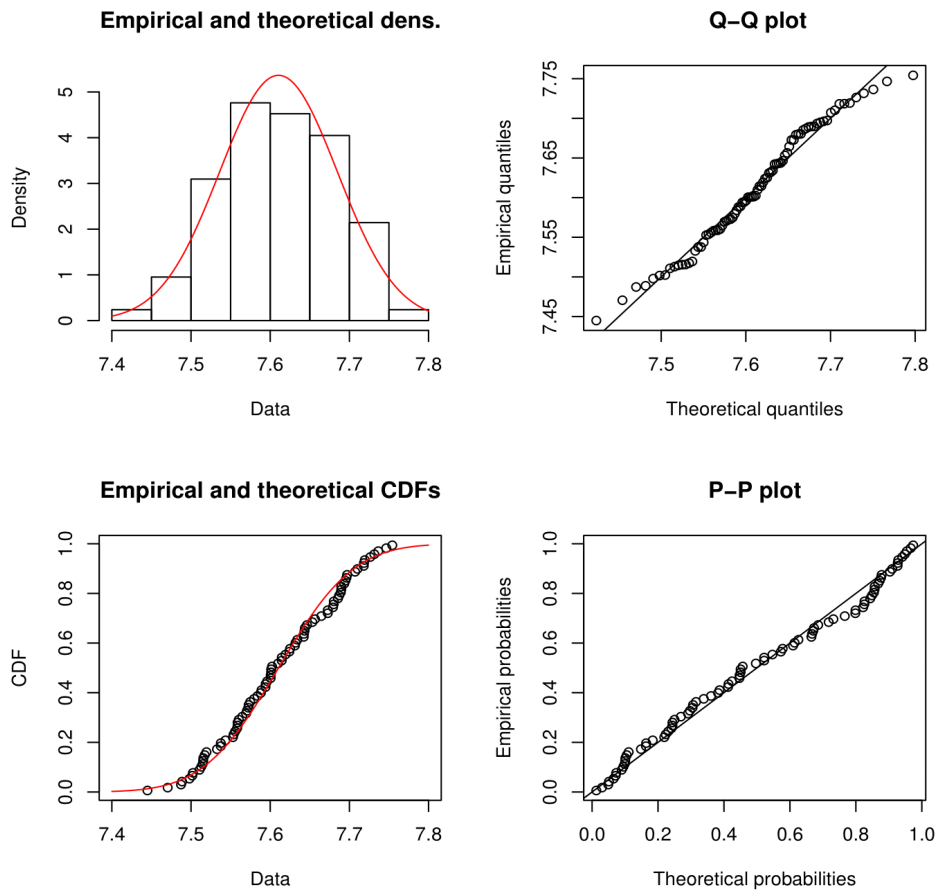

Figure C.3: Diagnostic plots for 15 m span: normal distribution fitted to transformed monthly maxima.

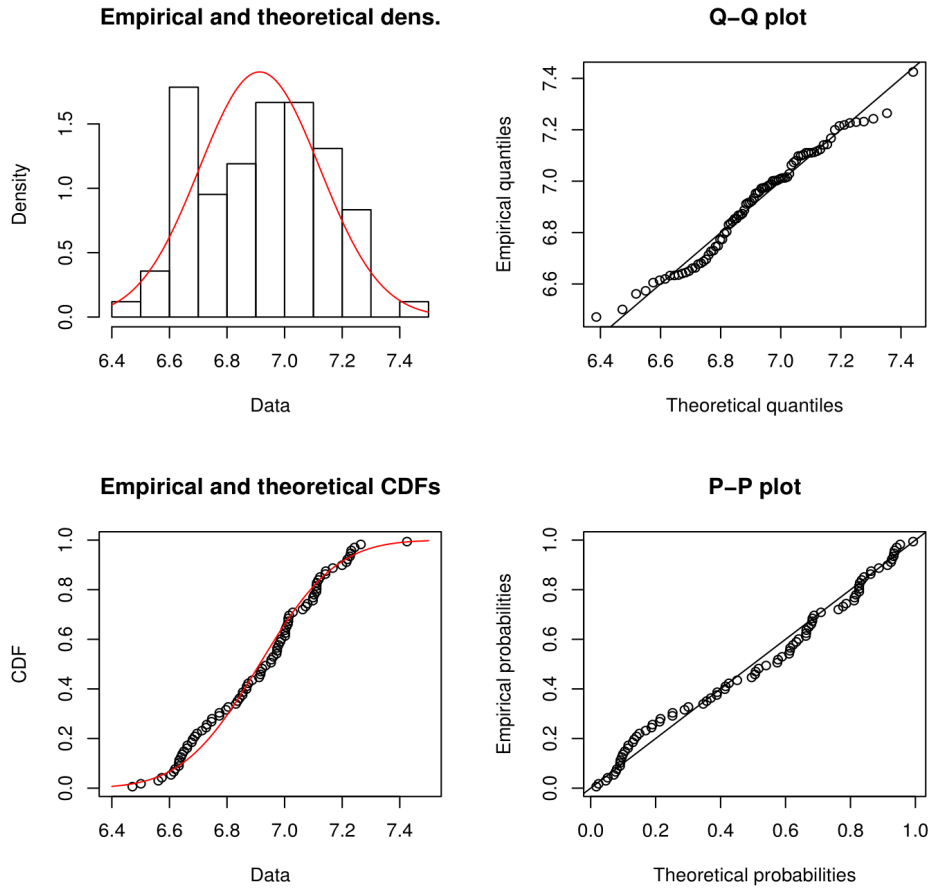

Figure C.4: Diagnostic plots for 20 m span: normal distribution fitted to transformed monthly maxima.

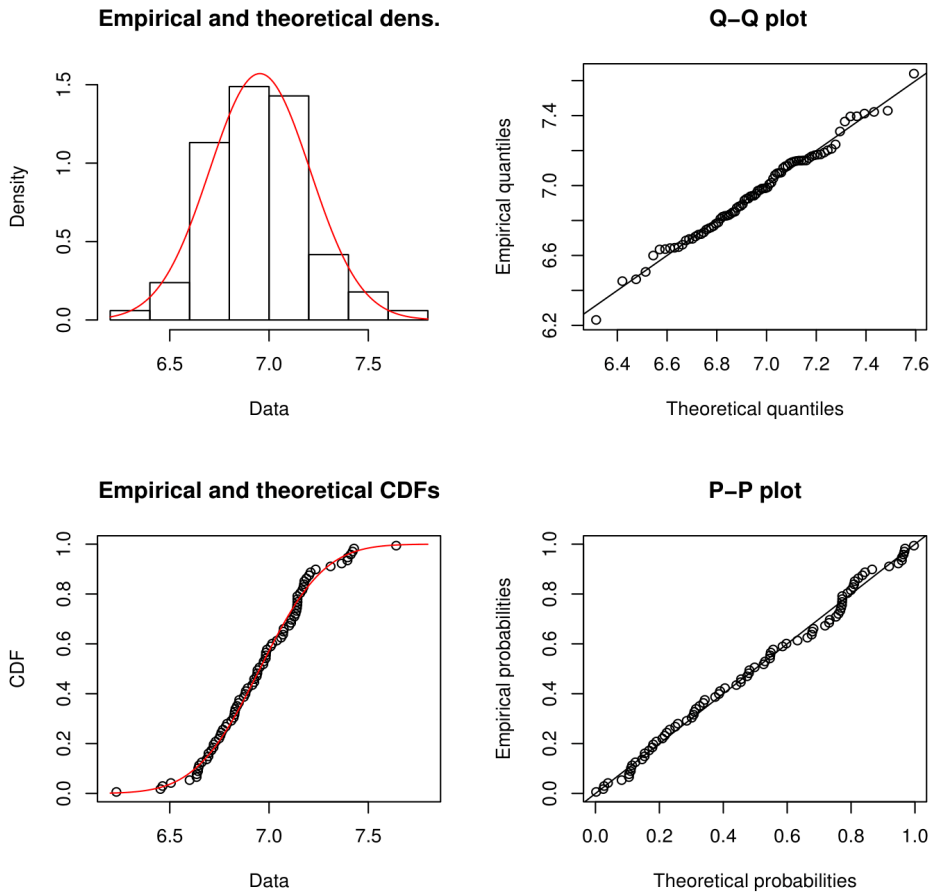

Figure C.5: Diagnostic plots for 25 m span: normal distribution fitted to transformed monthly maxima.

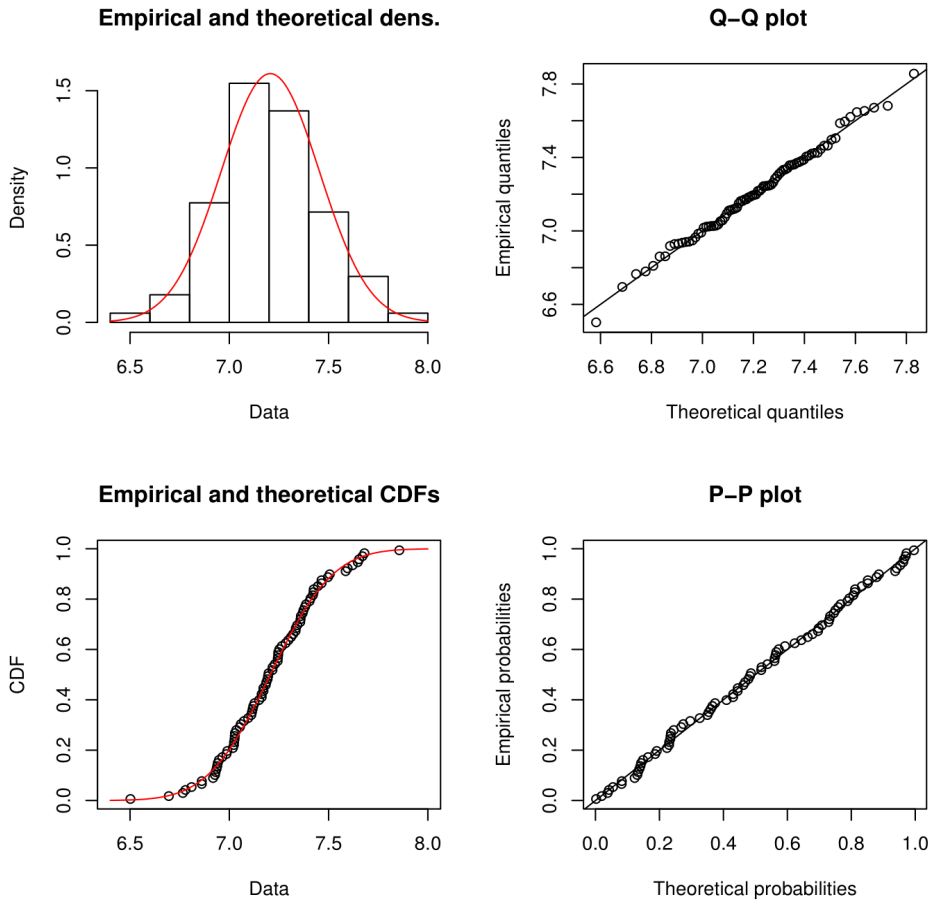

Figure C.6: Diagnostic plots for 30 m span: normal distribution fitted to transformed monthly maxima.

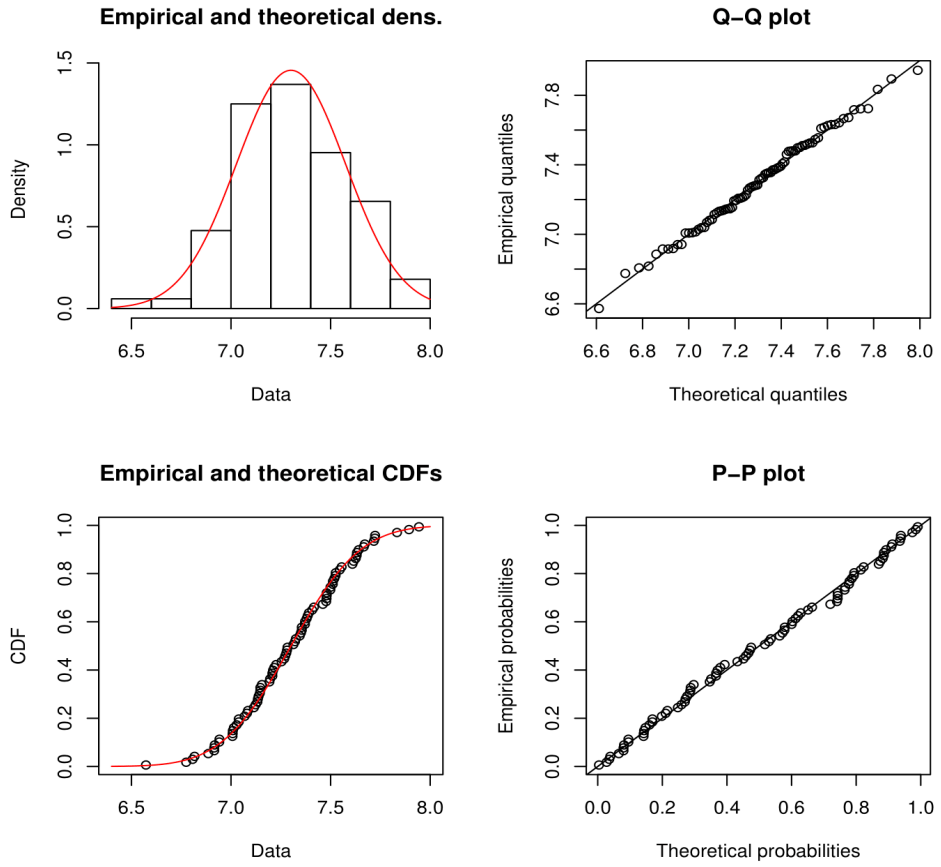

Figure C.7: Diagnostic plots for 35 m span: normal distribution fitted to transformed monthly maxima.

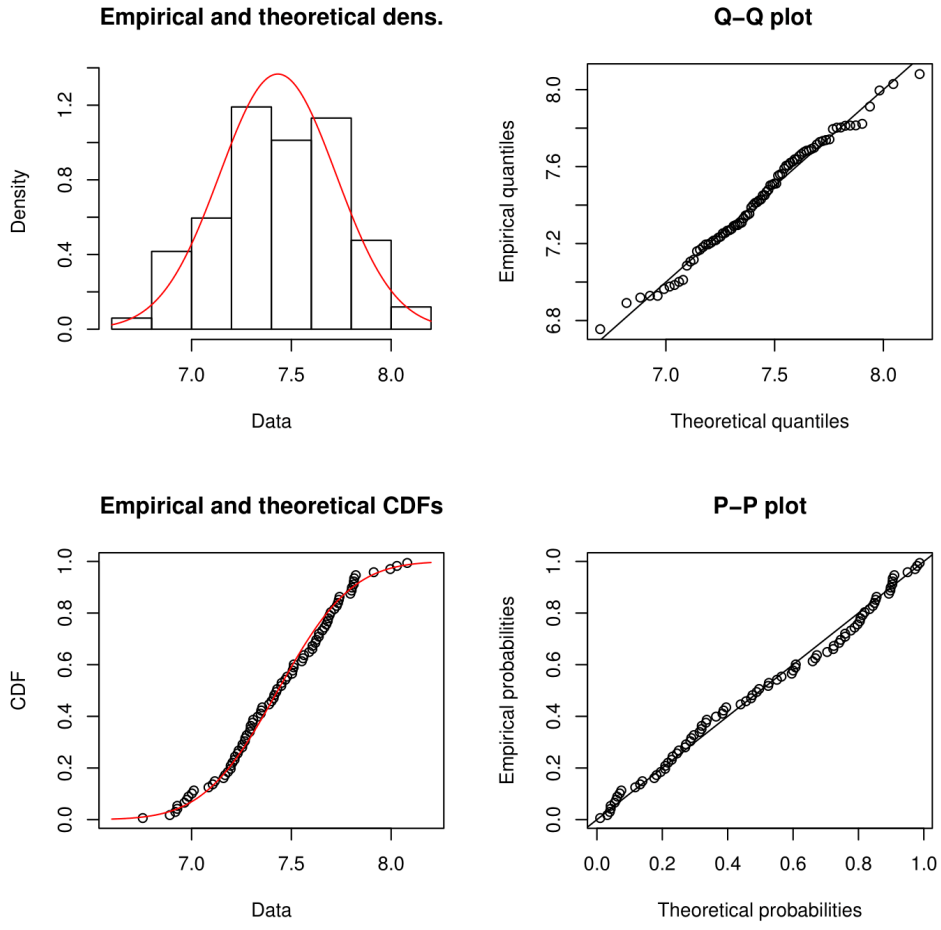

Figure C.8: Diagnostic plots for 40 m span: normal distribution fitted to transformed monthly maxima.

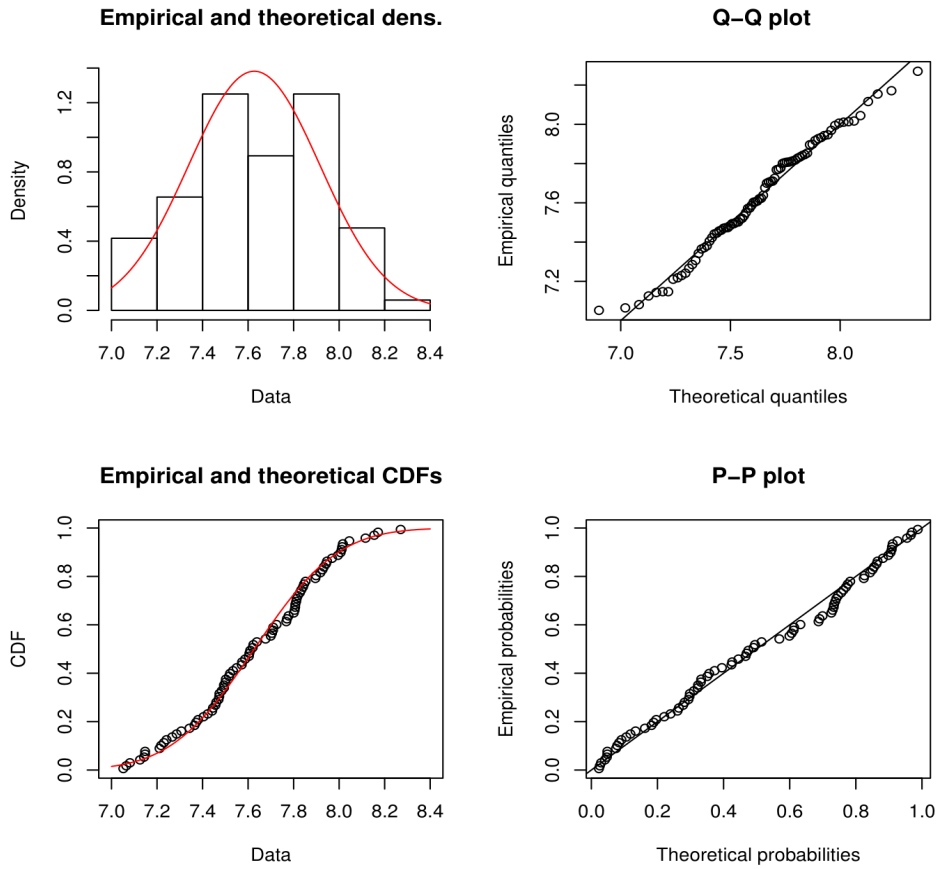

Figure C.9: Diagnostic plots for 45 m span: normal distribution fitted to transformed monthly maxima.

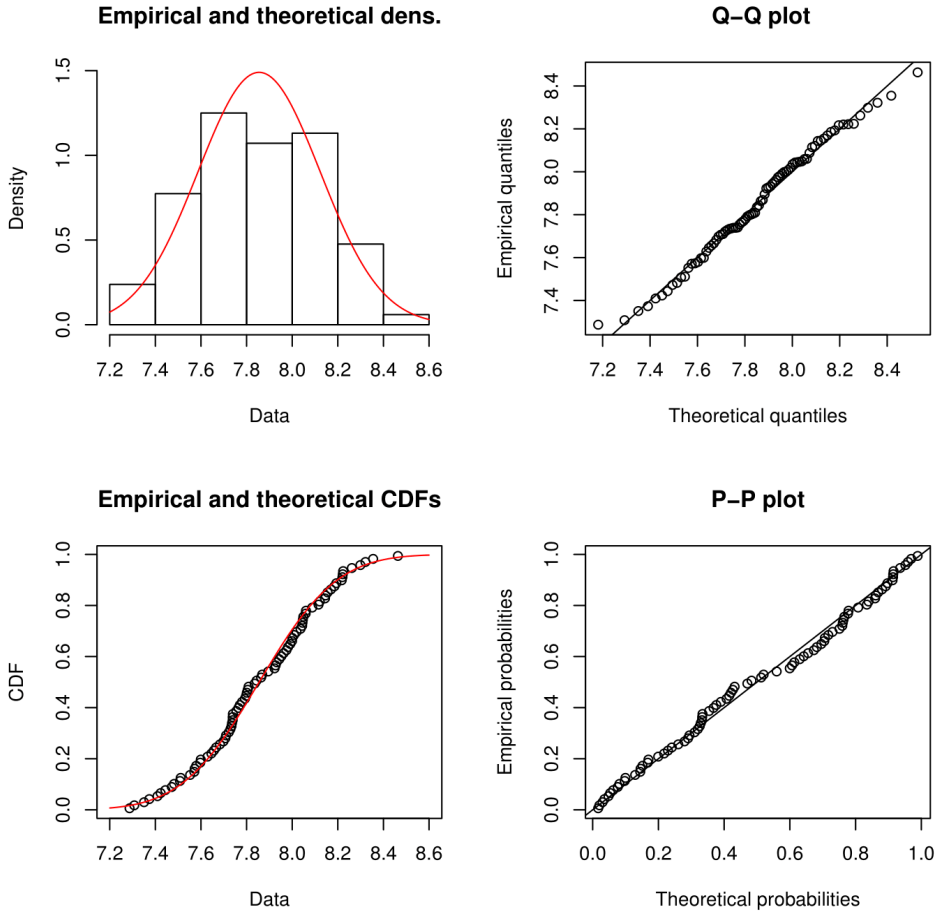

Figure C.10: Diagnostic plots for 50 m span: normal distribution fitted to transformed monthly maxima.

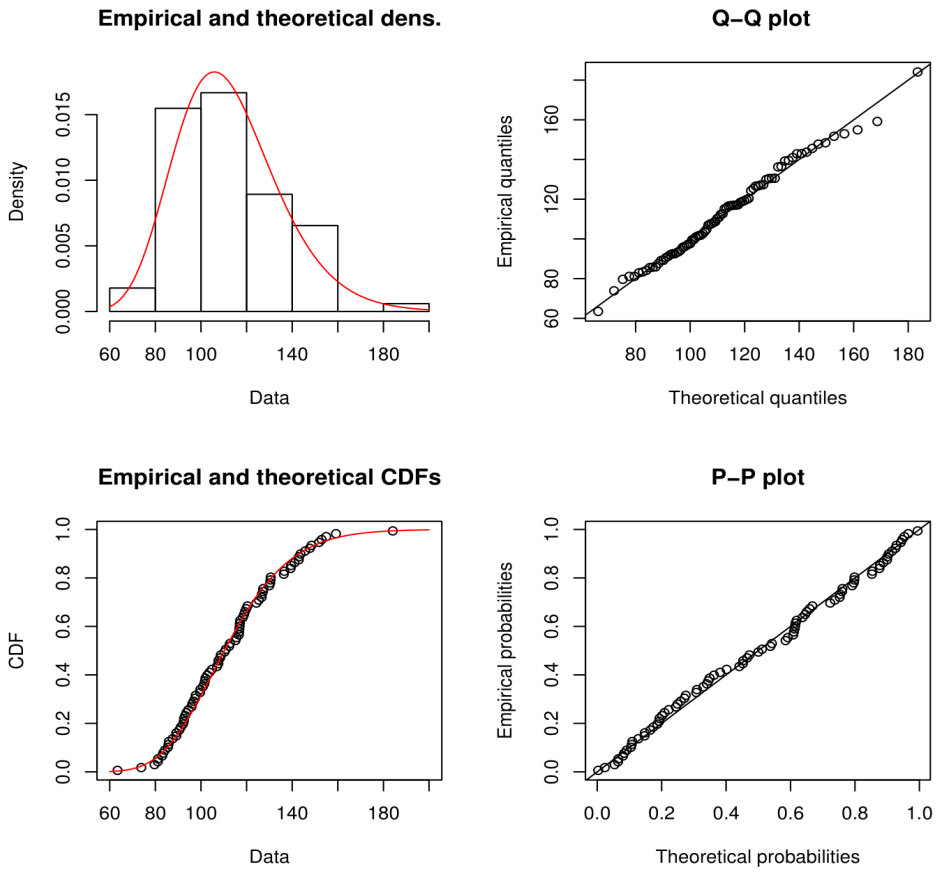

Figure C.11: Diagnostic plots for 5 m span: LN distribution fitted to shifted monthly maxima.

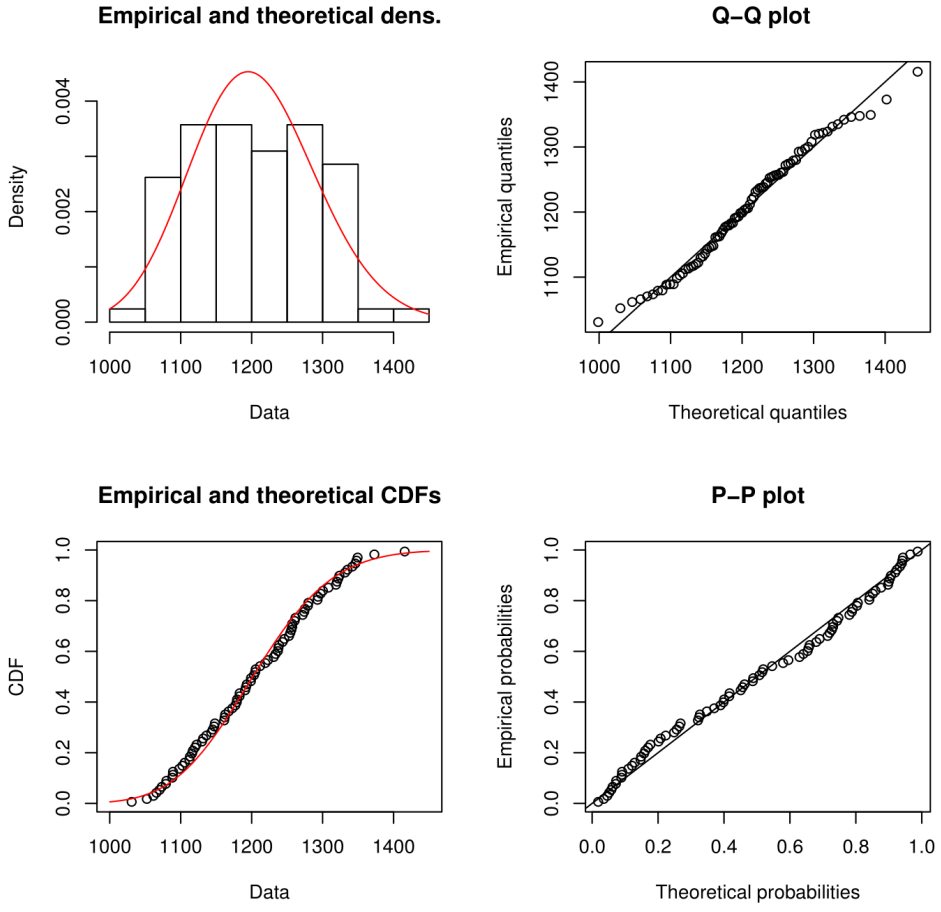

Figure C.12: Diagnostic plots for 10 m span: LN distribution fitted to shifted monthly maxima.

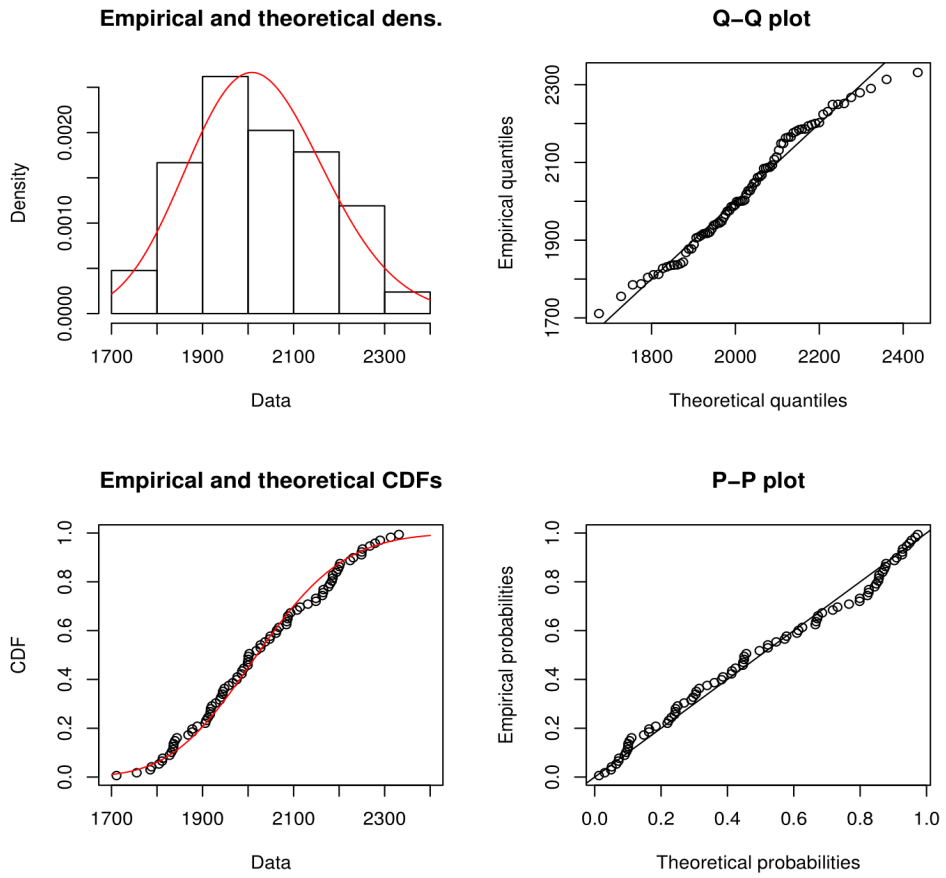

Figure C.13: Diagnostic plots for 15 m span: LN distribution fitted to shifted monthly maxima.

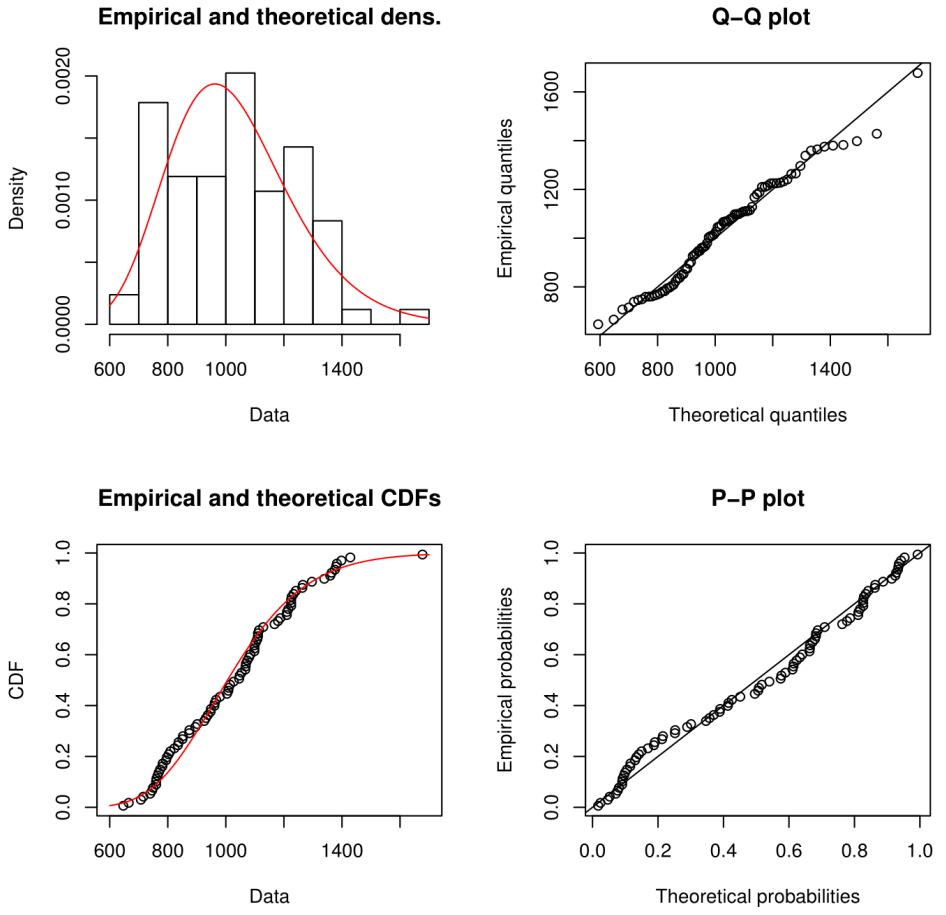

Figure C.14: Diagnostic plots for 20 m span: LN distribution fitted to shifted monthly maxima.

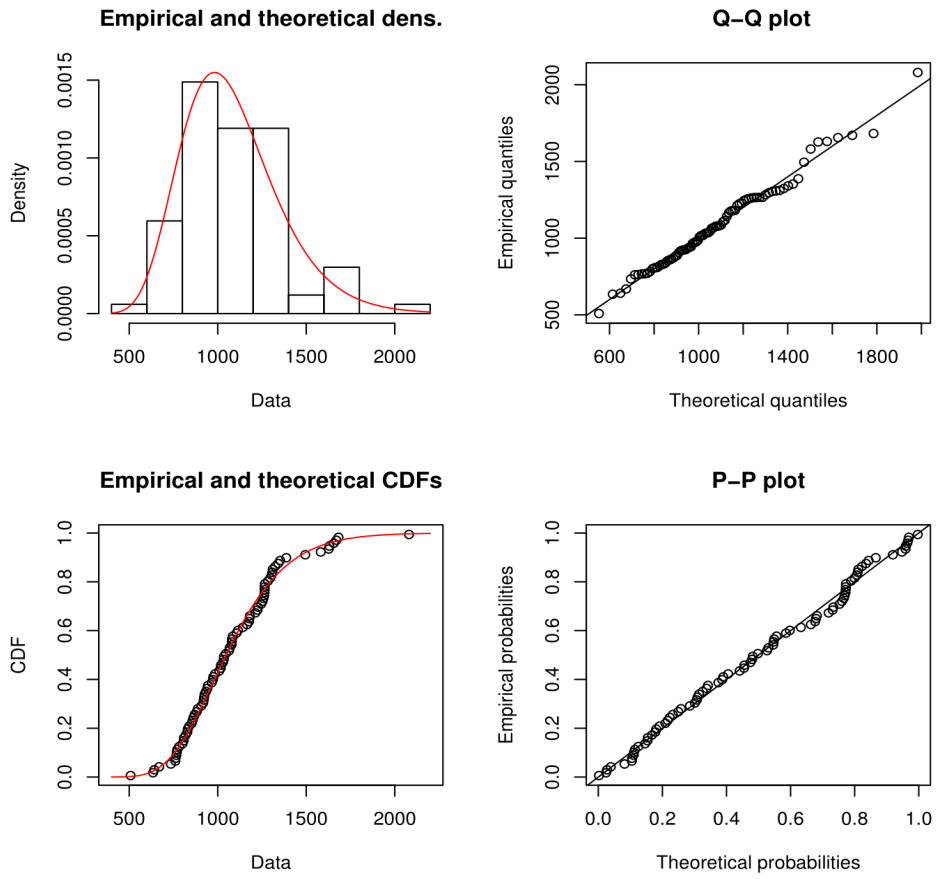

Figure C.15: Diagnostic plots for 25 m span: LN distribution fitted to shifted monthly maxima.

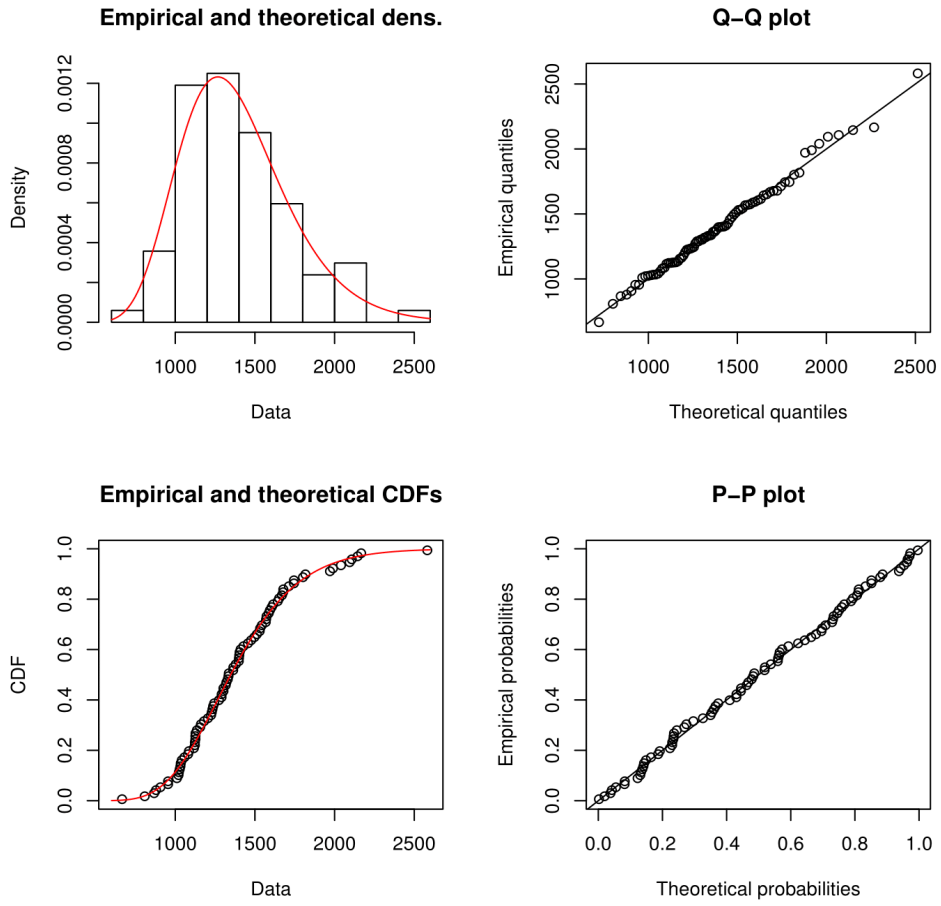

Figure C.16: Diagnostic plots for 30 m span: LN distribution fitted to shifted monthly maxima.

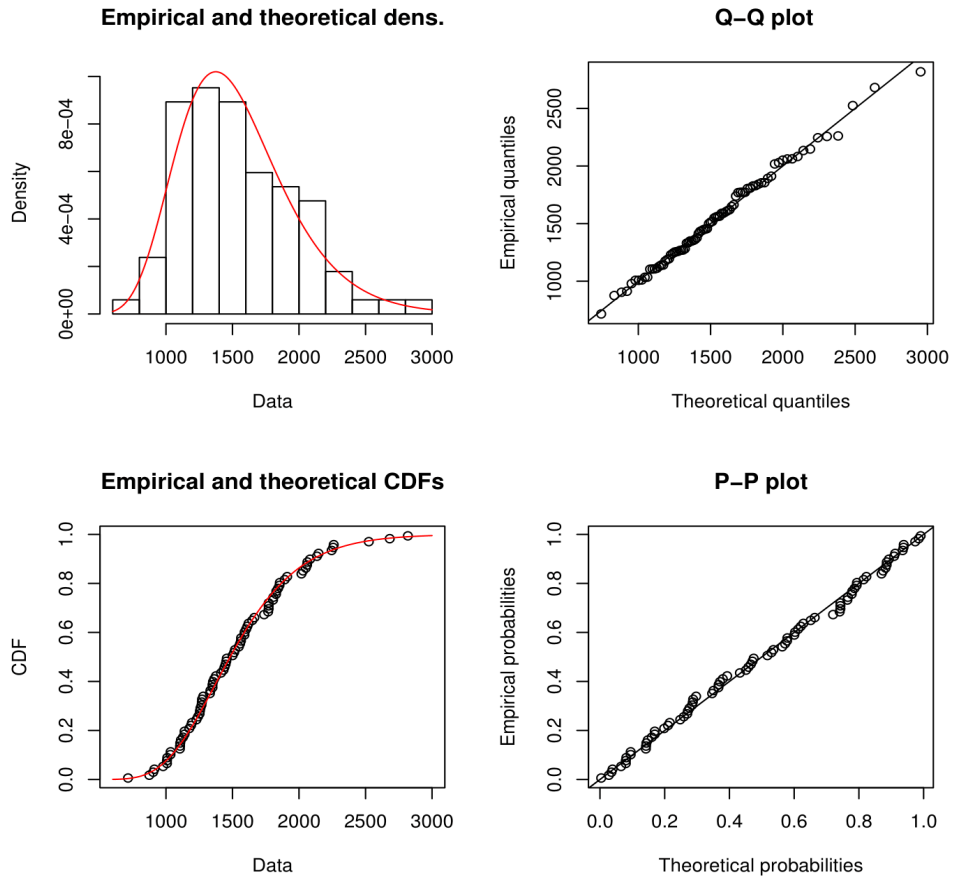

Figure C.17: Diagnostic plots for 35 m span: LN distribution fitted to shifted monthly maxima.

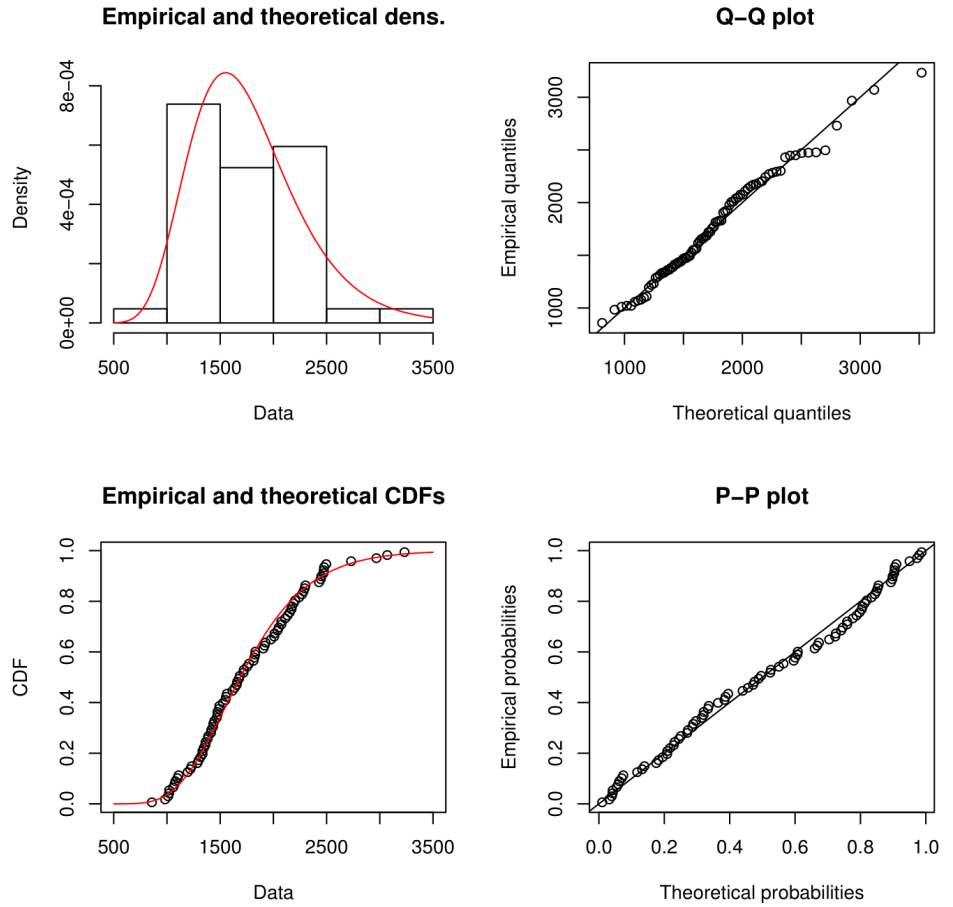

Figure C.18: Diagnostic plots for 40 m span: LN distribution fitted to shifted monthly maxima.

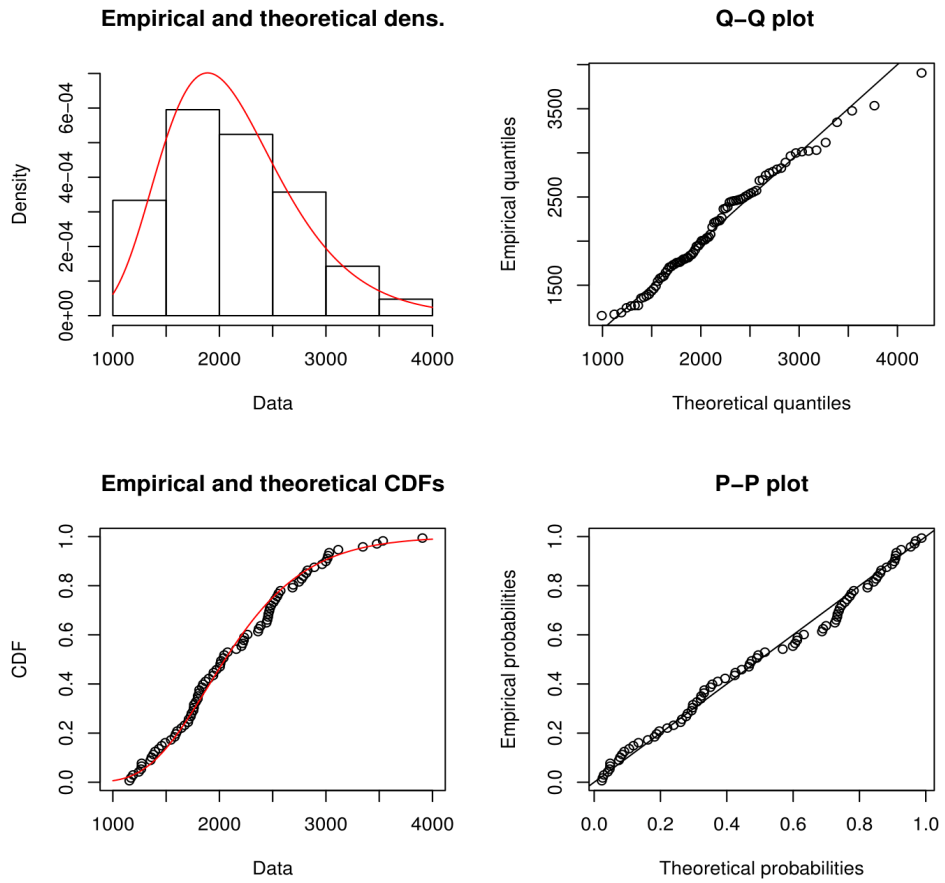

Figure C.19: Diagnostic plots for 45 m span: LN distribution fitted to shifted monthly maxima.

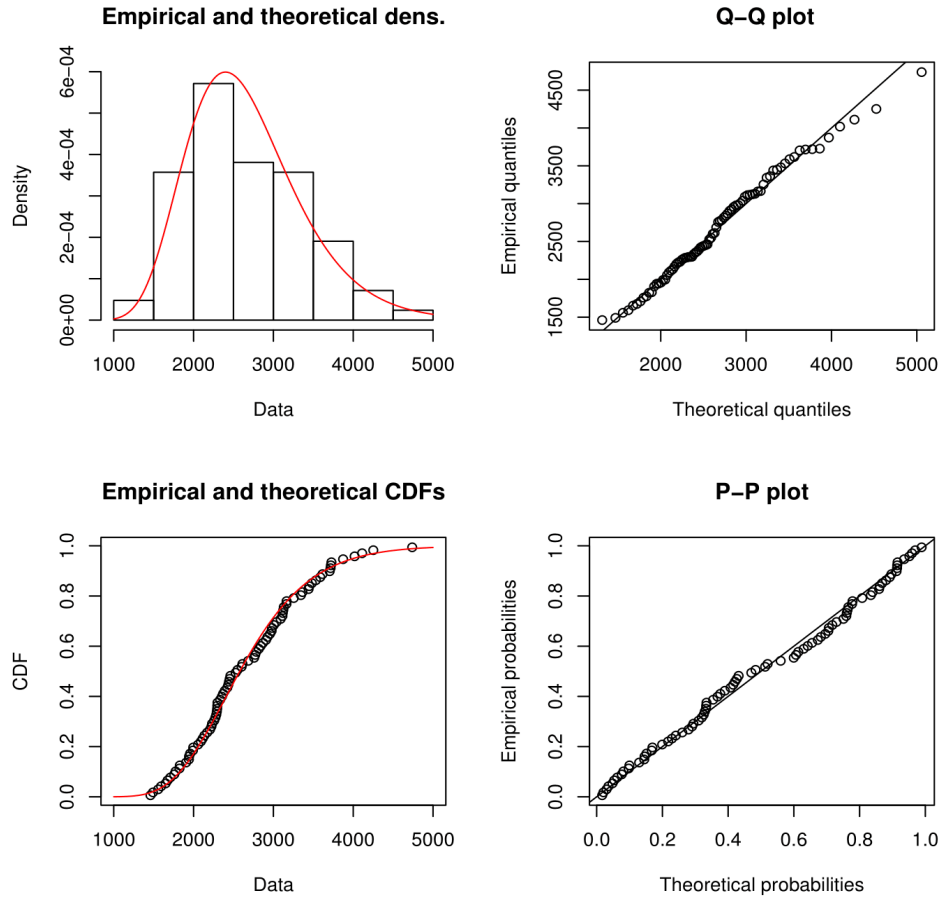

Figure C.20: Diagnostic plots for 50 m span: LN distribution fitted to shifted monthly maxima.

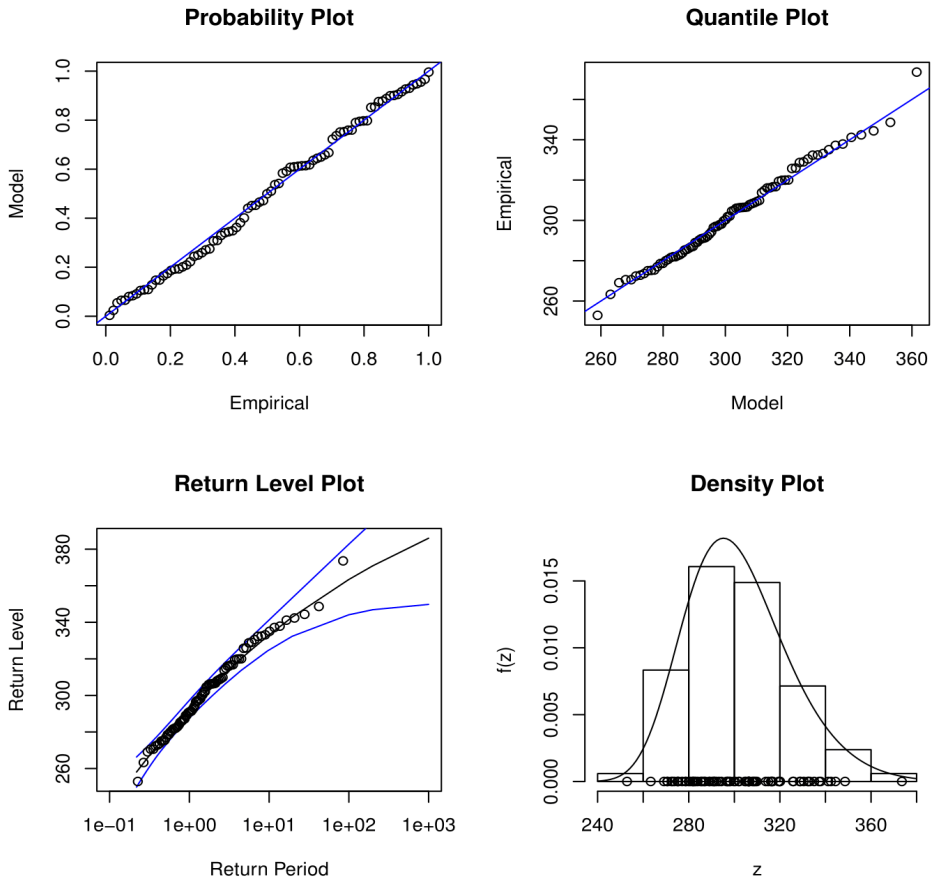

Figure C.21: Diagnostic plots for 5 m span: GEV distribution fitted to monthly maxima.

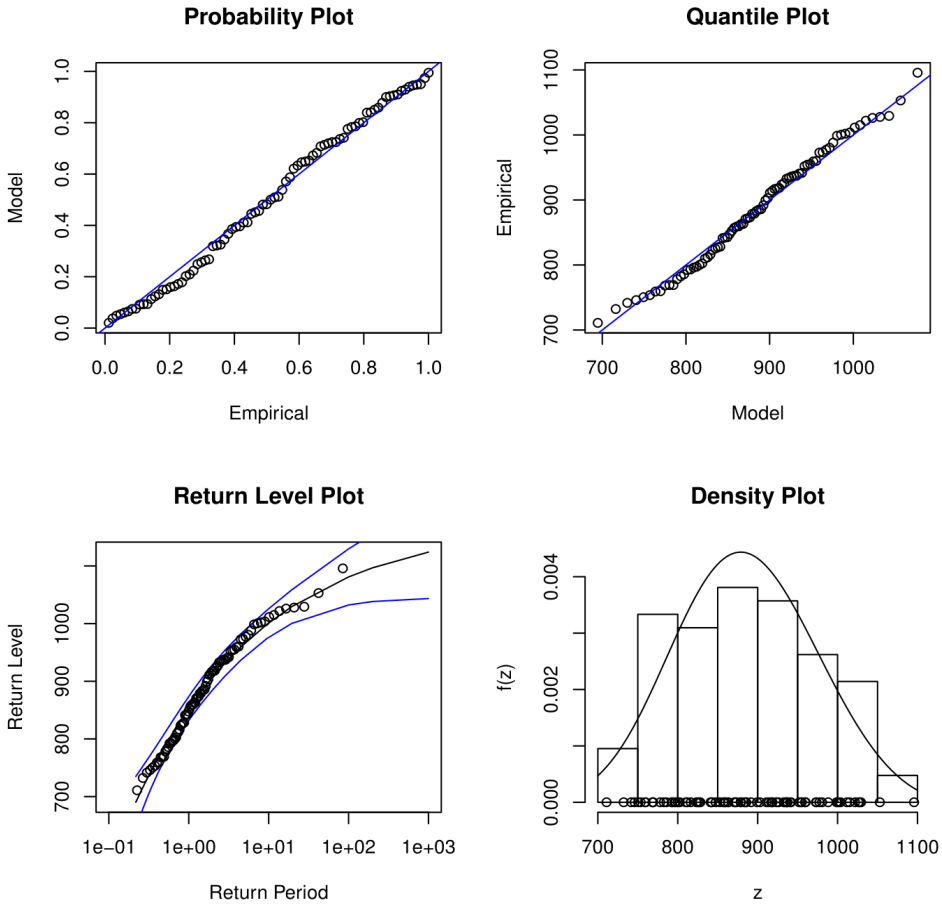

Figure C.22: Diagnostic plots for 10 m span: GEV distribution fitted to monthly maxima.

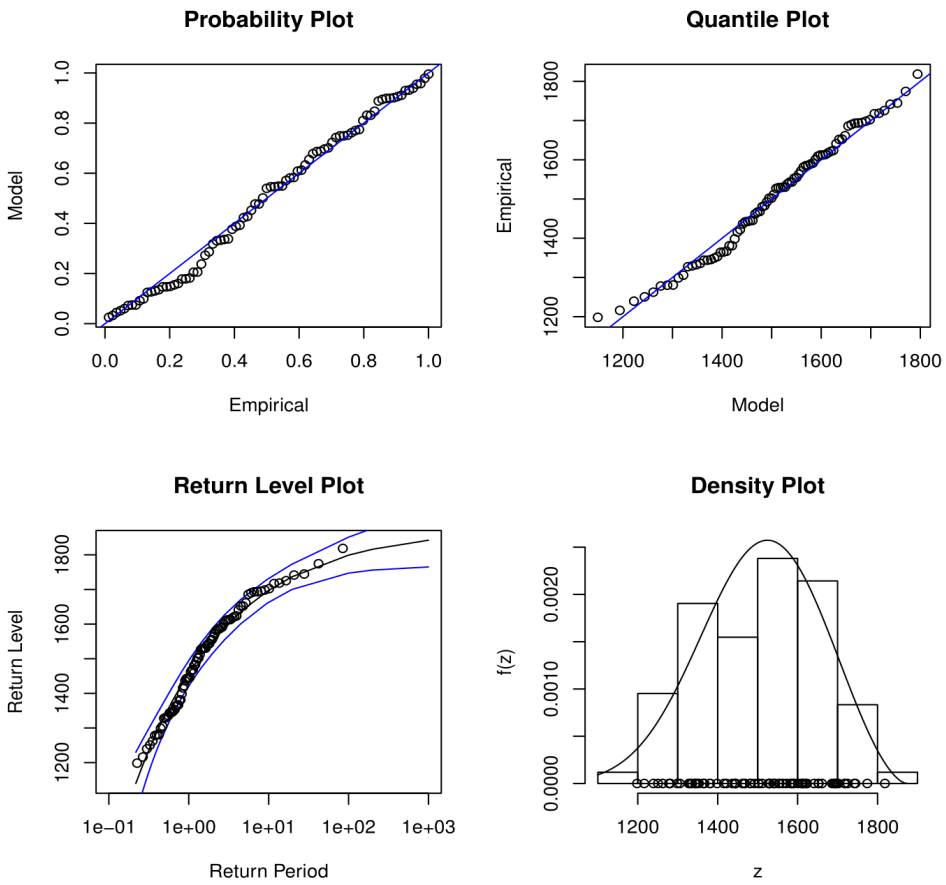

Figure C.23: Diagnostic plots for 15 m span: GEV distribution fitted to monthly maxima.

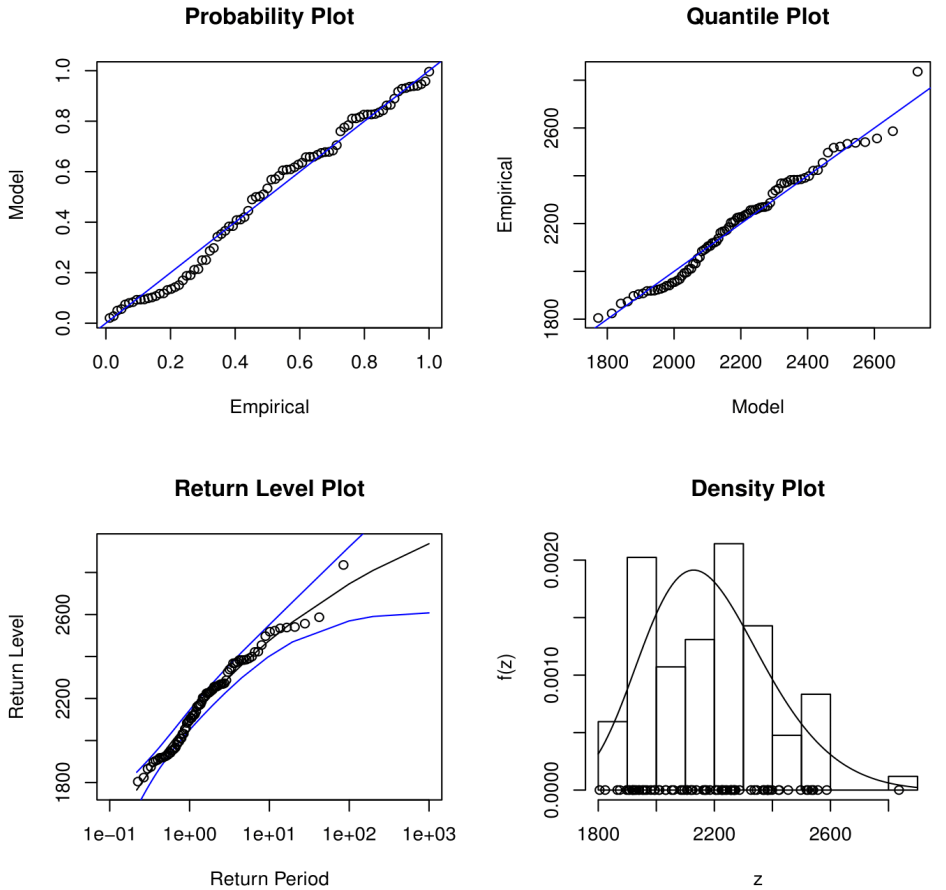

Figure C.24: Diagnostic plots for 20 m span: GEV distribution fitted to monthly maxima.

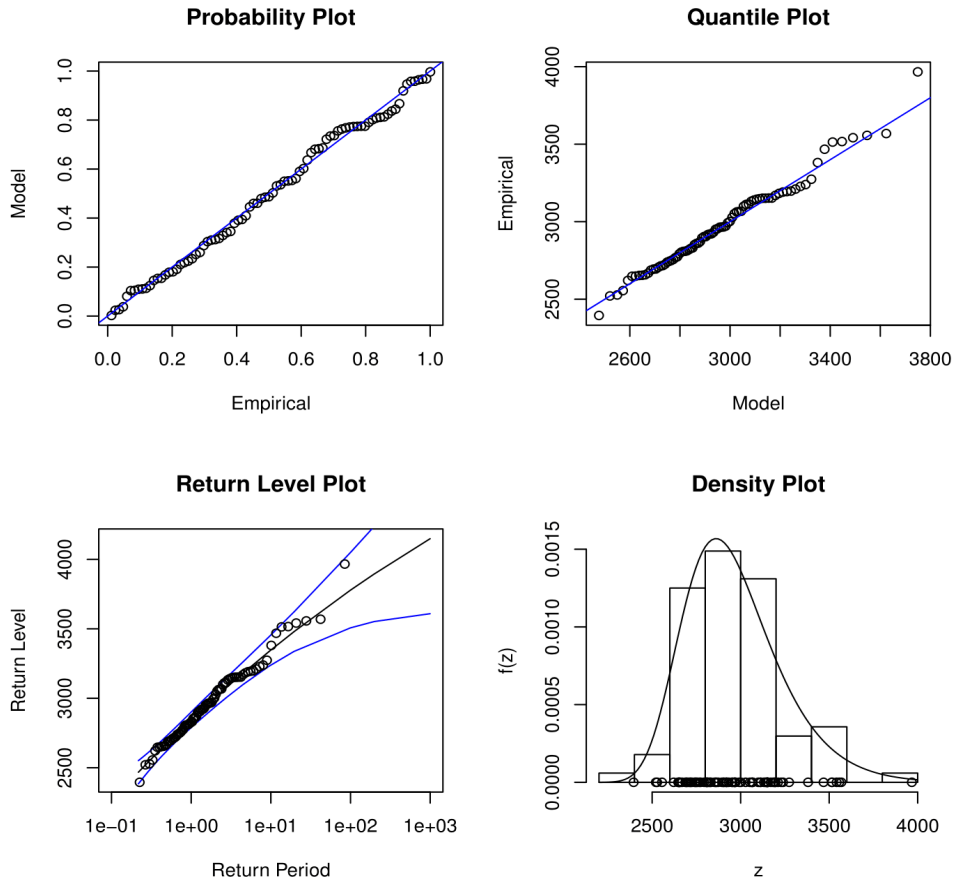

Figure C.25: Diagnostic plots for 25 m span: GEV distribution fitted to monthly maxima.

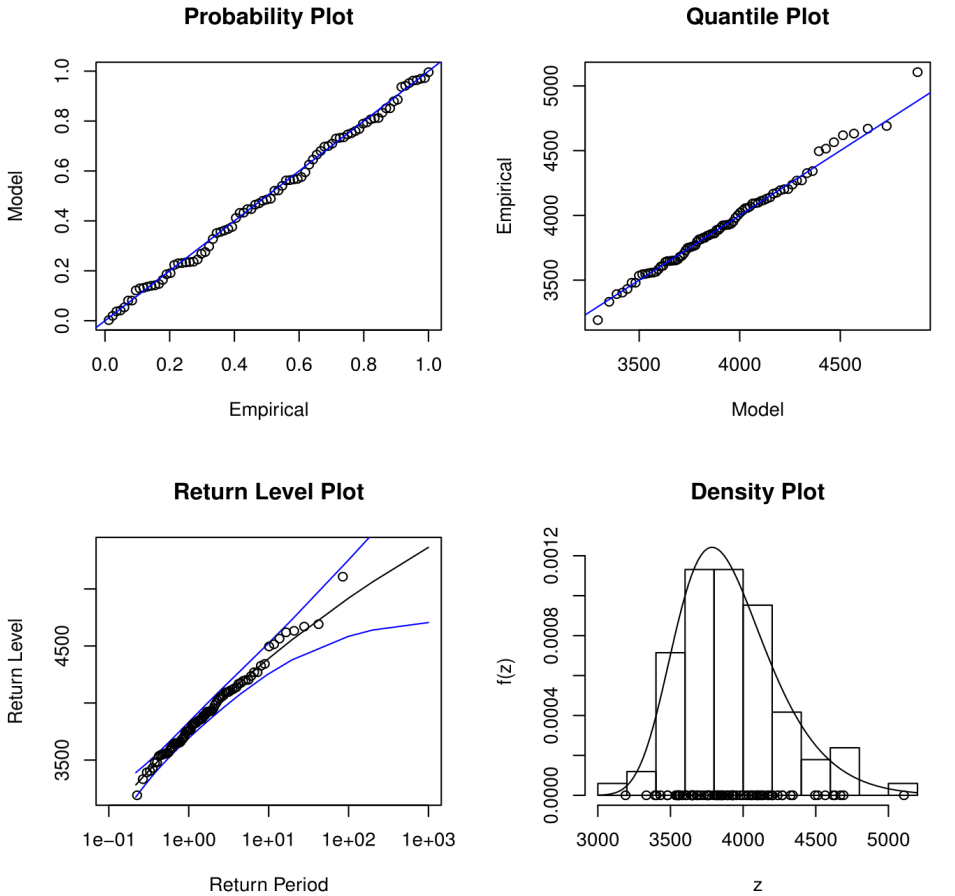

Figure C.26: Diagnostic plots for 30 m span: GEV distribution fitted to monthly maxima.

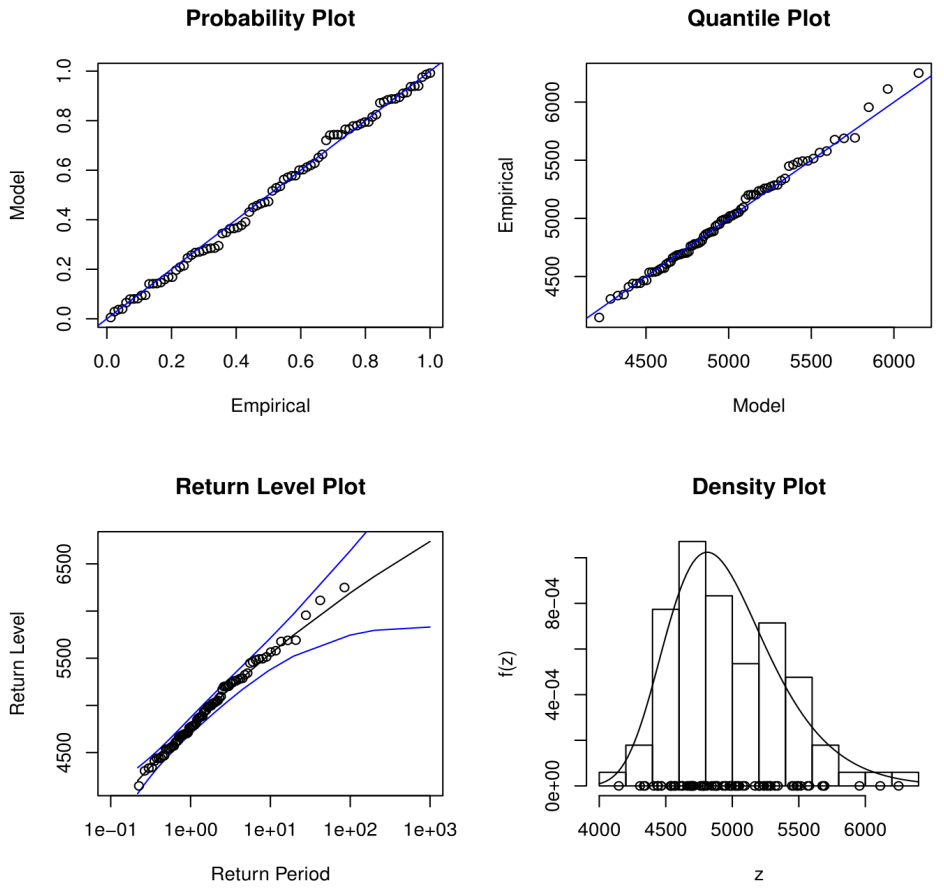

Figure C.27: Diagnostic plots for 35 m span: GEV distribution fitted to monthly maxima.

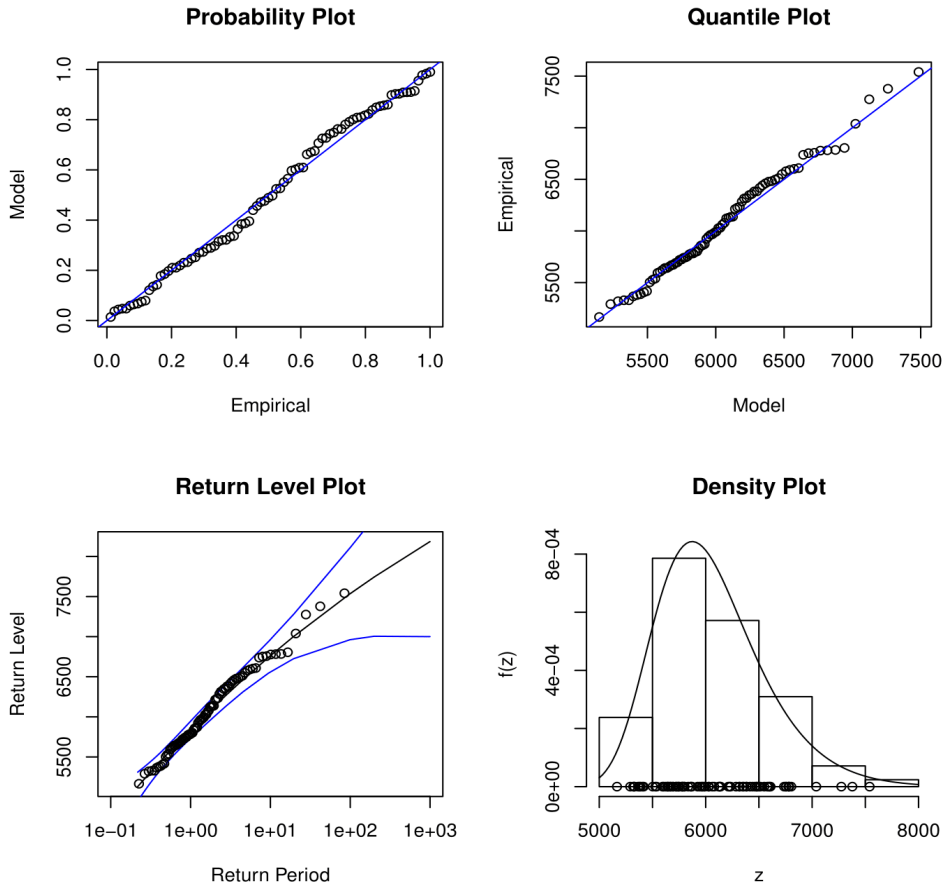

Figure C.28: Diagnostic plots for 40 m span: GEV distribution fitted to monthly maxima.

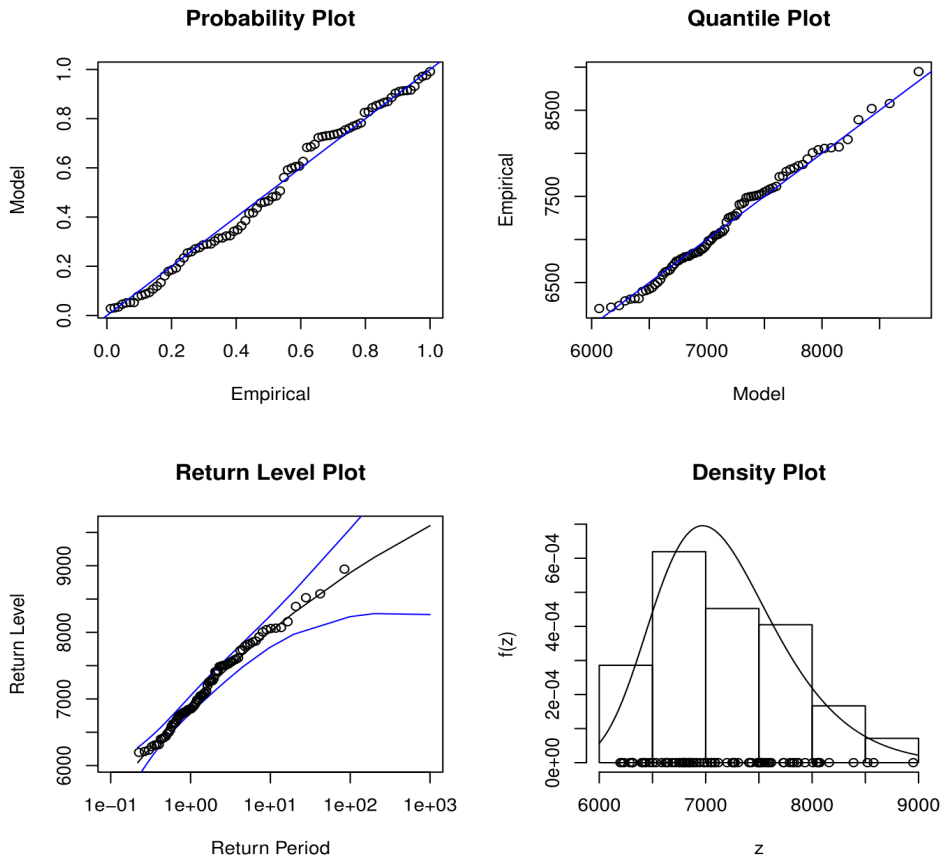

Figure C.29: Diagnostic plots for 45 m span: GEV distribution fitted to monthly maxima.

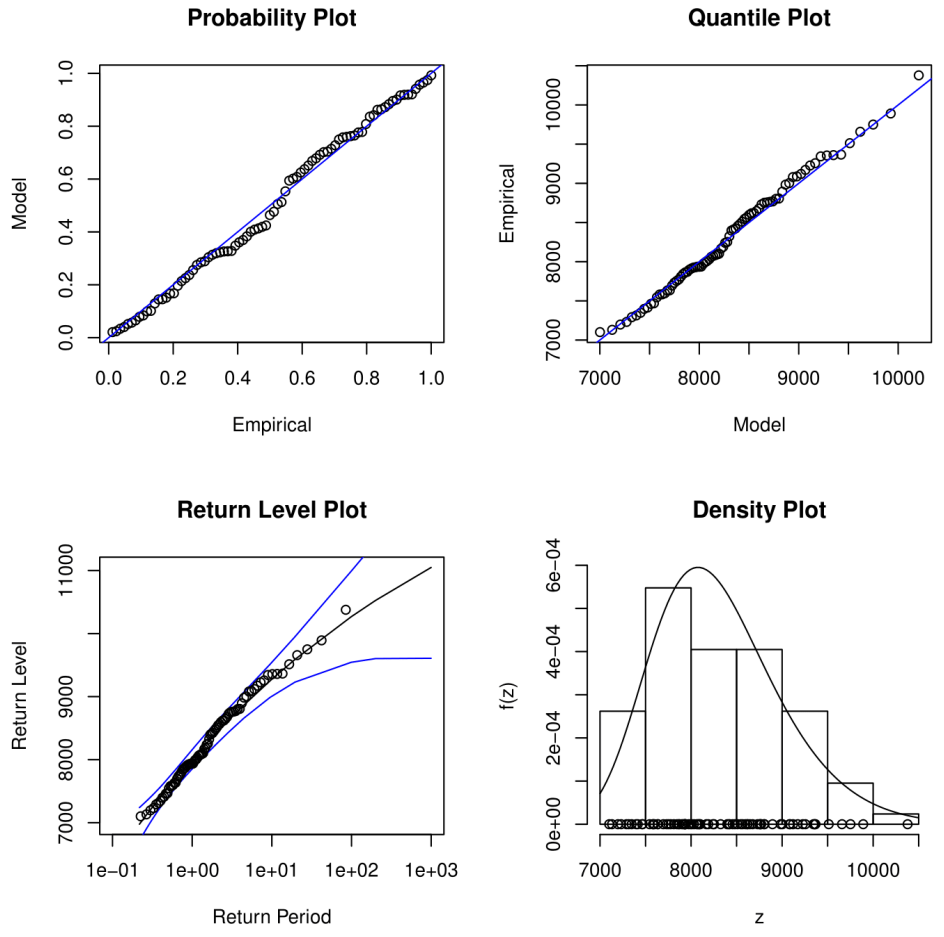

Figure C.30: Diagnostic plots for 50 m span: GEV distribution fitted to monthly maxima.

Appendix D: Diagnostic Plots for Kilner Park Case Study

The relevant diagnostic plots for Chapter 4 Section 4.5.2 are provided in this section. The data represents the combined monthly maxima (measured in kNm) carried by the critical spine beam. Figure D.1 to Figure D.8 represent the diagnostic plots for the three-parameter lognormal (LN3) distribution, where a two-parameter lognormal (LN) distribution is fitted to the shifted data. Figure D.9 to Figure D.16 show the diagnostic plots for the generalised extreme value (GEV) distribution fitted to the data. Load Case 1 to 8 are described in Section 4.4.2 and labelled in the figures according to which traffic lane is closest to the critical spine beam (in descending order). The notation for two traffic lanes is $(Q_1;Q_2)$ and for three traffic lanes is $(Q_1;Q_2;Q_3)$.

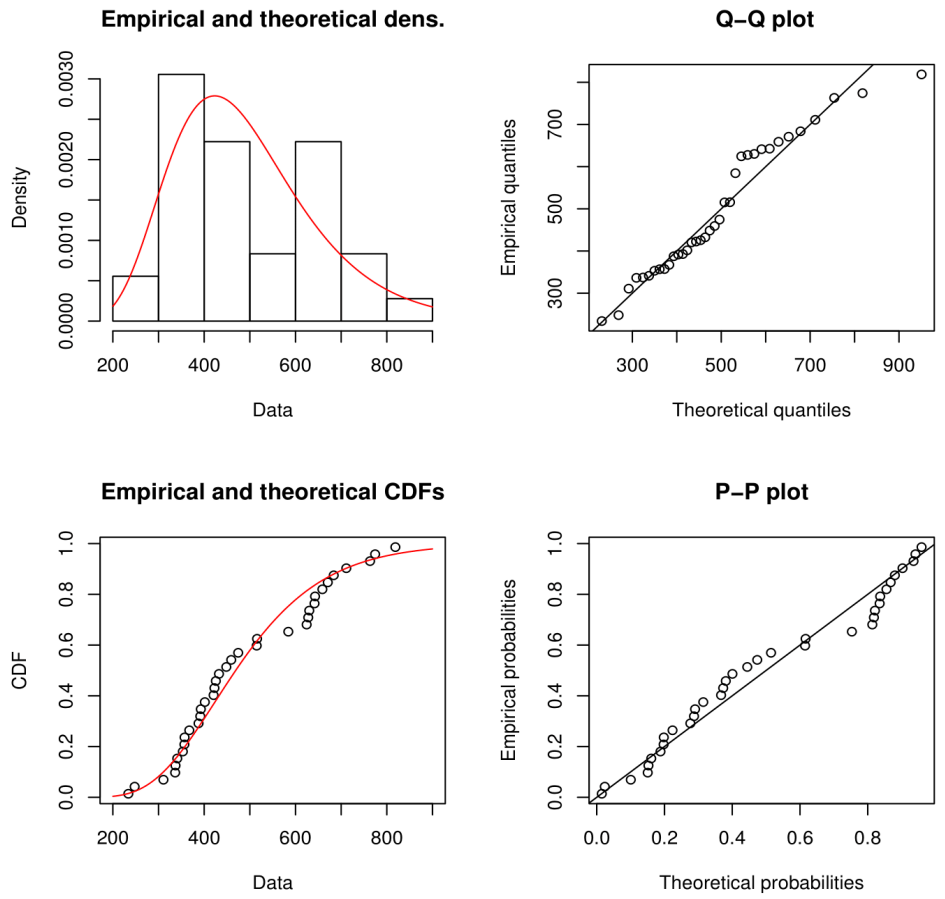

Figure D.1: Diagnostic plots for Load Case 1 (*Nb1*;*Nb2*): LN distribution fitted to shifted data.

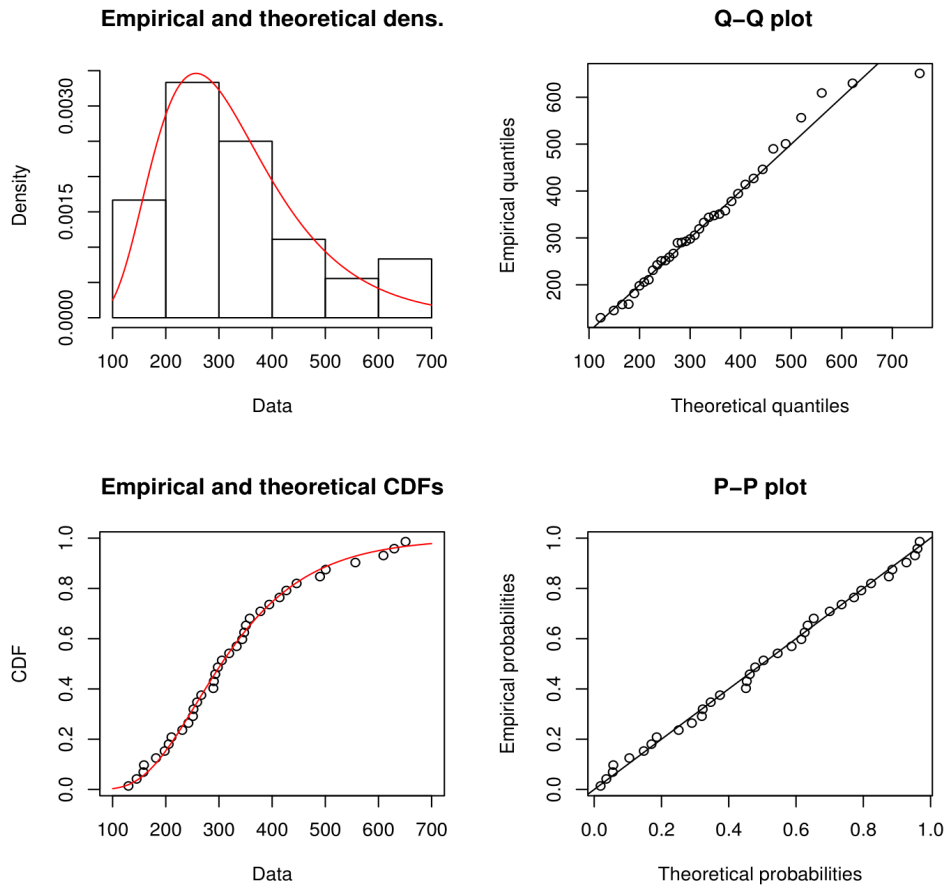

Figure D.2: Diagnostic plots for Load Case 2 (*Sb1*;*Sb2*): LN distribution fitted to shifted data.

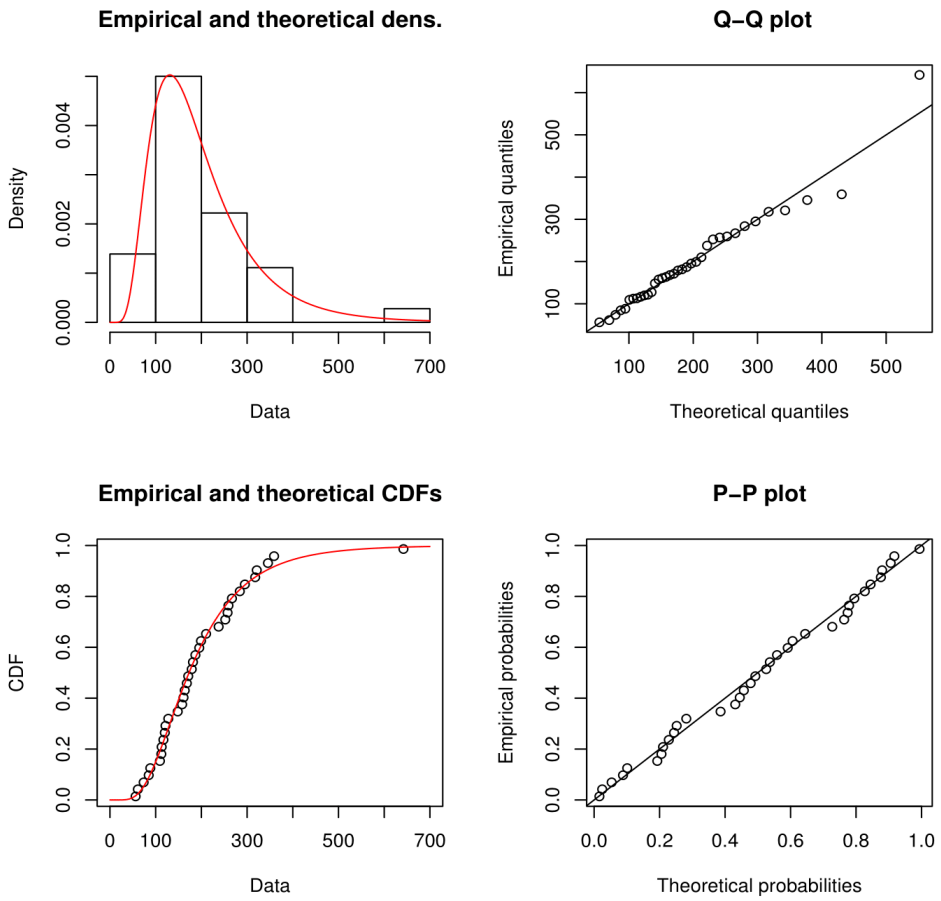

Figure D.3: Diagnostic plots for Load Case 3 (*Nb2*;*Nb1*): LN distribution fitted to shifted data.

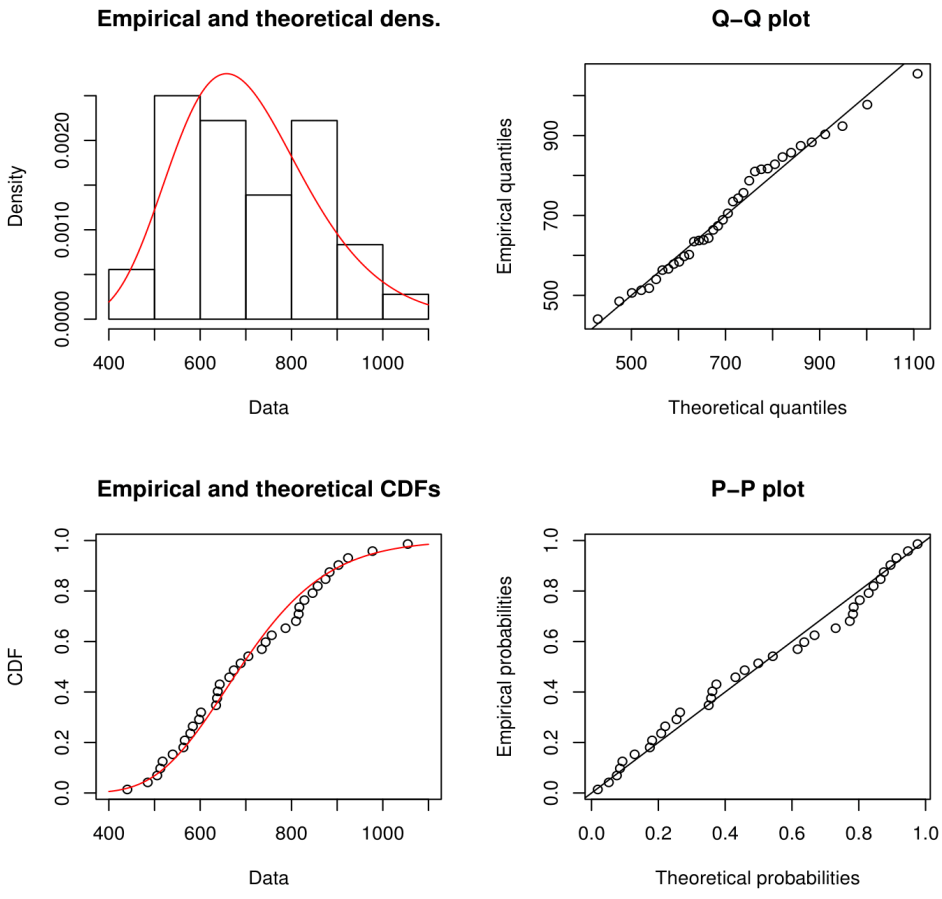

Figure D.4: Diagnostic plots for Load Case 4 (*Sb2*;*Sb1*): LN distribution fitted to shifted data.

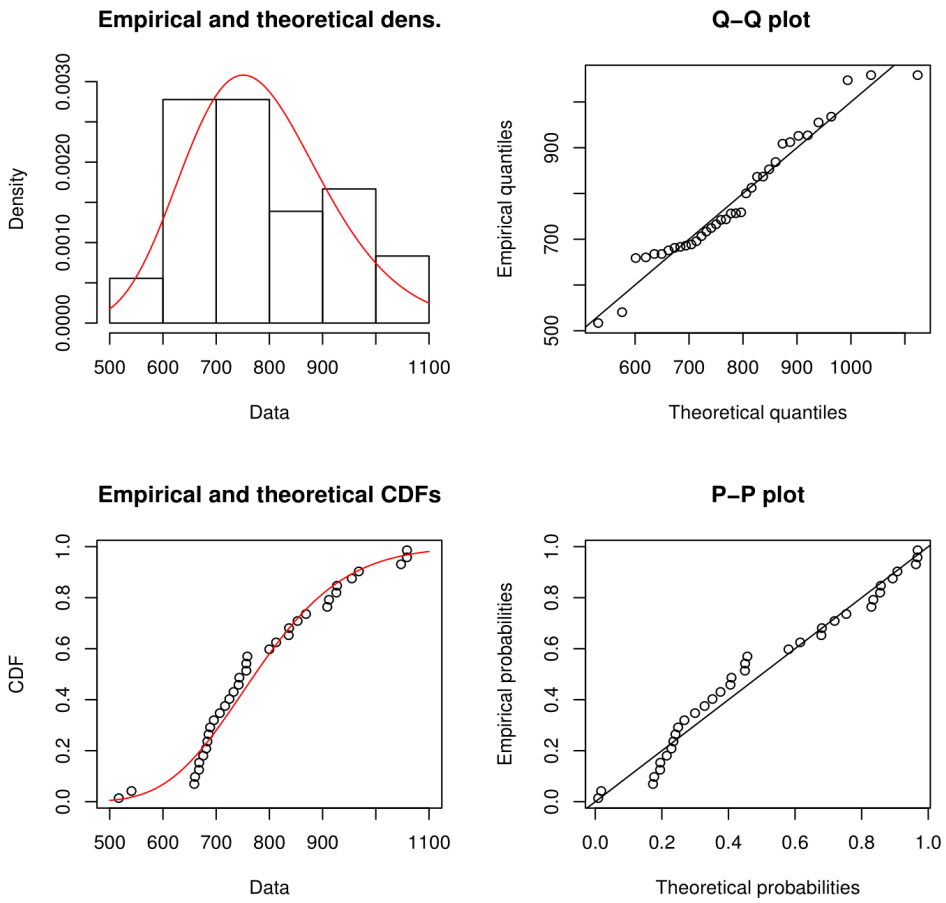

Figure D.5: Diagnostic plots for Load Case 5 (*Nb1*;*Sb1*): LN distribution fitted to shifted data.

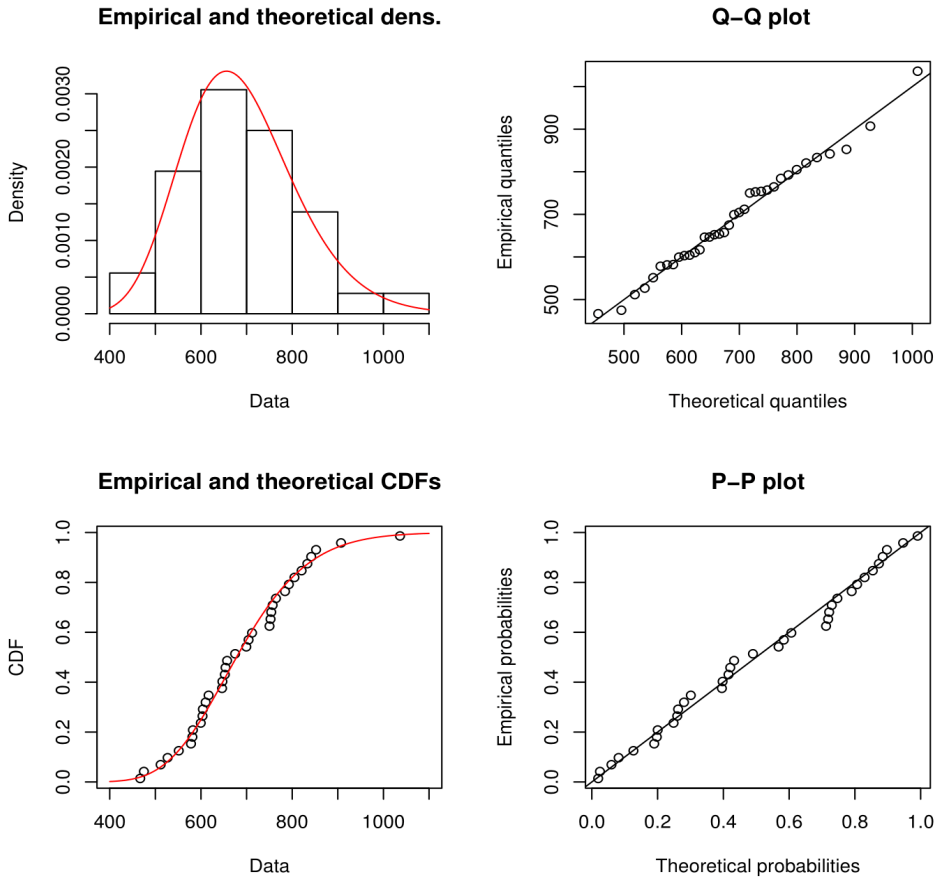

Figure D.6: Diagnostic plots for Load Case 6 (*Sb1*;*Nb1*): LN distribution fitted to shifted data.

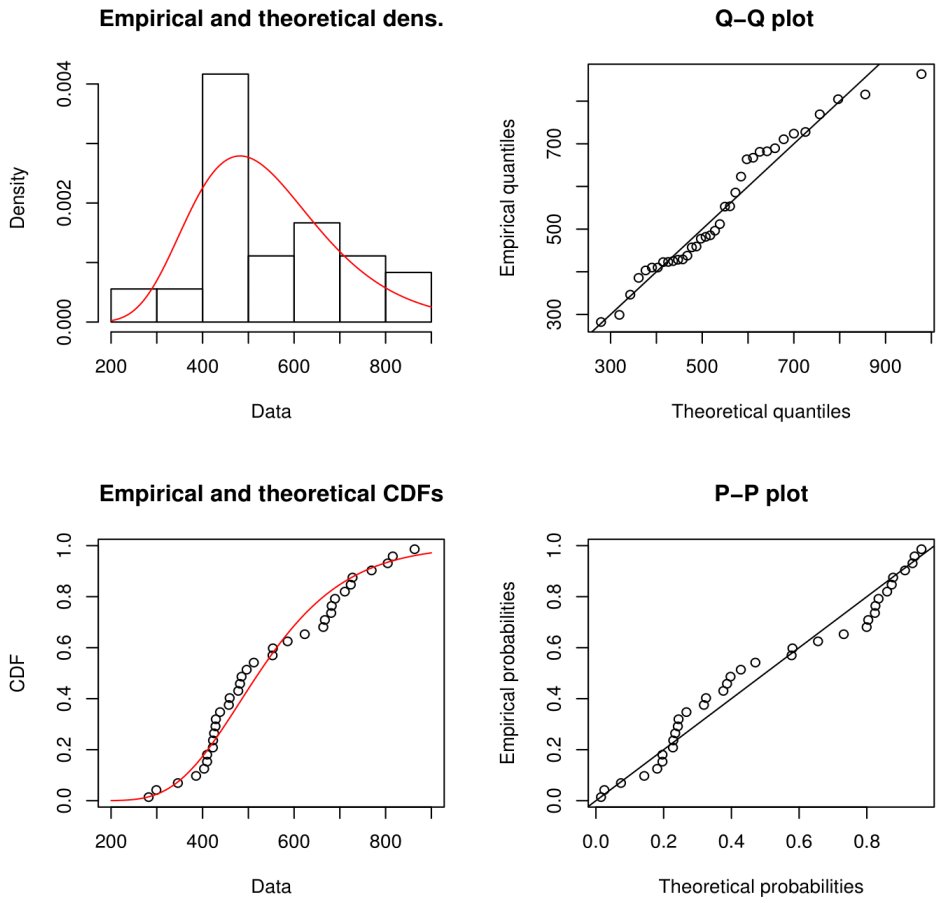

Figure D.7: Diagnostic plots for Load Case 7 (*Nb1*;*Nb2*;*Sb2*): LN distribution fitted to shifted data.

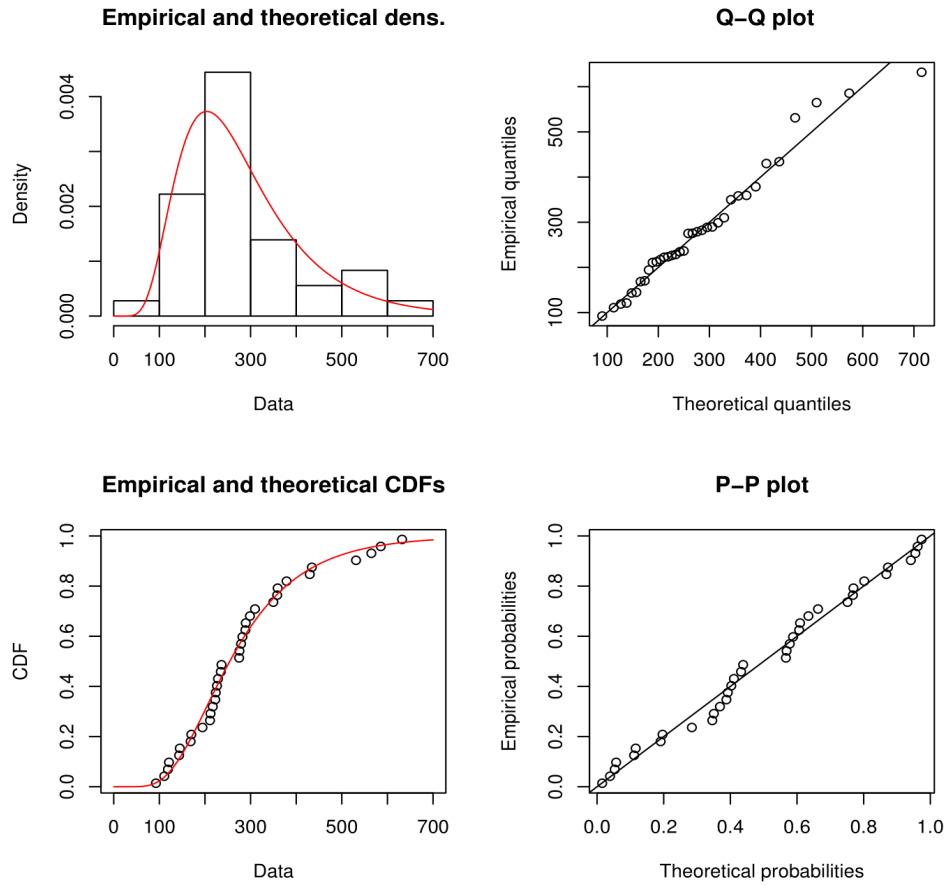

Figure D.8: Diagnostic plots for Load Case 8 (*Sb1*;*Sb2*;*Nb2*): LN distribution fitted to shifted data.

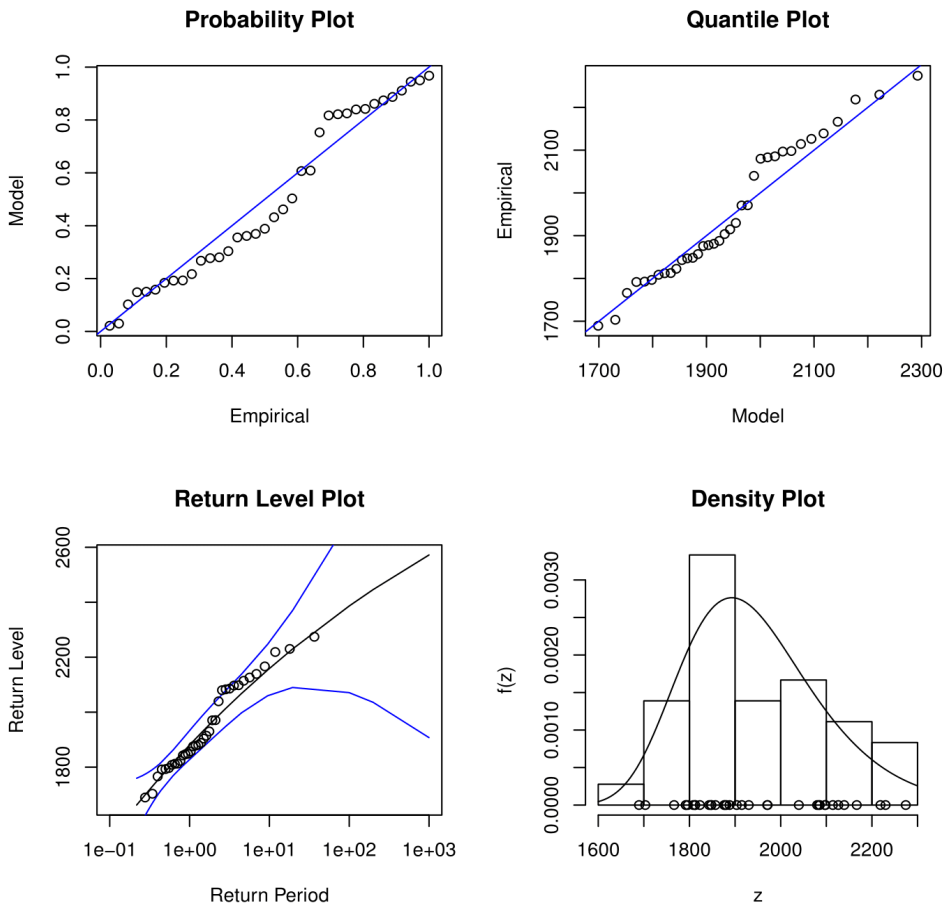

Figure D.9: Diagnostic plots for Load Case 1 (*Nb1*;*Nb2*): GEV distribution fitted to data.

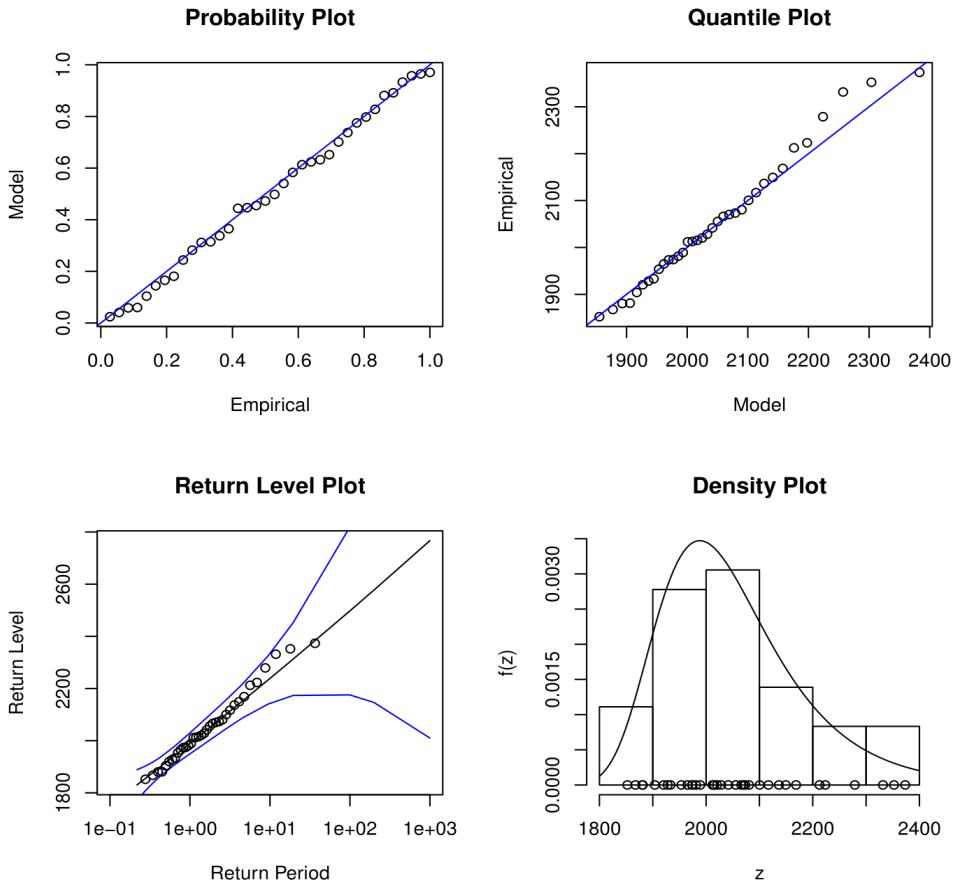

Figure D.10: Diagnostic plots for Load Case 2 (*Sb1*;*Sb2*): GEV distribution fitted to data.

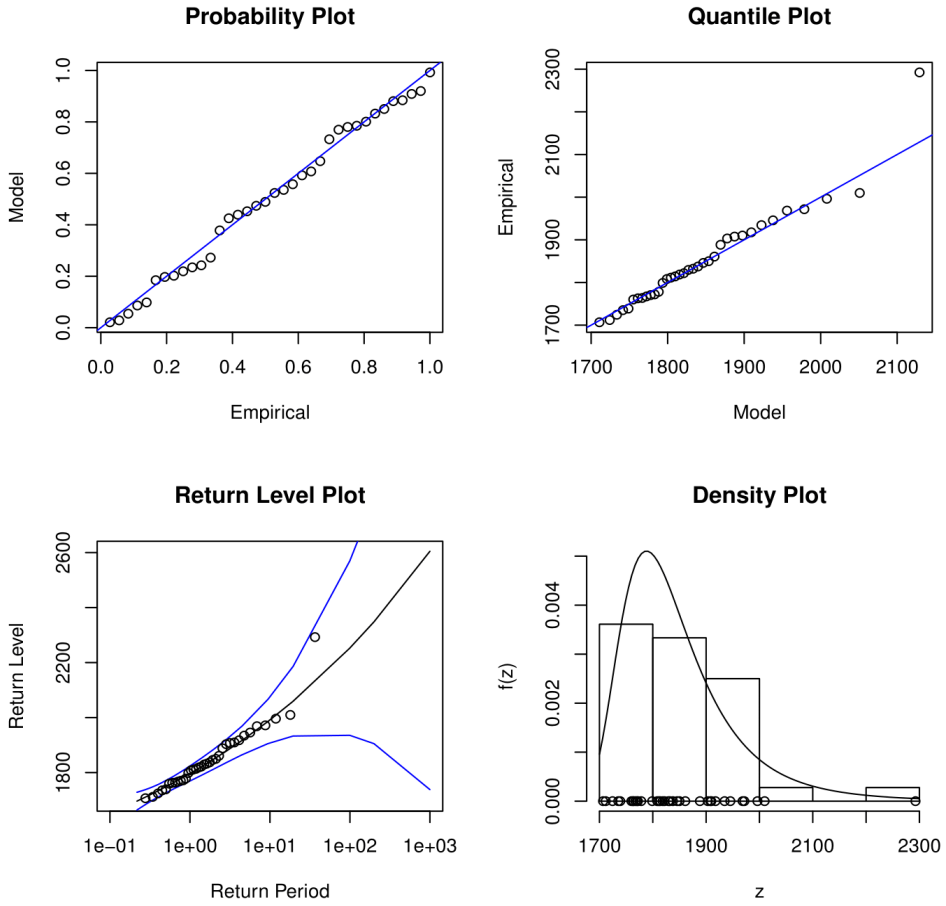

Figure D.11: Diagnostic plots for Load Case 3 (*Nb2*;*Nb1*): GEV distribution fitted to data.

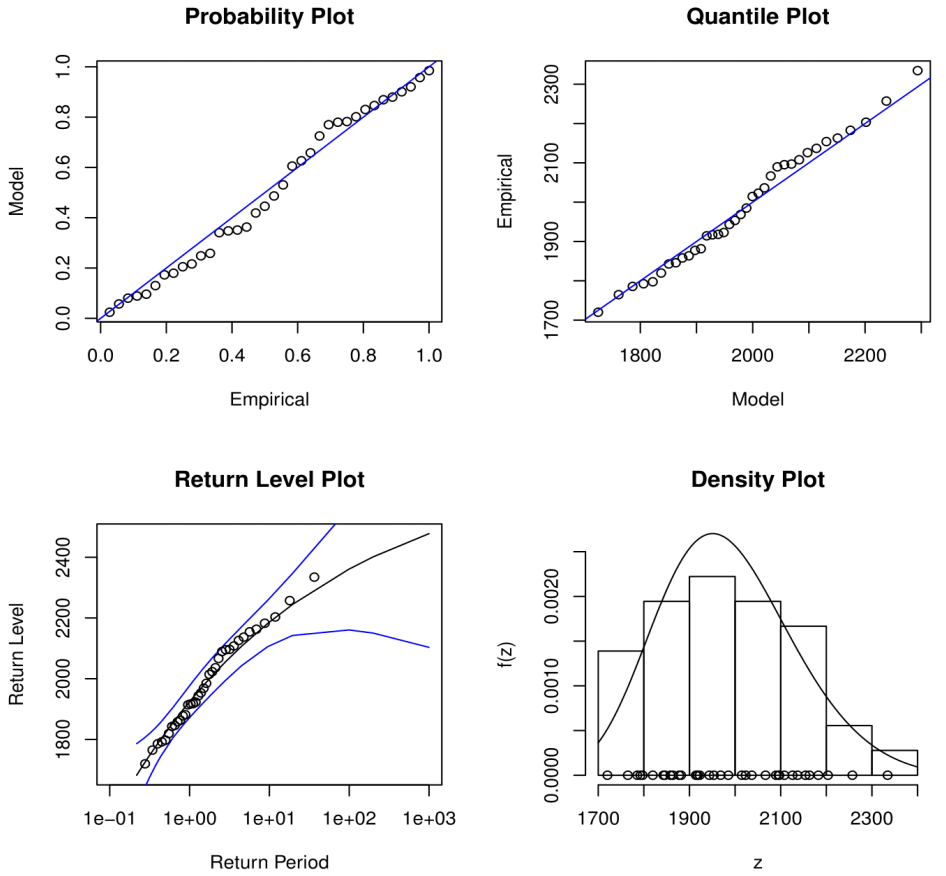

Figure D.12: Diagnostic plots for Load Case 4 (*Sb2*;*Sb1*): GEV distribution fitted to data.

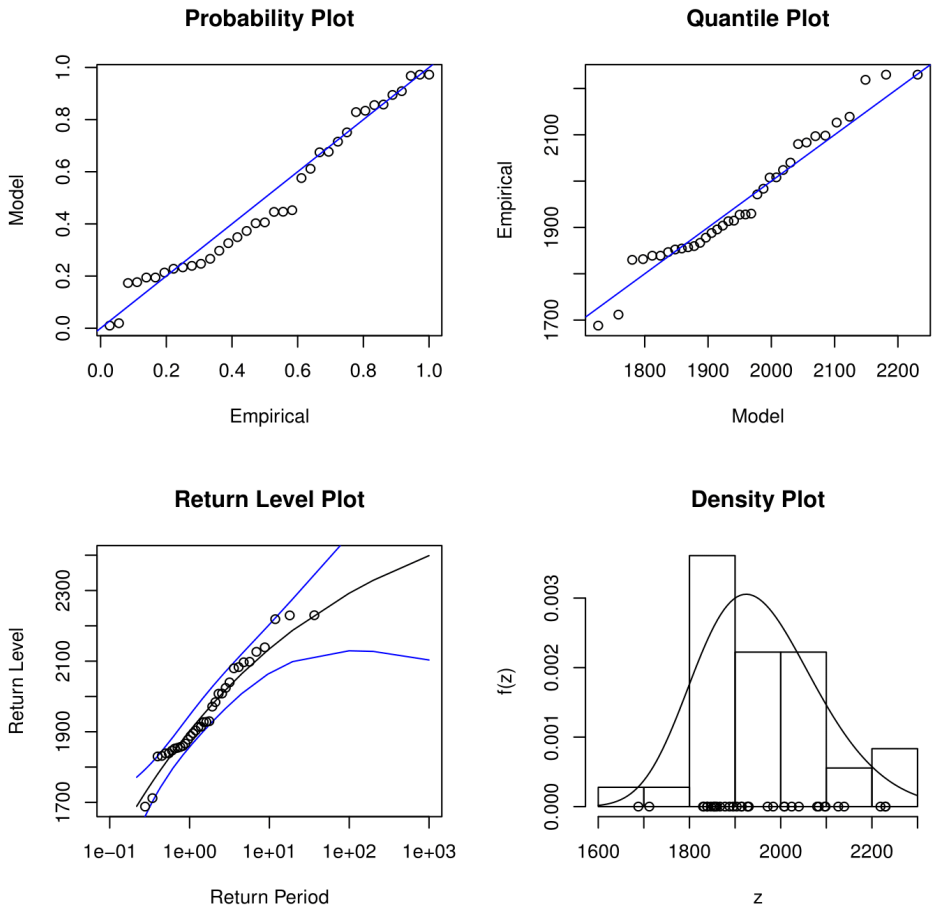

Figure D.13: Diagnostic plots for Load Case 5 (*Nb1*;*Sb1*): GEV distribution fitted to data.

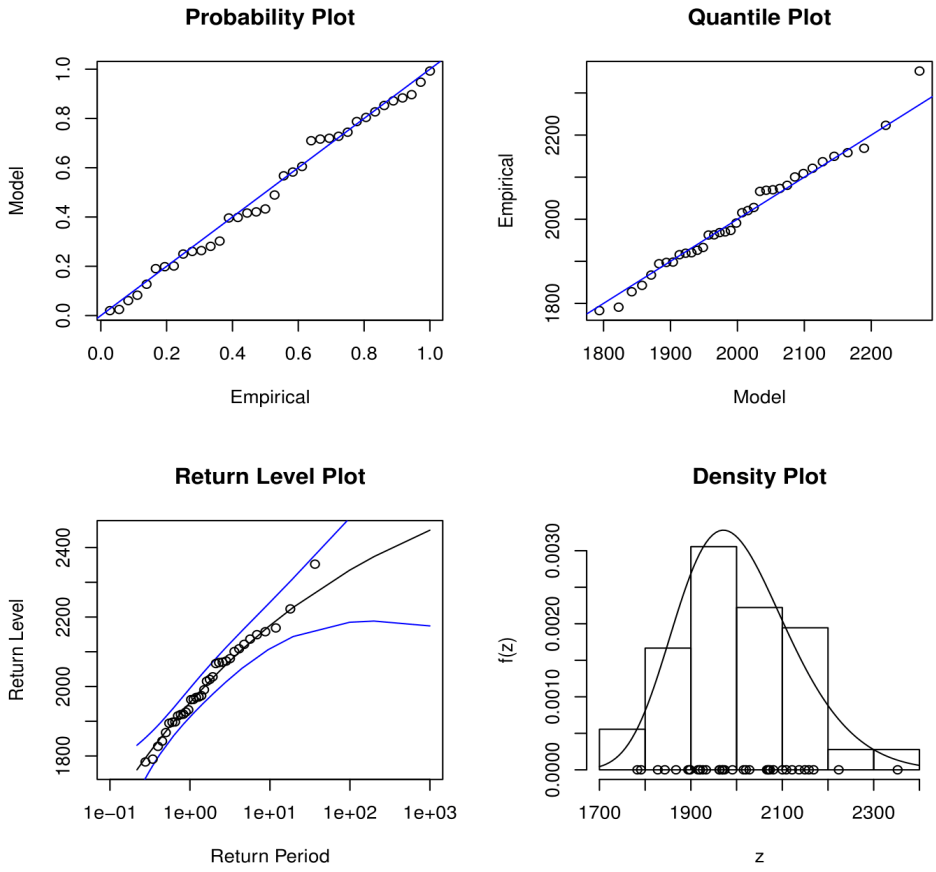

Figure D.14: Diagnostic plots for Load Case 6 (*Sb1*;*Nb1*): GEV distribution fitted to data.

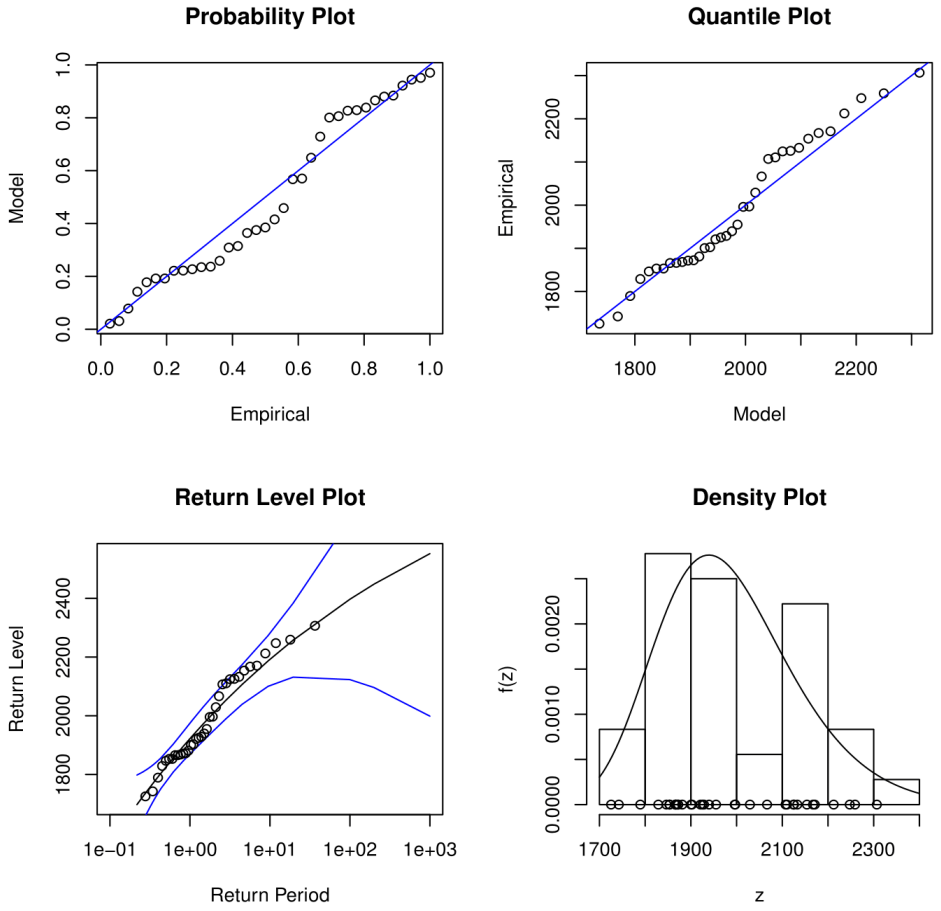

Figure D.15: Diagnostic plots for Load Case 7 (*Nb1*;*Nb2*;*Sb2*): GEV distribution fitted to data.

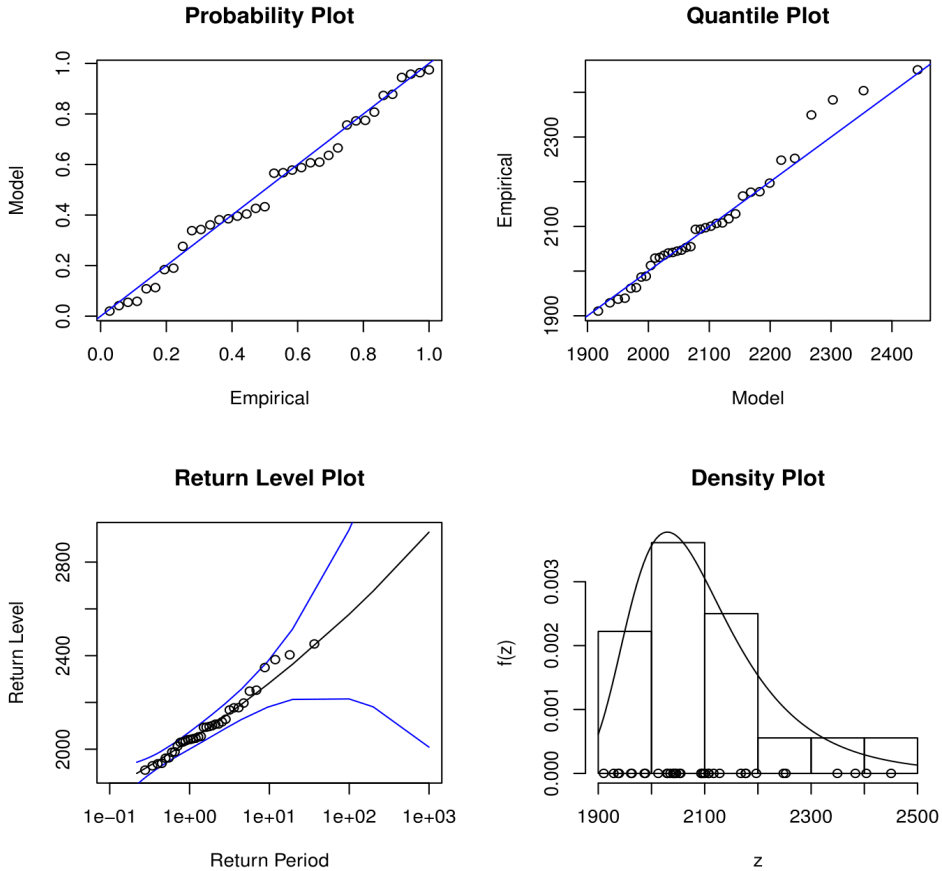

Figure D.16: Diagnostic plots for Load Case 8 (*Sb1*;*Sb2*;*Nb2*): GEV distribution fitted to data.